Deanship of Graduate Studies
Al – Quds University

Design, Synthesis and *In Vitro* Studies of Lipophilic Mixed Aliphatic/Aromatic Platinum(II/IV) Derivatives that are Encapsulated in Novel Drug Delivery Systems

Hebah Ibrahim Ali Damdoum

M.Sc. Thesis

Jerusalem – Palestine

1445/2024

Design, Synthesis and *In Vitro* Studies of Lipophilic Mixed Aliphatic/Aromatic Platinum(II/IV) Derivatives that are Encapsulated in Novel Drug Delivery Systems

Prepared by:

Hebah Ibrahim Ali Damdoum

B. Sc. Biology minor medical technology,

From Al-Quds University/Palestine

Supervisor: **Dr. Yousef Najajreh, PhD, Associate Professor**

Co-supervisor: **Dr. Mohyeddin Assali, PhD, Associate Professor**

A thesis submitted in partial fulfillment of the requirement for the Degree of Master of Biochemistry and Molecular Biology / Faculty of Medicine \ Al-Quds University

1445/2024

Al – Quds University
Deanship of Graduate Studies
Department of Molecular Biology and Biochemistry

Thesis approval

Design, Synthesis and *In Vitro* Studies of Lipophilic Mixed Aliphatic/Aromatic Platinum(II/IV) Derivatives that are Encapsulated in Novel Drug Delivery Systems

Prepared by: Hebah Ibrahim Ali Damdoum

Registration No: 22010005

Supervisor: Dr. Yousef Najajreh

Co-Supervisor: Dr. Mohyeddin Assali

Master thesis submitted and accepted date 14/5/2024

The names and signatures of the examining committee members are as follows:

1. **Head of committee:** Dr. Yousef Najajreh Signature:
2. **Internal examiner:** Dr. Sawsan Salameh Signature: Sawsan Salameh
3. **External Examiner:** Dr. Ahmad Mustafa Eid Signature:

Jerusalem-Palestine

1445/2024

Dedication

I want to dedicate my thesis to my mother, whom I always had by my side and who endured this journey with me, with all the love, encouragement, and support in the world.

To my dear Father in heaven (Al-Jannah by Allah's mercy)

Many thanks go to my supervisors, my teachers, my siblings, the rest of my family, friends, and coworkers for enduring me and supporting me, and everyone who supported me in my graduate studies.

May Allah be with my people and bless them.

May Allah be with them every step in the way.

We apologize for letting you down.

Hiba Ibrahim Damdoum

Declaration

I certify that this thesis submitted for the degree of Master, is the result of my own research, except where otherwise acknowledged, and that this study or any part of it has not been submitted for a higher degree to any other university or institution.

Signature:

Hebah Ibrahim Damdoum

Date: 14/5/2024

Acknowledgments

I thank Allah always and forever for giving me the strength, endurance, and courage to complete this journey of my life. I would like to thank my mother for believing in me and for being a support system throughout my life.

This project would not have been possible without the support of many people. First, I would like to thank my supervisor, Dr. Yousef Najajreh, who accompanied me throughout the project and was a great helper and supervisor I could not have wished for better. I would also like to give my gratitude and thanks to my co-supervisor, Dr. Mohyeddin Assali, who without his help in the biological aspect of this project alongside his respected fellow students Alaa Ratrot and Ahmed Musa with all of the difficult circumstances this project wouldn't have seen the light. Many thanks to Dr. Ismail Badran as well for leading the computational study for this project.

My special thanks go to Rima Aburish, who believed in me and my abilities and gave me all the support I needed in different forms.

I would also like to thank my mother, who encouraged and supported me along the way, my friends, and all the doctors at Al-Quds University Faculty of Medicine, who taught and supported me on my way to my master's degree.

I would also like to thank the laboratory staff of Dr. Mohammad Abul Haj who helped me access the analytical instruments to continue my thesis.

Title

Design, Synthesis and *In Vitro* Studies of Lipophilic Mixed Aliphatic/Aromatic Platinum (II/IV) Derivatives that are Encapsulated in Novel Drug Delivery Systems

Prepared by: Hebah Ibrahim Damdoum

Supervisor: Dr. Yousef Najajreh and Co-Supervisor: Dr. Mohyeddin Assali

Abstract

Research on synthesizing new anticancer compounds with minimal side effects is ongoing, with platinum-based drugs renowned worldwide for their anti-tumor properties. The main hypothesis of our study is that the choice of suitable chelating ligands for the platinum center in both oxidation states (Pt(II) or Pt(IV)) significantly influences the processing of these molecules and the nature of the lipid-based nano-delivery system. The physicochemical properties of the ligand substituents coordinated to the Pt center also strongly affect the dispersion of Pt-based complexes in drug delivery systems, such as niosomal layers.

This study focuses on the synthesis and investigation of new platinum(II/IV) derivatives with aliphatic and aromatic ligands encapsulated in niosomal vesicles. Characterization was performed using Attenuated Total Reflectance-Fourier *Trans*form Infrared (ATR-FTIR) spectroscopy and nuclear magnetic resonance

(NMR). The influence of the encapsulated ligands of platinum-loaded niosomal formulations on size, polydispersity, and loading efficiency was highlighted by using various novel types of platinum ligands. In vitro, studies on liver cancer cells (HepG2 and Hep3B) and the human hepatic stellate cell line (LX2) showed promising cytotoxic effects compared to those of cisplatin, miriplatin, and oxaliplatin.

The results indicated that smaller and more compact ligands, such as NBA, have better loading efficiency in the niosomal formulation compared to bulkier ligands like DACH. There were also clear connections between compounds with high lipophilicity, such as myristate, and increased potency against cancer cell lines, likely due to interactions with lipidic compounds and non-ionic surfactants in the niosomes.

In conclusion, this study introduces novel platinum(II/IV) compounds that show significant cytotoxic effects in liver cancer cells, highlighting the need for further investigation. This underscores the critical role of achieving well-balanced lipophilicity in drug delivery systems to enhance anticancer activity, minimize drug resistance, and ensure efficient tumor penetration. Further research is essential to understand and optimize these promising platinum-based formulations fully.

العنوان

تصميم و تصنيع لمشتقات البلاتين(II/IV) المختلطة الأليفاتية/العطرية المحبة للدهون دراساتها داخل خلايا من خلال تغليفها في أنظمة توصيل الأدوية الجديدة

إعداد:

هبة ابراهيم دمدوم

اشرف:

د.يوسف نجاجرة و المشرف المشارك: د.محيي الدين عسالي

الملخص:

لا تزال الأبحاث مستمرة حول تصنيع مركبات جديدة مضادة للسرطان مع الحد الأدنى من الآثار الجانبية، حيث تشتهر الأدوية المعتمدة على البلاتين في جميع أنحاء العالم بخصائصها المضادة للأورام.

الفرضية الرئيسية لدراستنا هي أن اختيار الرابطة او الروابط المناسبة لمركز البلاتين في كلتا حالتي الأكسدة (Pt(II) أو Pt(IV)) لها تأثير كبير على كيفية استقبال الدواء من خلال الجزيئات في انطمة تسليم الخلايا النانو ذات التركيبة الدهنية حيث ان تشتت الدواء البلاتيني المصنع في أنظمة توصيل الدواء مثل طبقة دهنية في حويصلات نيوزوم و ليبوزوم ، يتأثر بشدة بالخصائص الفيزيائية والكيميائية الروابط المنسقة مع مركز البلاتين.

تركز هذه الدراسة على تصنيع مركبات جديدة من مشتقات البلاتين (II/IV) مع بروابط أليفاتية وعطرية مغلفة في حويصلات نيوزومية. تم فحص هذه المركبات باستخدام التحليل الطيفي للأشعة تحت الحمراء (FTIR) / (ATR) والرنين النووي المغناطيسي (NMR). في المختبر، و أظهرت الدراسات التي أجريت على خلايا سرطان الكبد (HepG2 و-Hep3B) وخلايا الكبد البشرية (LX2) تأثيرات سامة للخلايا واعدة مقارنة بالسيسبلاتين. وميريبلاتين وأوكساليبلاتين.

أشارت النتائج إلى أن الروابط الأصغر والأكثر إحكاما، مثل NBA، تتمتع بكفاءة تحميل أفضل في تركيبة النيوزومال مقارنة بالروابط الأكبر حجمًا مثل DACH. كانت هناك أيضًا روابط واضحة بين المركبات ذات

المحبة العالية للدهون، مثل الميريستات، وزيادة الفعالية ضد خطوط الخلايا السرطانية، ويرجع ذلك على الأرجح إلى التفاعلات مع المركبات الدهنية والمواد السطحي غير الأيونية في النيوزومات.

في الختام، تقدم هذه الدراسة مركبات البلاتين(II/IV) جديدة التي تظهر تأثيرات سامة للخلايا على خلايا الكبد السرطانية، مما يشير إلى الحاجة إلى مزيد من التحقيق. وكما إنه يسلط الضوء على الدور الحاسم لتحقيق توازن بين تصنيع المركب و نظام توصيل الدواء لتعزيز النشاط المضاد للسرطان، وتقليل مقاومة الأدوية، وضمان اختراق الورم بكفاءة. يعد إجراء مزيد من الأبحاث أمرًا ضروريًا لفهم هذه التركيبات الواعدة القائمة على البلاتين وتحسينها بشكل كامل.

Table of Contents

List of Tables

List of Figures

List of Scheme

List of Abbreviation

Abbreviation	Full name
Pt	Platinum
E. coli	*Escherichia coli*
TNBC	Triple-Negative Breast Cancer
IV	Intravenously
CTR1	Copper *Trans*porter Protein
DNA	Deoxyribonucleic acid
RNA	Ribonucleic acid
NER	Nucleotide Ex*cis*ion Repair
FDA	Food and Drug Administration
CBDCA	1,1-cyclobutane dicarboxylate
DACH	1*R*, 2*R*-diaminocyclohexane
HCC	Hepatocellular Carcinoma
EPR Effect	The Enhanced Permeability and Retention
NADH	nicotinamide adenine dinucleotide (NAD) + hydrogen (H)
H_2O_2	Hydrogen Peroxide
I_2	Iodine
Br_2	Bromine
Cl_2	Chlorine
$KMnO_4$	Potassium permanganate
HDAC	Histone Deacetylase Inhibitors
COXis	Cyclooxygenase Inhibitors
DTDS	Drug Targeting and Delivery Systems
RES	Reticuloendothelial System
SUVs	Small Unilamellar Vesicles
LUVs	Large Unilamellar Vesicles
MUVs	Multilamellar Vesicles

GUV	Giant Unilamellar Vesicles
°C	Degree Celsius
THF	Thin-film hydration
Tc	*Trans*ition Temperature
PH	Potential of Hydrogen
REV	Reverse-Phase Evaporation
O/W	Oil in Water
NDDP	*Cis*-bis-neodecanoato-*trans*-*R,R*-1,2-diaminocyclohexane platinum(II)
DMPC	1,2-Dimyristoyl phosphocholine
DMPG	1,2-Dimyristoyl phosphatidylcholine
DPPC	Dipalmitoyl phosphatidyl choline
SPC	Soy phosphatidylcholine
HSPC	Hydrogenated Soy Phosphatidylcholine
DSPE-PEG2000	1,2-distearoyl-sn-glycero-3-phosphoethanolamine-N-[methoxy(polyethylene glycol)-2000] (ammonium salt)
DPPG	1,2-dipalmitoylsn-glycero-3-phospho-(1′-rac-glycerol) (sodium salt)
DSPC	1,2-distearoyl-sn-glycero-3-phosphocholine
DSPG	1,2-distearoyl-sn-glycero-3-phospho-(1′-rac-glycerol) (sodium salt)
GM1	Monosialoganglioside
PEG	Polyethylene Glycol
MPEG	Methoxy polyethylene glycol
MPS	Mononuclear Phagocyte System
TF	*Trans*ferrin
Cmax	maximum plasma concentration
AUC	Area under the curve

MTD	Maximum Tolerated Dose
HMGB1	High mobility group box 1
GOx	Glucose oxidase
TPZ	Triapazamine
RRD4	Phosphaplatin platinum(IV)
CanPt	Cantharidin-platinum(IV)
IC_{50}	Half-maximal inhibitory concentration
CHEMS	Cholesteryl Hemisuccinate
$CdCl_3$	Deuterated Chloroform (Chloroform-D)
DDW	Double-distilled water
MeOH	Methanol
DMF	Dimethyl Formamide
DMSO	Dimethyl Sulfoxide
KI	Potassium Iodide
EN	Ethylenediamine
NH_4OH 25%	Ammonium Hydroxide
DACH	((1*R*,2*R*)-1,2-diaminocyclohexane))
TFA	Trifluoroacetic Acid
$NaHCO_3$	Sodium Hydrogen Carbonate
HCl conc 37%	Concentrated hydrochloric acid
K_2PtCl_4	Potassium tetrachloroplatinate(II)
$AgNO_3$	Silver nitrate
EtOH	Ethanol
H_2O_2 3%	Hydrogen peroxide
ATR/FTIR	Attenuated total reflection /Fourier *trans*form infrared spectroscopy
^{1}H-NMR	Proton nuclear magnetic resonance
(ppm, δ)	per million
(d)	Doublet
(dd)	Doublet of doublets
(m)	Multiplet

(q)	Quartet
(t)	Triplet
(s)	Singlet
UV-VIS	Ultraviolet-visible
DLS	Dynamic Light Scattering
AFM	Atomic Force Microscopy
RBF	Round Bottom Flask
MYR	Myristato
EZB	Ethylbenzoato
TFBA	Trifluoromethylbenzoato
KOH	Anhydrous potassium hydroxide

Chapter One

Introduction

1.1 History of Cisplatin

More than five decades ago, Dr. Barnett Rosenberg, a biophysicist at Michigan State University, investigated the impact of the electrical field on cell division in *Escherichia coli (E. coli)* bacteria. Dr. Rosenberg *et al.,* added platinum rods to the growth chamber, assuming that they would not interfere with the study because of their inert nature. Surprisingly, bacterial division ceased after the application of an electric current to the field. *E. coli* continued to grow as an abnormally long filament. Once the electrical current was turned off, it began to divide normally. After two years of investigation of the strong effect of the electric field on bacterial growth, they found that the compound released from platinum rods affected cell growth. After another two years, *Rosenberg et al.* identified this complex. It was later named cisplatin(Rosenberg et al., 1965).

The compound diamminedichloroplatinum(II), [*cis*-[$Pt(NH_3)_2Cl_2$], cisplatin] **(10)** was first synthesized in the mid-1840s by Italian chemist Michele Peyronie. It is known as Peyrone's chloride or Peyrone's salt, and its structure was determined by Werner in 1893(Kauffman et al., 2010).

Cisplatin received little attention until the mid-1960s when Dr. Barnnet Rosenberg discovered its remarkable therapeutic properties in 1965. His research showed that cisplatin **(10)** demonstrated exceptional anticancer effects against sarcoma and leukemia in mice as an animal model. In 1978, the US Food and Drug Administration (FDA) approved its usage for treating testicular cancer, as it improved the cure rate by up to 90% and caused a significant decrease in the death rate for testicular cancer by two-thirds(Mayer et al. 2002). Cisplatin **(10)** is a breakthrough metal-containing anticancer drug that has gained international recognition. before all chemicals, natural products, or synthetic organic compounds that are used to treat cancer(Ghosh, 2019). Cisplatin is a fundamental component of the development of new metal-based drugs, establishing a benchmark for their effectiveness and safety. It is effective not only in testicular cancer but also in numerous solid tumors, such as ovarian, neck, bladder, cervical, esophageal, and small-cell lung cancers(Ratzon et al., 2016).

In clinical practice, cisplatin **(10)** is often used in combination with radiation treatment and other anticancer drugs such as taxanes or gemcitabine to increase its therapeutic efficiency. Furthermore, research has found that the combination of cisplatin and

docetaxel is significantly effective, particularly in treating triple-negative breast cancer (TNBC)(Sánchez-Escribano Morcuende, Alés-Martínez, and Aramburo González, 2007).

1.1.1 Mechanism of Action of Cisplatin

Cisplatin **(10)** is typically administered intravenously (I.V.) with saline or alongside other therapeutic drugs. The mechanisms of action include cellular uptake, activation, DNA binding leading to Pt-DNA adduct formation, and the cellular processing of these adducts for apoptosis(Feng, 2019; Johnstone et al., 2016). Cisplatin conversion is impeded by elevated chloride ion levels (~100 mM) in the bloodstream(Daley-Yates & McBrien, 1985). Nevertheless, it is vulnerable to interactions with plasma proteins, especially those enriched in thiol groups such as albumin, which can deactivate cisplatin and result in side effects such as nephrotoxicity and neurotoxicity(Alderden et al., 2006; Ghosh, 2019; Ivanov et al., 1998).

Upon entering the cell, cisplatin undergoes aquation, activation, and attachment to nuclear DNA through processes such as passive diffusion or active transport using membrane transporters, such as the copper transporter protein (CTR1)(Basu & Krishnamurthy, 2010). When cisplatin completely penetrates cells, the activation process begins when the chloride atom (non-amine ligand) is exchanged with two water molecules because of the lower intracellular chloride concentration (~4-12 mM)(Lippard, 2007; Johnstone et al., 2016). It forms a new positive cationic platinum species [*cis*-$Pt(NH_3)_2Cl(H_2O^+)$], which is active and has a high affinity for negatively charged purine bases (guanine and adenine) of DNA and RNA. This prevents DNA replication and RNA transcription, where it binds to form an irreversibly cross-linked adduct either between strands or within the same strand (between N7 atoms of nearby pairs) with DNA. The primary cross-links were 1,2-intrastrand GpG cross-links (60–65%), ApG cross-links (25%), 1,3-intrastrand GpXpG cross-links (5-10%), and some minor Pt-D(GG) inter-stream cross-links(Eastman, 1987; Kartalou & Essigmann, 2001).

The production of Pt-DNA adducts has been reported to directly influence their cytotoxic effects by causing local structural changes in double-stranded DNA and triggering cellular responses(Siddik, 2003). This process involves altering the DNA structure to allow binding to the major groove and exposing a wide minor groove

surface to cellular proteins that inhibit replication and transcription, resulting in the deformation of the DNA strand. This process also triggers the release of cytochrome c and the activation of intracellular caspases, leading to apoptosis and ultimately cell death if damaged cells are not rapidly repaired. Cisplatin predominantly targets rapidly dividing cells, including cancer cells, making it an attractive treatment option(Cohen & Lippard, 2001; Rocha et al., 2018; Siddik, 2003).

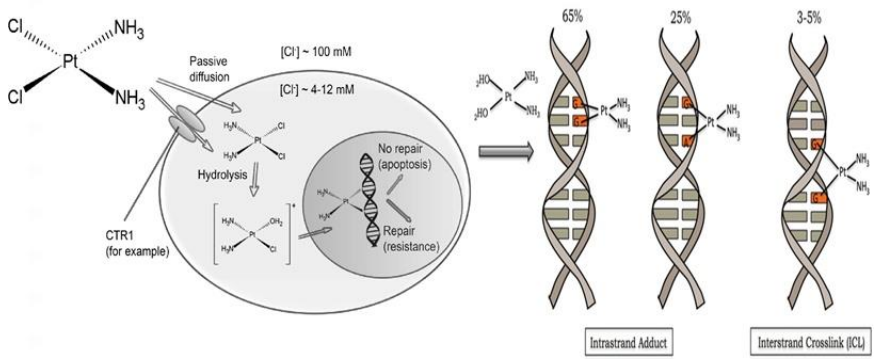

Figure 1.1.1: The structure and mechanism of action of cisplatin **(10)** damage DNA in the following manner: (A) it starts by exchanging the chloride atoms for water molecules (monosaturated and diaquated, respectively; (B) covalent bonds are formed between cisplatin and DNA, and intrastrand DNA adducts (cross-links) are formed initially. Percentages represent the frequency of each Pt-DNA adduct type(Siddik, 2003).

1.1.2 Drug Resistance and Toxicity of Cisplatin

The systemic administration of cisplatin **(10)** is associated with numerous severe adverse side effects, including metabolic instability. It is attached to albumin and other plasma proteins in the blood, leaving only a small fraction active and circulating in the bloodstream, with side effects ranging from general toxicity, such as nausea, diarrhea, vomiting, difficulty breathing, fever, and chills(Apps et al., 2015). A significant dose limitation of cisplatin **(10)** has been reported, which can be internalized inside rapidly dividing cells without any preference for cancerous cells or normal cells (such as hair, nails, skin cells, cells in the gastrointestinal tract, and blood cells in the bone marrow and others), and the kidney attempts to excreta the "harmful drug" for body protection. Nephrotoxicity is a composite result of the

transport of cisplatin into renal epithelial cells, injury to DNA, activation of multiple cell death and survival pathways, and initiation of a robust inflammatory response that limits and damages kidney function. With its repeated accumulation in the kidney tissue, over 25–35% of treated patients are affected by nephrotoxicity(Florea & Büsselberg, 2011; Kumar *et al.*, 2017). However, the systemic administration of cisplatin **(10)** is responsible for many other severe side effects, as it exhibits metabolic instability, as 90% of the drug is attached to albumin and other plasma proteins. Although nephrotoxicity can be controlled by fluid intake combined with saline administration before and after treatment, a significant dose-limiting toxic effect of cisplatin is a common adverse effect. Cisplatin treatment can potentially lead to neurotoxicity, which can result in symptoms such as peripheral neuropathy, numbness, or tingling of the hands and feet, as well as hearing loss (ototoxicity), tinnitus, electrolyte abnormalities, myelosuppressive hepatotoxicity, retinopathy, pancreatitis, seizures, and respiratory failure. The severity of these effects can vary depending on the dosage and duration of treatment and individual factors, such as age and overall health(Piccart *et al.*, 2001; Tsang et al., 2013; de Brito *et al.*, 2022). In addition, cisplatin treatment may cause infertility because it increases the induction of oxidative stress, which affects spermatogenesis by altering its structure, protein composition, cell count, and changes in testicular tissue histology and biochemistry(Yucel et al., 2019). In addition to its side effects, the clinical application of cisplatin is adversely affected by inherent and acquired resistance(Ho et al., 2016). Three main mechanisms underlying cisplatin **(10)** resistance have been identified.

I. Decreased cellular accumulation and increased drug efflux of cisplatin were associated with a reduction in CTR1 transporters. *Komatsu et al*. demonstrated that cisplatin accumulates in endosomes in cisplatin-resistant cancer cells and is prevented from reaching the DNA(Hall et al., 2008).

II. Cisplatin is detoxified by glutathione (GSH) and metallothioneins (MTs), and increased cellular GSH concentrations are correlated with cisplatin resistance in various cell lines(Hamaguchi et al., 1993). Cisplatin binds to GSH to form a complex that exports organic anion transporters and other proteins, such as thioredoxin, contributing to low cisplatin resistance(Kelley *et al.*, 1988; Boulikas, 2007; Stordal & Davey, 2007).

III. Enhanced DNA repair and tolerance. In initial studies, researchers assumed that nucleotide ex*cis*ion repair (NER) expression levels were related to

cisplatin sensitivity in tumor cells. However, cisplatin resistance is related to low mismatch repair efficiency rather than a simple relationship with NER levels(Mayer et al., 2002. Albertella *et al.)* indicated that platinum sensitivity was significantly affected by the absence of DNA polymerase(Malhotra-Kumar et al., 2007).

The three main mechanisms mentioned above result in the reduced efficacy of cisplatin.

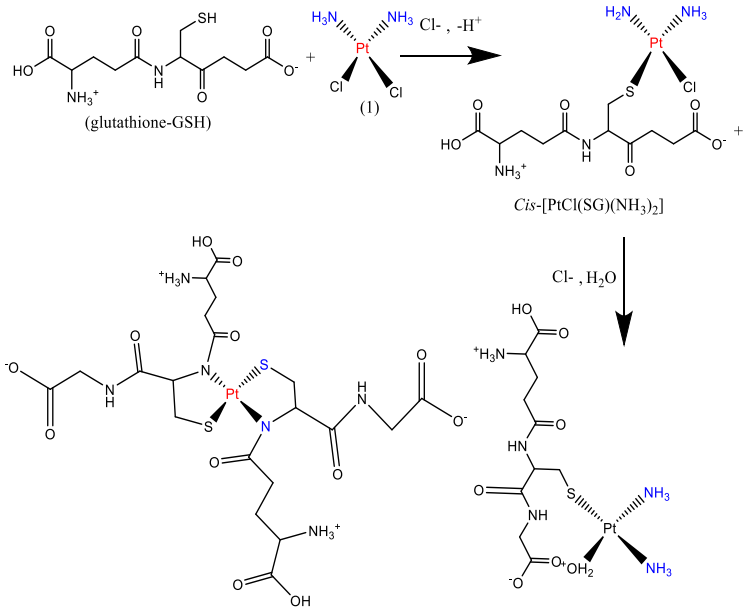

Figure 1.1.2: Synthesis of conjugated complexes of glutathione and cisplatin. Complexes can be removed from the cytoplasm of cells after their formation(Boulikas, 2007).

1.2 Related Platinum-based Drugs and their Mechanism of Action

Further exploration of platinum-based drugs and their combinations is necessary to reduce the toxicity and resistance associated with cisplatin and enhance anticancer effects with fewer side effects. The geometric isomers of cisplatin **(10)** and transplatin [*trans*-dichlorodiammineplatinum(II) (*trans*-platinum) **(52)**] (Figure 1.2.) exhibited toxicity, but no cytotoxic activity(Ratzon et al., 2016).

Cisplatin **(10)**
Clinically Active

Transplatin **(52)**
Clinically Inactive

Figure 1.2.1 The active compound (cisplatin **(10)**) is clinically approved for worldwide use and is inactive (transplatin **(52)**).

Of the nearly three thousand platinum complexes synthesized and tested, only two have been approved worldwide and five have been approved for therapeutic use in Asia(Wheate *et al.*, 2010; Johnstone et al., 2016).

Carboplatin **(53)**, a platinum-based drug licensed by the Food and Drug Administration (FDA) in 1989, is a second-generation platinum-based drug(Deo et al., 2018; Wheate et al., 2010) with a lower toxicity profile than cisplatin and, as such, can be administered at a higher dosage. This reduced toxicity is attributed to its distinct chelating leaving group, 1,1-cyclobutane dicarboxylate (CBDCA). Nevertheless, it still causes myelosuppression and shows cross-resistance with cisplatin **(10)**, due to sharing the same non-leaving group(R J Knox, F Friedlos, D A Lydall 1986.; Rixe et al., 1996).

[(1*R*,2*R*)-cyclohexane-1,2-diamine](ethanedioato-O,O')platinum(II); (Oxaliplatin) **(23)**, a third-generation platinum-based drug licensed in 2002, has a distinctive chelating ligand, oxalate, and (1*R*, 2*R*)-diaminocyclohexane (DACH), which acts as a non-leaving group(Deo et al., 2018; Wheate et al., 2010). Providing a different range of activities, such as action against colorectal cancer, which is typically resistant to cisplatin, helps to minimize cross-resistance with cisplatin, allowing for. Such notions are due to the dependency of drug uptake into cancer cells on organic cation transporters that are overexpressed in colon cancer, compared to copper transporters(Holzer et al., 2006; Zhang *et al.*, 2006). However, significant concern has been raised due to noticeable neurotoxicity, which is perceived as the most frequent dose-limiting toxicity(Rottenberg et al., 2021). Nevertheless, the drug demonstrated improved efficacy against colorectal cancer in combination with 5-fluorouracil (5-FU) and folinic acid (FA), both in metastatic and radically resected disease(Cheng et al., 2023; Pasetto et al., 2006).

Nedaplatin **(54)**, approved in Japan in 1995, is the second analog of cisplatin, with a similar activity profile but low renal, myelosuppression, and gastrointestinal toxicities. Heptaplatin

(55), on the other hand, was approved by the Korean FDA in 1999. Lobaplatin **(56)** received approval from the Chinese FDA in 2010 and is assumed to act by a similar mechanism of action to cisplatin i.e. involves DNA binding and transcription inhibition. The toxicity profiles included nephrotoxicity, and intra-abdominal bleeding The toxicity profile of heptaplatin **(55)** provides nephrotoxicity and intra-abdominal bleeding(Liu et al. 2016). In contrast, lobaplatin **(56)** exhibited lower cytotoxicity and higher efficiency than carboplatin tolerability, with minimal vomiting. Transient and reversible hematologic toxicity, neutropenia, and thrombocytopenia were noted 7–10 days after administration of lobaplatin(N. N. Zhou et al., 2018). A randomized and open-label phase II trial in triple-negative breast cancer (TNBC) patients revealed that the addition of lobaplatin to docetaxel and epirubicin chemotherapy regimen resulted in a pathologic complete response (pCR) overall response rate (ORR), which was accompanied by tolerable side effects(X. Wu et al., 2018). In addition, lobaplatin-based chemotherapy has been reported to be well-tolerated and effective in the treatment of advanced metastatic breast cancer(Y. Wu et al., 2019).

Miriplatin (**19** in Figure 1.2) was approved in Japan in 2009 for treating hepatocellular carcinoma (HCC) using lipiodolization. Miriplatin has a similar structure to oxaliplatin **(23)**, sharing a non-cleaving group, along with two myristate chains acting as cleaving groups. This configuration renders miriplatin a highly hydrophobic complex. Miriplatin is delivered into the hepatic artery in clinical settings combined with an oily lymphatic agent called Lipiodol Ultra-Fluide®, which serves as a carrier. This approach allows for the slow release of active platinum compounds into the aqueous phase, similar to the process observed for oxaliplatin. Miriplatin, [(1*R*,2*R*)-cyclohexane-1,2-diamine-*N*,*N*′]bis(tetradecanoato-*O*)platinum monohydrate **(19)**, is a third-generation platinum drug designed with the aim to improve drug delivery and reduce toxicity while enhancing the potency for treating HCC via hepatic artery administration as a sustained-release suspension with lipiodol. This formulation represents a promising method for treating hepatocellular cancer, demonstrating enhanced therapeutic efficacy with minimal adverse side effects(Tanaka et al., 2011).

Despite having less anticancer activity than cisplatin, all of these medications were approved by the Asian FDA due to their lowered toxicity in particular organs; nevertheless, the FDA did not approve them worldwide because they were not better than medications that were approved internationally(Deo et al., 2018; Wheate et al., 2010).

Few platinum-based anticancer agents have entered clinical trials but have not yet been approved, such as satraplatin **(57),** an orally active Pt(IV)-based prodrug, picoplatin **(58),** one ammine replaced with 2-picoline developed to overcome cisplatin resistance induced by overexpression of thiol-containing biomolecules; and ProLindac™ **(59),** an AP5346, 1*R*, 2*R*-diaminocyclohexane (DACH) platinum prodrug conjugated to water-soluble biocompatible polymers for advanced deliver(Apps et al., 2015; Eastman, 1987)). ProLindac exhibits efficacy at least equal to, and likely superior to, oxaliplatin while demonstrating excellent tolerability. Additional clinical studies of ProLindac in combination with other chemotherapeutic agents are planned(Wheate et al., 2010).

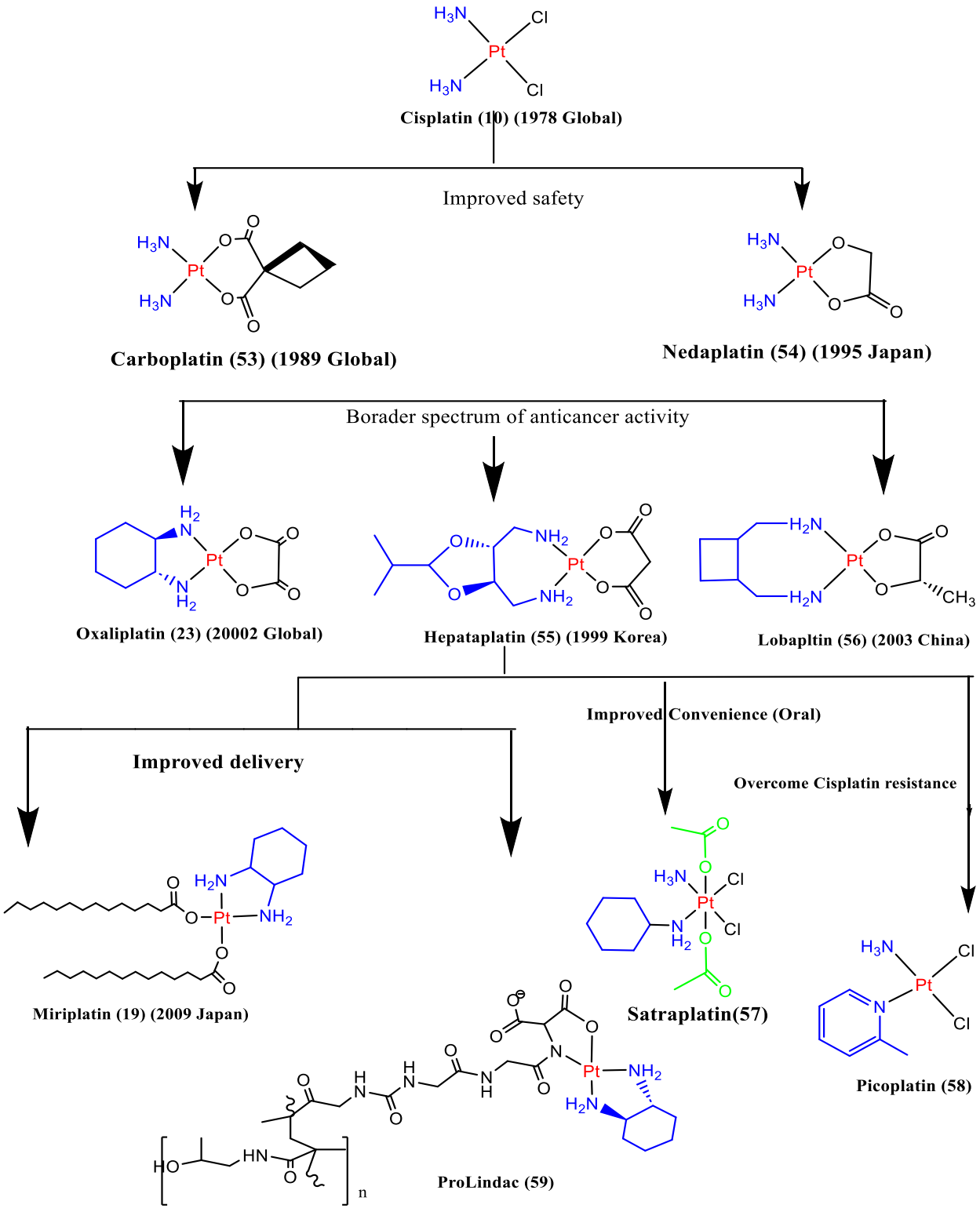

Figure 1.2.2: Structures of platinum anticancer agents have been approved for clinical use worldwide and nationally(Feng, 2019).

1.2.1 Modifying Platinum-based Drugs

Development of novel platinum-based anticancer drugs requires strategic modification of several structural features (Figure 1.2.3)(Wilson & Lippard, 2014). The non-leaving-group ligands of platinum complexes, L (monodentate or bidentate) in the *cis* configuration, are usually nitrogen donors that form thermodynamically stable bonds with platinum. These non-leaving ligands typically remain unchanged during drug activation and directly influence the nature of the final Pt-DNA adduct(Zhang et al., 2006). The ligands of the leaving group X in a *cis configuration*, typically chlorides, halides, and carboxylates, are labile and can be replaced by ligand substitution. Modification of ligand X can alter its activation kinetics, toxicity profile, and solubility(Lovejoy et al., 2008; Silverman et al., 2002). Axial ligands, *R*, are only present in higher-valence platinum complexes such as platinum(IV). These ligands will ultimately dissociate after biological reduction but can be used for tumor targeting or binding to nanoparticles(Lippard, 2014). Modifying these three ligand types also changes the lipophilicity and solubility of platinum molecules, which are critical physicochemical parameters for drug design and delivery(Markovic et al., 2018).

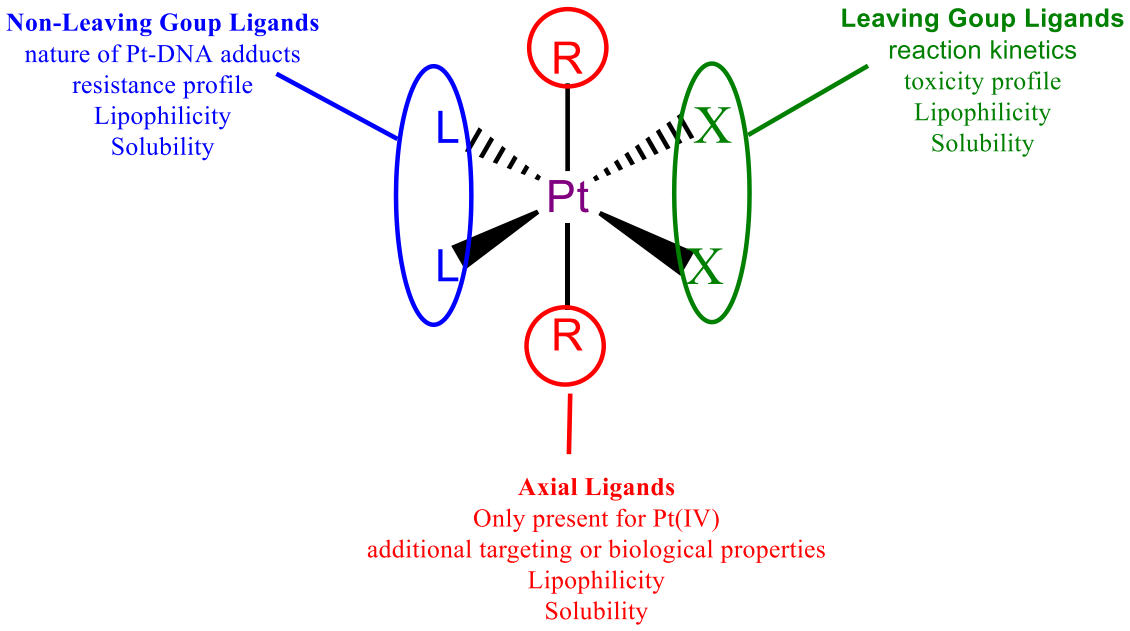

Figure 1.2.3: General structure of anticancer platinum agents(Wilson & Lippard, 2014).

Recently, there has been an increase in the generation of novel platinum-based anticancer drugs beyond the typical structure-activity relationships associated with reputable drugs such as cisplatin. New compounds mainly address the main obstacles facing drug development, including resistance, tumor selectivity, penetration and uptake, detoxification, and severe adverse effects. One approach to hunting compounds exerting improved action with minimal drawbacks is to exploit platinum(IV). Such an approach is justified by the realization of better pharmacokinetics, increased lipophilicity and bioactivity, and reduced side effects that are accompanied by higher stability, especially in acidic conditions. Compared to their respective reduced platinum(II) analogs, these qualities make them well-suited for oral administration, hypothetically permitting bioactive molecules with better drug-like properties with enhanced effectiveness, targeting, and efficacy(Venkatesh & Lippard, 2011; Venkatesh & Sadler, 2018).

Despite these prospective advantages, the FDA has not approved any of the Pt(IV) complexes that have been produced up to this point for clinical use. Therefore, the main goals of this current research are to fully understand how platinum(IV) derivatives undergo intracellular processing, illuminating their molecular mechanisms of action, and developing methods for carefully targeting their delivery to tumor sites while minimizing unfavorable side effects(Ravera, Gabano, et al., 2019).

Other approaches to developing non-typical structures of existing drugs were mentioned, such as *trans*-platinum complexes, which have a square-planar geometry. However, compared to *cis*-complexes, *trans*-complexes comprise a different arrangement of ligands around the Pt center. This structural dissimilarity is believed to be the basis for a distinct DNA-binding mode and mechanism of action, which lays the foundation for the potential ability to overcome emerging cancer resistance(Kalinowska-Lis et al., 2008).

There are also charged complexes, as some platinum complexes contain charged ligands that can affect cellular absorption and DNA binding. These charged complexes may alter pharmacokinetics and increase cancer cell selectivity(Ostrowski & Ford, 2009).

In addition, complexes with unusual DNA-binding modes and novel platinum complexes that can unexpectedly bind to DNA can be developed. This can potentially

disrupt the DNA repair processes and increase their cytotoxic effects, perhaps overcoming resistance mechanisms based on DNA repair(Oldfield et al., 2007).

Platinum complexes can be conjugated to ligands that target overexpressed enzymes, transporters, or receptors in cancer cells. These complexes can improve the selectivity of tumor cells by targeting specific pathways(Platts et al., 2001).

Platinum-based treatments can be coupled with other drugs or therapies to increase their efficacy and overcome drug resistance. For example, a combination of platinum drugs with immunotherapies or targeted therapies can have synergistic effects(Rottenberg et al., 2021).

A better understanding of the molecular mechanisms and drug resistance of cancer cells has driven the development of novel approaches to platinum-based chemotherapy. They aim to provide more effective and customized therapies while minimizing the side effects of standard platinum drugs, such as cisplatin.

1.3 Platinum(IV) Complex

To modulate issues related to resistance, side effects, and limited bioavailability associated with Pt(II) compounds, efforts have been directed toward the development of new platinum-based drugs designed to address these challenges. Pt(IV) complexes represent a class of prodrugs characterized by their relative inertness. A prodrug is a "derivative of a drug that is metabolized or activated in the body to release or generate the active drug." Containing a core platinum atom that, when activated, produces active Pt(II) derivatives, these compounds have the benefit of being able to circulate in the circulation in a somewhat stable oxidation state [Pt(IV)]. By controlling the reactivity of the drug and minimizing the loss of its active form, this approach aims to mitigate adverse effects frequently associated with platinum-based therapies(Deo et al., 2018).

The Pt(II) complexes had a square planar shape. In contrast, Pt(IV) complexes, the oxidized form of Pt(II), are coordinated in an octahedral coordination sphere with a low-spin Pt center in the d6 configuration. This geometry allows kinetic inertness(Madison et al., 2007). Glutathione, a critical cellular defense against toxins and oxidants, can neutralize electrophilic drugs, including some chemotherapeutic agents. It also plays a role in reducing Pt(IV) complexes to their active Pt(II) forms(Sluiter et al., 1992). Additionally, the significant amounts of reductants ascorbate, L-methionine, L-cysteine, and DL-homocysteine found in human plasma can reduce Pt(IV) complexes(Hall &

Hambley, 2002a; Jovanović *et al.*, 2013). Other biomolecules, such as serum albumin hemoglobin, and cytochrome c, can also activate Pt(IV) complexes. Various reducing agents have been used to highlight the complex mechanisms underlying Pt(IV) prodrug activation under various physiological conditions(Carr et al. 2006).

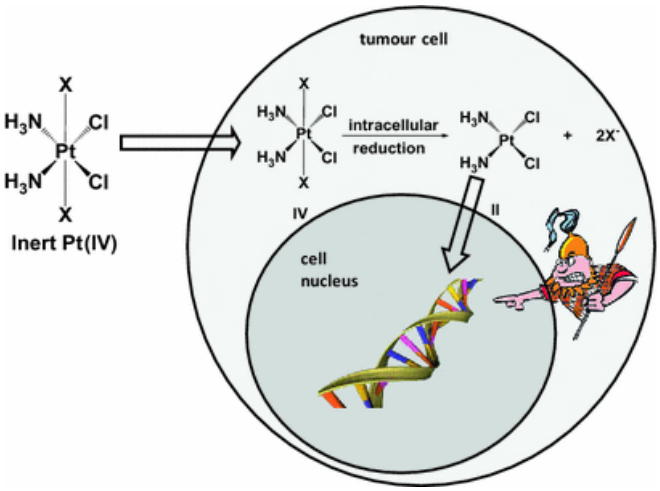

Figure 1.3. Illustrative drawing of the Pt(IV) prodrug hypothesis: reductive elimination of Pt(IV) prodrugs occurs with the release of the active Pt(II) moiety and two axial carboxylate ligands(Chen *et al.*, 2018).

1.3.1 Oxidation of Platinum(II) Complex

The final platinum(IV) product is determined by three key factors: platinum(II) precursor, oxidant, and solvent. The oxidant is significant because it can take two electrons from the Pt(II) core and occupy one of the axial ligand positions in the final product(Wilson and Lippard, 2014). An anion from the oxidant or solvent can simultaneously occupy the second axial site. One of the frequently used oxidizing agents is hydrogen peroxide (H_2O_2). Dihydroxidoplatinum(IV) complexes (*cis-, cis-, trans* $[PtL_2X_2(OH)_2]$) are usually produced. Oxidation using H_2O_2 generates two more OH groups occupying the axial positions (scheme **1.3.1**). Several organic protic solvents (ROH), including acetic acid, methanol, and ethanol, can be used as reaction media. To add ligands during the oxidation process, these solvents can coordinate with the Pt(IV) center(Chung et al., 2005). Because of the freedom in solvent selection, the reaction conditions may be adjusted to produce suitable platinum(IV) complexes with the desired characteristics(Lee et al., 2003).The

generation of more reactive carboxylic acid derivatives is an alternative strategy. Acyl chlorides, N-hydroxysuccinimide esters, acid anhydrides (both aliphatic and aromatic, such as glutaric, maleic, succinic, and phthalic anhydrides), acyl chlorides, N-hydroxysuccinimide esters, are suitable options. As shown in Scheme 1.3(Iv, 1996; Reithofer et al., 2011), these reactive derivatives reacted with axial OH ligands. Although acyl chloride and anhydride techniques are often used, they restrict the ligands that may be added to the axial locations of the Pt(IV) complexes. These techniques are often suitable for analyzing simple aliphatic and aromatic compounds(Zhang *et al.* 2013).

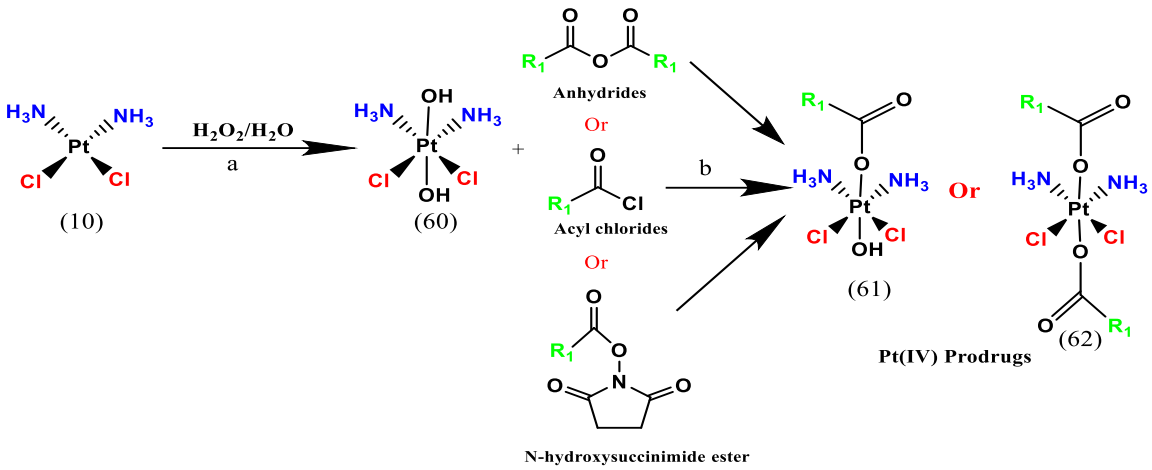

Scheme 1.3.1: General synthetic route for platinum(IV) prodrugs. a) Oxidation of Pt(II) by hydrogen peroxide (H_2O_2); b) acylation of dihydroxyplatinum(IV) using acid anhydrides, acyl chlorides, or N-hydroxysuccininide esters(Iv, 1996).

Halogens such as chlorine (Cl_2), bromine (Br_2), and iodine (I_2) have also been used as oxidizing agents for platinum(II).These halogens occupy two axial positions in the resulting Pt(IV) complexes(Johnstone et al., 2015; Xu et al., 2021). It is important to remember that the use of chlorine gas (Cl_2) in the laboratory requires specific handling and procedures because of safety concerns. Alternative and safer chlorinating compounds, such as iodobenzene dichloride ($PhICl_2$) or N, N-dichlorobenzene sulfonamide ($PhSO_2NCl_2$), are frequently used to address these safety issues. Although safer to handle, these compounds can progressively produce chlorine gas throughout the reaction(Johnstone et al., 2015; Xu et al., 2021).

Other oxidizing agents, such as $KMnO_4$, ozone in water, or the dichloride salt of dithiobis (formamidinium) were also used over the years. These agents can oxidize Pt(II) complexes to produce Pt(IV) derivatives(Lippard, 2014).

Reduction of Pt(IV) to its Pt(II) counterparts is a central step in the activation and exertion of anticancer activity. This reduction process significantly influences the biological activity of the Pt(IV) complexes(Hall & Hambley, 2002). The crucial step in the activation of Pt(IV) complexes is their reduction to Pt(II), which is influenced by several factors.

First, the biological activity of Pt(IV) complexes is significantly influenced by the reducing potential of the axial ligands, which differ from one another and thus affect the stability of the Pt(IV) complex and their reduction rate. The more electronegative the axial ligand is, the more it destabilizes the complex. For instance, some ligands, such as chloro-and trifluoroacetate ($OCOCF_3$), are more favorable for reduction, followed by carboxylate and hydroxo ligands [$OCOCF_3$ > Cl > OAc > OH](Johnstone et al., 2015; Olszewski et al., 2011).

Second, the rate of reduction is influenced by the bulkiness of the axial and equatorial ligands. For instance, the rate of reduction of JM-221 [$Pt(NH_3)(C_6H_{11}NH_2)(OCOC_3H_7)_2Cl_2$] is two-fold higher than that of JM-216 [(satraplatin) $Pt(NH_3)(C_6H_{11}NH_2)(OCOCH_3)_2Cl_2$], underlining the role of the bis-butyrate ($OCOC_3H_7$) axial ligand in destabilizing compound JM-221(Carr et al., 2006; Wheate *et al.*, 2010).

Pt(IV) complex carrier ligands may also influence the reduction rate. It was noticed that the reduction rate of Pt(IV) complexes with ethylenediamine is often lower than that of those with isopropyl amine and cyclohexylamine carriers. This was explained by the lower steric hindrance of ethylenediamine, which allowed for higher accessibility, resulting in a less stable six-coordinate state(Johnstone et al., 2016).

Notably, Pt(IV) complexes offer additional flexibility and the possibility of introducing innumerable groups into axial positions. These include derivatization with lipophilic groups, bioactive ligands (enhancing cellular uptake, e.g., polymers and nanoparticles), enzyme inhibitors (such as histone deacetylase (HDAC) inhibitors) to boost bioactivity, fatty acid conjugates to overcome resistance, and improved targeting ligands (e.g., folates) within axial ligands(Gibson, 2019). These modifications enable fine-tuning of Pt(IV) complexes to accomplish specific therapeutic goals and enhance their efficacy(Deo et al., 2019).

1.3.2 Pt(IV) Complex in the Clinical and Preclinical Phase

A wide range of Pt(IV) derivatives has been evaluated in the initial phases, and some have been assessed in clinical trials, such as satraplatin **(57)**, Iproplatin **(63)**, tetraplatin **(64),** and LA-12 **(65)**. Tetraplatin **(64)**, also known as ormaplatin, was assessed in phase I clinical trials that were terminated because of severe neurotoxicity at the maximum tolerated dose (MTD)(Johnstone et al., 2016). Iproplatin, *cis*-(dichloro)bis(isopropylamine)-*trans*-dihydroxyplatinum(IV) **(63)** was evaluated in phase I, II, and III clinical trials; however, these trials were terminated because of the inability to show superior performance compared to cisplatin or carboplatin in terms of effectiveness. The reduction in its activity may be due to the hydroxide ligands in the axial positions, which may have interpreted its reduction and activation by biological reducing agents(Olszewski *et al.*, 2011; Wexselblatt & Gibson, 2012).

Satraplatin **(57)**, (OC-6-43)-bis(acetato)-ammine(dichloro)-cyclohexylamine platinum(IV **(57)** was reported to be the most promising Pt(IV) derivative believed to act as a prodrug. It was orally administered as a platinum(IV) drug. It exhibited a more favorable toxicity profile with reduced side effects (such as ototoxicity, neurotoxicity, and nephrotoxicity) compared to cisplatin and carboplatin. Satraplatin was advanced to phase III trials in a study of 950 pediatric patients titled Satraplatin and Prednisone Against Refractory Cancer (SPARC). However, the overall patient survival rate did not improve significantly. Therefore, FDA approval for satraplatin **(57)** was sought but denied, and further trials on satraplatin **(57)** are ongoing(Ravera, Gabano *et al.*, 2019).

An analogous derivative of satraplatin **(57)**, LA-12 **(65)** [*trans*, *cis*, *cis*-bis(acetato)(1-adamantylamine)amminedichloridoplatinum(IV) **(65)**], comprising 1-adamantylamine as a non-leaving ligand, was synthesized. It is a more lipophilic derivative that exerts a higher cytotoxic effect and fewer side effects. However, the exact mechanism of action of LA-12 remains unclear(Apps et al., 2015; Ravera *et al.*, 2019).

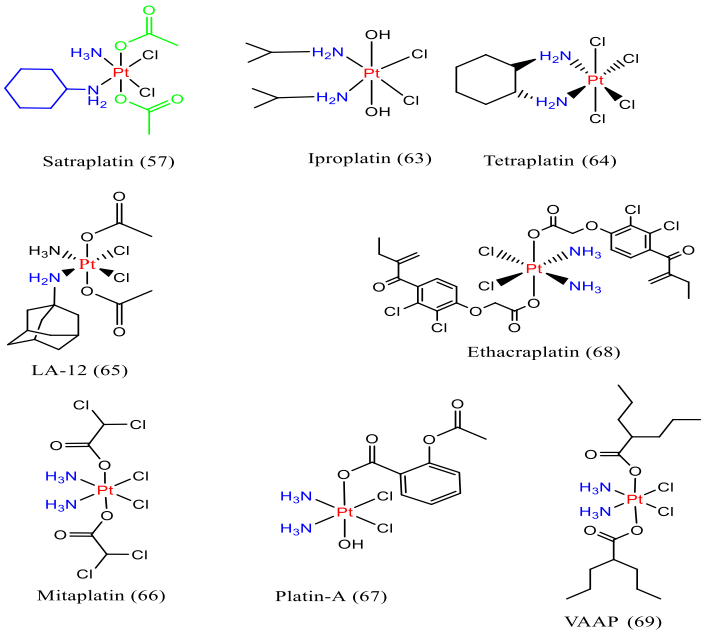

Figure 1.3.2 Examples of platinum(IV) anticancer agents include: 1) Pt(IV)-based derivatives evaluated in clinical trials including [satraplatin (**57**), iproplatin (**63**), tetraplatin (**64**), and LA-12 (**65**)] and 2) others in preclinical phases with biologically active axial ligands such as ethacraplatin (**68**), VAAP (**69**), mitaplatin (**66**), and platin-A (**67**)(Zhang & Sadler, 2017).

1.3.3 Dual Action of Platinum(IV) Derivatives

The reduction of Pt(IV) to obtain active Pt(II) species and a biologically active ligand is essential for the strategic development of bifunctional Pt(IV) prodrugs. This strategy seeks to help overcome drug resistance or increase the absorption and efficacy of platinum drugs. At this point, the most often used Pt(IV) cores are cisplatin, carboplatin, and oxaliplatin; bioactive ligands include inhibitors of histone deacetylase (HDAC), inhibitors of cyclooxygenase (COX), inhibitors of p53, and inhibitors of casein kinase 2 (CK2).

Several platinum(IV) complexes have been developed as dual-acting agents by adding two biologically active ligands at the axial positions. Additionally, Pt(IV)

conjugates exhibit a robust synergistic cytotoxicity profile and prolonged blood circulation times(Johnstone et al., 2013; Li et al., 2018).

Some of these complexes are currently in preclinical stages. Ethacraplatin, shown in (**68**, Figure 1.3.2), is a conjugated cisplatin with two ethacrynic acid (EA) ligands in the axial position. It is a diuretic drug known for its potency as an inhibitor of glutathione-S-*trans*ferase (GST), which is responsible for detoxifying several platinum agents. When ethacraplatin is intracellularly reduced, it elicits cisplatin, together with two equivalents of the GST inhibitor (EA). This novel strategy aims to reduce unwanted side effects and overcome resistance to cisplatin while concurrently improving the cellular absorption of EA(Johansson et al., 2011; Zanellato et al., 2011). Another notable example is represented by conjugating histone deacetylase (HDAC) inhibitors to the axial hydroxide ligands of Pt(IV). This includes the attachment of valproic acid or phenylbutyrate (PhB), ligands known for their ability to promote the apoptosis and differentiation of cancer cells when combined with platinum complexes. The bifunctional Pt(IV) valproate complex VAAP (**69**, Figure 1.3.2) has been reported to exhibit activity against both cisplatin-sensitive and cisplatin-resistant tumor cells. The conjugate derivatives displayed a remarkable enhancement of drug accumulation in tumor cells. Additional insights revealed that the axial ligands are capable of inhibiting HDAC, while the platinum moiety induces lesions in genomic DNA(Novohradsky et al., 2015, 2017).

The combined analog of oxaliplatin and VAAP (**70** in Table 1.3.2) has been synthesized in previous research, and while it shows lower cytotoxicity in cell culture compared to oxaliplatin alone, it is more effective than other Pt(IV) derivatives(Novohradsky et al., 2014). Recently, a group of Pt(IV) derivatives of [$PtCl_2$(1*R*,2*R*-diaminocyclohexane); [$PtCl_2$(DACH)]] was attached to two different bioactive molecules (*i.e.*, the histone deacetylase inhibitor 2-propyl pentanoic acid or valproic acid, and the potential antimetastatic agent 4-isopropenylcyclohexene-1-carboxylic acid (perillic acid, PA) as shown (**71** and **72** Table 1.3.2). Cytotoxic action of the newly synthesized compounds against four different human colon cancer cell lines (HCT116, RKO, HCT8, and HT29). *In vitro,* cell viability assays showed an enhanced antiproliferative effect, with an IC_{50} in the nanomolar range(Gabano et al., 2023). Mitaplatin (**66**, Figure 1.3.2) contains two dichloroacetate ligands (DCA) in the axial position. DCA, a pyruvate dehydrogenase kinase (PDK) inhibitor, treats lactic acidosis and restores regular mitochondrial activity. Although free cisplatin

causes DNA damage and apoptotic cell death, an intracellular decrease in mitaplatin releases DCA, which promotes mitochondrial apoptosis by freeing cytochrome c(Johnstone et al. 2009, Johnstone, et al. 2016).

The conjugation of cyclooxygenase inhibitors (COXis), such as ibuprofen and indomethacin, constitutes another class of Pt(IV) dual-action prodrugs. This strategy reduces the adverse effects of cisplatin while increasing its effectiveness. Acetylsalicylic acid is the axial ligand of the Pt(IV) complex known as platin-A (**67**, Figure 1.3.2), which has greater anticancer efficacy and a lower toxicity profile than cisplatin. Other COXis, including ketoprofen and naproxen, have been studied for their ability to conjugate with a platinum(IV) core(Ravera, Zanellato, et al., 2019). Thousands of compounds have been synthesized and tested; however, to date, none of these Pt(IV)-based prodrugs has been approved by the FDA. To design effective Pt(IV) complexes with the desired therapeutic performance, it is critical to understand the cellular processing and molecular mechanisms underlying this class of compounds.

Table 1.3.2 The different active ligands of platinum(IV) via the axial sites with a summary of their synthesized schemes

Pt(IV) Compounds	**Active ligand on the axial site**	**Synthetic procedure**
Satraplatin (**57**)	Di-acetate axial ligand	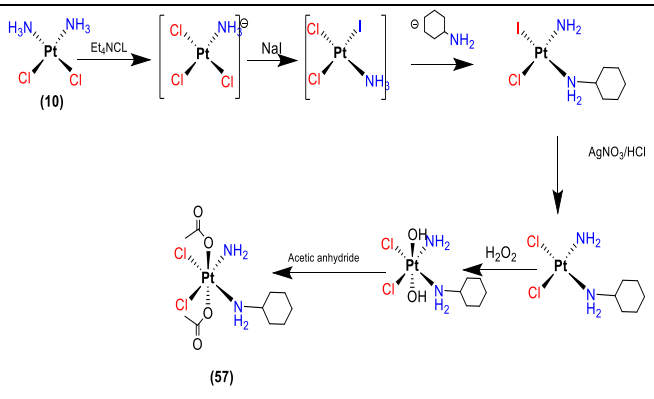
Iproplatin (**63**)	Di-hydroxide axial ligand	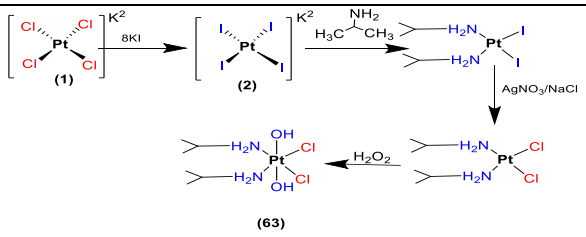

Tetraplatin (**64**)	Di-chloride axial ligand	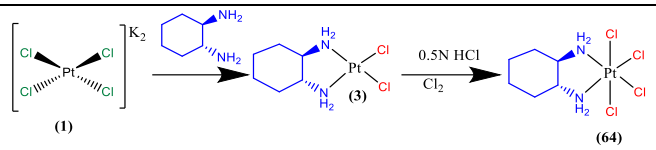
LA-12 (**65**)	Di-acetate axial ligand	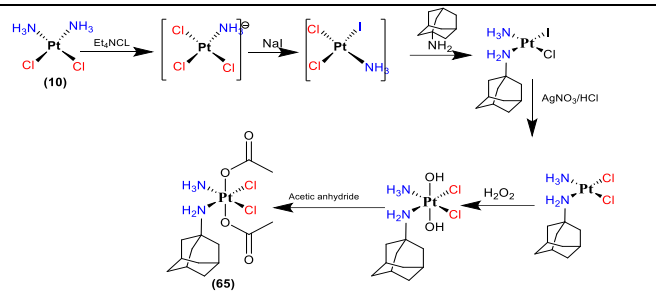
Ethacraplatin (**68**)	Di-Ethacrynic acid chloride axial ligand	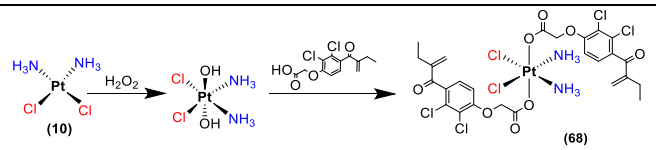
VAAP (**69**), and it analogous	Di-Valproic acid axial ligand	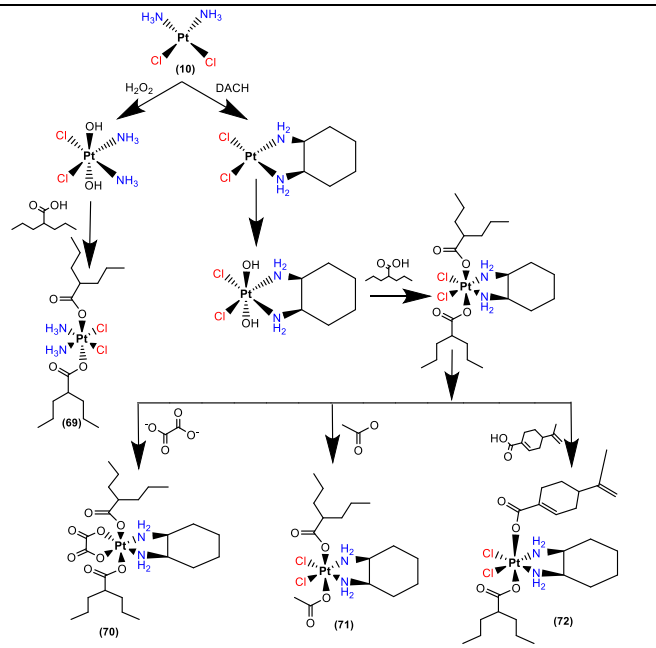
Mitaplatin (**66**)	Dichloroacetate axial ligands	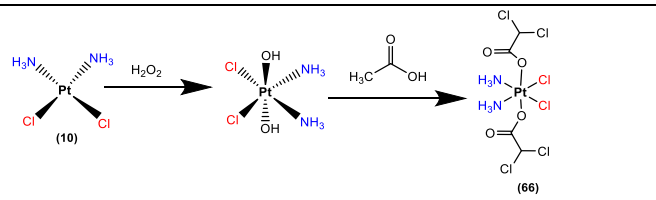
Platin-A (**67**)	Aspirin and hydroxide axial ligand	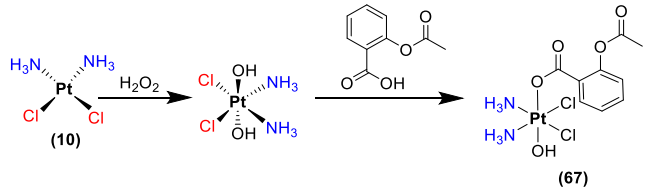

1.4 Effects of Lipophilic Ligands on the Physiochemical Properties of Platinum-based Drugs

Modification of platinum(IV) complexes by covalently introducing one or two ligands, which might be similar or dissimilar, to the axial sites is strongly believed to fine-tune the physicochemical properties of the final conjugate, including, but not limited to, solubility, lipophilicity, reactivity, and reduction rate(Klein & Hambley, 2006).

It was revealed that the cellular accumulation of the Pt(IV)diOA [*cis, cis, trans*-[Pt(IV)$(NH_3)_2Cl_2(OA)_2$] [Pt(IV)diOA] (OA = octanoato)] derivative of cisplatin-containing two OA units appended to the axial positions of a six-coordinate Pt(IV) center was significantly improved, which increased the concentration of both constituents, that is, the platinum moiety and the cleaved axial ligand (OA). The fact that Pt(IV)diOA was revealed to induce DNA hypermethylation and a reduction in mitochondrial membrane potential in cancer cells at a lower IC_{50} compared to free OA suggests a synergistic action of platinum and OA moieties. The significant advantage of lipophilic Pt(IV) derivatives with active axial ligands is the concurrent increase in the concentration of cleaved entities within cancer cells, which is facilitated by enhanced cellular uptake(Novohradsky et al., 2017).

The lipophilicity of platinum complexes plays an essential role in determining their capacity to passively traverse the lipid bilayers of biological membranes. This attribute is correlated with the relative solubility of compounds in lipid-rich surroundings, such as cellular membranes, compared to solubility in the hydrophilic environment of intra- and extracellular fluids(Oldfield et al., 2007).

Increasing the lipophilicity, of Pt(IV) complexes, as a result of attaching lipophilic ligands, was envisaged to improve the cellular accumulation, DNA platination, and cytotoxicity of the corresponding complexes. Synthetic strategies employed for this purpose include the incorporation of aromatic substituents or longer hydrocarbon chains(Shahabadi et al., 2011).

Platts *et al.*(2005) reported a strong correlation between the accumulation of certain platinum complexes inside the cells and their lipophilicity. This relationship was observed in five complexes synthesized by Loh *et al.*(1992) in human ovarian carcinoma cells(Platts et al., 2001), and in eight complexes prepared by Ang *et al.,* (2005) in both colon and lung carcinoma cells. A direct correlation was observed between improved cellular accumulation and increased cytotoxicity. This highlights the potential of

lipophilic ligands to enhance the anticancer activity of Pt-based agents(Ang et al. 2005; Loh et al. 1992).

Furthermore, lipophilic Pt-compounds aggregated more effectively in cisplatin-resistant cells. This bias may be attributable to their higher passive diffusion capacity, which allows them to avoid active transport pathways through which cisplatin relies on cellular entrance(Loh et al., 1992; Platts et al., 2001).

Kelland *et al.* (1993) investigated platinum(IV) complexes with the general formulas *cis-*, *trans-*, *cis*-[$PtCl_2(OCOR_1)_2NH_3(RNH_2)$]. Their research revealed an interesting pattern: as the lipophilicity of the *R* and R_1 substituents increased, so did their cytotoxicity(Kelland, 1993). This phenomenon was demonstrated by the increase in anticancer activity upon increasing the size of the *R* group from cyclobutene to cycloheptane as well as by the linear increase in cytotoxicity as the number of carbons in the R_1 substituent increased from R_1 =-CH_3 to -C_5H_{11}. For Pt(IV), the most successful drug was satraplatin **(57)**, which was attributed to its increased cellular accumulation, allowing it to overcome cisplatin resistance more effectively(O'Neill et al. 1999).

Krasnovskaya *et al.* (2022) reported the synthesis of novel unsymmetrically modified Pt(IV) prodrugs comprising the COX-inhibitor naproxen or long-chain hydrophobic stearic acid at one axial site with biotin as the second axial ligand. When assessing the bioactivity of the synthesized compounds, it was reported that the lipophilicity of the Pt(IV) complexes is decisive in the potency of cytotoxicity, with a minor impact on biotin receptor expression. Additionally, the reduction of Pt(IV), comprising naproxen and biotin as axial ligands, elicits the active drug cisplatin within 20 h of incubation in A549 cells(Spector et al., 2022). Enhancing the lipophilicity of Pt(IV) prodrugs by covalently introducing ligands at hydroxide axial sites is considered a strategic approach to improve transporter-independent cellular drug uptake. This approach aims to increase the activity of a prodrug by enhancing its lipophilicity. Furthermore, incorporating active ligands at the axial positions may synergistically inhibit cell proliferation by combining diverse bioactive entities. Therefore, the properties of axial ligands, including their chemical structure, functional groups, physicochemical properties, and bioactivity, play crucial roles in determining plasma protein interactions, cellular uptake, anticancer activity, and self-assembly patterns(Date et al., 2022).

1.4.1 Effect of Ligand Lipophilicity on Encapsulation of Pt(IV) Prodrugs on Drug Delivery Systems

Covalent conjugation of lipophilic (lipidic) chemical entities to small-molecule drugs was applied in developing agents that were successful in making them preclinical and some even for clinical administration. Ample evidence underlines the impact of lipophilic drug conjugates on pharmacokinetic and therapeutic profiles. Over the years, lipophilic conjugates (LC) have been shown to enhance drug encapsulation within engineered drug delivery systems, affording additional benefits for future applications of nanomedicine. Lipid-based drugs offer the advantage of enhanced absorption through biological barriers, notably the gastrointestinal epithelium and the blood-brain barrier. Moreover, their lipophilic nature facilitates easy passage across cell membranes, including those of kidney tubules, leading to prolonged circulation times(Huang et al., 2022; Zaro, 2015).

Prodrugs, which are inactive pharmacological compounds, have garnered significant attention for their inherent chemical modifications that allow for in *vivo* bioconversion, releasing various bioactive agents through enzymatic or chemical processes—a recognized approach in pharmacology(Huang et al., 2022; Zaro, 2015). Lipid-based drug delivery systems, such as emulsions(Dhaval et al., 2022), microemulsions(Tartaro et al., 2020), self-micro emulsifying drug delivery systems (SMEDDS)(Akula et al., 2014), solid lipid nanoparticles (SLN), nanostructured lipid carriers (NLC)(Dokania & Joshi, 2015), and liposomes, have garnered significant interest in recent years. They have been recognized for their ability to enhance the oral bioavailability of poorly water-soluble and lipophilic compounds. The integration of prodrugs with lipid-based drug delivery systems presents numerous advantages, such as enhanced pharmacokinetics, augmented absorption, an extended pharmacological half-life of drugs, and optimized targeting(Kaur & Kumar, 2018).

Lippard and Johnstone (2013) reported the synthesis of a group of cisplatin(IV) prodrugs with the general formula *cis, cis, trans*-[Pt-$(NH_3)_2Cl_2(OOCR)_2$], where R = methyl, ethyl, propyl, butyl, pentyl, hexyl, heptyl, octyl, or nonyl. A direct correlation between the increase in the length of the carboxylate ligand at the axial sites of cisplatin(IV) and the lipophilicity of cisplatin(IV) prodrugs was revealed, which in turn resulted in enhanced encapsulation efficiency (EE%) of these compounds in PLGA-PEG-COOH nanoparticles(Johnstone & Lippard, 2013).

Encapsulation of lipophilic Kiteplatin Pt(IV) prodrugs in PLGA-PEG micelles, were reported by Natile *et al.* (2016) to enhanced encapsulation of lipophilic kiteplatin Pt(IV) [*cis*, *trans*, *cis*-[$PtCl_2(OH)_2$(*cis*-1,4-DACH)]] prodrugs in PLGA-PEG micelles. The effect of aliphatic fatty acid chains (hexanoate, decanoate, acetate, and butanoate) on encapsulation efficiency (EE%) was evaluated. A correlation between the chain length of the axial carboxylate ligand and (EE%) in PLGA-PEG micelles was uncovered. The increase in chain length of the axial ligand, resulting in increased lipophilicity of the kiteplatin(IV) complex, resulted in increased (EE%) i.e. for bisacetato- (-0.23, 0.62), bisbutanoato- (1, 0.66), and bishexanoato (2.10, 0.71) up to bisdecanoato- (4.03, 0.76) for LogP and EE%, respectively(Giovanni Natile, 2016). In a follow-up study, the kiteplatin(IV) complex, namely *cis, trans, cis*-[$PtCl_2[CO_2(CH_2)4CH_3]_2$(*cis*-1,4-diaminocyclohexane)], *cis,-trans, cis*-[$PtCl_2[CO_2(CH_3)2CH_3]_2$(*cis*-1,4-diaminocyclohexane)], *cis, trans, cis*[$PtCl_2[CO_2(CH2)2CH_3]_2$(*cis*-1,4-diaminocyclohexane)], and *cis, trans, cis*-[$PtCl_2[CO_2(CH_2)8CH_3]_2$(*cis*-1,4-diamino cyclohexane)] were encapsulated in the core of polyethylene glycol (PEG)-stabilized solid lipid nanoparticles (PEG-SLNs). Nano-formulated prodrugs (Pt(IV)-prodrug/PEG-SLNs) were assessed for their capacity of Pt(IV)-Prodrug/PEG-SLNs to permeate BBB. For that sake, an in vitro BBB *trans* well model composed of a monolayer of polarized endothelial cells seeded on a porous membrane was set up, to allow the formation of an apical compartment (‘blood’ side) physically separated from the basolateral one (‘brain’ side). These investigations showed that PEG-SLN-encapsulated kiteplatin and the prodrug kiteplatin(IV) complexes exhibited an improved ability to reduce cell viability compared to their free counterparts, Additionally, the uptake of the tested Pt-based PEG-SLN-encapsulated drugs was magnified in U87 cells compared to their corresponding free counterparts after 4 hours of incubation(Arduino et al., 2020).

The conclusions of the above-mentioned studies clearly indicate that the development of a specialized delivery system is essential to address the side effects that are frequently linked to platinum-based drugs, including difficulties such as low solubility, treatment resistance, and non-specific targeting of cancer cells while avoiding unnecessary harm to normal cells. By improving drug solubility, targeting the distribution to specific cancer cells, and optimizing drug bioavailability, such a delivery system might help overcome these obstacles. Using this strategy, it is

possible to maximize the beneficial effects to achieve better therapeutic outcomes, which improves the safety and efficacy of platinum-based cancer treatments.

1.5 Drug Targeting and Delivery Systems (DTDS)

Since ancient times, medical science has focused on improving drug delivery techniques(Mahale et al., 2012). The need for patient-friendly and efficient drug delivery methods has increased over the past few decades(Tavano et al., 2013). Paul Ehrlich initially proposed the concept of targeted drug administration in 1909; he labeled it a "magic bullet," an approach to deliver drugs to damaged cells(Bini et al., 2012; Hong et al., 2009).

The goal of this strategy is to minimize contact with non-target tissues while delivering drugs to pre-identified target cells to minimize adverse effects and maximize effectiveness. Effective delivery of drugs to desired sites and molecular targets is hampered by different factors such as solubility, absorption, bioavailability, bio*trans*formation, and carrier characteristics. To address these shortages, novel drug delivery systems were developed to provide delayed drug release, improved solubility, prolonged drug action, improved specificity towards targeted regions, and minimized adverse side effects(Bini et al., 2012).

A perfectly engineered drug delivery system should limit adverse effects, prevent drug degradation, maintain therapeutic levels, control distribution patterns, shorten dose intervals, improve patient compliance, and deliver medications to intended targets. To achieve these objectives, intensive research efforts have been conducted globally, be it at the academic lab or the industry(Hong et al., 2009).

Site-specific drug delivery, as a targeting strategy, holds great promise in reducing off-target effects, decreasing unwanted toxicities, and thereby enhancing a drug's therapeutic efficacy(Tavano et al., 2014; Z. Zhao et al., 2020).

To that end, such an approach exploits ligands or carriers to deliver drugs to the infected organs or sites. To help evade the response of the immune system, the surface properties of the drug delivery system are modulated(Udofot et al., 2016; M. Wang et al., 2012). Although challenging, achieving targeted drug delivery is essential, particularly in cancer chemotherapy. The investigation of several carriers, including peptides, proteins, liposomes, synthetic polymers, niosomes, and microspheres, continues to progress rapidly in this field(Bini et al., 2012; Tavano et al., 2014).

These carriers may occur naturally or undergo structural modifications to specifically interact with cellular targets. This allows them to carry drug molecules close to pre-identified target cell lines for the most effective possible therapeutic results. These characteristics meet the criteria for an ideal drug delivery system(Bini et al. 2012):

- Non-immunogenicity, non-toxicity, and biodegradability.
- The ideal drug loading and release qualities match therapeutic requirements.
- Release of drug molecules upon internalization and identification near pre-identified target organs, tissues, or cells.
- The specificity of the drug delivery carrier should only be recognized by targeted tissues or cells and must maintain their activity.
- Capacity to pass across anatomical boundaries, such as the tumor vasculature, during chemotherapy.
- Bio-modules are used to identify and investigate carriers and non-ubiquitous sites to avoid crossover and maintain targeting efficacy.

Drug targeting and delivery systems (DTDS) can be classified into two basic types: active and passive. To ensure tailored delivery, active drug-targeting delivery systems depend on pre*cis*e biomolecular interactions between pharmaceuticals and cellular or tissue components. In a typical active DTDS system configuration, a pharmacophore is connected to the target component via a linker. The specific functionality of the *trans*porter, antigen, or receptor-based conjugate directs the drug toward the tumor tissue because of its binding affinity(Dancey & Chen, 2006).

Bioactive compounds, such as hormones, sugars, amino acids, peptides, and proteins, act as targeting ligands(Xiaoyong & Zijian, 2012). Biodegradable molecules such as polysaccharides, polyamino acids, proteins, and aliphatic polyesters such are PHBV (poly−β−hydroxybutyrate-co-β−hydroxy valerate), polyactides (PLA), polyglycolide (PGA), poly(lactide co-glycolides) (PLGA)(S. Zhang et al., 2014), and water-soluble poly(ethylene glycol) (PEG) form and function as delivery systems. The binding of the specific targeting functionality to the drug molecule may assist in distinguishing normal cells from cancer cells. This ensures enhanced efficacy and reduced side effects of the targeted drugs(Xiaoyong & Zijian, 2012).

Passive DTDS exploits the effect of enhanced permeability and retention (EPR) in tumor tissues(Frezza et al., 2010). The vascular system of tumors is disorganized and twisted

compared to that of normal tissues. Owing to the rapid proliferation of the vascular endothelium, there are many fenestrations and open junctions in tumor cells. These values range from 200 nm to 1.2 μM. Particles a few hundred nanometers in size can passively cross the tumor endothelial barrier through fenestrations, which are *trans*cellular pores that function as essential biological ultra-filers, permitting substrates to pass across cells via diffusive and convective pathways without relying on endocytosis or other receptor-mediated mechanism(Cogger et al., 2013).In addition, cancer cells lack functioning lymphatic networks, which prevents the efficient removal of excess fluid from solid tumor tissues(Apps et al., 2015).

Combining these two effects makes tumors hyperpermeable to circulating macromolecules, which extravasate owing to inefficient drainage through the lymphatic system and accumulate in solid tumor tissue, where they remain for prolonged periods. With this effect, the drug concentration in the tumor tissue is 20-30 times higher than that in the blood(Attia et al., 2019).

It also prolongs the circulation time of drug candidates in the blood(Xiaoyong & Zijian, 2012). Polymer-drug conjugates are an essential class of passive DTDS with platinum-based therapeutics. These advantages include (i) improved cellular uptake owing to the EPR effect and dynamic endocytosis characteristics of tumor cells, (ii) prolonged circulation time in blood vessels and residence time of the drug in tumors, and (iii) high loading capacity and water solubility of the drug(Haag & Kratz, 2006).

Multifunctional nanoparticles are formed by synthesizing different kinds of nanomaterials, both inorganic and organic, each with unique characteristics and functions. Inorganic nanomaterials involve gold, silver, silica, and iron oxide nanoparticles, but organic polymers have more advantages in terms of biocompatibility, stability, processability, targeted degradability, and better responsiveness to external stimuli such as light, heat, pH, or biological signals, helping them in a more controlled drug release(Alshammari et al., 2023).The organic nanomaterials themselves have more than one type of production, mainly, there are two types, first lipid-based such as liposomes, lipid emulsions, and niosomes, and polymer-based such as dendrimers, micelles, and polymerase(Alshammari et al., 2023; Rathee et al., 2022).

Liposomal and niosomal colloidal vesicular carrier systems have the potential to address the problems associated with oral drug bioavailability. These systems function as drug

reservoirs and regulate the release of the loaded drug molecules. They are well-known for their biocompatibility and lack of allergic and antigenic reactions. Furthermore, surface or compositional modification allows for efficient targeting of affected tissues, cells, or organs, which has important implications for cancer treatment(Ogata et al., 2009).

The niosome formulation is considered to have better advantages over the liposomal formulation in terms of stability, cost, and other factors that will be discussed in more detail in the next subtitle.

1.6 Niosomes Delivery System

The primary goal of nanodrug delivery system design is to develop effective formulations that specifically transport drugs to their intended locations without harming nearby healthy cells(Naderinezhad et al., 2017).

This was achieved by ensuring that the compounds were both compatible with the body and capable of breaking down naturally over time. Secondary aims include the prevention of sudden release of the drug, fine-tuning the drug dosage and release rate to achieve the desired therapeutic benefits, and reducing the frequency of drug administration to ensure patient adherence(Abdelkader et al., 2014b; Naderinezhad et al., 2017).

Niosomal drug delivery systems represent a possible solution to these goals, as niosomes are lipid-based delivery systems with great potential. The first niosomal formulations were developed and patented by L'Oreal in 1975 (part of the cosmetics industry). These vesicles mostly consist of non-ionic surfactants(Osanloo et al., 2018).

A microscopic bilayer lamellar structure is formed by combining non-ionic surfactants, such as spans or tweens, with cholesterol, followed by hydration in aqueous media(Sahin, 2007). The hydrophobic components of the bilayer lamellar structure were positioned away from the aqueous solvents, whereas the hydrophilic heads remained in contact with the aqueous solvents. Their structure can be utilized in hydrophilic, lipophilic, or amphiphilic drug molecules, allowing for a wide range of pharmacological combinations. The typical arrangement of the niosomes is shown in **Figure 1.6.**(Mishra et al., 2020). Additionally, they can be formulated with different ionic amphiphiles, such as dicetylphosphate and stearylamine, to achieve a stable suspension(Ruckmani & Sankar, 2010).

Niosomes are created by hydrating non-ionic surfactant films. They absorb or encapsulate aqueous liquids during hydration. In essence, niosomal vesicles do not form spontaneously(Matos et al., 2019). Their formation is thermodynamically stable and occurs under specific conditions, and they can only be formed when there is a correct combination of non-ionic surfactants and charge-inducing chemicals, which typically range in size from 100 nm to 300 nm(Abdelkader et al., 2014; Bagheri et al., 2014). The properties of niosomes can be altered by changing factors, such as their composition, surface charge, lamellarity, and tapping volume(Sankhyan & Pawar, 2012).

Niosomes are structurally similar to liposomes, which makes them viable alternatives to vesicular systems. These carriers are considered superior to liposomes for drug administration because of factors such as being more affordable, as the excipients, apparatus, and equipment used for the preparation of niosomes are cost-effective, enhanced physical stability under pH fluctuations, temperature stability, and being less vulnerable to light and sterilization. This formulation involves a simple technique that facilitates large-scale manufacturing, and the drug encapsulation effectiveness of these systems increases with higher concentrations and greater lipophilicity of the surfactant(Naderinezhad et al., 2017). Niosomes can function as drug reservoirs, have the duration of circulation for enclosed drugs, alter the distribution of the carrier system within organs, and enhance metabolic stability(He et al., 2017). Niosomes can alter the rate at which drugs are eliminated from the bloodstream, their distribution in tissues when metabolized, and the manner in which they interact with cells(Moghassemi and Hadjizadeh, 2014; Mishra *et al.*, 2020). They can be used as carriers for poorly bioavailable drugs to provide innovative drug delivery systems(Mahale et al., 2012).

Figure 1.6 Typical niosomes structures(Gharbavi et al., 2018).

Although niosomal delivery offers numerous advantages, it is essential to recognize potential stability challenges associated with aqueous niosomal suspensions. One concern is the potential for drug hydrolysis in an aqueous environment, which may compromise the efficacy of the encapsulated drugs over time(Gharbavi et al., 2018). Another issue is the risk of drug leakage from trapping sites within niosomes, leading to loss of drug payload and diminished therapeutic efficacy. Additionally, niosomes can aggregate, affecting their uniformity and effectiveness for drug delivery. Addressing these stability concerns is crucial in the development and optimization of niosomal drug delivery systems(Alemi et al., 2018; Gharbavi et al., 2018).

Niosomes are specialized drug delivery systems consisting of several essential components: i) Non-ionic Surfactants: These are amphiphilic molecules with polar heads and non-polar tails that enhance drug solubility and stability for practical drug delivery applications(Kumar and Rajeshwarrao, 2011). ii) Cholesterol modulates niosome characteristics, such as permeability and rigidity, and is typically mixed with surfactants in a 1:1 ratio(Bayindir & Yuksel, 2010; Onochie *et al.*, 2013). iii) Charge-inducing Molecules: Some formulations incorporate charge-inducing molecules to stabilize niosomes through electrostatic repulsion;

iv) Hydration Medium: Phosphate buffer serves as a common hydration medium for niosome formation(Abdelbary and Aboughaly 2015).

1.6.1 Preparation of Niosomes

Niosomes are lamellar structures similar to liposomes, which include small unilamellar vesicles (SUVs), large unilamellar vesicles (LUVs), and multilamellar vesicles (MLVs)(Sharma et al., 2018). Customizing the size of niosomes is essential for fulfilling pre*cis*e, targeted delivery requirements, leading to the use of several methods for developing flexible nanocarrier systems(Abdelbary & Aboughaly, 2015). The selection of the niosome preparation method depends on criteria such as the required vesicle size, size distribution, number of bilayers, encapsulation effectiveness of the aqueous phase, and membrane permeability. The production method involves mixing a surfactant and lipid blend with water at high temperatures (typically, above 60 °C). Optional methods to reduce the size can be used, resulting in the creation of a colloidal dispersion. This adjustable method for creating niosomes allows the tailoring of vesicle properties to suit certain therapeutic requirements, highlighting their effectiveness in drug delivery applications(Faheem and Abdelkader, 2019).

- Multilamellar vesicles (MLVs) are prepared using two main methods:

    - Thin-film hydration (THF)

        This begins with solvent dissolution and is often referred to as the hand-shaking method. Initially, a mixture of surfactant, cholesterol, and hydrophobic payload was dissolved in a powerful organic solvent such as chloroform, diethyl ether, ethanol, or methanol(Javani et al., 2021). Subsequently, the organic solvent was evaporated using a rotary evaporator, resulting in a thin, solid coating on the walls of the round-bottomed flask. The thin, dehydrated layer was hydrated using a water-based solution containing hydrophilic drugs. The hydration process occurs above the glass transition temperature (Tc) of the surfactant, which is usually above 60 °C, with mild stirring. Vesicle formation occurs under

hydration conditions(Matos et al., 2019). Intense hydration creates multilamellar niosomes of various sizes as the gentle hydration leads to the formation of large single-layered vesicles known as giant unilamellar vesicles (GUV). Small and uniform vesicles can be obtained using further size reduction methods, such as sonication, whether using a probe or a bath, to create small unilamellar vesicles (SUVs) with pre*cis*e specifications or extrusion. This means that consecutive extrusion through polycarbonate filters decreases the vesicle size, with the extent of reduction determined by the number of cycles and pore size(Ag Seleci et al., 2016). The primary challenge in using TFH is the limited entrapment of an aqueous core, resulting in low encapsulation efficiency for hydrophilic drugs. Nevertheless, various hydrophilic drugs can be effectively enclosed using this technique(Javani et al., 2021).

- Drug uptake via *trans*membrane pH gradient.

  This method is appropriate for ionizable hydrophobic payloads. Beginning with film formation, the hydrophobic payload, surfactant, and cholesterol were dissolved in chloroform, and the solvent was evaporated to create a thin film on the flask wall. The film was hydrated using a citric acid solution with a pH of 4.0 and then subjected to freeze-thaw cycles and sonication. An aqueous solution containing the drug was added, and the pH was set to 7.0-7.2, using a disodium phosphate solution. Vesicle generation was achieved by heating the mixture at 60 °C for 10 min(Y. Zhou et al., 2010). The neutral exterior of vesicles enables both protonated and unprotonated forms of the payload to pass through. The unprotonated form diffuses through the membrane and becomes protonated within it, confining it within the vesicle until equilibrium is reached(Rajera et al., 2011).

- The formation of small unilamellar vesicles (SUV) involves two methods.
    - Microfluidics.
        - This approach utilizes microchannels to regulate lipid flow and interact with an aqueous stream, leading to consistent niosome synthesis characterized by small size and low polydispersity(X. Zhao et al., 2014).
    - Using Sonication
        - Small and homogeneous unilamellar vesicles (SUVs) are created by homogenizing a mixture of surfactant, cholesterol, and a drug-containing aqueous phase at temperatures above the phase *trans*ition point, using a sonic probe for approximately 20 min(Ruckmani & Sankar, 2010).
- The Preparation of Large Unilamellar Vesicles involved the following methods.
    - Reverse-Phase Evaporation (REV)
        - The REV technique is beneficial for encapsulating hydrophilic payloads because it creates a more hydrophilic core than thin-film hydration. Cholesterol and surfactants were combined into a solution containing ether and chloroform. An aqueous solution containing the payload was added to the mixture, and the two resultant phases were sonicated at low temperatures. After sonication, an extra aqueous phase was introduced, and the organic phase was eliminated under reduced pressure using a rotary evaporator at approximately 40 °C. To form niosomes, the thick suspension was thinned using water and heated above the glass *trans*ition temperature (Tc) for 10 min. The drawback of this approach is the potential for residual solvent residues, which can result in unexpected biological consequences(Junyaprasert et al., 2013).
    - Ether Injection
        - The ether injection method involves gradually injecting niosome components into ether, ethanol, or isopropyl alcohol, using a needle, into a heated aqueous phase **(29)**. Niosome components are injected into an ether or equivalent solvent via a needle into a warmed aqueous phase at a regulated speed. Large unilamellar vesicles (LUV) are formed through the gradual evaporation of the solvent, creating an

ether gradient that extends toward the interface between the aqueous and non-aqueous phases. Nevertheless, this approach may result in varying vesicle sizes and small traces of ether, which may be disadvantageous(Mujoriya et al., 2011; ROGERSON et al., 1988).

Each approach has distinct benefits in niosome manufacturing, addressing certain requirements for drug administration. Unencapsulated drugs in niosome formulations can be recovered and refined using dialysis, gel filtration, and centrifugation/ultracentrifugation. Niosomes offer a versatile drug delivery platform that facilitates controlled drug release and improves drug solubility. Ongoing research is aimed at enhancing niosome formulations for diverse therapeutic applications. Various factors contribute to the formation of niosomes, impacting vesicular drug delivery systems(Tabbakhian *et al.*, 2006; Moghassemi et al., 2017; Akbari *et al.*, 2020).

1.7 Nanodelivery of Pt(II)-based Anticancer Agents

Platinum drugs are highly effective in cancer chemotherapy. Subsequently, a wide range of platinum-based compounds, including traditional platinum(II) (Pt(II)), non-traditional Pt(II) modifications, and platinum(IV) formulations, have been synthesized and currently employed as treatments for different types of solid tumors(Apps et al., 2015; Brown et al., 2019). Although they are effective, the risk of systemic toxicity and the development of drug resistance provide significant obstacles that limit their therapeutic efficacy(Xiaoyong & Zijian, 2012). To improve their pharmacological effects, researchers have investigated supramolecular nanocarrier-based drug delivery systems (NDDSs) that enable targeted administration of platinum drugs to tumor sites, reduce toxicity, and enhance therapeutic effectiveness, thereby representing a significant advancement in this field(Q. Zhang et al., 2023).

Cleavable spacers are frequently used to attach platinum components to the polymer backbone in polymer-platinum conjugates in platinum-based drug delivery systems. This linker ensures stability throughout *trans*portation and enables the release of the platinum component at the desired location upon cleavage. Passive drug targeting and delivery systems for platinum-based pharmaceuticals involve several nanoparticle-based platforms, such as micelles, liposomes, niosomes, lipids, and nanospheres, in addition to

polymer conjugates. The ideal particle size for the designed carriers usually ranges from 100 to 200 nm in diameter. This size range provides advantageous properties for effective medication delivery and increases concentrations at the desired location(Letchford & Burt, 2007; Gindy & Prud'homme, 2009).

The most widely tested delivery systems for platinum complexes and Nanodelivery systems that have entered clinical trials are liposomal delivery systems and micelles(Hang et al., 2016).

Liposomes are spherical structures composed of phospholipids that are arranged into either a single layer (unilamellar) or numerous layers (multilamellar) surrounding an aqueous center(FDA, 2018). These lipid-based molecules can function as effective drug-delivery systems with multiple benefits. They provide protection to enclosed substances, extend the duration of drug effectiveness, control drug release, and exhibit exceptional compatibility within the body and safety(Allen & Cullis, 2013). Furthermore, liposomes can selectively target specific regions of the disease either by passive or active diffusion. This results in a decrease in the overall side effects, an increase in the maximum tolerated doses, and an improvement in the therapeutic results(P. Liu et al., 2022). Several liposomal formulations of platinum drugs have entered clinical trials (Table 1.7), but none has been approved by the FDA(Hang et al., 2016).

Table 1.7.1 Liposomal formulations of platinum complexes evaluated clinically.

Formulation	**Aroplatin (L-NDDP)**	**SPI-077**	**Lipoplatin**	**Lipoxal**	**MBP-426**	**LiPla*Cis***
Encapsulated Drug	NDDP	Cisplatin	Cisplatin	Oxaliplatin	Oxaliplatin	Cisplatin
Lipid composition	DMPC/DMPG	HSPC/Cholesterol/DSPE-PEG2000	HSPC/DPPG/DSPE PEG2000	HSPC/DPPG/DSPE-PEG2000	TF-PEG-liposomes	DSPC/DSPG/DSPE-PEG2000
Clinical status	Phase II	Phase II	Phase II/III	Phase I	Phase I/II	Phase I

NDDP, *cis*-bisneodecanoato-*trans*-(1*R,*2*R)*-1,2-diaminocyclohexane platinum(II); DMPC, 1,2-dimyristoyl-snglycero-3-phosphocholine; DMPG, 1,2-dimyristoyl-sn-glycero-3-phospho-(1′-rac-glycerol) (sodium salt); HSPC, hydrogenated soy phosphatidylcholine; DSPE-PEG2000, 1,2-distearoyl-sn-glycero-3-phosphoethanolamine-N-[methoxy(polyethylene glycol)-2000] (ammonium salt); DPPG, 1,2-dipalmitoylsn-

glycero-3-phospho-(1′-rac-glycerol) (sodium salt); DSPC, 1,2-distearoyl-sn-glycero-3-phosphocholine; DSPG, 1,2-distearoyl-sn-glycero-3-phospho-(1′-rac-glycerol) (sodium salt).

In 2006, L-NDDP known as Aroplatin, was the first liposomal formulation studied in clinical trials for administering the cisplatin **(10)** analog (*cis bis-neodecanoato-trans-R*, *R*-1,2-diaminocyclohexaneplatinum II, NDDP). They were formed after reconstitution with 1,2-dimyristoyl phosphatidylcholine (DMPC), 1,2-dimyristoyl phosphatidylglycerol (DMPG), and acidified saline. Despite a drastic change in biodistribution compared to NDDP, L-NDDP causes myelosuppression in mice and diffuse hemorrhagic syndrome(Dragovich et al., 2006). The clinical use of non-PEGylated drugs is limited. Researchers created liposomes containing NDDP, phosphatidylcholine, cholesterol, and coated them with either monosialoganglioside (GM1) or polyethylene glycol (PEG) phosphatidylethanolamine. The accumulation of long-circulating liposomes was approximately three times higher than that of the standard phosphatidylcholine/cholesterol-based liposomes. In an *in vivo* RIF-1 tumor model in mice, the use of NDDP formulated in phosphatidylcholine resulted in a significant decrease in tumor growth rate. However, the dose escalation phase in 2005 had to be stopped early to surpass the maximum tolerable dose and observe drug instability and breakdown within the liposomes(Liu *et al.*, 2013).

SPI-77 is a cisplatin-coated methoxy polyethylene glycol (MPEG) liposomal formulation designed to avoid detection and removal by the Mononuclear Phagocyte System (MPS)(Meerum Terwogt et al., 2002). Although SPI-77 showed better effectiveness and tolerance than free cisplatin, its impact was hindered by inadequate drug release from liposomes, leading to reduced cytotoxicity compared to free cisplatin. To overcome this issue, Alavizadeh *et al*. (2014) encased cisplatin within liposomes containing phosphatidylcholines with different *trans*ition temperatures of phosphatidylcholines (HSPC, DPPC, DMPC, and soy phosphatidylcholine (SPC)). Their findings demonstrated that solid PEGylated liposomes, especially those containing DPPC and HSPC, had *trans*ition temperatures over 37 °C, resulting in excellent cisplatin release and significant anticancer effects(Alavizadeh et al., 2014). Tesauro *et al*.(2016) reported that cisplatin encapsulated in liposomes decreased cholesterol levels. Egg L-phosphatidylcholine increased platinum release and limited the development of platinum drug aggregates observed in SPI-077, which contained 44% cholesterol. His liposomal

formulation showed encouraging results in ovarian tumor cell lines, but additional research is needed to fully appreciate its potential(Ringhieri et al., 2016).

Lipoplatin, developed by Regulon Inc., is another liposomal cisplatin formulation, which includes cholesterol, dipalmitoyl phosphatidyl glycerol, methoxy-PEG-distearoyl phosphatidylethanolamine, and soy phosphatidylcholine. It has progressed through clinical phases I, II, and III, indicating greater efficacy, fewer side effects, and increased tumor accumulation compared to free cisplatin. This formulation is currently under further investigation(Ringhieri et al., 2016).

LiPla*Cis*, a liposomal cisplatin formulation developed by LiPlasome Pharma ApS, was also developed for degradation by secretory phospholipase A2, typically found in tumor regions. Despite these attempts, renal toxicity remains unresolved, resulting in study termination during Phase I. The same company also developed lipoxal, a liposomal formulation of oxaliplatin(Alavizadeh et al., 2014).

Lipoxal (oxaliplatin) has been shown to reduce myelotoxicity and gastrointestinal tract toxicity of oxaliplatin **(23)** while maintaining its antitumor potential(Shi et al., 2016). Miriplatin **(19)** was encapsulated in the lipid bilayer of liposomes containing DMPG by simple sonication. DMPG did not affect its antitumor activity by inducing apoptosis, showing promise for clinical application(Liu et al., 2016).

The liposomal formulation of oxaliplatin (MBP-426), transferrin (TF)-conjugated N-glutaryl phosphatidylethanolamine, was assessed in a clinical trial. Phase I showed that MBP-426 targets tumors more effectively by overexpressing the TF receptor in diverse cancers. The encapsulated oxaliplatin retained and reduced systemic circulation in *vivo* within the tumor tissues of colon 26, demonstrating its efficacy and potential to prevent off-target effects, and it inhibited tumor development better than pure oxaliplatin, at 226 mg/m2 of MBP-426 delivered every three weeks where safe, allowing for further clinical exploration, but one of the limitations was the dose of the drug, at 400 mg/m2, dose-limiting toxicities such as thrombocytopenia was noted, demanding a careful dose increase(Sankhala et al., 2009). After Phase I trials, Phase IIa/b studies examined the safety of MBP-426, particularly in conjunction with leucovorin and fluorouracil. This is a crucial step in evaluating its potential in combination therapy, advancing clinical validation, and improving patient outcomes(Thi et al., 2021).

Polymeric micelles are formed by amphiphilic block copolymers(Aliabadi & Lavasanifar, 2006) that have hydrophobic cores and hydrophilic shells. The architectural design of this system plays a critical role in determining how drugs are loaded, stabilized,

and released in a controlled manner. The inner core of the system contains the drug load, whereas the outer shell determines the behavior of the drug in terms of its movement and absorption in the body(Gong et al., 2012). The stability of polymeric micelles is greatly improved by incorporating anticancer drugs such as cisplatin into their inner core. This technique provides a notable opportunity to enhance the therapeutic effectiveness of platinum-based anticancer compounds. Currently, clinical trials are being conducted on two forms of polymeric micelles containing platinum-based anticancer complexes, specifically, NC-6004 and NC-4016. These attempts signify an important step in utilizing nanotechnology to improve the administration and effectiveness of platinum-based chemotherapy drugs, potentially improving treatment results for individuals with cancer(Uchino et al., 2005).

Table 1.7.2 Polymeric micelles containing platinum-based drugs in clinical trials.

Formulation	**NC-6004**	**NC-4016**
Encapsulated drug	Cisplatin	DACH-Pt
Micelles composition	Poly(ethyleneglycol)-β-poly(glutamic acid)	Poly(ethyleneglycol)-β-poly(glutamic acid)
Clinical state	Phase II/III	Phase I

Thus, NC-6004 represents a notable breakthrough in cancer treatment. This involves the use of polymeric micelles composed of a block copolymer including PEG (outer shell) and poly(glutamic acid) (pGlu) (inner core), which are combined with cisplatin to form coordinated *cis*-diammineplatinum moieties. Preclinical evaluations have shown that cisplatin has a longer duration in the bloodstream and a higher level of exposure to tumors than free cisplatin. This suggests that the drug is more effective in treating tumors. Although there was no significant disparity in tumor suppression between NC-6004 and cisplatin in specific models, NC-6004 demonstrated a positive safety profile up to 120 mg/m2 during Phase I clinical trials, but renal impairment and hypersensitivity reactions occurred at this dose, prompting a recommended Phase II dose of 90 mg/m^2(Uchino et al., 2005). The pharmacokinetic profile demonstrated a notable decrease in the maximum plasma concentration (Cmax) and an increase in the area under the curve (AUC) compared with free cisplatin. No complete or partial responses were detected, whereas 41.2% of the patients had stable illnesses. NC-6004 was evaluated in separate Phase I/II studies for advanced solid tumors and metastatic pancreatic cancer when used in

combination with gemcitabine. The maximum tolerated dose (MTD) for the combined therapy was 90 mg/m^2(Doi et al., 2017; Volovat et al., 2020). The adverse effects on neutrophil and white blood cell counts decreased. 55% of patients with metastatic pancreatic cancer experienced tumor reduction, with 15% showing partial responses and 70% maintaining a stable illness. Ongoing investigations are being conducted to compare the efficacy of NC-6004/gemcitabine with that of gemcitabine alone in a Phase III study of locally advanced or metastatic pancreatic cancer. However, the results of this study have not been published(X. Zheng et al., 2021).

In contrast, NC-4016 is a micellar formulation of oxaliplatin carried by PEG-P(Glu) designed to reduce the immediate harmful effects and development of resistance to cisplatin treatment (Ueno et al., 2014). Oxaliplatin differs from cisplatin and carboplatin by having free amino groups attached to platinum, leading to less toxicity and minimizing tumor resistance. It exhibits a comparable structural composition to NC-6004. Preclinical studies have demonstrated that NC-4016 shows higher stability and reduced cytotoxicity than free oxaliplatin. Additionally, it exhibited a longer blood circulation time and improved tumor targeting. NC-4016 was created by oxaliplatin, initially forming an aqueous combination with silver nitrate, and then separated from the precipitated silver chloride using centrifugation and filtration. Methoxy PEG-P(Glu) is added to the oxaliplatin aqueous complex solution and reacts to form oxaliplatin-incorporating micelles. Research at the University of Texas MD Anderson Cancer Center investigated the dosage escalation and pharmacokinetics of NC4016 in patients with advanced solid tumors or lymphoma. NC4016 was administered intravenously at doses of 15 mg/m2 and 80 mg/m2 every three weeks. The results of this study have not been published yet(Lovejoy et al., 2008; Ueno et al., 2014; X. Zheng et al., 2021). Both NC-6004 and NC-4016 demonstrate the potential of nanocarrier-based drug delivery systems to improve the effectiveness and decrease the toxicity of platinum-based anticancer drugs, thereby enhancing their therapeutic index(Hang et al., 2016).

These are all platinum(II)-based drugs encapsulated in lipid nanocarriers that have officially entered clinical trials, although none to date have been officially approved by the FDA(Hang et al., 2016). Thousands of novel platinum-based drugs and nanodrug delivery systems are being developed, similar to micelles and liposomes, such as niosomes, which have new advantages and could emerge as new drug delivery systems to be approved by the FDA.

1.8 Nanodelivery of Pt(IV)-based Anticancer Agents

Liposomal delivery systems are considered a favored design strategy for Pt(IV) prodrugs because they form complexes with identical equatorial ligands, such as cisplatin **(10)**, and axial ligands that provide additional physicochemical properties(Johnstone *et al.*, 2014; Johnstone et al., 2016). Pt(IV) axial positions can target the receptors on the outer surfaces of cancer cells. These advancements in platinum-based formulations based on liposomes and nanoparticles offer intriguing opportunities to enhance the effectiveness and safety of platinum-based chemotherapy for cancer treatment.

In a recent study, Pt(IV) complexes have been linked to estrogen-targeted estrogen receptor-positive breast and ovarian cancer cells, leading to upregulated HMGB1 expression and reduced DNA repair capacity(Singh et al., 2020).

Utilizing bioactive ligands at the axial positions of Pt(IV) complexes enhances their targeting ability, although these positions can also be used for encapsulation in nanodelivery systems. Hydrophobic carboxylates have been employed to deliver platinum complexes within the cores of nanoparticles formed from amphiphilic block copolymers(Bas and Soucek, 2012). Another study used cholesterol as a bioactive ligand for a Pt(IV) prodrug to enhance its affinity for liposomes(Z. Li et al., 2022). Browning et al. explored liposomal platinum(IV) prodrugs coupled with microbubbles for delivery, ultrasound-triggered drug release, and increased drug concentration in breast cancer cells(Browning et al., 2017). Chen *et al.* (2021) developed nanoparticles containing glucose oxidase (GOx) and tirapazamine (TPZ) in a hydrophilic cavity, enhancing intracellular hypoxia and improving cytotoxicity against drug-resistant malignancies(Chen et al., 2021).

Belkacemi *et al.* (2018) formulated liposomal platinum(IV) complexes (RRD4), which demonstrated enhanced therapeutic effects on breast tumor development and metastasis with lower toxicity than free drug(Belkacemi et al., 2018).Yang *et al.* (2017) synthesized hybrid cantharidin-platinum(IV) liposomes (CanPt) by combining cantharidin and platinum(IV) prodrugs to mitigate adverse effects and enhance drug absorption and release, leading to cancer cell apoptosis(X. Yang et al., 2017). Ravera *et al.*(2017) investigated cationic liposomes containing valproate, which, when combined with lipophilic Pt(IV), exhibited significant antiproliferative activity and increased cellular accumulation(Ravera et al., 2017). Furthermore, Chen *et al.* (2018) devised a nanoparticle-based delivery system for platinum complexes, such as *Cis*Pt(IV) and

OxaPt(IV), demonstrating cell cycle arrest, overcoming cisplatin resistance, and rapid drug release under specific conditions(Q. Chen et al., 2018). Targeted delivery of platinum drugs using long-circulating liposomes is an efficient strategy for improving drug efficacy and reducing toxicity. Enhancing the bioactive ligand attached to the Pt(IV) prodrug may improve its compatibility with the liposomal capsule, thereby enhancing the drug release, stability, and efficiency.

1.9 Literature Review

Platinum compounds have demonstrated exceptional efficacy in the treatment of different types of solid tumors, including ovarian, testicular, and lung malignancies, by causing DNA damage and inhibiting cell division(Apps et al., 2015; Brown et al., 2019). Although they have the potential to be ideal chemotherapeutic drugs, their clinical application is frequently impeded by issues such as toxicity, resistance, and the ability to reach the target site(Ghosh, 2019). Researchers have explored various strategies to address these challenges, such as altering the composition of platinum drugs and improving their administration methods(Browning et al. 2017).

Initially, the primary focus was on altering and modifying the structural and oxidation states of platinum compounds, such as cisplatin, carboplatin, and oxaliplatin, to enhance their effectiveness against tumors while minimizing side effects such as resistance and toxicity(Wilson & Lippard, 2014b).

Platinum drugs have undergone several alterations, including adjustments to the ligands linked to the Pt core, to make them more compatible with the drug delivery system(Allen & Cullis, 2013; Haag & Kratz, 2006). The most successful drug delivery systems containing platinum-based drugs are liposomes and micelles, and eight drug-encapsulated drugs have been successfully used in clinical trials(Hang et al., 2016).

Increasing the lipophilicity of platinum derivatives is one of the methods that has been exploited, as lipophilic drugs have improved solubility in lipid-base carriers, facilitating the development of drug delivery systems such as liposomes, niosomes, micelles, and other lipid nanoparticles, which enhance their ability to enter cell membranes, resulting in higher cellular absorption and perhaps improved therapeutic effectiveness, enhancing stability in biological settings, which is essential for preserving the integrity of the drug while circulating and reaching the intended spot(Johnstone et al., 2016). Encased in lipid-based nanoparticles for targeted distribution to certain tissues or cells, which is beneficial

for cancer treatment. Lipophilic drugs have extended circulation periods in the bloodstream when integrated into nanodelivery systems, which can improve their bioavailability and therapeutic benefits(Naderinezhad et al., 2017). By enhancing the lipophilicity of drugs and employing nanodelivery methods, researchers can improve drug *trans*port and therapeutic effects and potentially minimize the side effects associated with cancer treatment(Johnstone et al., 2016; Naderinezhad et al., 2017).

One of the earliest studies was conducted by Al-Baker *et al.* (1992) who synthesized novel highly lipophilic platinum complexes. These complexes were then enclosed in liposomal delivery systems to improve the delivery and efficacy of platinum-based chemotherapy by increasing the drug-to-lipid ratio in liposomal formulations. The series were *cis*-[$(RNH_2)_2PX_2$] where R = ethyl, propyl, isopropyl, butyl, cyclopropyl, cyclopentyl, or neopentyl, and X = either long-chain carboxylate, such as decanoate, laurate, myristate, heptade-canoate, stearate, nonadecanoate, or 2,2,3,3-tetramethylcyclopropylcarboxylate, or branched-chain carboxylate, such as neopentanoate, neohexanoate, neoheptanoate, neononanoate, or neodecanoate.

Among these compounds, *cis*-*bis*-neodecanoato-*trans*-R and R-1,2-diamocyclohexane platinum(II) (NDDP) have demonstrated promising antitumor activity. Nevertheless, NDDP encounters obstacles, such as myelosuppression, toxicity, chemical instability, and degradation when encapsulated within liposomes, which are crucial for the anticancer action of the complex *in vivo*. As a result, L-NDDP fails to meet the requirements for the chemical stability of a therapeutic product(Al-Baker et al., 1992).

In a complementary study based on NDDP, by focusing on the impact of the spatial configuration of the leaving group on intraliposomal stability and synthesizing new platinum complexes with linear aliphatic carboxylate ligands to overcome these limitations, researchers have developed formulations of highly lipophilic DACH compounds that maintain the chemical stability of platinum complexes within liposomes before administration for human use and within the change in liposomal formulation. The results of this study suggest that the structure of the leaving group significantly influences the intraliposomal stability of these compounds. Compounds with ten or fewer linear carbon leaving groups are more stable than compounds with branching leaving groups within the liposomes(Perez-Soler et al., 1994).

Subsequently, Mori *et al.* (1996) DMPC/DMPG liposomes accumulated in the liver and formulated NDDP-containing unilamellar phosphatidylcholine/cholesterol-based liposomes with either monosialoganglioside (GM1) or polyethylene glycol (PEG)-

phosphatidylethanolamine as the surface coating to avoid particle uptake by the organs and enhance circulation in vitro, *and in vivo* PEG-phosphatidylethanolamine, but not GM1, significantly enhanced the cytotoxicity of liposomal NDDP(Mori et al., 1996).
As mentioned above, it moved up to the second clinical trial, but the study was prematurely stopped because it exceeded the maximum tolerable dose, and drug instability and breakdown within the liposomes were observed(Liu *et al.*, 2013).

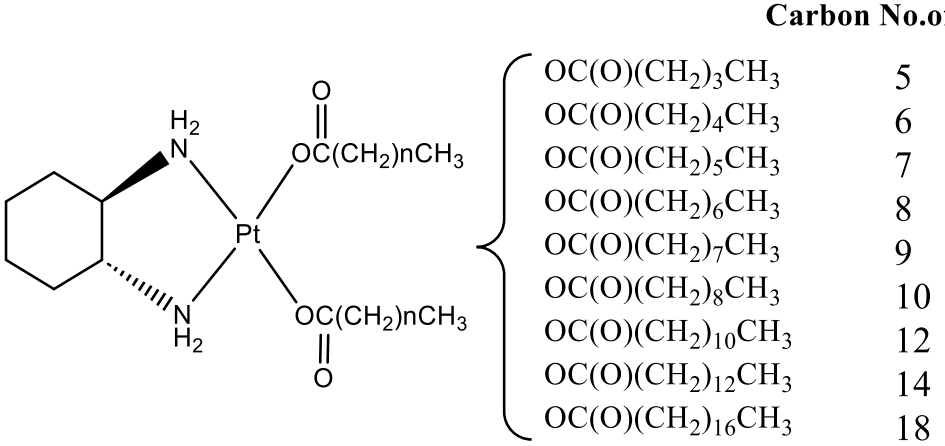

Figure 1.9. Chemical composition of linear alkyl carboxylate ligands in lipophilic di-minocyclohexane platinum (II) complexes. The reduced number of platinum complexes matches the number of carbons in the leaving group(Perez-Soler et al., 1994).

Ongoing research in this field continues to explore new platinum drug derivatives and innovative drug delivery systems for improving cancer treatment outcomes. Lipophilic platinum complexes have been developed by modifying the coordination of bioactive ligands to the platinum ion Pt(II) or Pt (IV) oxidation, which influences the cellular uptake and accumulation of Pt(II) drugs within tumor cells(Z. Li et al., 2022).
The niosomal formulation loaded with platinum-based drugs has been investigated in several studies, as it has more advantages and stability than liposomal drug delivery systems, and could be used as a better alternative(Kaur & Kumar, 2018; Kopermsub et al., 2011). They focused on the preparation of drug-loaded niosomes with optimized formulations using a response surface D-optimal factorial design for colorectal cancer treatment using either oxaliplatin or paclitaxel separately at different concentrations, demonstrating the effectiveness of niosomes in incorporating hydrophilic and hydrophobic drugs, and their release patterns were studied *in vitro* using the HT-29 colon cancer cell line(El-Far et al., 2022). In another study, carboplatin-loaded niosomal

nanoparticles were tested for their effectiveness against brain cancer cells. They used Span 40, PEG 400, and cholesterol. The nano-niosomal formulation of carboplatin showed superior cytotoxicity compared to standard carboplatin with sustained release of carboplatin from the nanoparticles, and the inclusion of PEG in the nanoparticle composition improved stability and drug delivery. The nanodrug had an IC_{50} of 90.5-2.1 uM, demonstrating its effectiveness(Abbasi et al., 2023). Additionally, a study developed pH-responsive cisplatin-loaded niosomes for targeted anticancer drug delivery. The niosomes showed a high encapsulation efficiency of 89% of cisplatin with better cytotoxicity compared to free cisplatin against breast cancer cells, MCF-7, pH-responsive cisplatin-loaded niosomes were developed using Span 60 and Tween 60 derivatized by cholesteryl hemisuccinate (CHEMS) and ergosterol as a helper lipid. The most responsive release was shown at pH 5.4 and 7.4 as the pH-responsive niosomes can release the drug in acidic tumor environments(Sargazi et al., 2021) The efficiency of niosomes loaded with cisplatin was also demonstrated by Kanaani *et al*. (2017), as the cytotoxicity of cisplatin increased by one and a half time compared to free drugs against breast cancer. The niosomes were prepared by reverse-phase evaporation, but this time cisplatin had a low encapsulation and loading efficiency (2.3-0.15 percent). and a burst release was observed as most of the drug release occurred in the first four hours along with crystalization in the suspension of nanoparticles containing cisplatin(Kanaani, Mazloumi Tabrizi, et al., 2017). Niosomal cisplatin was used to treat B16F10 melanoma, which reduced pulmonary nodules in a murine melanoma model and protected against bone marrow toxicity, weight loss, and leukopenia, which are normally observed when treated with free cisplatin. Niosomal cisplatin combined with theophylline showed a significant reduction in lung nodules; however, theophylline did not show antimetastatic effects alone or in combination with cisplatin or activated macrophages, and activated macrophages reduced secondary tumor growth in the lungs(Gude et al., 2002). In another study niosomes formulation containing low-dosage of gemcitabine and cisplatin (NGC) for lung cancer treatment was prepared using a simple heating method while optimizing the formulation using a D-optimal mixture design, the aerosol output of 96.22% indicates suitability for aerosolized delivery with the optimized NGC formulation inhibit the lung cancer cell growth against A549 and the results of the cytotoxicity study showed that the NGC formulation had reduced cytotoxicity compared to using cisplatin and gemcitabine alone this was noticed for both normal (1.56 µg/ml very toxic) and lung cancer cells (46 µg/ml very toxic) as the IC_{50} value indicated that the optimized NGC formulation was

less toxic to normal lung cell (280 µg/ml weakly toxic) and had a further reduction in cytotoxicity for lung cancer cells(Saimi et al., 2021).

These studies demonstrate the potential of niosomal formulations for delivering platinum-based drugs for cancer treatment.

1.10 Statement of the Problem

Despite the design, synthesis, and development of more than 3000 Pt-based cytotoxic agents over the last four decades, only thirty-five compounds have been clinically assessed. A key conclusion of previous studies is based on the notion that the pharmacological profile of Pt-based compounds is dependent on the characteristics of the leaving and non-cleaving (spectator) ligands. The main hypothesis is that appropriately chelated ligand(s) to the platinum center in either the oxidation state (Pt(II) or Pt(IV)) are highly influential and affect the processing of the molecules and the type of lipidic base nanodelivery system. In addition, the dispersion of Pt-based complexes in niosomes is highly affected by the physicochemical properties of ligand substituents coordinated to the Pt center.

1.11 Specific Objectives of the Study

1. Design, synthesis, purification, and characterization of a novel series of Pt(II/IV) derivativescontaining mixed aliphatic and aromatic ligands.
2. Encapsulate the synthesized compounds in a niosomal formulation.
3. Physicochemical characterization of the prepared niosomal formulations and assessment of encapsulation efficiency, loading, size, and morphology.
4. The cytotoxic effects of the synthesized Pt-based compounds encapsulated in niosomes were investigated against both cancer cell lines and normal cells.

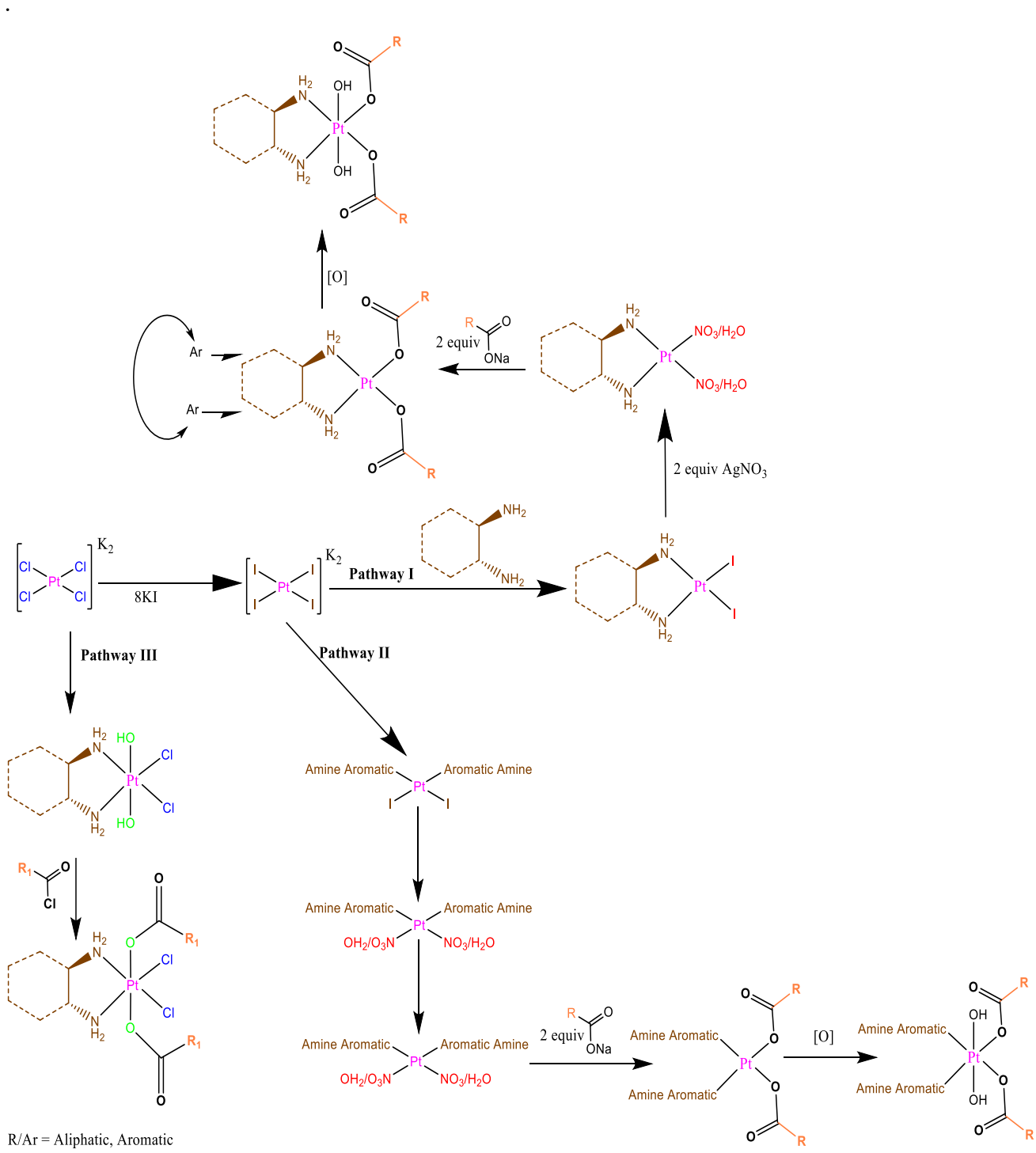

Scheme 1.11 General scheme depicting synthetic pathways and planned platinum-based cytotoxic compounds.

Chapter Two

Experimental part

2 Experimental part

General considerations

Reactions were carried out in a fume hood in the dark. Solvents and reagents were used as received from commercial sources without further drying or purification. Purified water was used, and organic solvents were of analytical grade.

2.1 Materials

Chemicals: Double-distilled water (DDW), methanol (MeOH), dimethyl formamide (DMF), dimethyl sulfoxide (DMSO), acetone, potassium iodide (KI), ethylenediamine (EN), ammonium hydroxide (NH_4OH 25%), ((1*R*,2*R*)-1,2-diaminocyclohexane)) “DACH" ($C_6H_{10}(NH_2)_2$); carboxylic acids: 4-ethyl benzoic acid (97%), acetic acid, trifluoroacetic acid (TFA) octanoic acid, sodium oxalate, 4-ethylbenzoic acid ($C_9H_{10}O_2$), 4-(trifluoromethyl)benzoic acid, aromatic amines: (pyridine), aliphatic amines (n-butyl amine), cyclic-aliphatic amine; piperidine; n-hexane, and were all purchased from ACROS Chemicals Ltd. and used without any further purification.

Concentrated hydrochloric acid (HCl 37%), sodium hydrogen carbonate ($NaHCO_3$), and myristic acid ($CH_3(CH_2)_{12}COOH$) were purchased from Merck Ltd, USA.

Potassium tetrachloroplatinate(II) (K_2PtCl_4), chloroform, and acetonitrile were purchased from Aldrich Chemicals Ltd, USA.

Silver nitrate ($AgNO_3$) and ethanol (EtOH) were purchased from Thermo Scientific, USA. Dioxane was purchased from J.T. Baker, USA. Ethyl acetate was purchased from MACRON Fine Chemicals, USA. Diethyl ether was purchased from EMSURE in Germany. Hydrogen peroxide (H_2O_2 3%) was purchased from Floris, UK.

Tween 80 were purchased from Arcos Organics, USA. Cholesterol was purchased from Merck. MTS reagent and trypsin-EDTA solution 1X were bought from Promega, USA.

2.2 Instruments and Equipment

Chemical hazards fuming hood, magnetic stirrers, hotplates, filtration apparatus, vacuum pumps, using sintered filtrated glass (pore size 3), celite, desiccators, and rotary evaporator are available at anticancer drugs research Lab, ATR/FT-IR spectroscopy was done at the Al-Quds Center for Measurement & Analysis, and proton nuclear magnetic resonance spectroscopy (^{1}H-NMR) was performed at the department of chemistry at Al-Najah National University.

2.2.1 Attenuated Total Reflectance-Fourier Transform Infrared (ATR-FTIR) Spectroscopy

All measurements were carried out on a TENSOR(II) FTIR Routine Spectrometer from Bruker Optic. All spectra were recorded by attenuated total reflection (ATR). The sample is placed onto the ATR crystal and pressed down using the swivel press to ensure optimal contact between the sample and the crystal. The FTIR measurements were recorded between 4,000 and 400 cm^1. Each spectrum was obtained by averaging 128 scans recorded at a resolution of 4 cm^1. The FTIR data of the spectra were pre-processed by baseline correction, and they were smoothed at a final resolution of 4 cm^{-1} by apodization of their Fourier *trans*forms by a Gaussian line. The processing of the spectra was carried out by OPUS software generated in the lab of the Al-Quds Center for measurement and analysis.

2.2.2 Proton nuclear magnetic resonance (^{1}H-NMR)

All measurements were conducted using 80 MHz NMR Spinsolve 80 from Magritek.^{1}H-NMR spectra Samples were run in deuterated chloroform chemical shifts ($CDCl_3$) or deuterated acetone solvent and are reported in parts per million (ppm, δ) downfield from tetramethyl Silan (TMS). The processing of the spectra was carried out by MNOVA software. Spin multiplicities are described as doublet (d), doublet of doublets (dd), singlet (s), triplet (t), quartet (q), and multiple (m).

2.2.3 Spectrophotometer 7315

A spectrophotometer 7315 (Jenway, UK) was used to measure the ultraviolet-visible (UV-VIS) spectra using 10-mm quartz cuvettes.

2.2.4 Water Bath Sonicator

A water bath sonicator (Elmasonic S70Hz; Elma, Germany) was used to improve the sparsity of the niosomes and their formation.

2.2.5 Dynamic Light Scattering (DLS) & PDI

Dynamic Light Scattering (DLS) was used for hydrodynamic size and polydispersity measurements obtained at an angle of scattering of 90 degrees and a temperature of 25 °C (NanoBrook Omni, Brookhaven Instruments, USA).

2.2.6 Atomic Force Microscopy (AFM)

Atomic Force Microscopy (AFM) images were captured by a NanoSurf Core AFM microscope, and the images were analyzed using Gwyddion software. The samples were prepared by drop-casting niosomes solution on mica substrates and then vacuum drying at 120ºC.

2.3 Synthesis of platinum complexes

2.3.1 General procedure for synthesis of *cis*-(alkylamine)diiodoplatinum(II) complexes [*cis*-$(NHR)_2PtI_2$]

All *cis*-(alkylamine)diiodoplatinum(II) complexes were synthesized according to previously reported procedures (Al-baker & Dabrowiak, 1987).

2.3.1.1 Synthesis of [(1*R*,2*R*)-cyclohexane-1,2-diamine](diiodoplatinum(II)); [*cis*-Pt(DACH)I_2] (3), is given as an example:

Potassium tetrachloropaltinate(II) [K_2PtCl_4] **(1)** (0.5 g, 1.20 mmol) were dissolved in 40 ml distilled water (DW) to which 8 equivalents of potassium iodide (KI) (1.60 g, 9.64 mmol) were added. The mixture was stirred at room temperature for 30 min through which the color turned to dark brown. To the stirred mixture (1*R*, 2*R*)-diaminocyclohexane "DACH" ($C_6H_{14}N_2$) (0.14 g, 1.20 mmol) was added, and the reaction mixture was stirred overnight. The formed yellow precipitate [(1*R*,2*R*)-cyclohexane-1,2-diamine](diiodoplatinum(II)); [*cis*-Pt(DACH)I_2] **(3)**, was collected via filtration (sintered fritted glass; pore size 3) and washed twice with 10 ml of DW After drying under suction for two hours, the product **(3)** was transferred into a vial and dried under vacuum in a desiccator (with KOH). The dried product was used in the following steps without any further purification.

Yield: 81% (548 mg, 0.973 mmol).

[Ethylenediamine](diiodoplatinum(II)); [*cis*-Pt(EN)I_2] **(4)**, same procedure (K_2PtCl_4) **(1)** (0.50 g, 1.20 mmol) with **(**81.42 µl, 1.20 mmol**)** of ethylenediamine.

Yield: 88% (468 mg, 0.919 mmol).

[*Cis*-di(n-butylamine)(diiodoplatinum(II)); [*cis*-Pt$(NBA)_2(I)_2$] **(5)**, same procedure (K_2PtCl_4) **(1)** (250 mg, 0.60 mmol) with **(**118.59 µl, 1.20 mmol**)** of n-butyl amine. Yield: 78.4% (280 mg, 0.470 mmol).

[*Cis*-di(piperidine)(diiodoplatinum(II)); [*cis*-Pt$(Pip)_2I_2$] **(6),** same procedure (K_2PtCl_4) **(1)** (250 mg, 0.60 mmol) with **(**118.53 µl, 1.20 mmol**)** of piperidine.

Yield: 88.66% (329.5 mg, 0.532 mmol).

2.3.2 Synthesis of diamminedichloridoplatinum(II) , [*cis*-[$Pt(NH_3)_2Cl_2$], Cisplatin] (10)

2.3.2.1 Synthesis of *cis*-diamminediiodideplatinum(II), [*cis*-[$Pt(NH_3)_2I_2$] (7)

The synthesis of cisplatin was performed according to Dhara's synthesis method for cisplatin(Dhar & Lippard, 2009). Briefly, potassium tetrachloroplatinate(II) [K_2PtCl_4] **(1)** (100 mg, 0.240 mmol) were dissolved in 10 ml double distilled water (DDW), to which eight equivalents (383 mg, 1.92 mmol) of potassium iodide (KI) were added. The mixture was stirred at room temperature for 20 minutes. Three equivalents of ammonium hydroxide (NH_4OH 25%) (55 µl, 0.72 mmol) were added, reaction mixture were stirred for 2 hours at room temperature. A fine yellow precipitate *cis*-diaminodiiodoplatinum(II) (*cis*-$Pt(NH_3)_2I_2$) **(7)** was produced. The product **(7)** was collected by filtration, washed with water, and dried under a vacuum. Yield: 78.3% (91 mg, 0.188 mmol).

2.3.2.2 Synthesis diamminedichloridoplatinum(II), [*cis*-[$Pt(NH_3)_2Cl_2$], Cisplatin] (10)

Cis-diaminodiiodoplatinum(II) (*cis*-$Pt(NH_3)_2I_2$) **(7)** prepared in the previous step was used subsequently without any further purification. In an aluminum foil-covered round bottom flask (RBF), (91 mg, 0.19 mmol) *cis*-$Pt(NH_3)_2I_2$ **(7)** was suspended in 10 mL DDW, to which two equivalents of $AgNO_3$ (64 mg, 0.38 mmol) were added. The mixture was stirred for 36 hours at room temperature. The precipitate of AgI was filtered off and washed twice with 5 ml DDW. The filtrate containing *cis*-diamminodiaquaplatinum(II)/ *cis*-diamminodinitratoplatinum(II) [*cis*-$Pt(NH_3)_2(H_2O)_2$ **(8)** and *cis*-$Pt(NH_3)_2(NO_3)_2$ **(9)**] were collected and treated with 0.5 ml of 37% HCl and stirred overnight at room temperature. The resulting yellow precipitate was collected by filtration, washed with DDW, and dried under vacuum. The final product diamminedichloridoplatinum(II), [*cis*-[$Pt(NH_3)_2Cl_2$], Cisplatin] **(10)** was collected as a yellow powder.

Yield: 63.8% (35 mg, 0.12 mmol). FTIR: 3281, 3200 (N-H stretching), 487 (Pt-N stretching).

2.3.3 Synthesis of [(1*R*,2*R*)-cyclohexane-1,2-diamine-N,N′]bis(tetradecanoato-O)platinum; [*cis*-Pt(DACH)$(MYR)_2$], Miriplatin] (19)

For the synthesis of diam(m)inedicarboxylatoplatinum(II) complexes the corresponding sodium carboxylate ligands ought to be synthesized in advance.

2.3.3.1 Synthesis of sodium carboxylates (sodium myristate (12), sodium 4-trifluoromethyl benzoate (14), and sodium 4-ethyl benzoate (16)).

The general synthesis of sodium carboxylates was carried out using previously published methods(Zacharie et al., 2009).

Synthesis of sodium myristate (12) is given as an example:

Myristic acid **(11)** (2.06 g, 8.76 mmol) was dissolved in ethanol (13 ml) at room temperature. The mixture was stirred for 15 minutes, a clear solution was formed. To the clear solution of myristic acid, 0.97 equivalents of sodium bicarbonate (0.71 g, 8.50 mmol) were added portion-wise. The resulting cloudy mixture was heated, under reflux for three hours. While heated a white-colored precipitate started to form. At the end of the 4-hour reflux, the reaction mixture was allowed to cool down and left at room temperature overnight. The volatiles were evaporated to dryness under reduced pressure using a rotary evaporator. The white solid sodium myristate **(12)** was scratched out using a spatula and collected in a 50 ml vial without further purification. Yield: 95.54% (2.095 g, 8.37 mmol).

Sodium 4-trifluoromethyl benzoate **(14)**, same procedure, trifluoromethyl benzoic acid **(13) (**0.5 g, 2.629 mmol**)**. Yield: 84 % (468 mg, 2.21 mmol).

Sodium 4-ethyl benzoate **(16),** same procedure, 4-ethylbenzoic acid **(15) (**0.5 g,3.329 mmol). Yield: 90% (518 mg, 3.0 mmol).

2.3.3.2 Synthesis of [(1*R*,2*R*)-cyclohexane-1,2-diamine]bis(chloroplatinum(II)); [*cis*-Pt(DACH)Cl_2] (17)

K_2PtCl_4 **(1)** (1 g, 2.409 mmol) was dissolved in (40 ml) DDW at room temperature. While stirring (1*R*, 2*R*)-1,2-diaminocyclohexane "DACH" (275 mg, 2.409 mmol) was added. The mixture was stirred at room temperature overnight. A fine yellow precipitate of [(1*R*,2*R*)-cyclohexane-1,2-diamine]bis(chloroplatinum(II)); [*cis*-Pt(DACH)Cl_2] **(17)** was formed. The compound was collected by filtration under a vacuum and washed with 10 ml of DDW. The product *cis*-Pt(DACH)Cl_2 **(17)** was transferred to a vial and dried in a desiccator (anhydrous KOH) under vacuum for 48 hours. Product **(17)** was used in the subsequent steps without further purification.

Yield: 60.77% (556.8 mg, 1.464 mmol).

2.3.3.3 Synthesis of [(1*R*,2*R*)-cyclohexane-1,2-diamine-N,N′]bis(tetradecanoato-O)platinum; [*cis*-Pt(DACH)(MYR)$_2$], Miriplatin] (19)

Method 1

Sodium myristate ($CH_3(CH_2)_{12}COONa$ **(12))** (131.7 mg, 0.53 mmol) were dissolved in (5 ml) DDW at 60ºC, two equivalents of $AgNO_3$ (89.30 mg, 0.53 mmol) were dissolved in a 3 ml of DDW and added to the dissolved sodium myristate **(12)** solution. The mixture was stirred for 0.5 hr., at 60 ºC and the white precipitate (silver myristate $CH_3(CH_2)_{12}COOAg$) **(18)** (176.36 mg, 0.53 mmol) was filtered off, washed with DDW and ethanol, and then suspended in 5 ml of DDW. *cis*-Pt(DACH)Cl_2 **(17)** (100 mg, 0.26 mmol) was added to the suspension of silver myristate **(18)**. The mixture was stirred overnight at room temperature, the precipitate was filtered off, washed with DDW and ethanol, the precipitate was stirred in 20 ml of ethanol at 80 ºC, after 15 min the silver chloride AgCl was filtered off, 5 ml of DDW was added to the filtrate, the white precipitate [(1*R,*2*R*)-cyclohexane-1,2-diamine-N,N′]bis(tetradecanoato-O)platinum; [*cis*-Pt(DACH)(MYR)2], Miriplatin] **(19)** was filtered off, washed with ethanol. The precipitate was transferred to a 10 mL vial and dried under a vacuum. The amount produced was insufficient.

Method 2

Cis-Pt(DACH)I_2 **(3)** (100 mg, 0.18 mmol) was suspended in DDW (10 ml) in an aluminum foil-covered round-bottom flask, to which 1.99 equivalents of $AgNO_3$ (60 mg, 0.36 mmol) were added. The mixture was stirred at room temperature for 48 hours. The yellow insoluble precipitate turned into a gray-colored one. The precipitate containing AgI was filtered off under suction using sintered fritted glass; pore size 3. Following washing with an additional 20 ml of DDW, the filtrate **[***cis*-Pt(DACH)$(NO_3)_2$ / *cis*-Pt(DACH)$(H_2O)_2$ **(20) / (21)]** was collected and used in the next step without further purification. The clear filtrate **[***cis*-Pt(DACH)$(NO_3)_2$ / *cis*-Pt(DACH)$(H_2O)_2$ **(20) / (21)]** was transferred to 50 ml RBF, to which sodium myristate **(12)** (93 mg, 0.36 mmol) was added. The mixture was stirred at room temperature for 24 hours. The resulting precipitate was collected by filtration, washed with DDW, and dried under vacuum. The final product [(1*R,*2*R*)-cyclohexane-1,2-diamine-N,N′]bis(tetradecanoato-O)platinum; [*cis*-Pt(DACH)(MYR)2], Miriplatin] **(19)** was collected as a white powder.
Yield: 91% (125 mg; 0.164 mmol). FTIR: 3198,3109 (N-H stretching), 2917,2890 (C-H stretching), 1685 (C=O stretching), 1586 (C-C stretching), 1384(C-O stretching).

2.3.4 Synthesis of [(1*R*,2*R*)-cyclohexane-1,2-diamine](ethanedioato-O,O')platinum(II) ; (Oxaliplatin) (23)

Cis-Pt(DACH)Cl_2 **(17)** (250 mg, 0.66 mmol) was suspended in DDW (4 ml), and 1.99 equivalent (222.30 mg, 1.308 mmol) of $AgNO_3$ was added. The mixture was stirred at room temperature overnight. The obtained silver chloride (AgCl) was filtered off using celite within the filter glass, and then it was washed with 4 ml of water. The filtrate containing [*cis*-Pt(DACH)$(NO_3)_2$ / *cis*-Pt(DACH)$(H_2O)_2$ **(20)** / **(21)**] was collected. 1.1 equivalent sodium oxalate (97 mg, 0.72 mmol) **(22)** was dissolved in 1 ml of water and added in two portions to the obtained filtrate **(20)**/**(21)** and stirred overnight. The resulting precipitate was collected by filtration, washed with DDW, and dried under vacuum. The final product [(1*R,*2*R*)-cyclohexane-1,2-diamine](ethanedioato-O,O')platinum(II) ; (Oxaliplatin) **(23)** was collected as a garish powder.

Yield: 15.8% (41.6 mg, 0.104 mmol). FTIR: 3209, 3161 (N-H stretching), 2977,2890 (C-H stretching), 1653 (C=O stretching), 1378 (C-O stretching), 1473 (C-C stretching), 476 (Pt-O stretching), and 515 (Pt-N stretching).

2.3.5 Synthesis of [(1*R*, 2*R*)- cyclohexane-1,2-diamine]-bis-(acetate)platinum(II); [*cis*-Pt(DACH)(acetate)$_2$] (25)

Cis-Pt(DACH)Cl_2 **(17)** (259 mg, 1.05 mmol) was suspended in DDW (4 ml), and 1.99 equivalent (321 mg, 1.90 mmol) of $AgNO_3$ was added. The mixture was stirred at room temperature overnight. The obtained AgCl was filtered off using celite within the filter glass, and then it was washed with 4 ml of water. The filtrate containing [*cis*-Pt(DACH)$(NO_3)_2$ / *cis*-Pt(DACH)$(H_2O)_2$ **(20)** / **(21)**] was collected. 2.2 equivalent sodium acetate (123 mg, 1.12 mmol) **(24)** was dissolved in 1 ml of water and added in five portions to the obtained filtrate **(20)** / **(21)** and left stirring overnight. The resulting precipitate was collected by filtration, washed with DDW, and dried under vacuum. The final product [(1*R*,2*R*)-cyclohexane-1,2-diamine]-bis-(acetate)platinum(II); [*cis*-Pt(DACH)(acetate)$_2$] **(25)** was collected as a grayish powder.
Yield: 2% (23.9 mg; 0.019 mmol). FTIR 3192,3124 (N-H stretching), 2977,2890 (C-H stretching), 1687 (C=O stretching), 1378 (C-O stretching), 1597 (C-C stretching), 442 (Pt-O stretching) stretching), 519 (Pt-N stretching).

2.3.6 Synthesis of [(1*R*,2*R*)-cyclohexane-1,2-diamine]bis(4-ethylbenzoato)platinum(II); [*cis*-Pt(DACH)(EBZ)$_2$] (26)

Cis-Pt(DACH)I_2 **(3)** (100 mg, 0.18 mmol) were suspended in DDW (10 ml) in an aluminum foil-covered round-bottom flask, to which 1.99 equivalents of $AgNO_3$ (60 mg, 0.35 mmol) were added while stirring. The mixture was left to stir at room temperature for 48 hours. The yellow insoluble precipitate turned into a gray-colored one. The precipitate containing AgI was filtered off under suction. Following washing with an additional 10 ml of DDW, the filtrate [*cis*-Pt(DACH)$(NO_3)_2$ / *cis*-Pt(DACH)$(H_2O)_2$ **(20)** / **(21)**] was collected and used in the next step with no further purification. The clear

filtrate [*cis*-Pt(DACH)$(NO_3)_2$ / *cis*-Pt(DACH)$(H_2O)_2$ **(20)** / **(21)**] was transferred to 50 ml RBF, and 64 mg (0.36 mmol) of sodium 4-ethyl benzoate **(16)** was added. The mixture was stirred at room temperature overnight. The resulting precipitate was collected by filtration, washed with DDW, and dried under vacuum. The final product [(1*R*,2*R*)-cyclohexane-1,2-diamine]bis(4-ethylbenzoato)platinum(II); [*cis*-Pt(DACH)$(EBZ)_2$] **(26)** was collected as a white powder.

Yield: 72% (80 mg; 0.131 mmol). FTIR 3212,3088 (N-H stretching), 2964,2934 (C-H stretching), 1661 (C=O stretching), 1385 (C-O stretching), and 1600 (C-C stretching). 1H NMR (81 MHz, CDCl3) δ 7.56 (t, J = 7.1 Hz, 4H, Ar), 6.84 (t, J = 8.7 Hz, 4H, Ar), 2.28 (q, J = 7.6 Hz, 4H, 2CH2CH3), 1.69 (d, J = 9.4 Hz, 2H, 2CHN), 0.95-0.74 (m, , 13H, DACH, 2CH3).

2.3.7 Synthesis of [(1*R*,2*R*)-cyclohexane-1,2-diamine]bis(4-trifluoromethylbenzoato)platinum(II); [*cis*-Pt(DACH)$(TFBA)_2$] (27)

Cis-Pt(DACH)I_2 **(3)** (100 mg, 0.18 mmol) were suspended in DDW (10 ml) in an aluminum foil-covered round-bottom flask, to which 1.99 equivalents of $AgNO_3$ (60 mg, 0.35 mmol) were added while stirring. The mixture was left stirring at room temperature for 48 hours. The yellow insoluble precipitate turned into a gray-colored one. The precipitate containing AgI was filtered off under suction. Following washing with an additional 10 ml of DDW the filtrate [*cis*-Pt(DACH)$(NO_3)_2$ /*cis*-Pt(DACH)$(H_2O)_2$ **(20)**/**(21)**] was collected and used in the next step with no further purification. The clear filtrate [*cis*-Pt(DACH)$(NO_3)_2$ / *cis*-Pt(DACH)$(H_2O)_2$ **(20)** / **(21)**] was transferred to 50 ml RBF, (79 mg, 0.36 mmol) of sodium 4-trifluoromethyl benzoate **(14)** was added. The mixture was stirred at room temperature overnight. The resulting precipitate was collected by filtration, washed with DDW, and dried under vacuum. The final product [(1*R,2R*)-cyclohexane-1,2-diamine]bis(4-trifluoromethylbenzoato)platinum(II); [*cis*-Pt(DACH)($TFBA)_2$] **(27)** was collected as a white powder.

Yield: 93% (115 mg; 0.167 mmol). FTIR 3226,3109 (N-H stretching), 2943,2855 (C-H stretching), 1612 (C=O stretching), 1378 (C-O stretching), 1570 (C-C stretching), 1161

(C-F stretching). 1H NMR (81 MHz, CDCl3) δ 7.96 (t, J = 6.1 Hz, 4H, Ar), 7.58 (t, J = 6.7 Hz, 4H, Ar), 2.47 (s, 4H, 2NH2), 1.18-0.79 (m, J = 31.4 Hz, 10H, DACH).

2.3.8 Synthesis of (ethylenediamine)bis(myristato)platinum(II); [*cis*-Pt(EN)(MYR)$_2$] (30)

Cis-(ethylenediamine)diiodoplatinum(II) [*cis*-(EN)PtI$_2$] **(4)** (100 mg, 0.20 mmol) (100 mg, 0.18 mmol) were suspended in DDW (10 ml) in an aluminum foil-covered round-bottom flask, to which 1.99 equivalents of $AgNO_3$ (66.42 mg, 0.40 mmol) were added. The mixture was stirred at room temperature for 48 hours. The yellow insoluble precipitate turned into a gray-colored one. The precipitate containing AgI was filtered off under suction using sintered fritted glass; pore size 3. Following washing with an additional 20 ml DDW the filtrate **[***cis*-Pt(EN)$(NO_3)_2$ / *cis*-Pt(EN)$(H_2O)_2$ **(28)** / **(29)**] was collected and used in the next step with no further purification. The clear filtrate [*cis*-Pt(EN)$(NO_3)_2$ / *cis*-Pt(EN)$(H_2O)_2$ **(28)** / **(29)**] was transferred to 50 ml RBF to which sodium myristate **(12)** (103.03 mg, 0.393 mmol) was added. The mixture was stirred at room temperature for 24 hours. The resulting precipitate was collected by filtration, washed with DDW, and dried under vacuum. The final product [ethylenediamine]bis(myristato)platinum(II); [*cis*-Pt(EN)(MYR)$_2$] **(30)** was collected as a white powder.

Yield: 88% (125 mg; 0.176 mmol). FTIR 3086,3024 (N-H stretching), 2958,2878 (C-H stretching), 1702 (C=O stretching), 1366 (C-O stretching), 1427 (C-C stretching).

2.3.9 Synthesis of (ethylenediamine)bis(4-ethylbenzoato)platinum(II); [*cis*-Pt(EN)(EZB)$_2$] (31)

Cis-(EN)PtI$_2$ **(4)** (100 mg, 0.20 mmol).were suspended in DDW (10 ml) in an aluminum foil-covered round-bottom flask, to which 1.99 equivalents of $AgNO_3$ (66.42 mg, 0.40 mmol) were added. The mixture was stirred at room temperature for 48 hours. The yellow insoluble precipitate turned into a gray-colored one. The precipitate containing AgI was filtered off under suction using sintered fritted glass; pore size 3. Following

washing with an additional 20 ml DDW the filtrate **[***cis*-Pt(EN)$(NO_3)_2$ / *cis*-Pt(EN)$(H_2O)_2$ **(28)** / **(29)**] was collected and used in the next step with no further purification. The clear filtrate **[***cis*-Pt(EN)$(NO_3)_2$ / *cis*-Pt(EN)$(H_2O)_2$ **(28)** / **(29)**] was transferred to 50 ml RBF to which sodium 4-ethyl benzoate **(16)** (103.03 mg, 0.40 mmol) was added. The mixture was stirred at room temperature overnight. The resulting precipitate was collected by filtration, washed with DDW, and dried under vacuum. The final product [ethylenediamine]bis(4-ethylbenzoato)platinum(II); [*cis*-Pt(EN)$(EZB)_2$] **(31)** was collected as a white powder.

Yield: 69.4% (69.1 mg; 0.125 mmol). FTIR: 3171,3088 (N-H stretching), 2969,2932 (C-H stretching), 1679 (C=O stretching), 1378 (C-O stretching), 1513 (C-C stretching).

2.3.10 Synthesis of [ethylenediamine]bis(4-trifluoromethylbenzoato)platinum(II); [*cis*-Pt(EN)$(TFBA)_2$] (32)

Cis-(EN)PtI_2 **(4)** (100 mg, 0.20 mmol) were suspended in DDW (10 ml) in an aluminum foil-covered round-bottom flask. 1.99 Equivalents of $AgNO_3$ (66.42 mg, 0.40 mmol) were added to the solution. The mixture was stirred at room temperature for 48 hours. The yellow insoluble precipitate turned into a gray-colored one. The yellow precipitate became an insoluble, gray-colored precipitate, then it was filtered off under suction using sintered fritted glass; pore size 3. Followed by washing with an additional 20 ml DDW, the filtrate **[***cis*-Pt(EN)$(NO_3)_2$ / *cis*-Pt(EN)$(H_2O)_2$ **(28)** / **(29)**] was collected and used in the next step with no further purification. The clear filtrate **[***cis*-Pt(EN)$(NO_3)_2$ / *cis*-Pt(EN)$(H_2O)_2$ **(28)** / **(29)**] was transferred to 50 ml RBF to which sodium 4-trifluoromethyl benzoate **(14)** (103.03 mg, 0.40 mmol) was added. The mixture was stirred at room temperature overnight. The resulting precipitate was collected by filtration, washed with DDW, and dried under vacuum. The final product of [ethylenediamine]bis(4-trifluoromethylbenzoato)platinum(II); [*cis*-Pt(EN)$(TFBA)_2$] **(32)** was collected as a white powder.

Yield: 85% (107.2 mg; 0.17 mmol). FTIR: 3282,3103 (N-H stretching), 2980,2970 (C-H stretching), 1617 (C=O stretching), 1372 (C-O stretching), 1511 (C-C stretching), 1161 (C-F stretching).

2.3.11 Synthesis of [*cis*-di(n-butylamine)]bis(myristato)platinum(II); [*cis*-$Pt(NBA)_2(MYR)_2$] (35)

Method 1

Cis-di(n-butylamine)diiodoplatinum(II) [*cis*-$(NBA)_2PtI_2$] **(5)** (100 mg, 0.17 mmol) was suspended in DDW (10 ml) in aluminum foil-covered round-bottom flask, to which 1.99 equivalents of $AgNO_3$ (56.78 mg, 0.33 mmol) were added. The mixture was stirred at room temperature for 48 hours. The RBF was heated for 30 minutes at 50 °C before filtration. The filtrate containing [*cis*-$Pt(NBA)_2(NO_3)_2$ / *cis*-$Pt(NBA)_2(H_2O)_2$ **(33)** / **(34)**] was collected and used in the next step with no further purification. The clear filtrate was transferred to 50 ml RBF to which sodium myristate **(12)** (84 mg, 0.32 mmol) was added. The mixture was stirred at room temperature for 24 hours. The milky color mixture was formed but most of it was stuck around the RBF, 10 ml of diethyl ether was added to the mixture, and it was left without stirring overnight, the precipitate formed a top layer crystal. The resulting precipitate was collected by filtration, washed with DDW, and dried under vacuum. The final product [*cis*-di(n-butylamine)]bis(myristato)platinum(II); [*cis*-$Pt(NBA)_2(MYR)_2$] **(35)** was collected as a white crystal.

Yield: 58.8% (74.5 mg; 0.1 mmol). FTIR: 3221,3115 (N-H stretching), 2945,2880 (C-H stretching), 1668 (C=O stretching), 1320 (C-O stretching).

Method 2

Cis-$(NBA)_2PtI_2$ **(5)** (102.7 mg, 0.17 mmol) were dissolved in chloroform (10 ml), two equivalents of sodium myristate **(12)** (86.40 mg,0.35 mmol) were added to the mixture, and dissolved, a clear yellow mixture was formed, to which two equivalent of $AgNO_3$ (58.5 mg,0.345 mmol) were added. The mixture was left stirring overnight, it turned into a cloudy dark yellow, and it filtrated off using celite within a filter glass then it was washed with 4 ml chloroform. The filtrate was evaporated to dryness using a rotary evaporator. an orange thin brownish layer was formed around the RBF. It was left at room temperature for 15 minutes then it was put in the fridge overnight. A light brownish

solid was obtained through recrystallization after 1 ml of ethyl acetate was added then it was heated for five minutes at 50 °C left to cool down at room temperature it was put in the fridge overnight, and another 1.5 ml of hexane was added to the mixture resulting the precipitate of the product to be formed, it was collected by filtration and dried under vacuum. The final product [*cis*-di(n-butylamine)]bis(myristato)platinum(II); [*cis*-$Pt(NBA)_2(MYR)_2$] **(35)** was collected as light brownish powder.

Yield: 66.4% (106.3 mg, 0.133 mmol). Same FTIR as method 1: 3221,3115 (N-H stretching), 2945,2880 (C-H stretching), 1668 (C=O stretching), 1320 (C-O stretching).

2.3.12 Synthesis of [*cis*-di(n-butylamine)]bis(4-ethylbenzoato)platinum(II); [*cis*-$Pt(NBA)_2(EZB)_2$] (36)

Method 1

Cis- $(NBA)_2PtI_2$ **(5)** (100 mg, 0.17 mmol) were suspended in DDW (10 ml), in an aluminum foil-covered round-bottom flask to which 1.99 equivalents of $AgNO_3$ (57 mg, 0.33 mmol) were added. The mixture was stirred at room temperature for 72 hours. The yellow insoluble precipitate turned into a gray-colored one. The precipitate containing AgI was filtered off under suction. Following washing with an additional 10 ml DDW the filtrate [*cis*-$Pt(NBA)_2(NO_3)_2$ / *cis*-$Pt(NBA)_2(H_2O)_2$ **(33)** / **(34)**] was collected and used in the next step with no further purification. The clear filtrate was transferred to 50 ml RBF to which sodium 4-ethyl benzoate **(16)** (61 mg, 0.34 mmol) was added. The mixture was stirred at room temperature for 48 hours. A milky precipitate was formed, 5 ml of diethyl ether was added to the mixture, and it was left stirring for 90 minutes. The resulting precipitate was collected by filtration, washed with DDW, and dried under vacuum. The final product [*cis*-(di-n-butylamine)]bis(4-ethylbenzoato)platinum(II); [*cis*-$Pt(NBA)_2(EZB)_2$] **(36)** was collected as a white powder.

Yield: 35% (38.2 mg; 0.059 mmol). FTIR: 3182,3115 (N-H stretching), 2960,2928 (C-H stretching), 1611 (C=O stretching), 1314 (C-O stretching).

Method 2

Similar to the first method *cis*- $(NBA)_2PtI_2$ **(5)** (105 mg, 0.17 mmol) were suspended in DDW (10 ml), to which 1.99 equivalents of $AgNO_3$ (57 mg, 0.33 mmol) were added. The mixture was left stirring at room temperature for 48 hours. The mixture was filtrated from AgI to obtain the clear filtrate [*cis*-$Pt(NBA)_2(NO_3)_2$ / *cis*-$Pt(NBA)_2(H_2O)_2$ **(33)** / **(34)**] which was collected and used in the next step with no further purification. To the clear filtrate sodium 4-ethyl benzoate **(16)** (61 mg, 0.34 mmol) were added. The mixture was stirred at room temperature for 24 hours. A milky precipitate was formed. The fine white precipitate was transferred to a 50 ml tube and centrifuged. the above filtrate was removed, and the product was put to dry in a desiccator. The final product [*cis*-(di-n-butylamine)]bis(4-ethylbenzoato)platinum(II); [*cis*-$Pt(NBA)_2(EZB)_2$] **(36)** was collected as a white powder.

Yield: 42% (45.3 mg; 0.071 mmol).: FTIR: 3182,3115 (N-H stretching), 2960,2928 (C-H stretching), 1611 (C=O stretching), 1314 (C-O stretching).

2.3.13 Synthesis of [*cis*-di(n-butylamine)]bis(4-trifluoromethylbenzoato)platinum(II); [*cis*-$Pt(NBA)_2(TFBA)_2$] (37)

Cis- $(NBA)_2PtI_2$ **(5)** (100 mg, 0.17 mmol) was suspended in DDW (10 ml), in an aluminum foil-covered round-bottom flask to which 1.99 equivalents of $AgNO_3$ (57 mg, 0.33 mmol) were added. The mixture was stirred at room temperature for 72 hours. 10 ml of ethanol were added to the mixture turning the mixture into a smooth yellowish-gray color it was left stirring at room temperature overnight. The yellow insoluble precipitate turned into a gray-colored one. The precipitate containing AgI was filtered off under suction. Following washing with an additional 10 ml DDW the filtrate [*cis*-$Pt(NBA)_2(NO_3)_2$ / *cis*-$Pt(NBA)_2(H_2O)_2$ **(33)** / **(34)**] was collected and used in the next step with no further purification. The clear filtrate was transferred to 50 ml RBF to which sodium 4-trifluoromethyl benzoate **(14)** (75 mg, 0.34 mmol) were added. The mixture was stirred at room temperature for 48 hours. The resulting precipitate was collected by filtration, washed with DDW, and dried under vacuum. The final product [*cis*-(di n-butylamine)]bis(4-trifluoromethylbenzoato)platinum(II); [*cis*-$Pt(NBA)_2(TFBA)_2$] **(37)** was collected as a white powder.

Yield: 82.35% (101 mg; 0.14 mmol). FTIR: 3200,3146 (N-H stretching), 2959,2928 (C-H stretching), 1611 (C=O stretching), 1384 (C-O stretching), 1161 (C-F stretching)

2.3.14 Synthesis of [*cis*-di(piperidine)]bis(myristato)platinum(II); [*cis*-Pt(PIP)$_2$(MYR)$_2$] (40)

Cis-di(piperidine)diiodidoplatinum(II) (*cis*-(PIP)$_2$PtI$_2$) **(6)** (100 mg, 0.16 mmol) was suspended in DDW (10 ml) in an aluminum foil-covered round-bottom flask, to which 1.99 equivalents of $AgNO_3$ (55 mg, 0.32 mmol) were added. The mixture was stirred at room temperature for 72 hours. Yellow insoluble precipitate turned into a yellowish-gray-colored one. The precipitate containing AgI was filtered off under suction. Following washing with an additional 10 ml DDW the filtrate [*cis*-Pt(PIP)$_2$(NO$_3$)$_2$ / *cis*-Pt(PIP)$_2$(H$_2$O)$_2$ **(38)** / **(39)**] was collected and used in the next step with no further purification. The clear filtrate was transferred to 50 ml RBF to which sodium myristate **(12)** (85 mg, 0.32 mmol) were added. The mixture was stirred at room temperature for 48 hours. The resulting precipitate was collected by filtration, washed with DDW, and dried under vacuum. The final product [*cis*-di(piperidine)]bis(myristato)platinum(II); [*cis*-Pt(PIP)$_2$(MYR)$_2$] **(40)** was collected as a white powder.
Yield: 95.6% (126 mg; 0.153 mmol). FTIR: 3200,3147 (N-H stretching), 2918,2851 (C-H stretching), 1612 (C=O stretching), 1380 (C-O stretching), 552 (Pt-N stretching), 435 (Pt-O stretching).

2.3.15 Synthesis of [*cis*-di(piperidine)]bis(4-ethylbenzoato)platinum(II); [*cis*-Pt(PIP)$_2$(EBZ)$_2$] (41)

Cis-di(piperidine)bis(iodido)platinum(II) (*cis*-(PIP)$_2$PtI$_2$) **(6)** (105 mg, 0.17 mmol) was suspended in DDW (10 ml) in an aluminum foil-covered round-bottom flask, to which 1.99 equivalents of $AgNO_3$ (58 mg, 0.34 mmol) were added. The mixture was stirred at room temperature for 72 hours. Yellow insoluble precipitate turned into a yellowish-gray-colored one. The precipitate containing AgI was filtered off under suction. Following washing with an additional 10 ml DDW the filtrate [*cis*-Pt(PIP)$_2$(NO$_3$)$_2$ / *cis*-

$Pt(PIP)_2(H_2O)_2$ **(38)** / **(39)**] was collected and used in the next step with no further purification. The clear filtrate was transferred to 50 ml RBF to which sodium 4-ethyl benzoate **(16)** (61.30 mg, 0.34 mmol) was added. The mixture was stirred at room temperature for 48 hours. The resulting precipitate was collected by filtration, washed with DDW, and dried under vacuum. The final product [*cis*-di(piperidine)]bis(4-ethylbenzoato)platinum(II); [*cis*-$Pt(PIP)_2(EBZ)_2$] **(41)** was collected as a white powder.
Yield: 44.7% (51 mg; 0.076 mmol). 3200,3155 (N-H stretching), 2974,2922 (C-H stretching), 1601 (C=O stretching), 1378 (C-O stretching), 436 (Pt-O stretching).

2.3.16 Synthesis of [*cis*-di(piperidine)]bis(4-trifluoromethylbenzoato)platinum(II); [*cis*-$Pt(PIP)_2(TFBA)_2$] (42)

Cis-$(PIP)_2PtI_2$) **(6)** (100 mg, 0.16 mmol) was suspended in DDW (10 ml) in an aluminum foil-covered round-bottom flask, to which 1.99 equivalents of $AgNO_3$ (55 mg, 0.32 mmol) were added. The mixture was stirred at room temperature for 72 hours. Yellow insoluble precipitate turned into a yellowish-gray-colored one. The precipitate containing AgI was filtered off under suction. Following washing with an additional 10 ml DDW the filtrate [*cis*-$Pt(PIP)_2(NO_3)_2$ / *cis*-$Pt(PIP)_2(H_2O)_2$ **(38)** / **(39)**] was collected and used in the next step with no further purification. The clear filtrate was transferred to 50 ml RBF to which sodium 4-trifluoromethyl benzoate **(14)** (72 mg, 0.32 mmol) was added. The mixture was stirred at room temperature for 48 hours. The resulting precipitate was collected by filtration, washed with DDW, and dried under vacuum. The final product [*cis*-di(piperidine)]bis(4-trifluoromethylbenzoato)platinum(II); [*cis*-$Pt(PIP)_2(TFBA)_2$] **(42)** was collected as a white powder.
Yield: 88.2% (110 mg; 0.15 mmol). 3100,3050 (N-H stretching), 2976,2896 (C-H stretching), 1607 (C=O stretching), 1324 (C-O stretching), 1166 (C-F stretching), 488 (Pt-N stretching), 435 (Pt-O stretching).

2.3.17 Synthesis of [*cis*-di(piperidine)]bis(acetate)platinum(II); [*cis*-$Pt(PIP)_2(acetate)_2$] (43)

Cis-$(PIP)_2PtI_2$) **(6)** (107.80 mg, 0.17 mmol) was dissolved in chloroform (10 ml) in an aluminum foil-covered round-bottom flask, to which two equivalents of sodium Acetate **(24)** (82 mg,0.35 mmol) were added and dissolved as well. To the mixture two equivalents of $AgNO_3$ (59 mg,0.35 mmol) were added. The mixture was left stirring overnight and was filtrated off using celite within filter glass then it was washed with 4 ml chloroform. The filtrate was evaporated to dryness using a rotary evaporator. an orange-yellowish layer was formed around the RBF. 1 ml of methanol was added then it was left overnight at room temperature. The resulting precipitate was collected by filtration and dried under a vacuum. The final product [*cis*-(di(piperidine)]bis(acetate)platinum(II); [*cis*-$Pt(PIP)_2(acetate)_2$] **(43)** was collected as dark brownish powder. Yield: 21.8% (18.1 mg, 0.037 mmol).

2.3.18 Synthesis of [*cis*-di(pyridine)]bis(myristato)platinum(II)[*cis*-$Pt(PYR)_2(MYR)_2$] (47)

2.3.18.1 Synthesis of [*cis*-di(pyridine)]bis(chloroplatinum(II)); [*cis*-$Pt(PYR)_2(Cl)_2$] (44)

Potassium tetrachloroplatinate K_2PtCl_4 **(1)** (205 mg, 0.494 mmol) were dissolved in DDW (20 ml) at room temperature. While stirring Pyridine (80 µl, 0.988 mmol) were added. The mixture was stirred at room temperature overnight. A fine yellow precipitate of [*cis*-di(pyridine)]bis(chloroplatinum(II)); [*cis*-$Pt(PYR)(Cl)_2$] **(44)** was formed. The compound was collected by filtration, washed with 10 ml DDW, and dried by vacuum filtration, [*cis*-$Pt(PYR)_2Cl_2$) **(44)** was transferred to a vial and dried in a desiccator (KOH) under vacuum for 48 hr. They were used subsequently without any further purification. Yield: 82.38% (172.8 mg, 0.407 mmol)

2.3.18.2 Synthesis of [*cis*-di(pyridine)]bis(myristato)platinum(II)[*cis*-$Pt(PYR)_2(MYR)_2$] (47)

Cis-Pt $(PYR)_2(Cl)_2$ **(44)** (64.2 mg, 0.15 mmol) was suspended in DDW (10 ml) in an aluminum foil-covered round-bottom flask, to which 1.99 equivalents of $AgNO_3$ (51.16

mg, 0.30 mmol) were added. The mixture was stirred at room temperature for 48 hours. Yellow insoluble precipitate turned into a milky yellow color, and the precipitate containing AgI was filtered off under suction. Following washing with an additional 10 ml DDW the filtrate [*cis*-$Pt(PYR)_2(NO_3)_2$ /*cis*-$Pt(PYR)_2(H_2O)_2$ **(45)**/**(46)**] were collected and used in the next step with no further purification. The clear filtrate was transferred to 50 ml RBF to which sodium myristate **(11)** (79.56 mg, 0.302 mmol) was added. The mixture was stirred at room temperature for 24 hours. The fine white precipitate was transferred to a 50 ml tube and centrifuged. The above filtrate was removed, and the product was put to dry in a desiccator. The final product [*cis*-di(pyridine)]bis(myristato)platinum(II)[*cis*-$Pt(PYR)_2(MYR)_2$] **(47)** was collected as a white powder.

Yield: 28.7% (35.4 mg; 0.043 mmol). FTIR: 2967,2916(C-H stretching), 1581 (C=O stretching), 1381 (C-O stretching), 1285 (C-N stretching), 433 (Pt-O stretching).

2.3.19 Synthesis of [*cis*-di(pyridine)]bis(4-ethylbenzoato)platinum(II); [*cis*-$Pt(PYR)_2(EBZ)_2$] (48)

Cis-Pt-$(PYR)_2(Cl)_2$ **(44)** (118.3 mg, 0.28 mmol) was suspended in DDW (10 ml) in an aluminum foil-covered round-bottom flask, to which 1.99 equivalents of $AgNO_3$ (95 mg, 0.56 mmol) were added, and the mixture was stirred at room temperature for 48 hours. Yellow insoluble precipitate turned into a milky-colored precipitate, and the precipitate containing AgI was filtered off under suction. Following washing with an additional 10 ml DDW the filtrate [*cis*-$Pt(PYR)_2(NO_3)_2$ / *cis*-$Pt(PYR)_2(H_2O)_2$ **(45)** / **(46)**] were collected and used in the next step with no further purification. The clear filtrate was transferred to 50 ml RBF to which sodium 4-ethyl benzoate **(16)** (96 mg, 0.56 mmol) was added. The mixture was stirred at room temperature for 24 hours. The resulting precipitate was collected by filtration, washed with DDW, and dried under vacuum. The final product [*cis*-(di(pyridine)]bis(4-ethylbenzoato)platinum(II); [*cis*-$Pt(PYR)_2(EBZ)_2$] **(48)** was collected as a white powder.

Yield: 14.6% (26.6 mg; 0.041 mmol). FTIR: 2977, 2924 (C-H stretching), 1667 (C=O stretching), 1383 (C-O stretching), 1250 (C-N stretching).

2.3.20 Synthesis of [*cis*-di(pyridine)]bis(4-trifluoromethylbenzoato)platinum(II); [*cis*-Pt(PYR)$_2$(TFBA)$_2$] (49)

Cis-Pt(PYR)$_2$(Cl)$_2$ **(44)** (108 mg, 0.25 mmol) was suspended in DDW (10 ml) in an aluminum foil-covered round-bottom flask, to which 1.99 equivalents of AgNO3 (86 mg, 0.50 mmol) were added, and the mixture was stirred at room temperature for 48 hours. Yellow insoluble precipitate turned into a milky, yellow-colored. The precipitate containing AgI was filtered off under suction. Following washing with an additional 10 ml DDW the filtrate [*cis*-Pt(PYR)$_2$(NO$_3$)$_2$ / *cis*-Pt(PYR)$_2$(H$_2$O)$_2$ **(45)** / **(46)**] were collected and used in the next step with no further purification. The clear filtrate was transferred to 50 ml RBF to which sodium 4-trifluoromethyl benzoate **(14)** (113.26 mg, 0.51 mmol) was added. The mixture was stirred at room temperature for 24 hours. The resulting precipitate was collected by filtration, washed with DDW and dried under vacuum. The final product [*cis*-(di-pyridine)]bis(4-trifluoromethylbenzoato)platinum(II); [*cis*-Pt(PYR)$_2$(TFBA)$_2$] **(49))** was collected as a white powder.

Yield: 36.4% (66.6 mg; 0.091 mmol). FTIR: 2974,2927 (C-H stretching), 1609 (C=O stretching), 1379 (C-O stretching), 1252 (C-N stretching), 1165 (C-F stretching), 487 (Pt-N stretching).

2.3.21 Synthesis of [ethylenediamine]bis(4-ethylbenzoatodihydroxyplatinum(IV)); [*cis, cis, trans*-Pt(EN)(EZB)$_2$(H$_2$O)$_2$] (50)

Cis-Pt(EN)(EZB)$_2$ **(31)** (23.6 mg, 0.043 mmol) were added to 1 ml of hydrogen peroxide (H_2O_2), in an aluminum foil-covered round-bottom flask. The mixture was stirred at room temperature for 24 hours. The resulting precipitate was collected by filtration and dried under a vacuum. The final product of [ethylenediamine]bis(4-ethylbenzoatodihydroxyplatinum(IV)); [*cis, cis, trans*-Pt(EN)(EZB)$_2$(H$_2$O)$_2$] **(50)**) was collected as a whitish powder. Yield: 58.14% (15 mg; 0.025 mmol).

2.3.22 Synthesis of [*cis*-di(piperidine)]bis(4-trifluoromethylbenzoatodihydroxyplatinum(IV)); [*cis, cis, trans*-$Pt(PIP)_2(TFBA)_2(H_2O)_2$] (51)

Cis-$Pt(PIP)_2(TFBA)_2$ **(42)** (21.3 mg, 0.029 mmol) were added to 1 ml of hydrogen peroxide (H_2O_2), in an aluminum foil-covered round-bottom flask. The mixture was stirred at room temperature for 24 hours. The resulting precipitate was collected by filtration and dried under vacuum. The final product of [*cis*-(di-piperidine)]bis(4-trifluoromethylbenzoatodihydroxy-platinum(IV)); [*cis, cis, trans*-$Pt(PIP)_2(TFBA)_2(H_2O)_2$] **(51)** was collected as whitish powder.
Yield: 69 % (15.6 mg; 0.020 mmol).

2.4 Preparation of the Platinum Derivatives Loaded in Niosomes

The technique used to prepare niosomes was the thin film hydration technique. 1 mg of the platinum derivative with a cholesterol mixture with Tween 80 (100:100 mM ratio) were weighed adequately and then dissolved in a 10 ml chloroform mixture. Subsequently, the solvent was evaporated by a rotary evaporator, and the solvent mixture was evaporated until dry, obtaining a thin film of the lipid with a white appearance. Followed by the addition of 10 mL of Milli-Q water to hydrate the film. The flask was heated to 55ºC for 60 minutes while stirring at 20 rpm to obtain a white suspension. After that, the obtained suspension was sonicated for 20 minutes to get fine vesicles and then kept at 4 ºC for additional analysis.

2.5 Platinum Derivatives Loading Efficiency

Once the Pt derivative was loaded into the Niosome nanoparticles, they were centrifuged at 5000 rpm for 10 min to remove the excess free Pt derivative. Then, the loaded amount was determined by UV-Vis spectroscopy based on a developed calibration curve at its λ_{max}. Loading efficiency of Pt derivative (%) = (amount of the loaded Pt derivative/total amount of Pt derivative applied)*100%.

2.6 Anticancer Activity

2.6.1 *Cell Culture*

The anticancer activity of the developed Niosomes was evaluated on liver cancer cells (Hep-G2, Hep-3B) and normal liver cells (LX2). The cells have been cultured in T-175 cell culture flasks added with a cell culture growth medium (CGM) consisting of RPMI basal medium supported with FBS (10%), *L*-glutamine (1%), and penicillin/streptomycin (1%). The cells were stored in a standard cell culture incubator under special circumstances; 99% humidity, 5% CO_2 and 37 ºC.

During the sub-culturing stage, the medium has been suctioned and then washed with an excess of Ca^{2+}-free phosphate-buffered saline. Afterward, the cells were incubated with 0.025% trypsin for 5 minutes inside the cell culture incubator until sufficient cells were separated from the flask. Subsequently, trypsin has been inactivated by CGM, the cell suspension has been assembled, and the viable cell count has been measured by using trypan blue stain before adjusting the cell concentration to 50.000 cells/ml. Lastly, the cells have been cultivated in a 96-well plate with 5000 cells/well. The cells have been left to attach and accommodate the whole night before making any test.

2.6.2 *Cytotoxicity Test*

A concentration-dependent cytotoxicity experiment was performed for pt derivatives loaded niosomes (11.172-75 µM) under a 7.4 pH condition, where 100 µl of the test medium was used per well. After overnight incubation with the test conditions, 20 µl of MTS reagent was added to the whole wells and then incubated for 1 hour in a cell culture incubator. Finally, the absorbance was determined at 490 nm by a plate reader.

Chapter Three

Results and Discussion

3 Result and Discussion

The group of drugs known as platinum-based drugs (Pt-based) have proven to be an excellent example of a type of therapy that has broad anticancer efficacy, especially in patients with solid tumors(Kilari et al., 2016). However, despite their initial success, they are obstructed by two primary challenges: cellular resistance and severe toxicity profiles due to the lack of specificity, causing kidney damage, neurotoxicity, ototoxicity, and other cell damage associated with cisplatin treatment and other established platinum drugs(Kasparkova et al., 2008; Lee et al., 2003; Y. R. Zheng et al., 2014). In response to these limitations, significant investigations have been conducted on the compounds themselves by synthesizing several analogs characterized through the modification of ligands or alterations in the oxidation state of the metal from platinum(II) to platinum(IV), and using a suitable drug delivery system(DDS) to enhance therapeutic efficacy and reduce adverse reactions to these compounds. This influences the loading efficiency, encapsulation yield, formulation stability, cellular uptake, and drug release(J. Chen et al., 2021; Dilruba & Kalayda, 2016; S. Liu et al., 2016).

Several platinum drugs have been encapsulated in many types of DDS, liposomes and the micelles encapsulation system were the most successful. They have successfully entered the clinical trials, but none were approved, some due to enabling the therapeutic effect of the already existing drugs or reducing the side effects from the toxicity and resistance of the cells and the slow release of the drug itself from the DDS(Belkacemi et al., 2018; D. Liu et al., 2013; Xiaoyong & Zijian, 2012).

The idea of having a compatible drug design with the use of DDS has emerged as a way to handle the side effects of the encapsulated drug with the advantage of being less toxic and more pre*cis*e by delivering it through DDS. One of the methods is to incorporate Pt-synthetic derivatives of cytotoxic drugs into lipid-based drug formulations, which could be a strategic way to combat increasing drug resistance and reduce the side effects of these drugs(S. Liu et al., 2016; Ringhieri et al., 2016). With the use of an appropriate vesicular drug delivery system such as niosomes(Abdelkader et al., 2011; Obeid et al., 2023).

Niosomes are spherical vesicles composed of nonionic surfactants. They have a similar structure to the liposomal formulation but offer more advantages, including improved stability as they have non-ionic surfactants that are more stable compared to the phospholipids in the liposomes, which are more fragile and need a special condition in

storing them, and lower manufacturing costs compared to the liposomes as well(Kaur & Kumar, 2018).

In this study, we designed, synthesized, purified, and characterized novel Pt(II/IV) complexes comprising aromatic–lipophilic ligands that were encapsulated in a niosomal formulation and evaluated their dispersion in the niosomes, which is influenced by the physicochemical characteristics of the substituent's ligand with the coordination to the Pt-core, anticancer activity in *vitro* using liver cancer cells (Hep-G2 and Hep-3B) and normal liver cells (LX2).

3.1 Synthesis of the Platinum Compound

The design of the novel platinum(II/IV) compounds involved three steps:

1. Synthesizing the intermediate materials, the chelating ligands of Pt(II) complex are bidentate amine (DACH and EN) or monodentate amine (NBA, PIP, and PYR) [*cis*-$(NHR)_2PtI_2$]/ [*cis*-$(NHR)_2PtCl_2$].
2. Synthesizing of the lipophilic leaving ligand of sodium carboxylate
    a. Sodium myristate (aliphatic tail with high lipophilicity)
    b. Sodium 4-trifluoromethyl benzoate and sodium ethylbenzoate (aromatic tail).
3. Synthesis of the novel platinum compound through the combination of the intermediate complex with the carboxylate ligand.

3.1.1.1 Synthesis of diamminedichloridoplatinum(II), [*cis*-[$Pt(NH_3)_2Cl_2$], Cisplatin] (10)

Cisplatin is the first platinum-based anticancer drug to be used and is considered one of the positive controls in this study for the cytotoxic effects of the other synthesized drugs. It was synthesized according to the Dhar method in 1970(Dhar and Lippard, 2009).

Starting from potassium tetrachloropaltinate(II) [K_2PtCl_4] **(1)** dissolving in water, a light brown color mixture was subjected to ligand exchange by adding an excess amount of a saturated solution of potassium iodide (KI) to form tetraiodoplatinate(II) [K_2PtI_4] **(2).** The dark brown mixture was stirred for 20 to 30 minutes, which is

enough time for the exchange to occur. The addition of an excess amount of a saturated solution of KI is to ensure that K_2PtCl_4 **(1)** is completely converted to K_2PtI_4 **(2)**, (**Scheme 3.1.1**) The halides like Cl, Br and I are known as libeled ligands that are easily replaced by inert ligands like amines that are needed in the second step. After adding the ammonia (NH_3), it replaced the iodide ligand. The first exchange of (NH_3) is done easily, but the second exchange position of the ammine group has an option, either exchange with the iodide ligand that is in the *trans* position with the first reacted ammonia, or exchange with the ligand that is in the *cis* position with the first reacted ammonia (*trans* with the other iodide ligand). Due to the strong *trans* effect of the iodide ligand, which influences the substation of the NH_3 ligand to a transposition with the other iodide ligand (*cis* with the NH_3 ligand), ensuring the formation of the insoluble intermediate compound *cis*-diaminodiiodoplatinum(II) (*cis*-$Pt(NH_3)_2I_2$) **(7)**. However, if K_2PtCl_4 **(1)** is directly converted into **[**$PtCl_2(NH_3)_4$] by adding the ammonia and then treated with HCl, it might yield transplatin **(52)** as the final product instead of cisplatin **(10)** as the Cl is kinetically competitive with NH_3 thus yielding a small portion of the *trans* isomer(Wilson & Lippard, 2014a).

Cis-$Pt(NH_3)_2I_2$) **(7)** is collected by filtration and dried under suction as a yellow powder. The insoluble *cis*-$Pt(NH_3)_2I_2$) **(7)** was treated with $AgNO_3$ in water, for the substitute of iodide ligand with nitrate or water forming the soluble intermediate *cis*-diamminodiaquaplatinum(II)/*cis*-diamminodinitratoplatinum(II) [*cis*-$Pt(NH_3)_2(H_2O)_2$ **(8)/** *cis*-$Pt(NH_3)_2(NO_3)_2$ **(9)]** and the insoluble byproduct AgI as precipitate, which was filtered out. Excess HCl was added to the filtrate containing *cis*-$Pt(NH_3)_2(H_2O)_2$ **(8)** / *cis*-$Pt(NH_3)_2(NO_3)_2$ **(9)** to obtain cisplatin [*cis*-$Pt(NH_3)_2Cl_2$] **(10)** which was filtrated out and dried as a pure yellow powder**.** Yield**:** 63.8%.

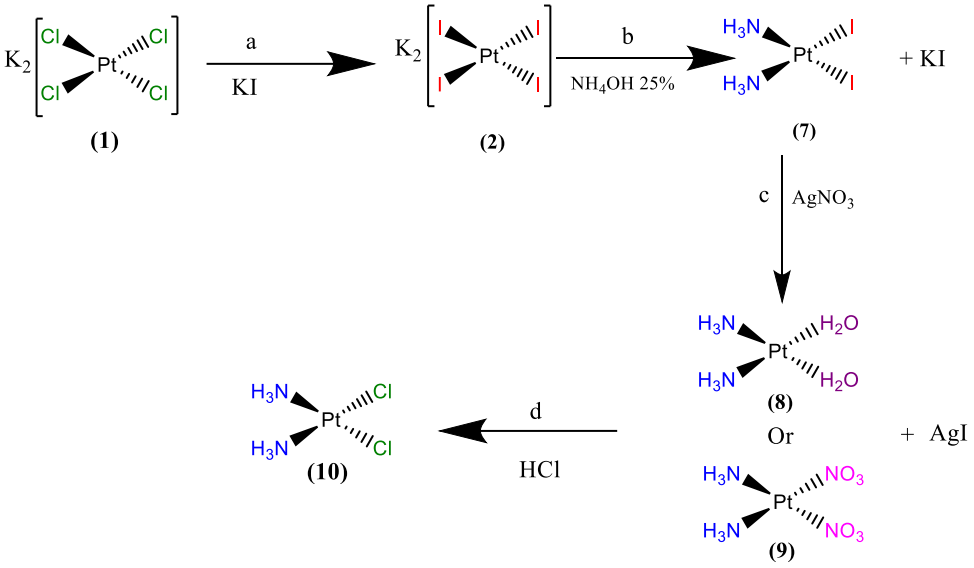

Scheme 3.1.1 Synthesis of cisplatin **(10)** starting from (K_2PtCl_4) **(1)**. Reagents and conditions; a) 8 equiv. (KI), 10 ml DDW, r.t, 20 min ;b) 3 equiv. NH_4OH 25%, 10 ml DDW, r.t, 24 hr., filtration and drying under suction, yield: 78.3%, ;c) 2 equiv. ($AgNO_3$), 10 ml of DDW, r.t, 36 hr., filtrate, wash ;d) (35% HCl),10 ml of DDW r.t, 24 hr., filtrate and drying under suction, 63.8%.

3.1.2 Synthesis of *cis*-(alkylamine)diiodoplatinum(II) complexes [*cis*- $(NHR)_2PtI_2$]

To synthesize the Pt(II) complex of interest the chelate ligand of the type *cis*-(alkylamine)diiodoplatinum(II) complexes [*cis*-$(NHR)_2PtI_2$] needed to be synthesized. The [*cis*-$(NHR)_2PtI_2$], were synthesized according to the previously reported procedure(Al-baker & Dabrowiak, 1987).

Starting from potassium tetrachloropaltinate(II) [K_2PtCl_4] **(1)**, ligand exchange was performed to synthesize tetraiodoplatinate(II) [K_2PtI_4] **(2)** by adding a saturated solution of KI. After twenty to thirty minutes of stirring the mixture, the intermediate materials are added to the stirred mixture, reaction time varies from 24 to 72 hours depending on the intermediate ligand. The bidentate ligand (1*R*,2*R*)-diaminocyclohexane "DACH", and ethylenediamine (EN)) forms a more stable complex compared to the complex with a monodentate ligand, The exchange reaction with the labile ligand are exchanged at once in the case of the bidentate ligand, and forming the bidentate ligands between the two amine ligands in the compound

ensures the formation of a *cis* compound (**Scheme 3.1.2**). As for the other intermediate, the *cis* formulation is determined by the strong *trans* effect of the iodide ligand.

The yield ranges from very good to acceptable 81%, 88%, 78.4%, 88.67% , 60.77% and 82.38% receptively [*cis*-Pt(DACH)I_2] **(3)**, [*cis*-Pt(EN)I_2] **(4)**, [*cis*-Pt(NBA)$_2I_2$] **(5)**, [*cis*-Pt(PIP)$_2I_2$] **(6)**, [*cis*-Pt(DACH)Cl_2] **(17)**, [*cis*-Pt(PYR)$_2Cl_2$] **(44)]**.

The yield of this type of complex is usually excellent as reported in the literature, with 96% for both *cis*-Pt(DACH)I_2 **(3)** and [*cis*-Pt(DACH)Cl_2] **(17)** and 92% for *cis*-Pt(PIP)$_2I_2$ **(6)**(De Oliveira et al., 1996; Marzo et al., 2018; Pažout et al., 2011).

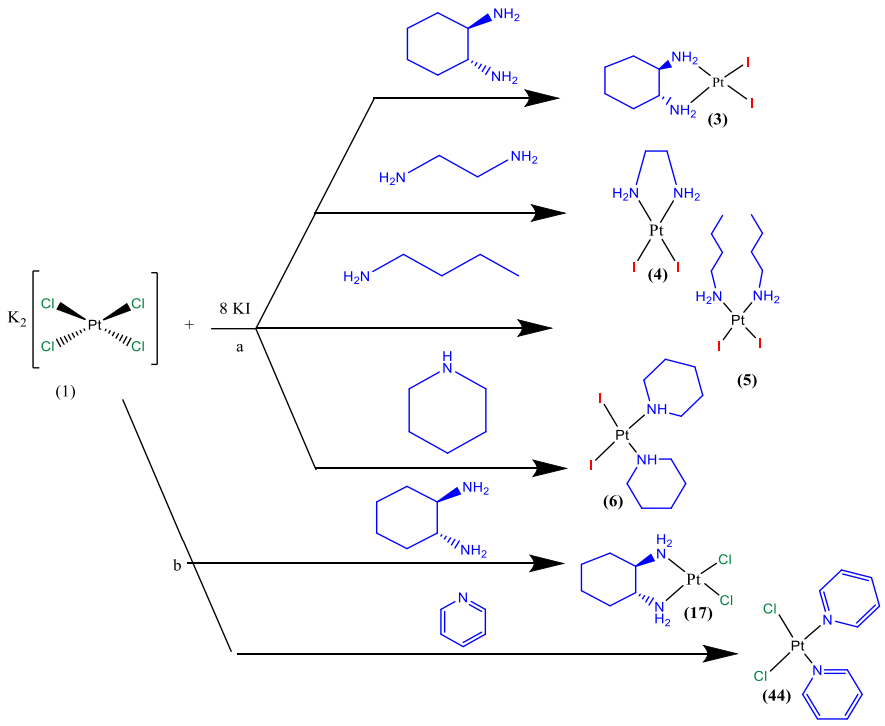

Scheme 3.1.2 Synthesis of *cis*-(alkylamine)diiodoplatinum(II) complexes [*cis*-(RNH,)PtI_2], [*cis*-(DACH)PtI_2] **(3)**, [*cis*-(EN)PtI_2] **(4)** [*cis*-(NBA)$_2PtI_2$] **(5)**, [*cis*-(Pip)$_2PtI_2$] **(6)**, from (K_2PtCl_4) **(1).** Reagents and conditions; a) KI, 40 ml of DDW, r.t, 20 minutes, 2 equiv. intermediate materials (DACH, or ethylenediamine, or piperidine, or n-butyl amine) r.t., 24 to 72 hr., filtrate, drying under suction, Yield: **(3)** 81%; **(4)** 88%; **(5)** 78.4%; **(6)** 88.66%; b) 2 equiv. intermediate materials, (DACH or Pyridine**),** 20 ml of DDW r.t., 24 hr., filtrate, drying under suction. Yield: **(17)**, 60.77%, **(44)** 82.38%.

3.1.3 Synthesis of [(1*R*,2*R*)-cyclohexane-1,2-diamine-N,N′]bis(tetradecanoato-O)platinum; [*cis*-Pt(DACH)(MYR)$_2$], Miriplatin] (19)

3.1.3.1 Synthesis of carboxylate ligands [sodium myristate (12), sodium 4-trifluoromethyl benzoate (14) and sodium 4-ethyl benzoate (16)]

To synthesize the Pt(II) complexes of interest the carboxylate ligands needed to be prepared. The carboxylate ligands were synthesized as the corresponding sodium salt employing documented procedures(Zacharie et al., 2009). The desired acid was initially dissolved in ethanol (EtOH) and .95 equivalents of sodium bicarbonate ($NaHCO_3$) were added. The cloudy mixture was stirred under reflux for a period of 3-4 hours through which CO_2 gas was liberated and the acid was converted to its corresponding sodium salt. It was noticed that in the case of sodium 4-trifluoromethyl benzoate **(14)** and sodium 4-ethyl benzoate **(16)** a white precipitate started to appear after two hours of heating, while more time was needed before any precipitate was formed in the case of sodium myristate **(12)**. One explanation, the difference in the solubility between the sodium salts is rooted in lipophilicity difference. After cooling to room temperature and to allow completion of the reaction and quantitative precipitation, the mixture was stirred overnight. The volatile compounds were removed under reduced pressure using a rotary evaporator. The product was collected from the rotary evaporator by scabbing using a spatula and then placed in a desiccator (with KOH). It is worth mentioning that when filtration was used to collect and dry the final product, the precipitate blocked the pores of the sintered glass, which made the filtration a tedious and lengthy step, and most importantly, a lot of the product was lost, resulting in a lower yield. The yield in this step ranged from very good to excellent. For example, the yields of sodium myristate **(12)**, sodium 4-trifluoromethyl benzoate **(14)**, and sodium 4-ethyl benzoate **(16)** were 95.54 %, 90%, and 84%, respectively, this yields are expected to be high similarly to the documented procedures(Zacharie et al., 2009).

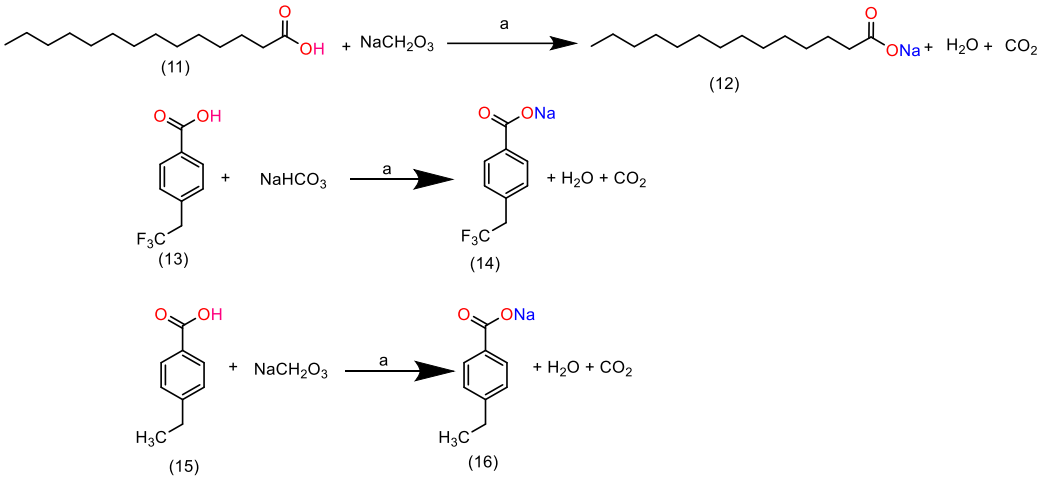

Scheme 3.1.3.1 Synthesis of sodium carboxylates by reacting acids and sodium bicarbonate. Reagents and conditions: a) EtOH ml, stirring, reflux for 3 to 4 hr., and drying using a rotary evaporator, dry in a desiccator (with anhydrous KOH), **(12)** yield: 95.54% **(14)** yield: 84% and **(16)** yield: 90%(Zacharie et al., 2009).

3.1.3.2 Synthesis of (1*R*,2*R*)-diaminocyclohexanedimyristato platinum(II) [Miriplatin; (*cis*-Pt(DACH)(MYR)$_2$] (19)

[(1*R*,2*R*)-cyclohexane-1,2-diamine-N,N′]bis(tetradecanoato-O)platinum; [*cis*-Pt(DACH)(MYR)$_2$], Miriplatin] **(19)** was prepared in the current study. Two methods were tried.

Method 1

Based on(Q. Wang & Pu, 2015) synthetic procedure, silver myristate [$CH_3(CH_2)_{12}COOAg$; **(18)**] was synthesized by reacting sodium myristate $CH_3(CH_2)_{12}COONa$ **(12)** with silver nitrate ($AgNO_3$). The reaction was performed at 60 °C and the ion exchange was quick and quantitative. To get rid of the $NaNO_3$ traces the precipitate was suspending in water, washed, and filtrated. The next step. i.e. ligand exchange of chlorides with myristate was accomplished by reacting silver myristate with [(1*R*,2*R*)-cyclohexane-1,2-diamine]bis(chloroplatinum(II)); [*cis*-Pt(DACH)Cl_2] **(17)** in double-distilled water. Though the ligand exchange was fast and quantitative, the precipitation of AgCl precipitate off was tedious compared to the filtration of AgI. Seemingly due to a similar degree of solubility, both AgCl and miriplatin **(19)** got concurrently precipitated. Purifying miriplatin **(19)** by simple filtration and while heating the solution turned out to be problematic.

Efforts to purify miriplatin **(19)** by solubility-based differences in water turned out to be fruitless as well. Initially by adding extra volume of DDW or by warming the solution ended up in a reduced amount of the desired product. Realizing that AgCl forms finer particles (reduced size) compared to AgBr or AgI and that AgCl has higher water solubility compared to AgI (Ksp = 1.77×10^⁻10 and 8.52 × 10 ^⁻17 for AgCl and AgI respectively). Both facts lead us to adopt a two-step AgI-based approach(Pažout et al., 2011; Q. Wang & Pu, 2015).

The desired product (miriplatin) **(19)** was collected as a white-to-beige colored powder after filtration, washing with ethanol, and drying under vacuum. Compound **(19)** was stored desiccated over anhydrous potassium hydroxide. The produced amount was insufficient.

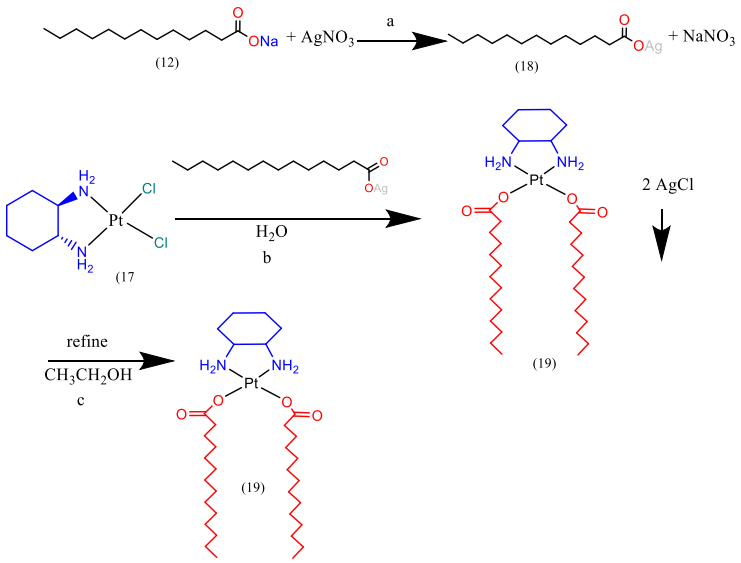

Scheme 3.1.3.2.1 Synthesis of miriplatin **(19)** starting from silver myristate **(18)** and Pt(DACH)Cl_2 **(17)** via synthesis of silver myristate **(18)** from sodium myristate and adding it to Pt(DACH)Cl_2 **(17)** and refining the product. Reagents and conditions: a) 2 equiv. $AgNO_3$, 3 ml DDW, stirring at 60 °C, r.t, 0.5 hr., washing with DDW and ethanol.; b) 5ml DDW, stirring. r.t. 24 hr., filtration, washing with DDW and ethanol; c) 20 ml ethanol, stirring at 80 °C, .r.t, 15 min, filtration, washing with DDW and ethanol(Q. Wang & Pu, 2015).

Method 2

In this method, miriplatin **(19)** was prepared following an alternative sequence of ligand exchange steps and by employing the iodide form of platinum(II) species. Briefly, Pt(DACH)I_2 **(3)** was allowed to react with $AgNO_3$ under dark conditions. The diaqua/dinitrato intermediate *cis*-Pt(DACH)$(H_2O)_2$/*cis*-Pt(DACH)$(NO_3)_2$ **(20)**/**(21)** was collected following filtrating the precipitate AgI off.

The previously prepared sodium myristate **(12)** was added to the diaqua/dinitrato [*cis*-Pt(DACH)$(H_2O)_2$/*cis*-Pt(DACH)$(NO_3)_2$ **(20)**/**(21)**] and left to stand at room temperature overnight. Displacement of diaqua/dinitrato by myristate resulted in affording miriplatin **(19)** as a white-to-beige colored precipitate. **(19)** was collected by filtration, washed with DDW, and dried under suction. Yield: 91%.

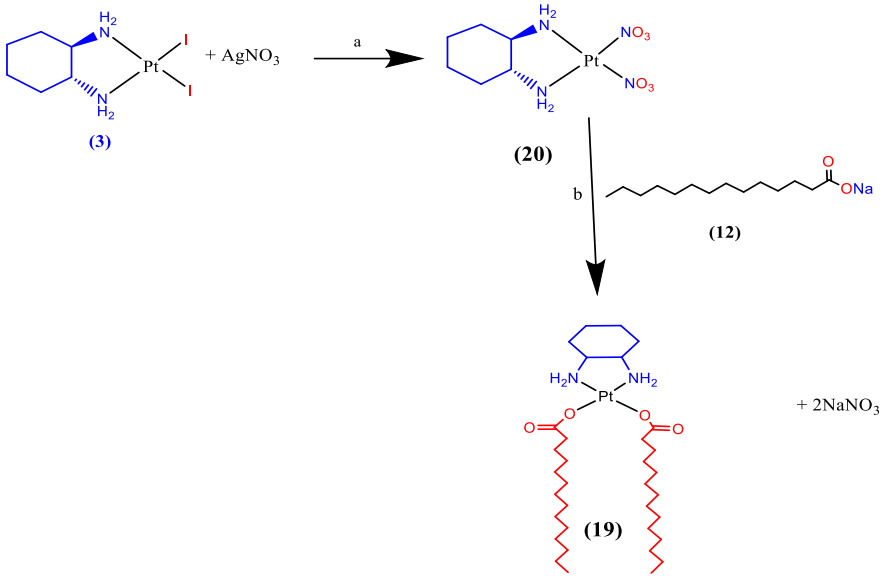

Scheme 3.1.3.2.2 Synthesis of miriplatin **(19)** from Pt(DACH)I_2 **(3)**. Reagents and conditions: a) 1.99 equiv. silver nitrate ($AgNO_3$), 10 ml DDW, r.t, 48 hr.; b) filtration, sodium myristate **(12)**, r.t, 24 hr., filtration, drying under suction. Yield: 91%.

3.1.4 Synthesis of [(1*R*,2*R*)-cyclohexane-1,2-diamine](ethanedioato-O,O')platinum(II) (Oxaliplatin) (23)

The synthesized [(1*R*,2*R*)-cyclohexane-1,2-diamine]bis(chloroplatinum(II)); [*cis*-Pt(DACH)Cl_2] **(17)** was converted to the diaqua/dinitrato [*cis*-Pt(DACH)$(H_2O)_2$/ *cis*-

$Pt(DACH)(NO_3)_2$ **(20)/(21)]** by ligand exchange reaction with silver nitrate ($AgNO_3$). After filtrating off AgCl and washing with water the filtrate was collected. Sodium oxalate **(22)** was dissolved in a little DDW (1 to 2 ml) and it was added portion-wise to the filtrate, this proved to be a more efficient way than adding it at once without dissolving it first to which the produced amount would not be accurate as the amount of used DDW played an important part it needs to be the minimum, some of the product would be soluble in the filtrate and need to be extracted due to the solubility of as every 6 mg/ml it is soluble in DDW. The mixture was stirred at room temperature overnight during which a white-creamy precipitate was formed. The desired oxaliplatin was collected by filtration. After washing with cold DDW and drying using suction, the powder was transferred into a vial stored as desiccated over anhydrous potassium hydroxide. A fine white garish of [(1*R*,2*R*)-cyclohexane-1,2-diamine](ethanedioato-O,O')platinum(II) ; (Oxaliplatin) **(23)** was synthesized. Yield: 15.8%.

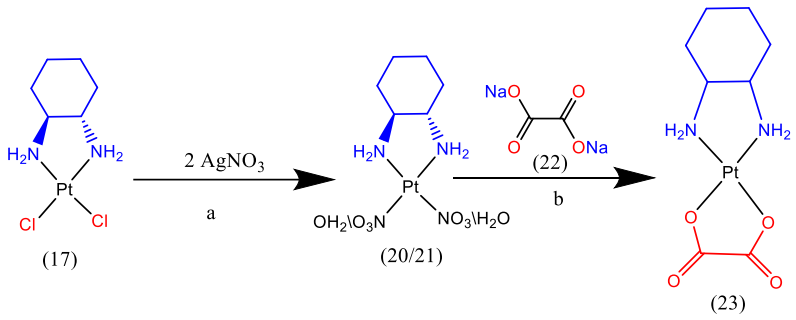

Scheme 3.1.4 Synthesis of oxaliplatin **(23)** starting from $Pt(DACH)Cl_2$ **(17)** and $AgNO_3$ via the intermediate *cis*-$Pt(DACH)H_2O$/ *cis*-$Pt(DACH)NO_3$ **(20)/(21)** from the reaction with, finally adding sodium oxalate **(22)** to form oxaliplatin. Reagents and conditions: a) 2 eqiuv. $AgNO_3$, 10 ml DDW, stirring at room temperature, 48 hr.; b) filtration, sodium oxalate **(22)**, stirring at room temperature, r.t., 24h, filtration, drying under suction. Yield: 15.8%.

3.1.5 Synthesis of [(1*R*, 2*R*)- cyclohexane-1,2-diamine]bis(acetato)platinum(II); [*cis*-Pt(DACH)(acetate)$_2$] (25)

Similar to (Oxaliplatin) **(23)** the reaction was repeated with different types of sodium. The synthesized [(1*R*,2*R*)-cyclohexane-1,2-diamine]bis(chloroplatinum(II)); [*cis*-Pt(DACH)Cl_2] **(17)** was converted to the diaqua/dinitrato [*cis*-Pt(DACH)$(H_2O)_2$/ *cis*-Pt(DACH)$(NO_3)_2$ **(20)/(21)]** by ligand exchange reaction with silver nitrate ($AgNO_3$). After filtrating off AgCl and washing with water the filtrate was collected. Sodium acetate **(24)** was dissolved in a minimal amount of DDW and added to the filtrate in very small portions, as the sodium acetate solubility in water is 119 g/ 100 ml, The mixture was stirred at room temperature overnight The desired [(1*R*,2*R*)-cyclohexane-1,2-diamine]-bis-(acetate)platinum(II); [*cis*-Pt(DACH)$(acetate)_2$] **(25)** was collected by filtration. After washing with cold DDW and drying using suction, the powder was transferred into a vial stored as desiccated over anhydrous potassium hydroxide. A fine white garish of [(1*R*,2*R*)-cyclohexane-1,2-diamine]-bis-(acetate)platinum(II); [*cis*-Pt(DACH)$(acetate)_2$] **(25)** was synthesized.

The formation indication of the product was noticed here for the first time after several trials due to its high solubility and low yield. Yield: 2%.

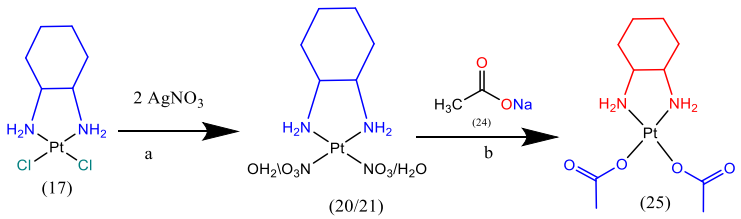

Scheme 3.1.5 Synthesis of [*cis*-Pt(DACH)$(acetate)_2$] **(25)** starting from Pt(DACH)Cl_2 **(17)** and $AgNO_3$ via the intermediate *cis*-Pt(DACH)H_2O/ *cis*-Pt(DACH)NO_3 **(20)/(21)** from the reaction with, finally adding sodium acetate **(24)** to form [*cis*-Pt(DACH)$(acetate)_2$] **(25)**. Reagents and conditions: a) 2 equiv $AgNO_3$, 10 ml of DDW, stirring, r.t, 48 hr.; b) filtration, 2 equiv sodium acetate **(24)**, stirring, r.t., 24 hr., filtration. Yield:2%.

3.1.6 Synthesis of [(1*R*,2*R*)-cyclohexane-1,2-diamine]bis(4-ethylbenzoato)platinum(II); [*cis*-Pt(DACH)$(EBZ)_2$] (26) and [(1*R*,2*R*)-cyclohexane-1,2-diamine]bis(4-trifluoromethylbenzoato)platinum(II); [*cis*-Pt(DACH)(TFBA)$_2$] (27)

The synthesized [(1*R*,2*R*)-cyclohexane-1,2-diamine]bis(iodoplatinum(II)); [*cis*-Pt(DACH)I_2] **(3)** was converted to the diaqua/dinitrato [Pt(DACH)$(H_2O)_2$/ Pt(DACH)$(NO_3)_2$ **(20)/(21)]** by ligand exchange reaction with silver nitrate ($AgNO_3$). After filtrating off AgI and washing with water the filtrate was collected. Sodium 4-trifluoromethyl benzoate **(14)** was added and in a similar reaction 4-ethyl benzoate **(16)** were added. Both of those sodium's have similar structures with different substituents (ethyl or 4-thrifluoromethyl substituent); CF_3 is considered more stable than CH_3 and is one of the most powerful electron-withdrawing groups given it a more stable formation during the reaction with lower solubility(Blint et al., 1974; O'Connor et al., 2010). This may explain the higher yield of [(1*R*,2*R*)-cyclohexane-1,2-diamine]bis(4-trifluoromethylbenzoato)platinum(II); [*cis*-Pt(DACH)$(TFBA)_2$] **(27)** (93%) compared to [(1*R*,2*R*)-cyclohexane-1,2-diamine]bis(4-ethylbenzoato)platinum(II); [*cis*-Pt(DACH)$(EBZ)_2$] **(26)** (72%), even though both were under the same conditions.

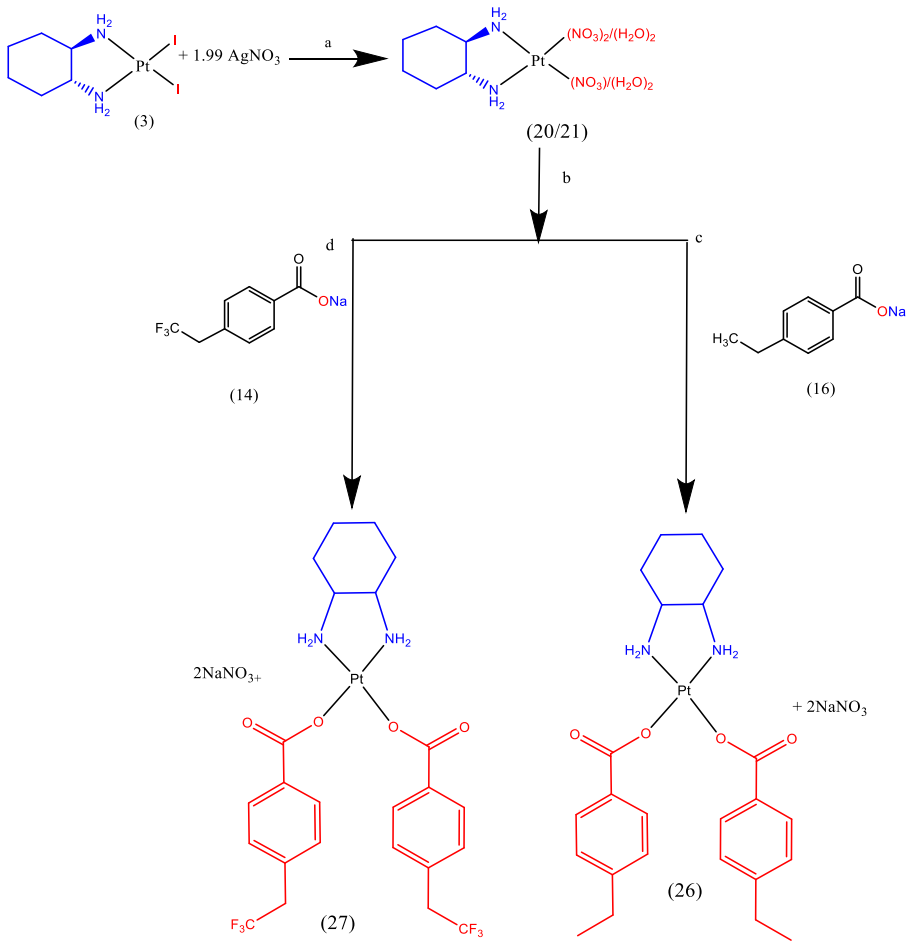

Scheme 3.1.6 Synthesis of [*cis*-Pt(DACH)(EBZ)$_2$] **(26)** and [*cis*-Pt(DACH)(EBZ)$_2$] **(27)** starting from Pt(DACH)I$_2$ **(3)** and $AgNO_3$ via the intermediate *cis*-Pt(DACH)(H$_2$O)$_2$/*cis*-Pt(DACH)(NO$_3$)$_2$ **(20)/(21)** from the reaction with, finally adding sodium (4-trifluoromethyl benzoate **(14)** 4-ethyl benzoate **(16)** to form [*cis*-Pt(DACH)(EBZ)$_2$] **(26)**/[*cis*-Pt(DACH)(EBZ)$_2$] **(27)**. Reagents and conditions: a) $AgNO_3$, 10 ml DDW, stirring, r.t, 48 hr.; b) filtration; c) sodium (4-trifluoromethyl benzoate **(14)** / ;d) 4-ethyl benzoate **(16))** stirring, r.t., 24 hr., filtration.

3.1.7 Synthesis of [ethylenediamine]bis(carboxylate)platinum(II); [*cis*-Pt(EN)(A)$_2$], A = myristato (30), 4-ethylbenzoato (31) and 4-trifluoromethylbenzoato (32) ligand.

The synthesized [ethylenediamine]bis(iodoplatinum(II)); [*cis*-Pt(EN)I$_2$] **(4)** was converted to the diaqua/dinitrato [*cis*-Pt(EN)(H$_2$O)$_2$/*cis*-Pt(EN)(NO$_3$)$_2$ **(28)/(29)]** by ligand exchange reaction with silver nitrate ($AgNO_3$). After filtrating off AgI and washing with water the filtrate was collected. To the filtrate, the desired sodium was added (Sodium myristate **(12)**, sodium 4-trifluoromethyl benzoate **(14)**, sodium 4-ethyl benzoate **(16)**). The synthesized complex contains ethylenediamine (EN) as its amine ligand which is commonly used in the synthesis of platinum(II) drugs as it forms bidentate ligands forming very stable chelating compounds(Kostrhunova et al., 2011). The yields of the three products [*cis*-Pt(EN)(MYR)$_2$] **(30)**, ([*cis*-Pt(EN)(TFBA)$_2$] **(32)**, and ([*cis*-Pt(EN)(EZB)$_2$] **(31)** ranged from very good to good respectively 88%, 85%), 69.4%, the difference in the yield could be due to the lipophilicity of the carboxylated ligands.

In the absence of organic solvents, the effect of lipophilicity on the yield of synthesized complexes may be indirect but significant. Even in aqueous conditions, the lipophilicity of carboxylate ligands can influence reactant interactions as well as the stability of intermediates and final products. For example, myristate, a long-chain fatty acid, is expected to give the resultant complex a more hydrophobic character [*cis*-Pt(EN)(MYR)$_2$]. This increased hydrophobicity may impact the solubility of the complex and its intermediates in water, potentially improving their stability during the synthesis process. In contrast, ligands such as 4-trifluoromethyl benzoate (TFBA) and 4-ethylbenzoate (EZB) may have varying degrees of hydrophobicity, which

could influence their interactions with water molecules and other reactants, potentially affecting synthesis efficiency and, ultimately, product yield.

In this context, the observed yield variations between the synthesized complexes [*cis*-Pt(EN)(MYR)$_2$] **(30),** [*cis*-Pt(EN)(EZB)$_2$] **(31)** and [*cis*-Pt(EN)(TFBA)$_2$] **(32)** could be related to the different hydrophobicities of the carboxylate ligands. Ligands having higher hydrophobicity, such as myristate, may induce more favorable interactions with the reactants, resulting in higher yields than ligands with lower hydrophobicity.

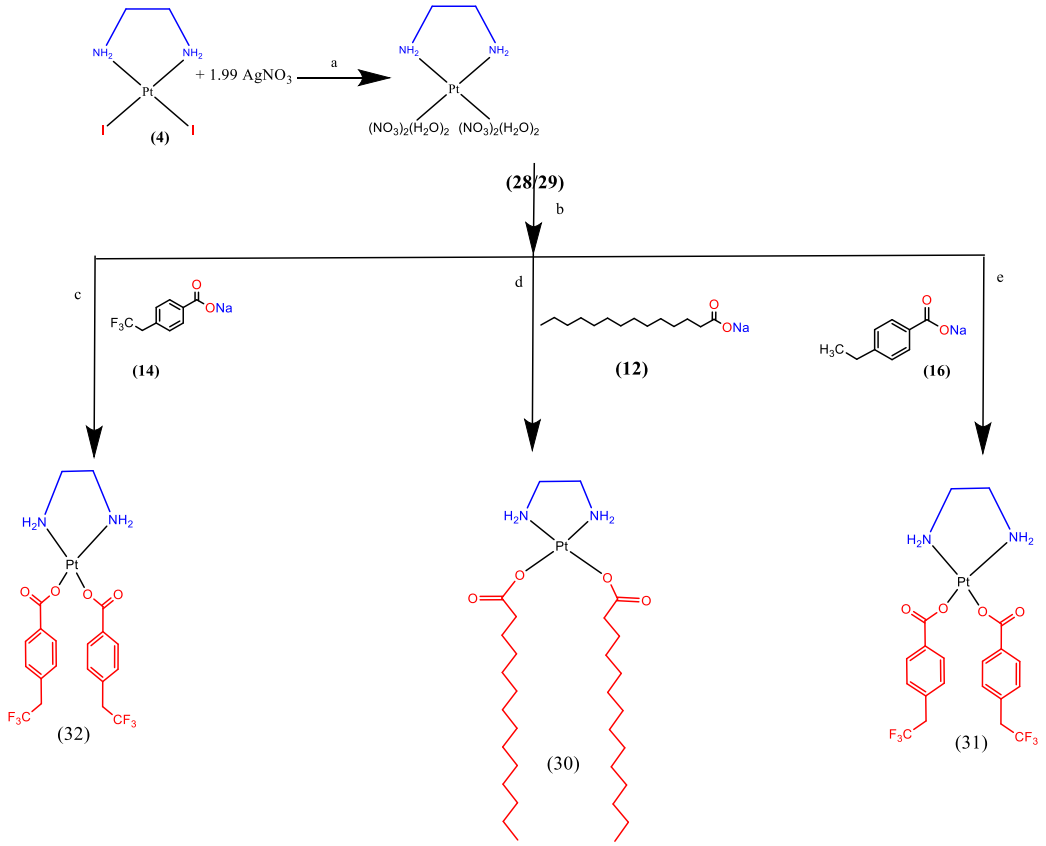

Scheme 3.1.7 Synthesis of [*cis*-Pt(EN)(MYR)$_2$] **(30)**, [*cis*-Pt(EN)(EBZ)$_2$] **(31),** and [*cis*-Pt(EN)(TFBA)$_2$] **(32)** starting from Pt(EN)I$_2$ **(4)** and $AgNO_3$ via the intermediate *cis*-Pt(EN)(H$_2$O)$_2$/ *cis*-Pt(EN)(NO$_3$)$_2$ **(28)/(29)** from the reaction with finally adding sodium (sodium myristate **(12)**, 4-trifluoromethyl benzoate **(14)** / 4-ethyl benzoate **(16)** to form the final product. Reagents and conditions: a) 2 equiv.$AgNO_3$, 10 ml H_2O, stirring r.t 48 hr..; b) filtration; c) adding 2 equiv. of sodium 4-trifluoromethyl benzoate **(14)**, stirring, r.t. 24 hr, at room temperature, filtration; d) adding 2 equiv. of sodium myristate **(12),** stirring at r.t., 24 hr., filtration; e) adding 2 equiv. of sodium 4-ethyl benzoate **(16)**, stirring atr.t., 24 hr., filtration.

3.1.8 Synthesis of [*cis*-di(n-butylamine)]bis(myristato)platinum(II); [*cis*-Pt(NBA)$_2$(MYR)$_2$] (35)

The synthesized complex of *cis*-Pt(NBA)$_2$(MYR)$_2$] **(35)** has high lipophilicity. For preparing [*cis*-Pt(NBA)$_2$(MYR)$_2$] **(35)** two methods were tried.

Method 1

The synthesized [*cis*-di(n-butylamine)diiodoplatinum(II) [*cis*-Pt(NBA)$_2$(I)$_2$] **(5)** was converted to the diaqua/dinitrato intermediate *cis*-Pt(NBA)$_2$(H$_2$O)$_2$/*cis*-Pt(NBA)$_2$(NO$_3$)$_2$ **(33)/(34)** by ligand exchange reaction with silver nitrate ($AgNO_3$). Unlike the previous experiments, this reaction took longer to finish, it was heated for half an hour at 50° to speed it.

After allowing the RBF to cool down the filtrating process were done through double filter paper precipitate After filtering AgI was filtered off and washed with water the filtrate was collected.

To be noticed the filtration process needs to be repeated more than once to get a clear filtrate without AgI byproduct, celite was later used to avoid this problem.

Sodium myristate **(12)** was added, mixture was stirred at room temperature overnight, the initially formed product was hard to manage, and most of the product was stuck around the RBF, diethyl ether was added to the mixture and left without stirring overnight. Displacement of diaqua/dinitrato by myristate resulted in affording [*cis*-di(n-butylamine)]bis(myristato)platinum(II); [*cis*-Pt(NBA)$_2$(MYR)$_2$] **(35)** as a white crystal colored layer. **(35)** was collected by filtration, washed with DDW, and dried under suction. Worth mentioning, that using diethyl ether on its own without the water or using another solvent such as dioxane didn't achieve a similar result nor the hoped product amount, and trying to centrifuge the product instead of normal filtration did not help in improving the yield as none of these methods delivered the hoped result or were as good as this method. Yield: 58.8%.

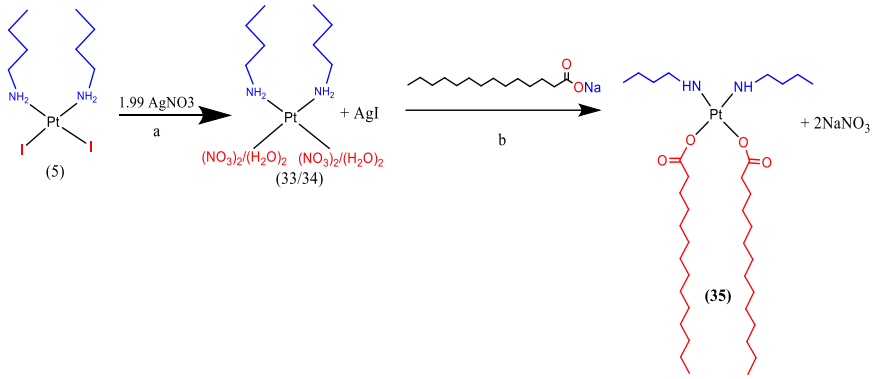

Scheme 3.1.8.1 Synthesis of [*cis*-Pt(NBA)$_2$(MYR)$_2$] **(35)** starting from *cis*-Pt(NBA)$_2$I$_2$ **(5)** and $AgNO_3$ via the intermediate *cis*-Pt(NBA)$_2$(H$_2$O)$_2$/ *cis*-Pt(NBA)$_2$(NO$_3$)$_2$ **(33)/(34)**, finally adding sodium myristate to form [*cis*-Pt(NBA)$_2$(MYR)$_2$] **(35)**. Reagents and conditions: a) 2 equiv. $AgNO_3$, 10 ml H$_2$O, stirring at r.t., 48 hr., 50 ºC for 30 min; b) filtration, adding 2 equiv. sodium myristate **(12)**, stirring r.t, 24 hr, 10 ml diethyl ether, without stirring r.t, 24 hr., filtration, dryness through suction. Yield: 58.8%.

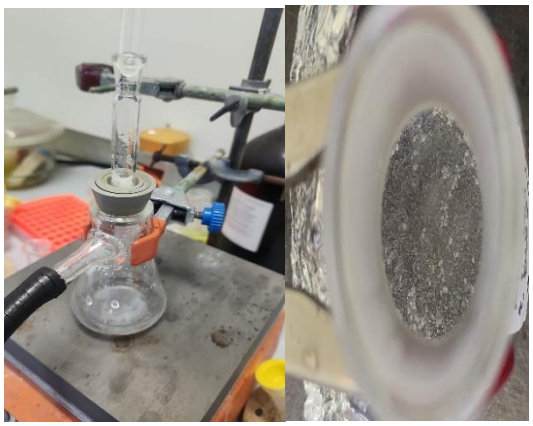

3.1.8.1 Visual observation of the formed layer after 24 hours of adding diethyl ether and the filtration of [*cis*-Pt(NBA)$_2$(MYR)$_2$] **(35)**.

Method 2

Based on(Al-Baker et al. 1992) synthetic procedure *cis*-Pt(NBA)$_2$I$_2$ **(5)** was first dissolved the in chloroform, obtaining a clear yellow mixture, sodium myristate was added to the mixture it dissolved completely as well, $AgNO_3$ were added, the reaction of the mixture color turned into a darker yellow with some precipitate indicating the

start of the ligand exchange reaction, After stirring overnight, the mixture was filtered through celite to remove the AgI, a clear deep yellow filtrate was obtained, the mixture were fully dried in the rotary evaporator. A brownish-orange layer was formed around the RBF, the recrystallization and purification of the product were done though a mixture of ethyl acetate which was heated over 50^{c} for five minutes and hexane. Other solvents were tried such as acetone and methanol, but none gave a good result, so they were removed using rotary evaporator. [*cis*-Pt(NBA)$_2$(MYR)$_2$] **(35)** were obtained as light brownish powder. Yield 66.4%.

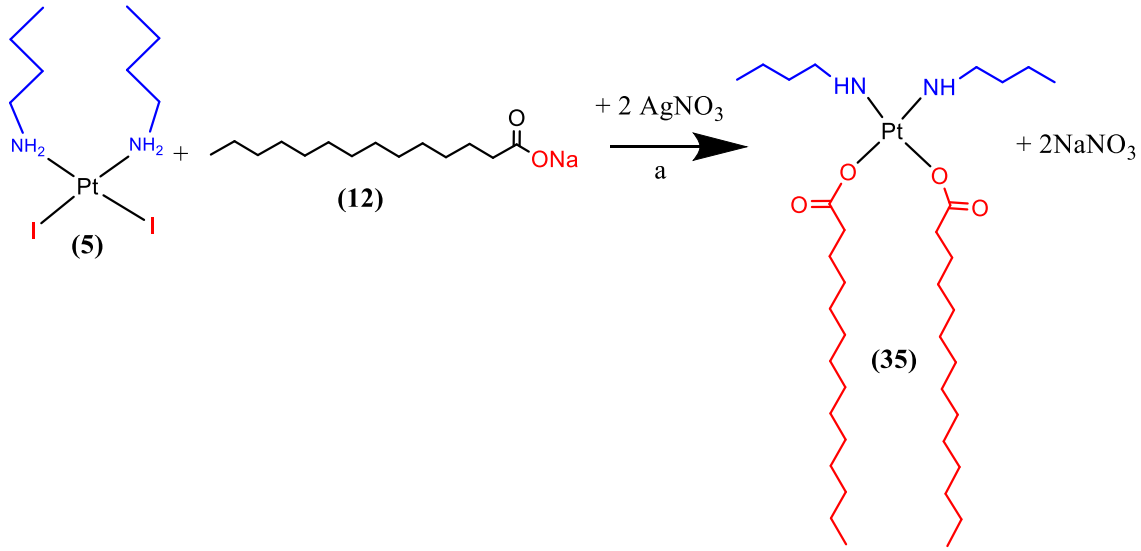

Scheme 3.1.8.2 Synthesis of [*cis*-Pt(NBA)$_2$(MYR)$_2$] **(35)** starting from *cis*-Pt(NBA)$_2$I$_2$ **(5)** and sodium myristate **(12)** dissolved in chloroform**.** Reagents and conditions: a) chloroform (10 ml), 2 equiv. $AgNO_3$, stirring, r.t. 24 hr., filtration, evaporation, refrigeration for 24 h., 1 ml of ethyl acetate, 50 $^{\circ}$C heat for 5 min, refrigerate, 1.5 ml hexane, filtrate. [*cis*-Pt(NBA)$_2$(MYR)$_2$] **(35)**. Yield: 66.4%.

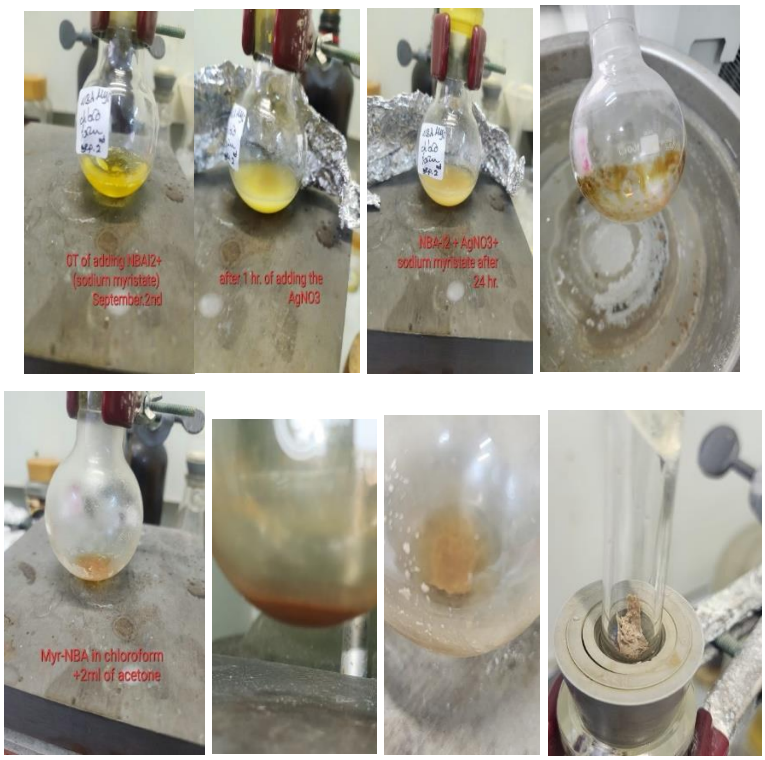

Figure 3.1.8.2 Visual observation of the change in color after adding sodium and silver nitrate, rotary evaporation, solvent addition, heat application (the color becomes deep brown), and filtration of [*cis*-Pt(NBA)$_2$(MYR)$_2$] **(35).**

3.1.9 Synthesis of [*cis*-di(n-butylamine)]bis(4-ethylbenzoato)platinum(II) [*cis*-Pt(NBA)$_2$(EZB)$_2$] (36)

The synthesized *cis*-Pt(NBA)$_2$I$_2$ **(5)** was converted to the diaqua/dinitrato intermediate *cis*-Pt(NBA)$_2$(H$_2$O)$_2$/*cis*-Pt(NBA)$_2$(NO$_3$)$_2$ **(33)/(34)**, by the ligand exchange reaction with AgNO$_3$. After filtering off the AgI and washing with water the filtrate was collected. Sodium 4-ethyl benzoate were added, the mixture was stirred at room temperature for 48 hr. similar to [*cis*-Pt (NBA) $_2$ (MYR)$_2$] **(35)** the initial formed product was hard to manage, and most of the product was stuck around the RBF, diethyl ether was added to the mixture and left stirring for an hour and half. Displacement of diaqua/dinitrato by 4-ethyl benzoate resulted in affording [*cis*-di(n-butylamine)]bis(4-ethylbenzoato)platinum(II); [*cis*-Pt(NBA)$_2$(EZB)$_2$] **(36)** as a white powder. **(36)** was collected bfiltration, washed with DDW and dried under suction .Yield: 35.5%.

Another similar method was tested to improve the yield, starting the same with the synthesized $Pt(NBA)_2I_2$ **(5)** and converted to the diaqua/dinitrato intermediate *cis*-$Pt(NBA)_2(H_2O)_2$/*cis*-$Pt(NBA)_2(NO_3)_2$ **(33)/(34)**, by the ligand exchange reaction with $AgNO_3$. filtering off the AgI washing with water, and finally collecting the filtrate. Sodium 4-ethyl benzoate **(16)** was added, the mixture was stirred at room temperature for 24 hr. But instead of the normal filtration procedure, the mixture was transferred into a centrifuge tube, in order to centrifuge the product to help it separate easily from the filtrate, the collected precipitate were dried in the desiccator with KOH, affording [*cis*-di(n-butylamine)]bis(4-ethylbenzoato)platinum(II); [*cis*-$Pt(NBA)_2(EZB)_2$] **(36)** as a white powder. Yield: 35%.

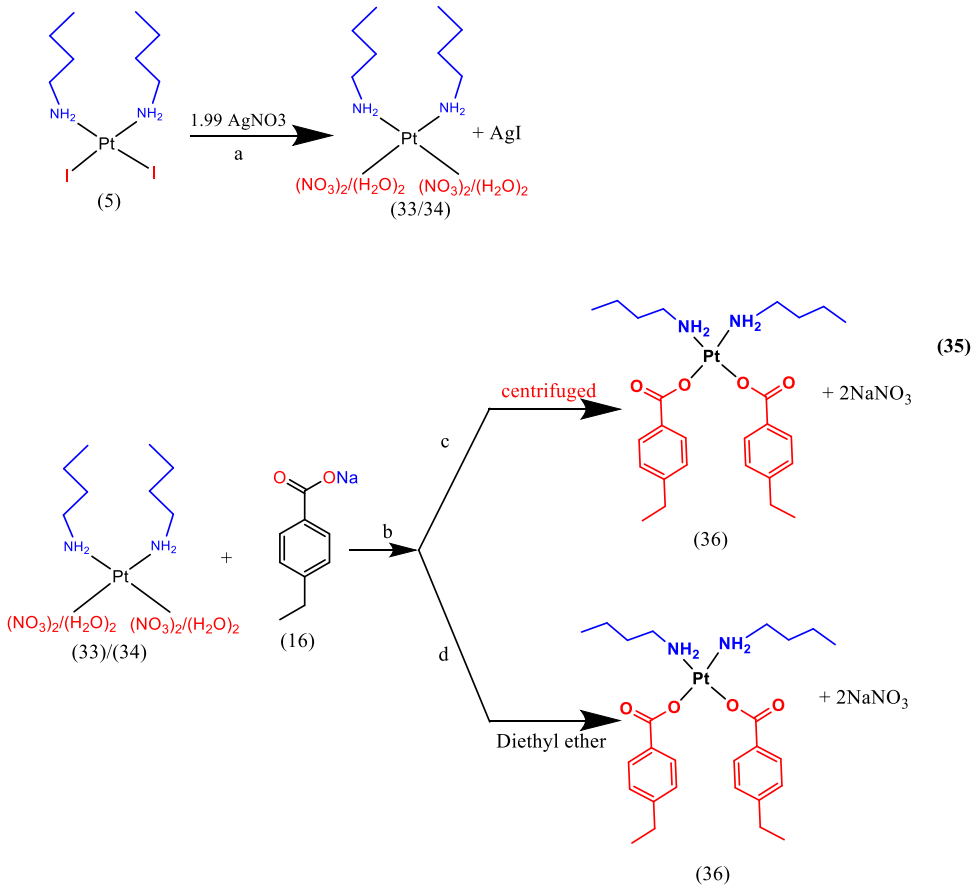

Scheme 3.1.9 Synthesis of [*cis*-$Pt(NBA)_2(EZB)_2$] **(36)** starting from $Pt(NBA)_2I_2$ **(5)** and $AgNO_3$ via the intermediate *cis*-$Pt(NBA)_2(H_2O)_2$/ *cis*-$Pt(NBA)_2(NO_3)_2$ **(33)/(34)**, finally adding sodium myristate to form [*cis*-$Pt(NBA)_2(EZB)_2$] **(36)**. Reagents and conditions: a) 2 equiv. $AgNO_3$, 10 ml H_2O, stirring r.t., 48 hr. ;b) filtration, 2 equiv. of sodium 4-ethyl benzoate **(16)**, stirring r.t, 24 hr. ;c) centrifuge, remove filtrate,

dryness the desiccator with anhydrous KOH. Yield 41.4 %; d). 5 ml diethyl ether, stirring r.t, 90 min, filtration, dryness through suction, Yield: 35%.

3.1.10 Synthesis of [*cis*-di(n-butylamine)]bis (4-trifluoromethylbenzoato)platinum(II); [*cis*-Pt(NBA)$_2$(TFBA)$_2$] (37)

Similarly, *cis*-Pt(NBA)$_2$(TFBA)$_2$ **(37)** was prepared following an alternative sequence of ligand exchange steps and by employing the iodide form of platinum(II) species. Briefly, Pt(NBA)$_2$I$_2$ **(5)** was allowed to react with $AgNO_3$ under dark conditions. The diaqua/dinitrato intermediate *cis*-Pt(NBA)$_2$(H$_2$O)$_2$/*cis*-Pt(NBA)$_2$(NO$_3$)$_2$ **(33)/(34)** was collected after adding ethanol to the mixture and stirred overnight, the filtrating process were done through double filter paper the precipitate AgI off. The previously prepared sodium 4-trifluoromethyl benzoate **(14)** was added to the diaqua/dinitrato [*cis*-Pt(NBA)$_2$(H$_2$O)$_2$/*cis*-Pt(NBA)$_2$(NO$_3$)$_2$ **(20)/(21)**] and left to stand at room temperature overnight. Unlike the previous platinum compound with NBA [*cis*-Pt(NBA)$_2$(TFBA)$_2$] **(37)** precipitate was easy to handle with regular filtration without adding any dissolvent. Displacement of diaqua/dinitrato by 4-trifluoromethyl benzoate resulted in a white product of [*cis*-di(n-butylamine)]bis(4-trifluoromethylbenzoato)platinum(II); [*cis*-Pt(NBA)$_2$(TFBA)$_2$] **(37),** the product was stored to dry into a vile as desiccated over KOH.

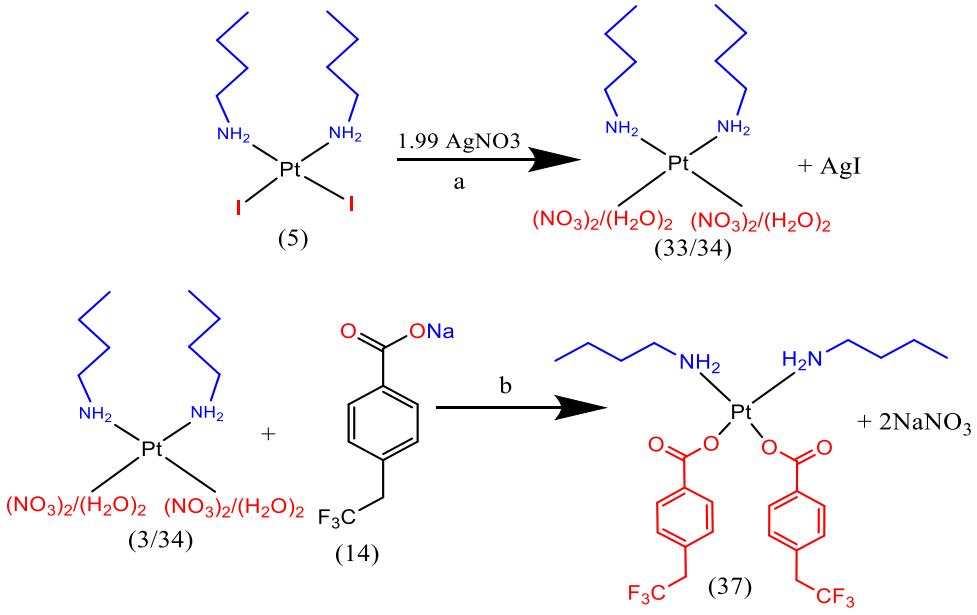

Scheme 3.1.10 Synthesis of [*cis*-$Pt(NBA)_2(TFBA)_2$] **(37)** starting from $Pt(NBA)_2I_2$ **(5)** and $AgNO_3$ via the intermediate *cis*-$Pt(NBA)_2(H_2O)_2$/ *cis*-$Pt(NBA)_2(NO_3)_2$ **(33)/(34)**, finally adding4-trifluoromethyl benzoate **(14)** to form [*cis*-$Pt(NBA)_2(TFBA)_2$] **(37)**. Reagents and conditions: a) $AgNO_3$, 10 ml H_2O, stirring r.t., 78 hr., ethanol 5 ml, stirring r.t. 24 hr.; b) filtration, sodium, stirring r.t, 24 hr., filtration, dryness through suction. Yield: 82.35%.

3.1.11 Synthesis of [*cis*-di(piperidine)]bis(myristato)platinum(II); [*cis*-$Pt(PIP)_2(MYR)_2$] (40) / [*cis*-di(piperidine)]bis(4-ethylbenzoato)platinum(II); [*cis*-$Pt(PIP)_2(EBZ)_2$] (41) / [*cis*-di(piperidine)]bis(4-trifluoromethylbenzoato)platinum(II); [*cis*-$Pt(PIP)_2(TFBA)_2$] (42)

The compounds *Cis*-$Pt(PIP)_2(MYR)_2$ **(40)/** [*cis*-$Pt(PIP)_2(EBZ)_2$] **(41)** / [*cis*-$Pt(PIP)_2(TFBA)_2$] **(42)** were prepared following an alternative sequence of ligand exchange steps and by employing the iodide form of platinum(II) species. Briefly, $Pt(PIP)_2I_2$ **(6)** was allowed to react with $AgNO_3$ under dark conditions. The diaqua/dinitrato intermediate *cis*-$Pt(PIP)_2(H_2O)_2$/*cis*-$Pt(PIP)_2(NO_3)_2$ **(38)/(39)** was collected, the filtrating process were done through celite the precipitate AgI was filtered off. The previously prepared sodium myristate **(12)** was added once and in a similar reaction sodium 4-ethyl benzoate **(16)** or sodium 4-trifluoromethyl benzoate **(14)** were added to the diaqua/dinitrato [*cis*-$Pt(PIP)_2(H_2O)_2$/ *cis*-$Pt(PIP)_2(NO_3)_2$ **(38)/(39)**] and left to stand at r.t. for overnight. Displacement of diaqua/dinitrato by myristate, 4-ethyl benzoate and 4-trifluoromethyl benzoate resulted in affording [*cis*-di(piperidine)]bis(myristato)platinum(II); [*cis*-$Pt(PIP)_2(MYR)_2$] **(40)/** [*cis*-di(piperidine)]bis(4-ethylbenzoato)platinum(II); [*cis*-$Pt(PIP)_2(EBZ)_2$] **(41)/** [*cis*-di(piperidine)]bis(4-trifluoromethylbenzoato)platinum(II); [*cis*-$Pt(PIP)_2(TFBA)_2$] **(42)** as a white colored precipitate. **(40)/(41)/ (42)** were collected by filtration, washed with DDW and dried under suction.

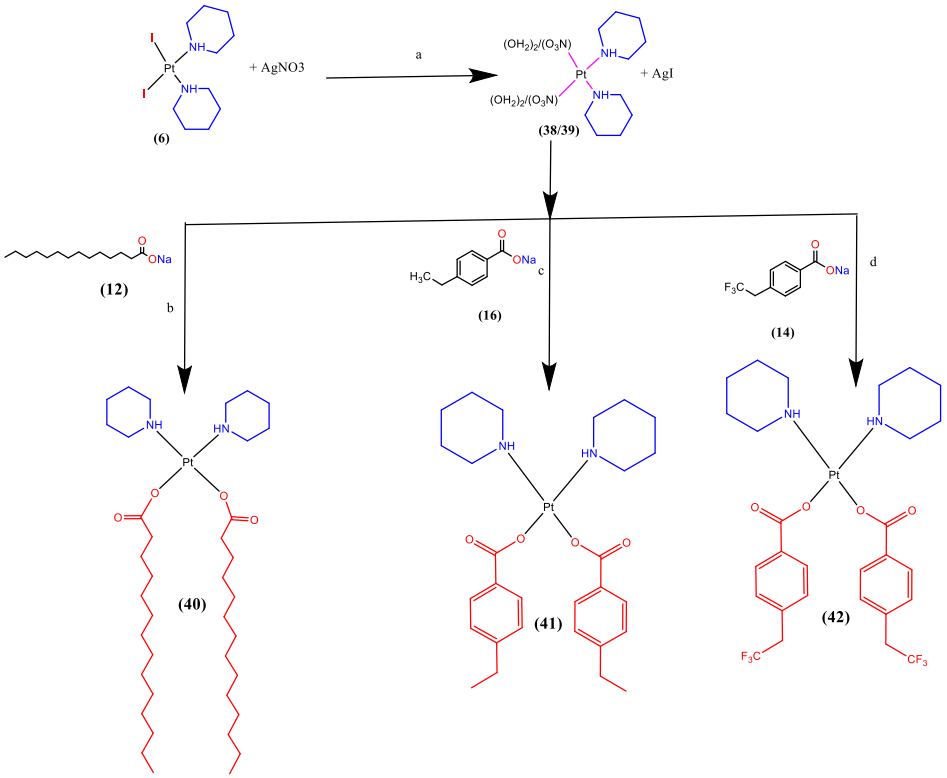

Scheme 3.1.11 Synthesis of [*cis*-Pt(PIP)$_2$(MYR)$_2$] **(40)/** [*cis*-Pt(PIP)$_2$(EBZ)$_2$] **(41)** / [*cis*-Pt(PIP)$_2$(TFBA)$_2$] **(42),** starting from Pt(PIP)$_2$I$_2$ **(5)** and $AgNO_3$ via the intermediate *cis*-Pt(PIP)$_2$(H$_2$O)$_2$/ *cis*-Pt(PIP)$_2$(NO$_3$)$_2$ **(38)/(39)**, finally adding sodium myristate **(12)** /sodium 4-ethylbenzoat **(16)** /sodium 4-trifluoromethyl benzoate **(14)** to form [*cis*-Pt(PIP)$_2$(MYR)$_2$] **(40)/** [*cis*-Pt(PIP)$_2$(EBZ)$_2$] **(41)** / [*cis*-Pt(PIP)$_2$(TFBA)$_2$] **(42)**. Reagents and conditions: a) 2 equiv. $AgNO_3$, 10 ml H$_2$O, stirring r.t., 78 hr. stirring, 4 hr; b) filtration, 2 equiv. sodium myristate **(12)**, stirring r.t, 24 hr., filtration, dryness through suction, yield 95.6%; c) filtration, 2 equiv. sodium 4-ethyl benzoate **(16)**, stirring r.t, 24 hr., filtration, dryness through suction, yield 44.7%.; d) filtration, 2 equiv. sodium 4-trifluoromethyl benzoate **(14)**, stirring r.t, 24 hr., filtration, dryness through suction, Yield: 88.2%.

3.1.12 Synthesis of [*cis*-di(piperidine)]bis(acetato)platinum(II); [*cis*-Pt(PIP)$_2$(acetate)$_2$] (43)

Based on(Al-Baker et al. 1992) synthetic procedure *cis*-(PIP)$_2$PtI$_2$ **(6)** was first dissolved in chloroform, obtaining a clear yellow mixture, sodium myristate was added to the mixture it dissolved completely as well, $AgNO_3$ were added, and the reaction of the mixture color turned into a yellow with some precipitate indicating

the start of the ligand exchange reaction, After stirring overnight, the mixture was filtered through celite to remove the AgI, a clear deep light yellow filtrate was obtained, the mixture were fully dried in the rotary evaporator. A brownish-orange layer was formed around the RBF, the recrystallization and purification of the product were done though adding 1 ml of methanol. The immediate resulting color were yellow to orange solvents, after it was left over night the color turned into brownish. [*cis*-Pt(PIP)$_2$(acetate)$_2$] **(43)** were obtained as brownish light powder. Yield: 22.8%

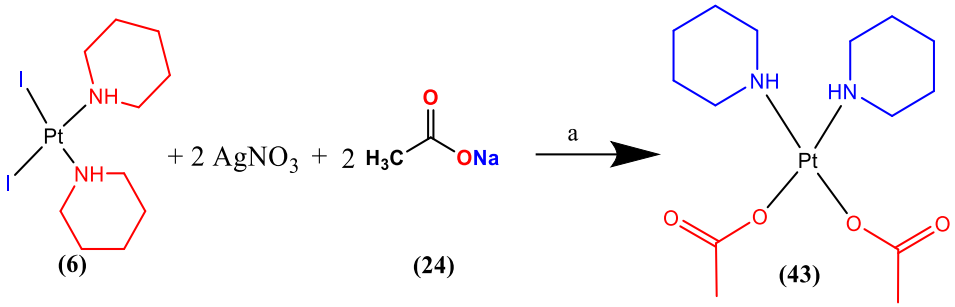

Scheme 3.1.2 Synthesis of [*Cis*-Pt(PIP)$_2$(acetate)$_2$] **(43)** starting from Pt(PIP)$_2$I$_2$ **(6)** and sodium acetate **(24)** dissolved in chloroform**.** Reagents and conditions: a) chloroform (10 ml), 2 equiv. $AgNO_3$, stirring at r.t. 24 hr., filtration, evaporation, refrigeration for 24 hr., 1ml of methanol, filtrate. [*Cis*-Pt(PIP)$_2$(acetate)$_2$] **(43)**. Yield: 21.7%.

3.1.13 Synthesis of [*cis*-di(pyridine)]bis(myristato)platinum(II) [*cis*-Pt(PYR)$_2$(MYR)$_2$] (47)

[*Cis*-di(pyridine)]bis(myristato)platinum(II); [*cis*-Pt(PYR)$_2$(MYR)$_2$] **(47)** was prepared following an alternative sequence of ligand exchange steps and by employing the iodide form of platinum(II) species. Briefly, Pt(PYR)Cl$_2$ **(3)** was allowed to react with $AgNO_3$ under dark conditions. The diaqua/dinitrato intermediate *cis*-Pt(PYR)$_2$(H$_2$O)$_2$/*cis*-Pt(PYR)$_2$(NO$_3$)$_2$ **(45)/(46)** was collected following filtrating the precipitate AgCl off. The previously prepared sodium myristate **(12)** was added to the diaqua/dinitrato intermediate *cis*-Pt(PYR)$_2$(H$_2$O)$_2$/*cis*-Pt(PYR)$_2$(NO$_3$)$_2$ **(45)/(46)** and stirred at r.t. for overnight. Displacement of diaqua/dinitrato by myristate resulted in affording *cis*-

$Pt(PYR)_2(MYR)_2$ **(47)** as a white-to-beige colored precipitate. The product **(47)** had small forming particles which led to the obstruction of the filtration process, the product was transferred to a centrifuge tube in order to get the product in an easier manner instead of the filtration process, the above supernatant were removed and the precipitate of **(47)** was put to dry. Yield 28.9%.

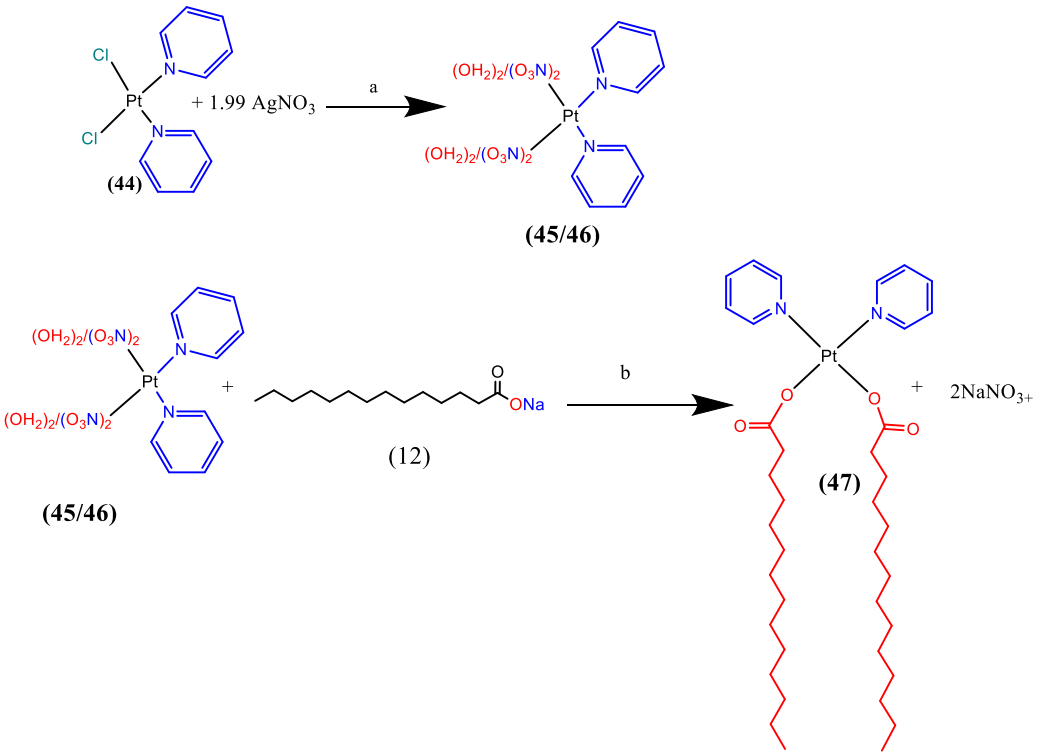

Scheme 3.1.2 Synthesis of [*cis*-$Pt(PYR)_2(MYR)_2$] **(47)**, starting from $Pt(PYR)_2I_2$ **(44)** and $AgNO_3$ via the intermediate *cis*-$Pt(PYR)_2(H_2O)_2$/ *cis*-$Pt(PIP)_2(NO_3)_2$ **(45)/(46)**, finally adding sodium myristate **(12)** to form [*cis*-$Pt(PYR)_2(MYR)_2$] **(47).** Reagents and conditions: a) 2 equiv. $AgNO_3$, 10 ml H_2O, stirring r.t., 78 hr., stirring r.t. 24 hr.; b) filtration, 2 equiv. sodium myristate **(12)**, stirring r.t, 24 hr., filtration, centrifugation, drying, Yield: 28.9%.

3.1.14 Synthesis of [*cis*-di(pyridine)]bis(4-ethylbenzoato)platinum(II); [*cis*-$Pt(PYR)_2(EBZ)_2$] (48) and [*cis*-di(pyridine)]bis(4-trifluoromethylbenzoato)platinum(II); [*cis*-$Pt(PYR)_2(TFBA)_2$] (49)

The compounds [*cis*-$Pt(PYR)_2(EBZ)_2$] **(48)**/[*cis*-$Pt(PYR)_2(TFBA)_2$] **(49)** were prepared following an alternative sequence of ligand exchange steps and by

employing the iodide form of platinum(II) species. Briefly, *cis*-Pt(PYR)$_2$Cl$_2$ **(44)** was allowed to react with $AgNO_3$ under dark conditions. The diaqua/dinitrato intermediate *cis*-Pt(PYR)$_2$(H$_2$O)$_2$/*cis*-Pt(PYR)$_2$(NO$_3$)$_2$ **(45)/(46)** was collected , the filtrating process were done through celite the precipitate AgCl was filtered off. The previously prepared sodium 4-ethylbenzoat **(16)** were added and in a similar reaction/sodium 4-trifluoromethyl benzoate **(14)** were added to the diaqua/dinitrato [Pt(PYR)$_2$(H$_2$O)$_2$/Pt(PYR)$_2$(NO$_3$)$_2$ **45)/(46)**] and left to stand at room temperature for overnight. Displacement of diaqua/dinitrato by 4-ethyl benzoate and 4-trifluoromethyl benzoate resulted in affording [*cis*-di(pyridine)]bis(4-ethylbenzoato)platinum(II); [*cis*-Pt(PYR)$_2$(EBZ)$_2$] **(48)**/[*cis*-di(pyridine)]bis(4-trifluoromethylbenzoato)platinum(II); [*cis*-Pt(PYR)$_2$(TFBA)$_2$] **(49)** as a white colored precipitate. **(48)/(49)** were collected by filtration, washed with DDW, and dried under suction.

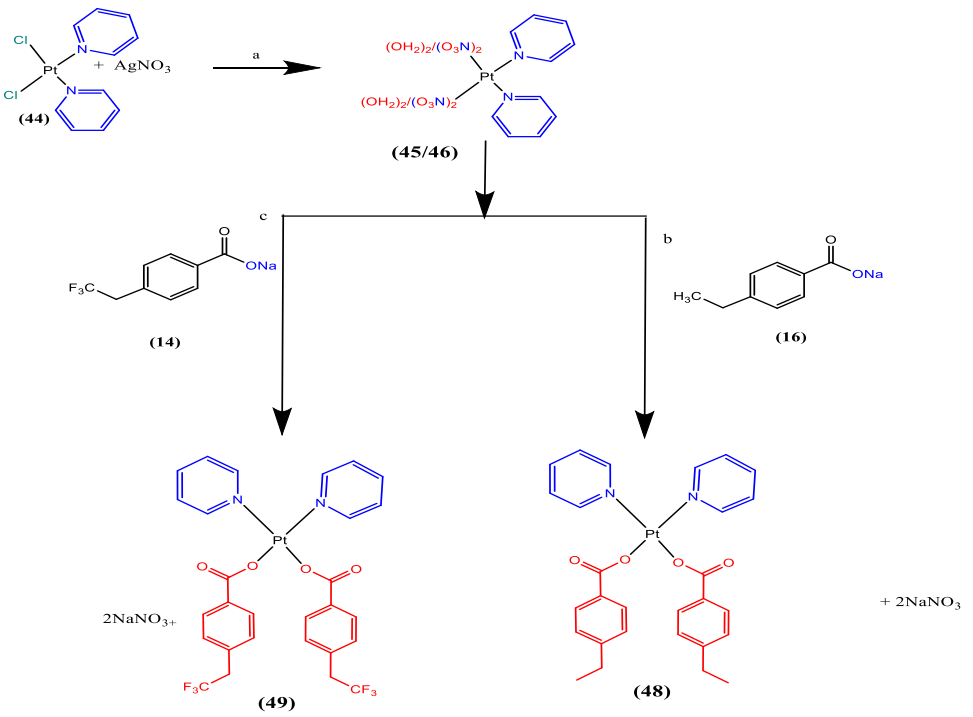

Scheme 3.1.14 Synthesis of [*cis*-Pt(PYR)$_2$(EZB)$_2$] **(48)/** [*cis*-Pt(PYR)$_2$(TFBA)$_2$] **(49)** **,** starting from Pt(PYR)$_2$I$_2$ **(44)** and $AgNO_3$ via the intermediate Pt(PYR)$_2$(H$_2$O)$_2$/ Pt(PIP)$_2$(NO$_3$)$_2$ **(45)/(46)** , finally adding sodium 4-ethyl benzoate **(16)** / sodium 4-trifluromethyl benzoate **(14)** to form [*cis*-Pt(PYR)$_2$(EZB)$_2$] **(48)/** [*cis*-

$Pt(PYR)_2(TFBA)_2$] **(49)**. Reagents and conditions: a) $AgNO_3$, 10 ml H_2O, stirring r.t., 78 h at room temperature, stirring r.t. 24h at room temperature b) filtration, sodium 4-ethyl benzoate **(16)**, stirring r.t, 24 h, filtration, yield 14.4%. c) filtration, sodium 4-trifluromethyl benzoate **(14)**, stirring r.t, 24 h, filtration, yield: 35.80%.

3.1.15 Synthesis of [ethylenediamine]bis(4-ethylbenzoatodihydroxyplatinum(IV)); [*cis, cis, trans*- $Pt(EN)(EZB)_2(H_2O)_2$] (50) and [*cis*-di(piperidine)]bis(4-trifluoromethylbenzoatodihydroxyplatinum(IV)); [*cis, cis, trans*-$Pt(PIP)_2(TFBA)_2(H_2O)_2$] (51)

Pt(IV) derivatives of [*Cis*-$Pt(EN)(EZB)_2(H_2O)_2$] **(50)** / [*Cis*-$Pt(PIP)_2(TFBA)_2(H_2O)_2$] **(51)** were synthesized by oxidizing previously prepared Pt(II) using hydrogen peroxide (H_2O_2). The oxidation of Pt(II) to Pt(IV) allowed the formation of two additional hydroxide ligands at the axial sites.

The process started from the previously prepared [*cis*-$Pt(EN)(EZB)_2$] **(31)** / [*cis*-$Pt(PIP)_2(TFBA)_2$] **(42)** reacting with 1 ml of 3% H_2O_2, with stirring for 24 hr. at room temperature. The white-colored precipitate **(50)/(51)** were collected by filtration, dried under suction, put in the desiccator with anhydrous KOH. Giving an average yield of 58.14% and 69% for (50) and (51) respectively.

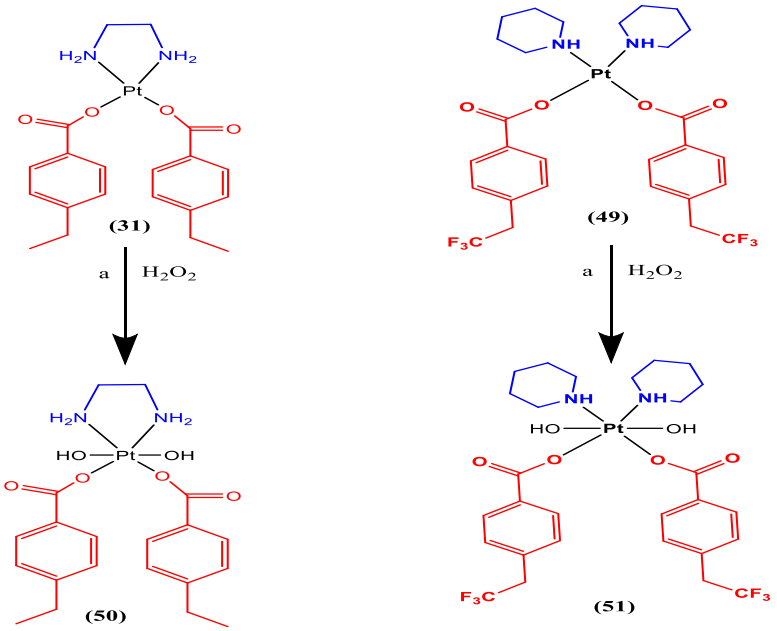

Scheme 3.1.15 Synthesis of [*cis*-$Pt(EN)(EZB)_2(H_2O)_2$] **(50)** / [*cis*-$Pt(PIP)_2(TFBA)_2(H_2O)_2$] **(51)** starting from reacting [*cis*-$Pt(EN)(EZB)_2$] **(31)** and

[*cis*-Pt(PYR)$_2$(TFBA)$_2$] **(49)** with 1 ml of 3% H_2O_2 . Reagents and conditions: a) 3% H_2O_2 (1 ml), r.t. 24 hr., stirring, filtration. Yield: 58.14%, 69% respectively

Table 3.1.1 The intermediate, cisplatin and oxaliplatin synthesized in the study

Compound's names	Compound's structure	Yield	Physical appearance
[*Cis*-Pt(DACH)I_2] **(3)**	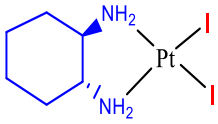	81% (548 mg, 0.973 mmol)	Yellow powder
[*Cis*-Pt(DACH)Cl_2] **(17)**	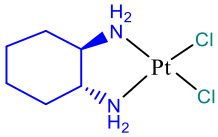	60.77% (556.8 mg, 1.464 mmol)	Yellow powder
[*Cis*-Pt(EN)I_2] **(4)**	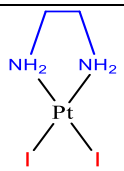	88% (468 mg; 0.919 mmol)	Yellow powder
[*Cis*-Pt(NBA)$_2I_2$] **(5)**	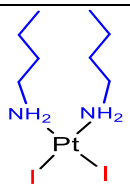	78.4% (280 mg; 0.470 mmol)	Yellow powder
[*Cis*-Pt(Pip)$_2I_2$] **(6)**	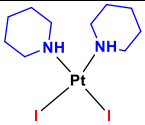	88.66% (329.5 mg; 0.532 mmol)	Yellow powder
[*Cis*-Pt(PYR)$_2Cl_2$) **(44)**	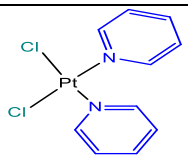	82.38% (172.8 mg, 0.407 mmol)	Light-Yellow powder
[*Cis*-[Pt(NH_3)$_2I_2$] **(7)**	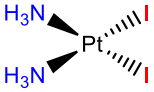	78.3% (91 mg; 0.188 mmol)	Yellow powder
(Cisplatin) **(10)**	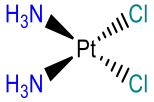	63.8% (35 mg, 0.12 mmol)	Yellow powder
(Oxaliplatin) **(23)**	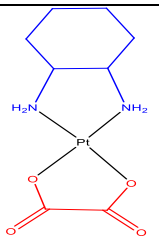	15.8% (41.6 mg, 0.104 mmol)	Garish powder

Table 3.1.2 Synthesized complexes with myristate ligands

Compound's names	Compound's structure	Yield	Physical appearance
Sodium myristate **(12)**	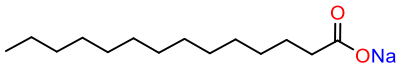	95.54%(2095 mg, 8.37 mmol)	White powder
[[*Cis*-Pt(DACH)(MYR)$_2$], Miriplatin] **(19)**	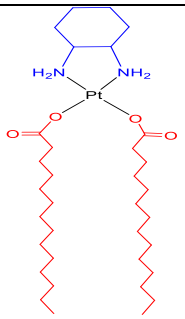	91% (125 mg; 0.164 mmol)	White powder
[*Cis*-Pt(EN)(MYR)$_2$] **(30)**	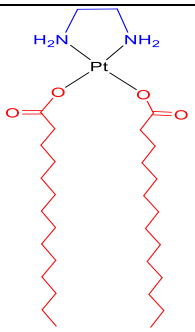	88% (125 mg; 0.176 mmol)	White powder
[*Cis*-Pt(NBA)$_2$(MYR)$_2$] **(35)**	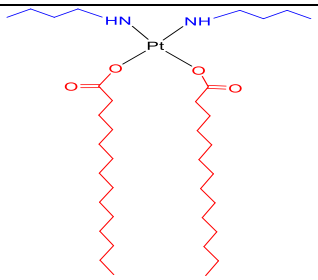	58.8% (74.5 mg; 0.1 mmol)	White crystals
		66.4% (106.3 mg, 0.133 mmol)	light brownish powder
[*Cis*-Pt(PIP)$_2$(MYR)$_2$] **(40)**	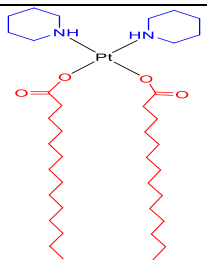	95.6% (126 mg; 0.153 mmol)	White powder

[*Cis*-Pt(PYR)$_2$(MYR)$_2$] **(47)**	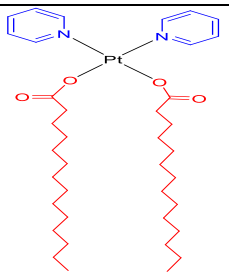	28.9% (35.4 mg; 0.043 mmol)	White powder

Table 3.1.3 Synthesized complexes with 4-ethyl benzoate ligands

Compound's names	Compound's structure	Yield	Physical appearance
Sodium 4-ethyl benzoate **(16)**	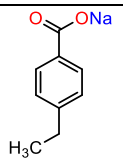	90% (518 mg, 3.0 mmol).	White powder
[*Cis*-Pt(DACH)(EBZ)$_2$] **(26)**	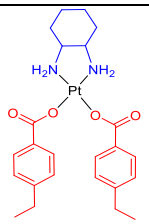	72% (80 mg; 0.131 mmol)	White powder
[*Cis*-Pt(EN)(EZB)$_2$] **(31)**	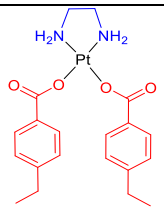	69.4% (69.1 mg; 0.125 mmol)	White powder
[*Cis*-Pt(NBA)$_2$(EZB)$_2$] **(36)**	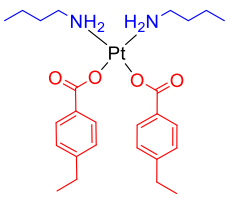	35% (38.2 mg; 0.059 mmol)	White powder
		42% (45.3 mg; 0.071 mmol)	White powder
[*Cis*-Pt(PIP)$_2$(EBZ)$_2$] **(41)**	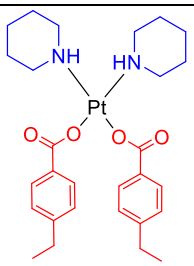	44.7% (51 mg; 0.076 mmol)	White powder

[*Cis*-Pt(PYR)$_2$(EBZ)$_2$] **(48)**	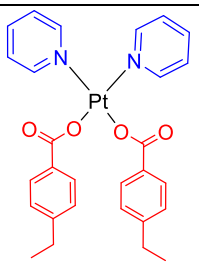	14.6% (26.6 mg; 0.041 mmol).	White powder

Table 3.1.4 Synthesized complexes with 4-trifluoromethyl benzoate ligands

Compound's names	Compound's structure	Yield	Physical appearance
Sodium 4-trifluoromethyl benzoate **(14)**	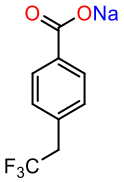	84% (468 mg 2.21 mmol)	White powder
[*Cis*-Pt(EN)(TFBA)$_2$] **(32)**	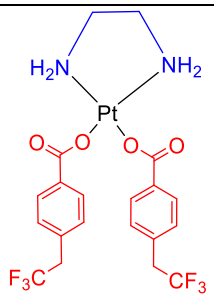	85% (107.2 mg; 0.17 mmol)	White powder
[*Cis*-Pt(DACH)(TFBA)$_2$] **(27)**	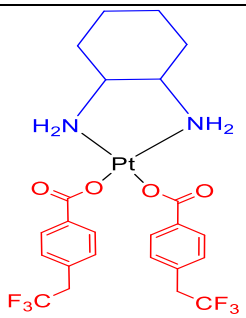	Yield: 93% (115 mg; 0.167 mmol)	White powder
[*Cis*-Pt(NBA)$_2$(TFBA)$_2$] **(37)**	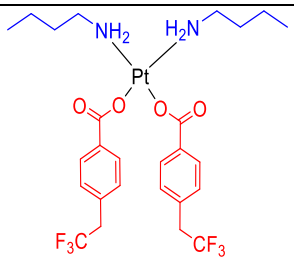	82.35% (101 mg; 0.14 mmol)	White powder

[*Cis*-Pt(PIP)$_2$(TFBA)$_2$] **(42)**	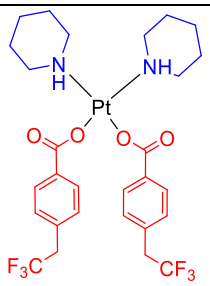	88.2% (110 mg; 0.15 mmol)	White powder
[*Cis*-Pt(PYR)$_2$(TFBA)$_2$] **(49)**	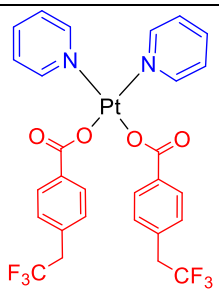	36.4% (66.6 mg; 0.091 mmol)	White powder

Table 3.1.5 Synthesized complexes with acetate ligands and Pt(IV) complexes

Compound's names	Compound's structure	Yield	Physical appearance
[*Cis*-Pt(DACH)(acetate)$_2$] **(25)**	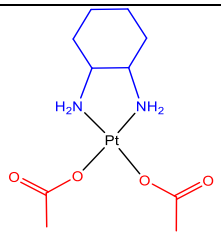	2% (23.9 mg; 0.019 mmol)	Garish powder
[*Cis*-Pt(PIP)$_2$(acetate)$_2$] **(43)**	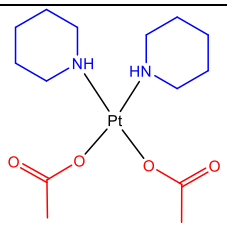	21.7% (18.1 mg, 0.037 mmol)	Dark brownish powder.
[*Cis*-Pt(EN)(EZB)$_2$(H$_2$O)$_2$] **(50)**	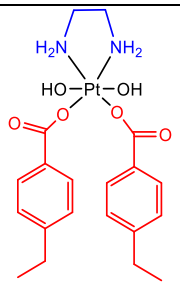	58.14% (15 mg; 0.025 mmol)	Whitish powder

[*Cis*-Pt(PIP)$_2$(TFBA)$_2$(H$_2$O)$_2$] **(51)**	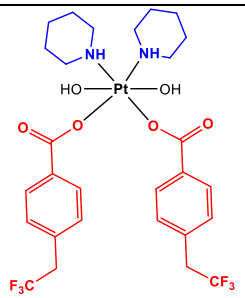	69% (15.6 mg; 0.020 mmol)	Whitish powder

The yield of the synthesized compounds varied from low to high. This variation may be attributed to differences in the lipophilicity of each compound, which affects their solubility in water. Compounds with higher water solubility may remain in the product filtrate, reducing the overall yield. Additionally, the duration of the final filtration step could impact the yield, as extended filtration times might contribute to variations in the recovered product.

3.2 Characterization of compounds using attenuated total reflection (ATR)/Fourier transform infrared spectroscopy (FTIR) and ^{1}H-NMR

The IR spectrum of *cis*-Pt(DACH)X$_2$ intermediate and their analogs are shown in (**Figure 3.2.1)** which crossbanded with a previous study regarding the IR result of *cis*-Pt(DACH)I$_2$(Pažout et al., 2011). It's noticed that the NH stretching has the highest intensity in the intermediate compound, the intensity is weakened after the substitute with the iodide ligand, the Pt(EN)X$_2$ are shown in (**Figure 3.2.2**)(Bahkali et al., 2021), Pt(NBA) $_2$X$_2$ are shown in (**Figure 3.2.3)**, Pt(PIP)$_2$X$_2$(Khan et al., 2000)are shown in (**Figure 3.2.4)**, Pt(PYR) $_2$X$_2$ are shown in (**Figure 3.2.5)**.

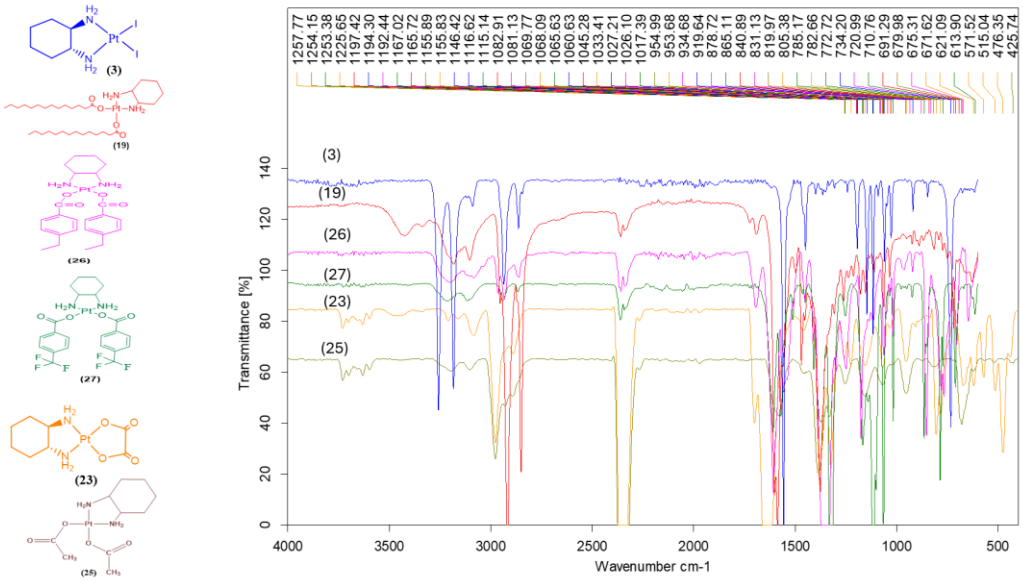

Figure 3.2.1 The FTIR/ATR spectra analysis of *cis*-Pt(DACH)X_2, where X = Iodide **(3)**, myristate **(19)**, 4-ethyl benzoate **(26)**, 4-trifluoromethyl benzoate **(27)**, oxalate **(23)**, and acetate **(25)**.

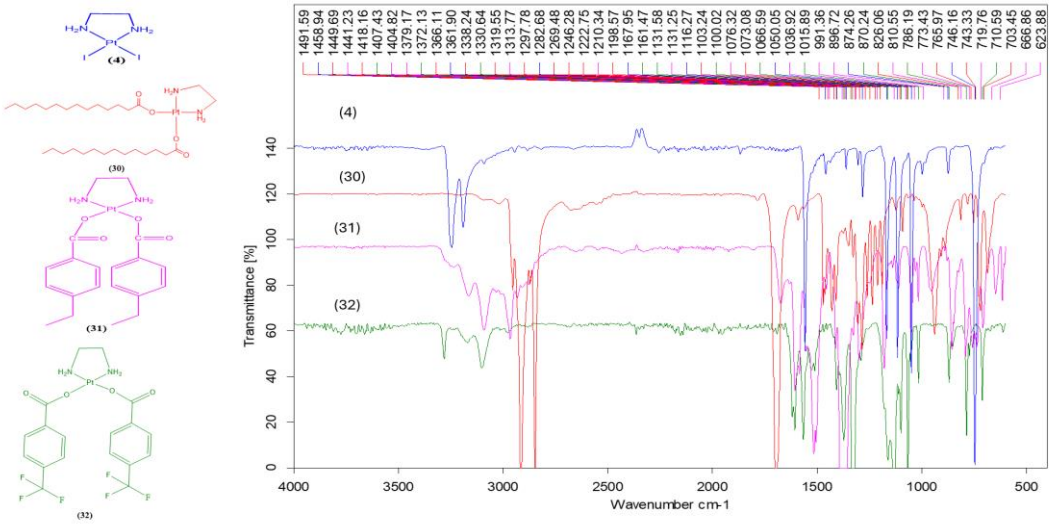

Figure 3.2.2 The FTIR/ATR spectra analysis of *cis*-Pt(EN)X_2, where X = iodide **(4)**, myristate **(30)**, 4-ethyl benzoate **(31)**, and 4-trifluoromethyl benzoate **(32)**.

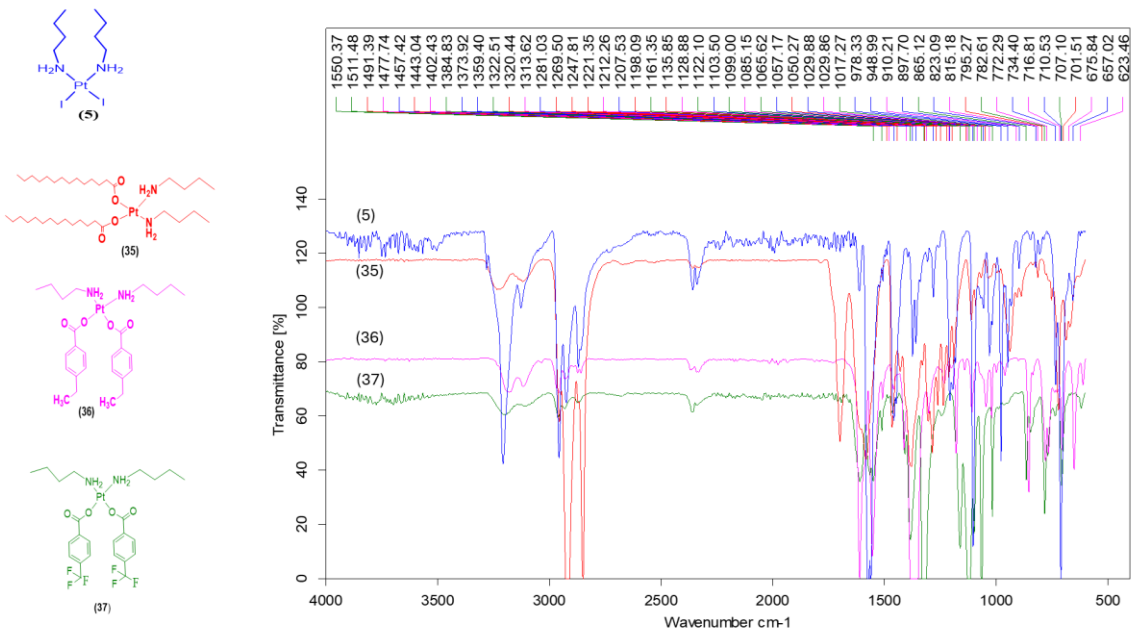

Figure 3.2.3 The FTIR/ATR spectra analysis of *cis*-Pt(NBA)$_2$X$_2$, where X = iodide **(5)**, myristate **(35)**, 4-ethyl benzoate **(36)**, and 4-trifluoromethyl benzoate **(37)**.

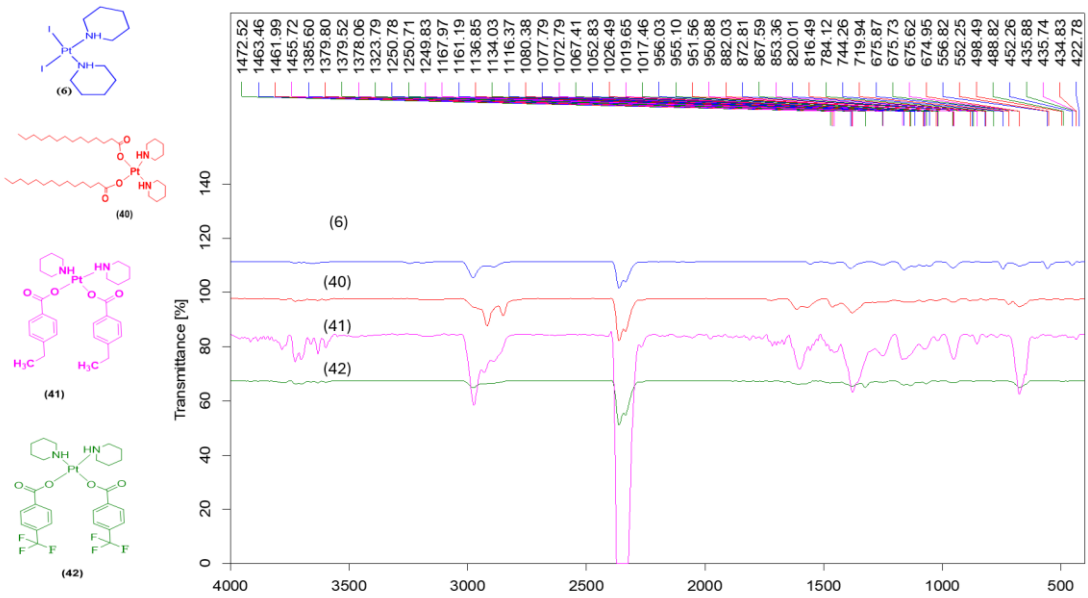

Figure 3.2.4 The FTIR/ATR spectra analysis of *cis*-Pt(PIP)$_2$X$_2$, where X = iodide **(6)**, myristate **(40)**, 4-ethyl benzoate **(41)**, and 4-trifluoromethyl benzoate **(42)**.

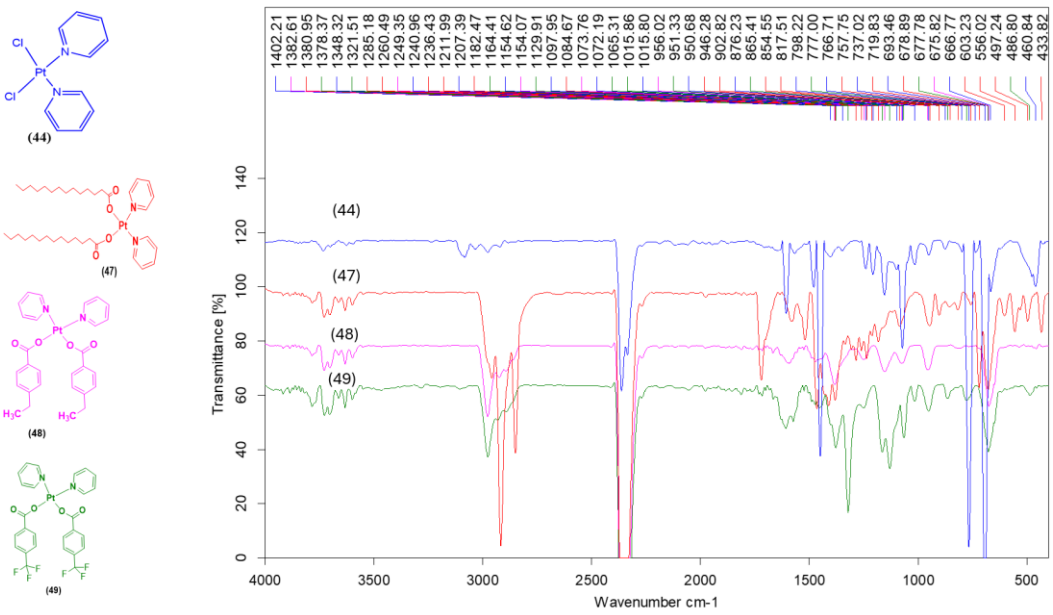

Figure 3.2.5 The FTIR/ATR spectra analysis of *cis*-Pt(PYR)$_2$X$_2$, where X = chloride **(44)**, myristate **(47)**, 4-ethyl benzoate **(48)**, and 4-trifluoromethyl benzoate **(49)**.

It clearly shows how the peak stretching and the intensity of the same chelating ligand are affected by the different leaving groups which is detailed in (**Table 3.2),** The range of 3400 and 3100 cm^{-1} have been attributed to the coordinate neutral amine ligand, C=O band appeared in the range of 1596-1680 cm^{-1} while C-O band appear in the range of 1340-1388 cm^{-1}, the Pt-I and Pt-Cl were supposed to appear around 300 while, the Pt-N were supposed to appear around 470-580 while The Pt-O were supposed to appear around 315-480(Khan et al., 2000). The FTIR/ ATR of each final complex was put in **Appendix 1**. The strong sharp peak at 2357 is suspected carbon O=C=O stretching, which was caused by wiping the FTIR/ATR with isopropanol.

Table 3.2 FTIR/ ATR spectroscopy of platinum (II) complex.

Complex	IR, cm^{-1}				
	^{V}N-H	^{V}C-H	^{V}C=O	^{V}C-O	^{V}C-C in-ring
[*cis*-Pt(DACH)(I)$_2$] **(3)**	3257-3184	2936-2864	____	____	1558
Miriplatin **(19)**	3198-3109	2917-2870	1685	1384	1586

Oxaliplatin **(23)**	3209-3161	2977-2890	1653	1378	1473	Pt-N 519	Pt-O 442
[*cis*-Pt(DACH)(acetate)$_2$] **(25)**	3192-3124	2977-2890	1687	1380	1597	Pt-N 515	Pt-O 476
[*cis*-Pt(DACH)(EZB)$_2$] **(26)**	3212-3088	2964-2934	1661	1385	1600		
[*cis*-Pt(DACH)(TFBA)$_2$] **(27)**	3226-3109	2943-2855	1612	1378	1570	CF 1161	
[*cis*-Pt(EN)(I)$_2$] **(4)**	3247-3190	2977-2888	___	__	1460	Pt-N 423	
[*cis*-Pt(EN)(MYR)$_2$] **(30)**	3086-3024	2958-2878	1702	1366	1427		
[*cis*-Pt(EN)(EZB)$_2$] **(31)**	3171-3088	2969-2932	1679	1378	1513		
[*cis*-Pt(EN)(TFBA)$_2$] **(32)**	3282-3103	2980-2970	1617	1372	1511	C-F 1161	
[*Cis*-Pt(NBA)$_2$I$_2$] **(5)**	3212-3134	2924-2870	1614	1359	1560		
[*Cis*-Pt(NBA)$_2$(MYR)$_2$] **(35)**	3221-3115	2945-2880	1668	1320	1491		
[*Cis*-Pt(NBA)$_2$(EZB)$_2$] **(36)**	3182-3115	2960-2928	1611	1314	1477		
[*Cis*-Pt(NBA)$_2$(TFBA)$_2$] **(37)**	3200-3146	2959-2928	1611	1384	1550	CF 1161	
[*Cis*-Pt(PIP)$_2$I$_2$] **(6)**	3246-3191	2977-2890	___	___	1555		
[*Cis*-Pt(PIP)$_2$(MYR)$_2$] **(40)**	3200-3147	2918-2851	1612	1380	1572	Pt-O 435	Pt-N 552
[*Cis*-Pt(PIP)$_2$(EBZ)$_2$] **(41)**	3200-3155	2974-2922	1601	1378	1557	Pt-O 435	
[*Cis*-Pt(PIP)$_2$(TFBA)$_2$] **(42)**	3100-3050	2976-2896	1607	1324	1524	C-F 1666	Pt-O 435	Pt-N 488

[*Cis*-Pt(PYR)$_2$Cl$_2$] **(44)**	____	2977-2922	____	____	____	C=N 1379	C-N 1348	
[*Cis*-Pt(PYR)$_2$(MYR)$_2$] **(47)**	___	2957-2916	1581	1381	1520	C-N 1285	Pt-O 433	
[*Cis*-Pt(PYR)$_2$(EBZ)$_2$] **(48)**	_____	2977-2924	1667	1383	1552	C-N 1250		
[*Cis*-Pt(PYR)$_2$(TFBA)$_2$] **(49)**	_____	2974-2927	1609	1379	1579	C-N 1252	C-F 1165	Pt-N 487

The ^{1}H-NMR data for [*cis*-Pt(DACH)(EBZ)$_2$] **(26)** which is shown in **(Figure 3.3.6),** recorded at 81 MHz in $CDCl_3$, The aromatic region shows triplets at δ 7.56 ppm (J = 7.1 Hz, 4H) and δ 6.84 ppm (J = 8.7 Hz, 4H), corresponding to the aromatic protons of the 4-ethyl benzoate (EBZ) ligands, indicating symmetry within the aromatic rings. The quartet at δ 2.28 ppm (J = 7.6 Hz, 4H) is assigned to the methylene protons in the ethyl groups (CH_2CH_3) attached to the benzoate rings, reflecting coupling with the adjacent methyl groups. A doublet at δ 1.69 ppm (J = 9.4 Hz, 2H) corresponds to protons on the cyclohexane-1,2-diamine (DACH) adjacent to nitrogen atoms (CHN). Finally, a broad multiplet between δ 0.95 and 0.74 ppm (13H) encompasses the aliphatic protons of the DACH structure and the methyl groups of the ethyl substituents, indicating a complex splitting pattern. This NMR data confirms the presence of aromatic rings, ethyl groups, and the DACH moiety, aligning well with the expected structure of the complex.

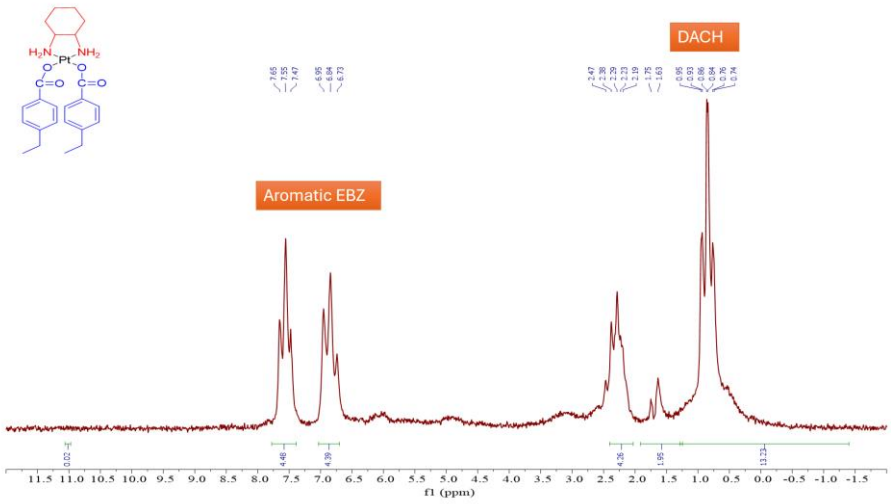

Figure 3.3.6 ^{1}H-NMR spectra of [*Cis*-Pt(DACH)(EBZ)$_2$] **(26)**

^{1}H-NMR data for [*cis*-Pt(DACH)(TFEB)$_2$] **(31)** which is shown in **(Figure 3.3.8),** recorded at 81 MHz in $CDCl_3$, The aromatic region exhibits triplets at δ 7.96 ppm (J = 6.1 Hz, 4H) and δ 7.58 ppm (J = 6.7 Hz, 4H), corresponding to the aromatic protons of the 4-trifluoromethylbenzoate (TFBA) ligands. This indicates the presence of two sets of equivalent aromatic protons, suggesting a symmetric arrangement within the aromatic rings. A singlet at δ 2.47 ppm with an integration of 4H corresponds to the amine protons (NH_2) in the cyclohexane-1,2-diamine (DACH) moiety, indicating the presence of two NH_2 groups that are not coupled to other protons. The broad multiplet between δ 1.18 and 0.79 ppm (10H) encompasses the aliphatic protons of the DACH structure, reflecting a complex splitting pattern typical for a cyclohexane ring with protons in different environments. This NMR data confirms the presence of aromatic rings, amine groups, and the DACH moiety, aligning well with the expected structure of the platinum complex.

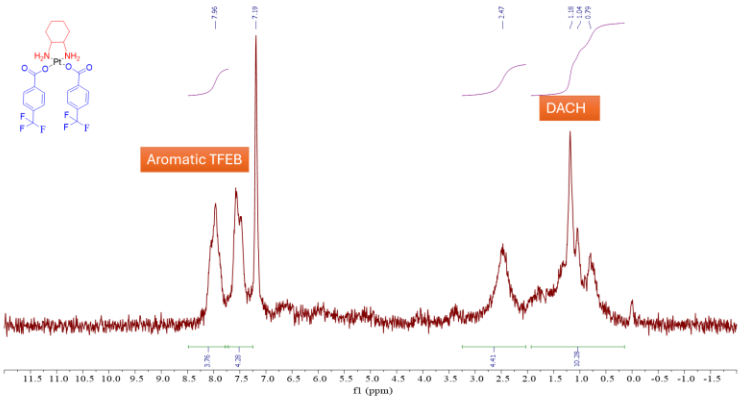

Figure 3.3.8 ^{1}H-NMA spectra of [*Cis*-Pt(DACH)(TFBA)$_2$] **(27)**

The ^{1}HNMR for compounds [*Cis*-Pt(PIP)$_2$(MYR)$_2$] **(40)** and [*Cis*-Pt(EN)(EBZ)$_2$] (31) were done the results indicate that these two compounds need to be repurified, as for the other compounds the ^{1}HNMR were not performed due to the unavailability at the time, its recommended to be done in the future.

3.3 Characterization of Pt-loaded niosomal formulations niosomes

The morphology and size of the loaded niosomes were determined using the atomic force microscope (AFM), as shown in Figure 3.3. Spherical loaded niosomes were obtained. Based on the analysis of AFM measurements the diameter was 160-270 nm for the blank niosomes, 150-190 nm for niosomal-miriplatin **(19)**, and 80-120 nm for niosomal [*cis*-$Pt(NBA)_2(MYR)_2$] **(35)** its small size could be due to the niosomes self-assembly and the interference with the lipophilic characteristics of the compound from its long aliphatic chain and the amine chain. Other Pt-niosomal formulations had bigger vesicles with diameters in the range of 215-340 nm, as shown in Table 3.3**.**

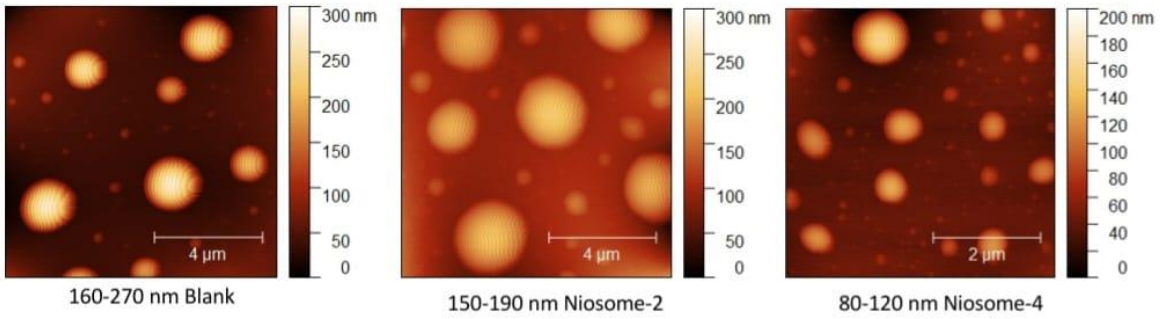

Figure 3.3: AFM images of the Pt-derivatives loaded in niosomal formulations.

The polydispersity index (PDI) of nanoparticles, which represents the distribution of size populations within a given sample, numerically ranges from 0.01 for a perfectly uniform sample concerning particle size 0.3 whereas a PDI index value of more than 0.3 indicates a broad particle size distribution of the formulation up to 1.0 (for a highly polydisperse sample with multiple particle size populations)(Silva & Press, 2019). Thus, PDI is considered one of the critical parameters for evaluating the consistency of the distribution of particle size in the niosomal formulations. The lower PDI indicates a narrow particle size distribution, and the smaller the distribution, the easier it is to make an accurate prediction of the particle behavior. The main technique for determining the PDI is dynamic light scattering (DLS), which measures particle size by examining the Brownian motion of particles. DLS offers a quick and easy means to determine the size of particles. Since it can measure a broad range of sizes, DLS is especially useful for native niosomal preparations(Silva & Press, 2019; Witika et al., 2022). The particle size distribution of freshly prepared niosomal formulations encompassing a group of newly synthesized Pt-based cytotoxic agents were determined using NanoBrook Omni.

Particle size and size distribution are pivotal parameters in evaluating nanoparticle performance(Bahari & Hamishehkar, 2016). Significant disparities in drug loading,

encapsulation efficiency, bioavailability, and efficacy of nanoformulations are observed with wide particle size distributions. Attaining nanoparticles with narrow size distributions, especially smaller particles, presents a notable challenge due to their uptake mechanisms via endocytosis or tight junctions of intestinal epithelial cells(Bahari & Hamishehkar, 2016; Joseph et al., 2023). Table 3.3 presents various formulations of Pt-loaded niosomes, detailing their size distribution, polydispersity index (PDI), loading efficiency, and corresponding *in vitro* activity against Hep-G2, Hep-3B, and LX2 cells, represented with an IC_{50} in the nanomolar range by the GraphPad.

It is noticed that the particle size of niosome nanoparticles at different weight ratios varies within the range of 80-120 nm and 150-190 nm, whereas unmodified CS/ALG core-shell nanoparticles at different weight ratios are comparatively larger and vary between 98-216 nm. However, in all the core-shell nanoparticle formulations, a minority population of very small particles is observed. Again, all the nanoparticle batches exhibit PDI index values of 0.25-0.65. So, it can be interpreted that the niosome nanoparticles will be more preferred for intestinal internalization over unmodified CS/ALG core-shell nanoparticles in delivering insulin via oral route due to their comparatively smaller size, particle size distribution, and more stable particles showing monodispersity(Y. Wang et al., 2024).

Our findings, as presented in Table 3.3, underscore the considerable influence of encapsulated ligands on the size, polydispersity, and loading efficiency of platinum-based compounds within the niosomal formulation. Interestingly, the impact of various ligand structures on particle size and polydispersity is notably diminished in compounds featuring more compact and smaller ligands. For instance, compounds like NBA (n-butyl amine) tend to exhibit smaller particle sizes compared to those with bulkier ligands such as (1*R*, 2*R*)-Diaimnocyclohexane (DACH), exemplified by *cis*-$Pt(NBA)_2(MYR)_2$ **(35)** at 109 nm versus *cis*-$Pt(DACH)(TFBA)_2$ **(27)** at 252.16 nm. Additionally, compounds with smaller ligands demonstrate lower polydispersity, indicative of a more uniform distribution of particle sizes.

Moreover, ligand selection significantly affects loading efficiency, with certain ligands showcasing notable improvements in encapsulation efficiency. For instance, *cis*-$Pt(NBA)_2(EZB)_2$ **(36)** and *cis*-$Pt(PYR)_2(EZB)_2$ **(48)** exhibit remarkable loading efficiencies of 71% and 78%, respectively, despite slightly larger particle sizes. This enhancement in loading efficiency suggests an intricate interplay between these ligands and the niosomal structure, but there's a noticeable difference in these compounds in

both dynamic light scattering (DLS) and polydispersity index (PDI). The cytotoxicity of **(36)** is found to be twice as potent as **(48)**, highlighting the significant influence of the aliphatic spectator ligand NBA in contrast to the heterocyclic ligand pyridine as well as facilitating more effective encapsulation of platinum compounds. For instance, combining NBA as a spectator ligand with TFBA as a leaving group notably improves loading efficiency, as evidenced by *cis*-Pt(NBA)$_2$(TFBA)$_2$ **(37)** achieving 64% loading compared to 58% and 51% for *cis*-Pt(EN)(TFBA)$_2$ **(32)** and *cis*-Pt(PIP)$_2$(MYR)$_2$ **(40)**, respectively. Furthermore, compounds featuring myristate as a leaving ligand demonstrate improved loading efficiency compared to oxaliplatin or cisplatin. However, even among compounds sharing similar ligands, loading efficiency may vary significantly. The comparatively low encapsulation observed in *cis*-Pt(DACH)(TFBA)$_2$ **(27)** with a loading efficiency of 15% appears unexpected when contrasted with *cis*-Pt(EN)(TFBA)$_2$ **(32)** at 58%. Both complexes feature two monodentate TFBA carboxylate ligands along with a spectator bidentate ligand, DACH, which is more lipophilic in **(27)** than EN in **(32)**. Notably, the loading efficiency for *cis*-Pt(EN)(TFBA)$_2$ **(32)** surpassed that of oxaliplatin **(23)** at 36%, suggesting a potential influence of the aromatic carboxylate ligand TFBA compared to oxalate, and the involvement of additional variables such as drug molecule interactions or ligand geometry. Optimizing drug delivery systems for cancer therapy necessitates a comprehensive understanding of the intricate interplay between ligand structure and the physicochemical properties of the niosomal formulation.

Table 3.3.1 The loading efficiency, DLS, polydispersity, and IC$_{50}$ of niosomes loaded with platinum derivatives with myristate ligand along with cisplatin and oxaliplatin.

Niosomes loaded with Pt derivatives		**IC$_{50}$ of the Pt-loaded Niosomes**			
Compound structure	**Loading Efficiency (LE)**	**Particle size and PDI**	**Hep G2**	**Hep 3B**	**LX2**
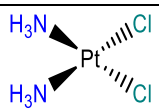	35%	170.2 nm, 0.2	0.7775 µM	0.5658 µM	1.129 µM

Cisplatin **(10)**					
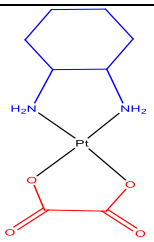 (Oxaliplatin) **(23)**	36%	246.69 nm, 0.279	0.9848 µM	0.6865 µM	0.4361 µM
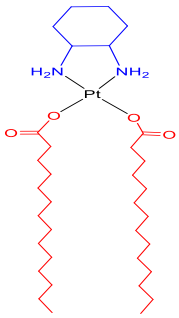 [[*Cis*-Pt(DACH)(MYR)$_2$], Miriplatin] **(19)**	39%	183.55 nm, 0.078	0.2015 µM	0.6906 µM	0.5207 µM
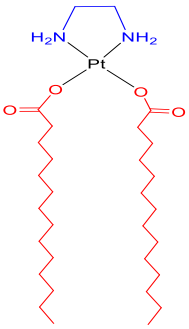 [*Cis*-Pt(EN)(MYR)$_2$] **(30)**	48%	227.76 nm, 0.284	0.5363 µM	0.3584 µM	0.5207 µM
	51%	279.81 nm, 0.349	0.6294 µM	0.3584 µM	0.1576 µM

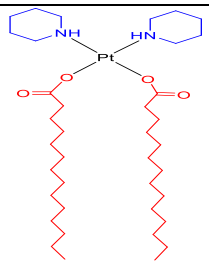 [*Cis*-Pt(PIP)$_2$(MYR)$_2$] **(40)**					
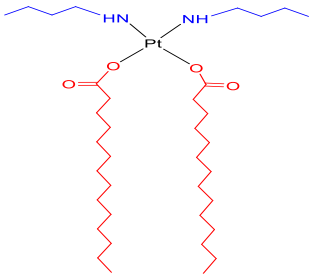 [*Cis*-Pt(NBA)$_2$(MYR)$_2$] **(35)**	39.5%	109 nm, 0.151	0.4424 µM	0.6014 µM	0.3051 µM
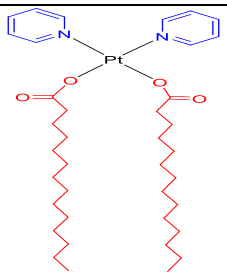 [*Cis*-Pt(PYR)$_2$(MYR)$_2$] **(47)**	46%	343.52 nm, 0.265	0.7999 µM	0.3896 µM	0.3749 µM

Table 3.3.2 The loading efficiency, DLS, polydispersity, and IC_{50} of niosomes loaded with platinum derivatives with 4-ethyl benzoate ligand.

Niosomes loaded with Pt derivatives	**IC_{50} of the Pt-loaded Niosomes**				
Compound structure	**Loading Efficiency (LE)**	**Particle size and PDI**	**Hep G2**	**Hep 3B**	**LX2**

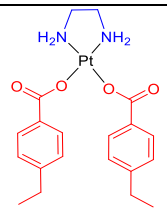 [*Cis*-Pt(EN)(EZB)$_2$] **(31)**	43%	220.91 nm, 0.164	1.062 uM	0.9038 uM	0.8486 uM
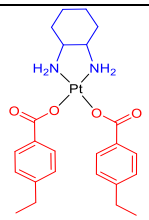 [*Cis*-Pt(DACH)(EBZ)$_2$] **(26)**	38%	256.65 nm, 0.333	0.6277 uM	0.5414 uM	0.5387 uM
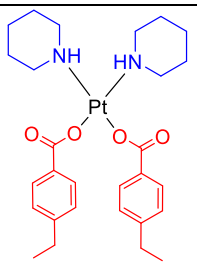 [*Cis*-Pt(PIP)$_2$(EBZ)$_2$] **(41)**	56%	212.87 nm, 0.322	0.7460 uM	0.4821 uM	0.6795 uM
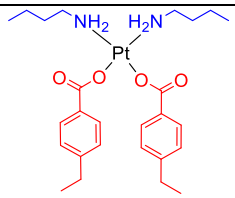 [*Cis*-Pt(NBA)$_2$(EZB)$_2$] **(36)**	71%	159.46 nm, 0.276	0.6260 uM	0.5358 uM	0.3399 uM
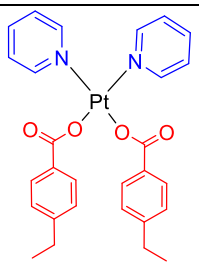 [*Cis*-Pt(PYR)$_2$(EBZ)$_2$] **(48)**	78%	209.48 nm, 0.208	1.162 uM	1.046 uM	0.6435 uM

Table 3.3.3 The loading efficiency, DLS, polydispersity, and IC_{50} of niosomes loaded with platinum derivatives with 4-trifluoromethyl benzoate ligand.

Niosomes loaded with Pt derivatives	IC_{50} of the Pt-loaded Niosomes				
Compound structure	**Loading Efficiency (LE)**	**Particle size and PDI**	**Hep G2**	**Hep 3B**	**LX2**
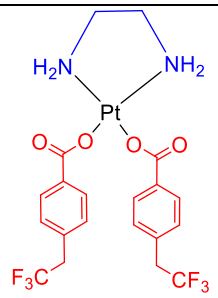 [*Cis*-Pt(EN)$(TFBA)_2$] **(32)**	58%	217.84 nm, 0.089	1.093 µM	0.7206 µM	0.9810 µM
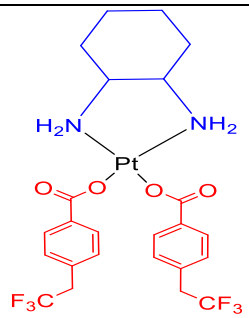 [*Cis*-Pt(DACH)$(TFBA)_2$] **(27)**	15%	252.16 nm, 0.164	0.5783 µM	0.4152 µM	0.09467 µM
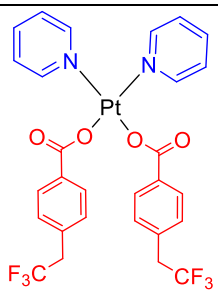 [*Cis*-Pt$(PIP)_2(TFBA)_2$] **(42)**	26%	206.75 nm, 0.294	0.5420 µM	0.5151 µM	0.2480 µM

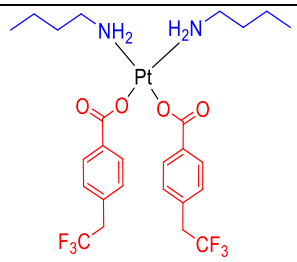 [*Cis*-Pt(NBA)$_2$(TFBA)$_2$] **(37)**	64%	272.09 nm, 0.286	0.8199 µM	0.7886 µM	0.7298 µM
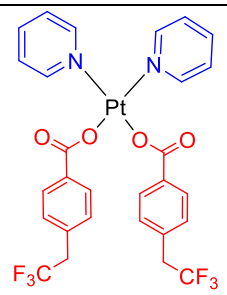 [*Cis*-Pt(PYR)$_2$(TFBA)$_2$] **(49)**	47%	330.62 nm, 0.281	0.6865 uM	0.4439 uM	0.4439 uM

Theoretically, the smaller vesicles could lead to lower IC_{50} values and a higher potency against cancer cells. Briefly, the niosomal formulation of *cis*-Pt(NBA)$_2$(MYR)$_2$**(35)** exhibited a good potency (IC_{50} = 0.4424 µM, 0.6014 µM, 0.3051 µM) against Hep-G2, Hep-3B, and LX2, respectively, compared to *cis*-Pt(PYR)$_2$(MYR)$_2$ **(47)** (343.52 nm), and it poses a good potency at the same time (IC_{50} = 0.7999 µM, 0.3896 µM, 0.3749 µM) against Hep-G2, Hep-3B, and LX2, respectively. It's still controversial and needs more investigation and study.

Low polydispersity in niosome formulations often results in more uniform vesicles, which can enhance their reliability and stability, leading to more consistent and predictable IC_{50} values across different cell lines. Higher polydispersity indicates a larger range of particle sizes, which might affect cellular uptake and drug release kinetics, potentially causing variability in IC_{50} values among different cell lines(Saimi et al., 2021). For instance, [*cis*-Pt(DACH)(MYR)$_2$], Miriplatin **(19)**, exhibited the lowest polydispersity (0.078) and the highest potency against the Hep-G2 cell line (0.2015 µM), supporting the theoretical connection between low polydispersity and high potency. Conversely, [*cis*-Pt(EN)(TFBA)$_2$] **(32)**, with the second-lowest polydispersity (0.089), showed one of the weakest potencies in the study (1.093 µM) against Hep-G2, indicating that other factors may also influence efficacy.

The low loading efficiency may also be due to the use of the film hydration techniques, as low loading efficiency is one of the disadvantages of these techniques(Karki et al., 2016), to overcome this and due to the high lipophilic characteristics of the novel synthetic compounds tween 80 were used, which possesses a low hydrophilic-lipophilic balance (HLB) value and is the best for utilization the niosomal formulation to enhance encapsulation efficiency(Ruckmani & Sankar, 2010). The loading efficiency of the drug was average compared to the previous published studies, especially regarding cisplatin and oxaliplatin, with loading efficiencies of 45% and 36% respectively. Cisplatin, oxaliplatin, and carboplatin have solubility in water of 1 mg/ml, 6 mg/ml, and 14 mg/ml, respectively. Spans were used in the niosomal formulations in all of the previous studies. They were used to compare niosomal cisplatin and free cisplatin in a murine B16-F10 melanoma model. The percentage entrapment efficiency (EE%) of cisplatin was 31.983 ± 0.72%(Gude et al., 2002). It was also used to prepare niosomal cisplatin against breast cancer, with an encapsulation efficiency and loading efficiency of 41 ± 2 and 2.3 ± 0.15%, respectively(Kanaani, Javadi, et al., 2017). In a n other studies against breast cancer, it was carried out with a PH-responsive agent, which provided a high encapsulation efficiency of 89%(Sargazi et al., 2021). Other than cisplatin, the oxaliplatin niosomal formulation was studied against colorectal cancer, and the EE% was 90.57 ± 2.05%(El-Far et al., 2022). Niosomal carboplatin was evaluated against brain carcinoma using Span 60, and the EE% was 60.2 ±2.3%(Abbasi et al., 2023). Span 40 was also used in another study that tested the efficiency of cisplatin against VX2 sarcoma; the EE% was 76.93 ± 2.67%(H. Yang et al., 2013).

3.4 Cytotoxicity of niosomal nanoparticulate formulations of Pt-based derivatives

Assessment of the cytotoxicity of the niosomal formulation of compounds prepared in the course of this study was done against three cell lines: Hep-G2 (nontumorigenic human hepatoma cells with high proliferation rates and an epithelial-like morphology that perform many differentiated hepatic functions), Hep-3B (immortalized human-derived hepatocyte carcinoma cell line), and LX2 (human hepatic stellate cell line) shown in Table 3.3. A concentration-dependent cytotoxicity study using an MTS assay was performed for Pt-derivatives loaded in the niosomal formulation. MTS was selected as the assay of choice since it does not require using DMSO for solubilizing, which is

advantageous when using platinum-based drugs known to be inactivated by this solvent(Lu, 2014). Our results indicate a notable connection between the structure of the compound and the cytotoxic effect on the cell line.

It is shown that the niosomal formulation of miriplatin **(19)** was most potent against the Hep-G2 hepatoma cell line compared to other platinum niosomal formulation. For instance, the miriplatin noisomal formulation was three-and-half-fold more active against Hep-G2 compared to Hep-3B, around five-fold more potent against it compared to the formulation of oxaliplatin, and around five-fold more potent against it compared to the formulation of cisplatin (**Figure** 3.5.1). A previous study (2011) conducted by Tanaka and his team has been recognized for its cytotoxicity against liver cancer cells(Tanaka et al., 2011). Miriplatin analogs *cis*-Pt(EN)$(MYR)_2$ **(30)**, *cis*-Pt$(PIP)_2(MYR)_2$ **(40),** and *cis*-Pt$(PYR)_2(MYR)_2$ **(44)** exhibited higher potency against the cell line Hep-3B (IC_{50} = 0.3584 μM, 0.3584 μM, and 0.3896 μM, respectively). Indicating that myristate, which is the common moiety in these compounds, has a role to play in improving the performance of the formulation in inhibiting the prefiltration of cells. It is believed that the lipophilic character of myristate may exert hydrophobic interaction with lipidic compounds (cholesterol or L-α-soya phosphatidylcholine) and with the non-ionic surfactants that are the main ingredients utilized for the preparation of niosomes. Nonionic surfactant has a hydrophilic head group and a hydrophobic tail, which affect the entrapment efficiency assumingly by accommodating hydrophobic drugs within the outer layers' hydrophobic shells. Additionally, lipid compounds are utilized to provide an unbending nature, appropriate shape, and adaptation to the niosomes.

The difference in potency between the two cell lines with the same compound may be due to their origin. As for the LX2, the compound that had the lowest IC_{50} value of 0.09467 μM on the LX2 cells in our study was *cis*-Pt(DACH)$(TFBA)_2$ **(27)**, which would have the most potency against the normal liver cell line, and it also had potency against the liver cancer cells of 0.5783 uM and 0.4152 uM for Hep-G2 and Hep-3B, respectively. The drug with the highest IC_{50} against the LX2 is cisplatin **(10),** which would be the least potent against the liver cancer cell line. Hep-G2 and Hep-3B cell lines were obtained from different biopsy specimens, representing distinct phases of liver cell differentiation. Hep-G2 originates from primary hepatoblastoma (HB), while Hep-3B originates from primary hepatocellular carcinoma (HCC). Proteome analysis showed that Hep-G2 cells retained more characteristics associated with hepatocytes, whereas

Hep-3B cells exhibited more characteristics associated with fibroblasts and epithelial to mesenchymal *trans*ition (EMT) markers. EMT is a reversible process important in tissue formation and conditions like fibrosis and tumor formation, influenced by various factors such as miRNAs, epigenetic changes, and transcription factors. EMT transforms fibroblasts into hepatocyte-like cells and vice versa. Hep-3B cells underwent EMT, whereas Hep-G2 cells did not show EMT signs. Differences in P53 status also play a role, with Hep-G2 having mutated P53 and Hep-3B having wild-type P53 similar to LX2, affecting activity against normal liver cells and LX2(Qiu et al., 2015).

The cytotoxicity of niosomal platinum compounds, using IC_{50} values as indicators, may vary based on the maturation stage and cellular features of Hep-G2, Hep-3B, and LX2 cells. Compounds with lower IC_{50} values against Hep-G2 cells derived from primary hepatoblastoma (HB) may be more susceptible to our niosomal platinum formulations because of their hepatocyte-like characteristics shown clearly in miriplatin **(19)**. Hep-3B cells may respond differently to niosomal platinum compounds due to epithelial-mesenchymal *trans*ition (EMT) and fibroblast-like features compared to Hep-G2 cells, as indicated by IC_{50} values. If certain drugs show selective cytotoxicity against cells undergoing EMT, such as Hep-3B, their IC_{50} values may be lower than those for Hep-G2 cells. As shown in Table 3.3, almost all of the synthesized compounds exhibit lower IC_{50} values for Hep-3B compared to Hep-G2 cells, which suggests selective toxicity against cells undergoing EMT. Differences in P53 status between Hep-G2 and Hep-3B cells may influence their reactions to our niosomal platinum compounds, resulting in varying IC_{50} values. Compounds that exclusively target cells with mutant P53, such as Hep-3B, may have decreased IC_{50} values against these cells while remaining relatively high against normal liver cells (LX2). For example, [*cis*-$Pt(NBA)_2(TFBA)_2$] **(37)** and [*cis*-$Pt(NBA)_2(EZB)_2$] **(36)** demonstrate selective cytotoxicity against Hep3B cells, which possess mutated P53, indicating their effectiveness in targeting P53-mutated cancer cells.

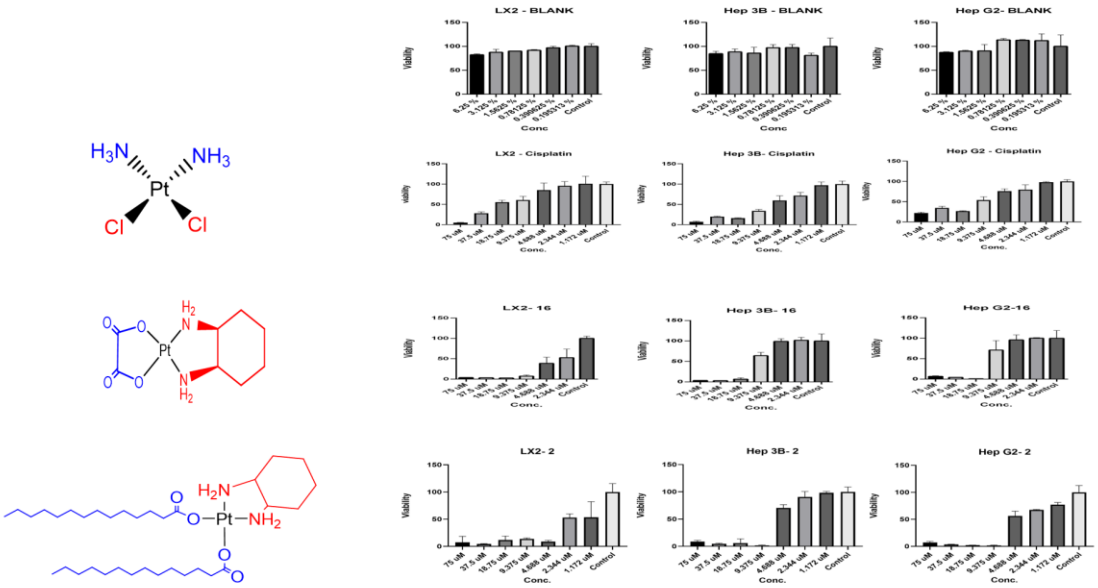

Figure 3.4.1 The IC_{50} of blank, loaded cisplatin, oxaliplatin and miriplatin.

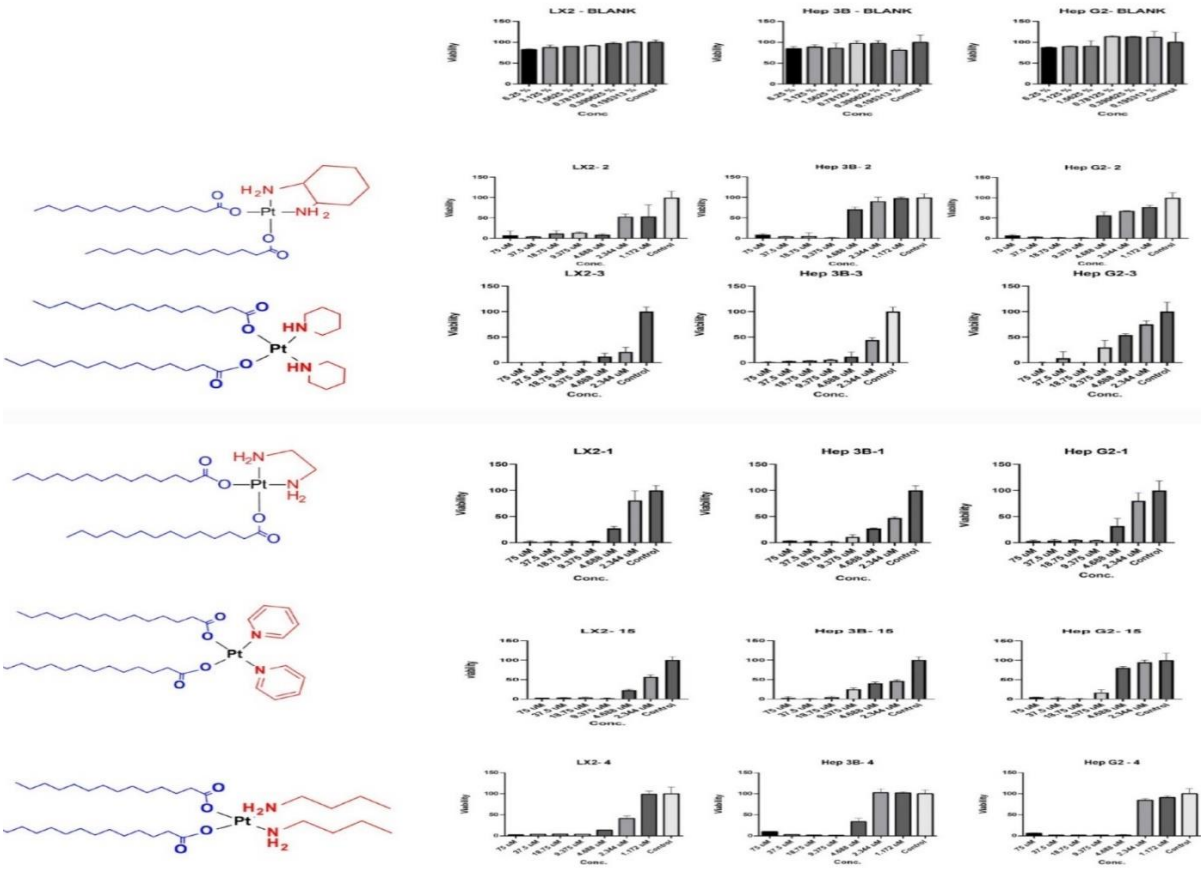

Figure 3.4.2: IC_{50} of blank, loaded miriplatin, and its analogs.

4 Conclusion

In conclusion, our study presents the design and synthesis of lipophilic mixed aliphatic/aromatic platinum(II/IV) derivatives and encapsulates these drugs in a novel drug delivery system, which, in our case, was niosome vesicles. The synthesis of the platinum compound was achieved through various routes with different yields and physical appearances. The purity and characteristics of the synthesized compounds were analyzed using analytical techniques such as FTIR/ATR ^{1}H-NMR, confirming their suitability for further preclinical and clinical investigation.

The characterization of the niosomal formulations resulted in critical information on loading efficiency and particle properties. Compounds like [*Cis*-Pt(NBA)$_2$(MYR)$_2$] **(35)** and [*Cis*-Pt(NBA)$_2$(EZB)$_2$] **(36)** have good loading efficiencies and reduced particle sizes, indicating promising drug delivery potential with homogeneous distributions inside niosomal formulations. Conversely, substances such as [*Cis*-Pt(DACH)(EBZ)$_2$] **(26)** have bigger particle sizes and greater polydispersity indices, indicating difficulties in attaining uniform drug distribution.

In vitro studies of these platinum compound-encapsulated niosomal formulations were assessed using the MTS assay on liver cancer cells (Hep-G2 and Hep-3B) and normal LX2, The cytotoxicity assays on these cell lines revealed important details about the anticancer activity of niosomal platinum compounds. Compounds such as [*Cis*-Pt(EN)(TFBA)$_2$] **(32)** and [*Cis*-Pt(NBA)$_2$(EZB)$_2$] **(36)** showed substantial cytotoxic effects with low IC_{50} values, indicating that they could be effective cancer therapies. Compounds having higher IC_{50} values, such as [*Cis*-Pt(EN)(EBZ)$_2$] **(31)** and [*Cis*-Pt(PYR)$_2$(EBZ)$_2$] **(48)**, may need more optimization to improve their therapeutic efficacy.

The platinum-based niosomal formulation showed promising results in terms of cytotoxic effects against the liver cell line, especially against Hep3B, which indicates the efficiency of these drugs against cell lines that either undergo EMT or have mutated P53. Niosomal platinum compounds may be interesting therapeutic choices for malignancies with P53 mutations, frequently associated with resistance to traditional chemotherapeutic drugs. By targeting specific vulnerabilities caused by P53 mutations, these drugs may overcome resistance mechanisms and enhance treatment results for patients with P53-mutated malignancies.

While our findings shed light on the link between niosomal platinum compounds and P53 status, more research is needed to unravel the underlying mechanisms causing the observed differences in sensitivity among cancer cell lines. Furthermore, preclinical and clinical studies are required to evaluate these drugs' efficacy and safety in P53-mutated malignancies, as well as to assess their clinical *trans*lation potential. In addition to the data presented in this study, future research should involve some computational studies to gain a clear understanding of Pt-dispersal inside the drug delivery system (DDS), and comprehensive animal trials to assess the efficacy and safety of niosomal platinum compounds for cancer treatment. While our in vitro trials give vital information about the cytotoxic effects of these compounds on cancer cell lines, animal studies are required to assess their therapeutic potential in a more physiologically relevant condition. Animal studies will enable pre*cis*e monitoring of drug release kinetics and pharmacokinetics, revealing critical information about the compound's distribution, metabolism, and elimination within the body. Tracking the drug's release from niosomal formulations over time allows us to better understand its pharmacological action and modify dose regimens for maximum therapeutic efficacy. Furthermore, animal studies allow for the evaluation of possible side effects and toxicity profiles related to niosomal platinum compounds. By closely monitoring animal subjects for adverse responses and physiological changes, we can detect possible safety issues and improve formulations or procedures for treatment to reduce patient risks.

References

Abbasi, M., Reihanisaransari, R., Poustchi, F., Hheidari, A., Ghanbarikondori, P., Salehi, H., Salehi, V., Izadkhah, M., Moazzam, F., & Allahyartorkaman, M. (2023). Toxicity of Carboplatin-Niosomal Nanoparticles in a Brain Cancer Cell Lineet. *Asian Pacific Journal of Cancer Prevention*, *24*(11), 3985–3991. https://doi.org/10.31557/APJCP.2023.24.11.3985

Abdelbary, A. A., & Aboughaly, M. H. H. (2015). Design and optimization of topical methotrexate loaded niosomes for enhanced management of psoriasis: Application of Box-Behnken design, in-vitro evaluation and in-vivo skin deposition study. *International Journal of Pharmaceutics*, *485*(1–2), 235–243. https://doi.org/10.1016/J.IJPHARM.2015.03.020

Abdelkader, H., Alani, A. W. G., & Alany, R. G. (2014a). Recent advances in non-ionic surfactant vesicles (niosomes): Self-assembly, fabrication, characterization, drug delivery applications and limitations. *Drug Delivery*, *21*(2), 87–100. https://doi.org/10.3109/10717544.2013.838077

Abdelkader, H., Alani, A. W. G., & Alany, R. G. (2014b). Recent advances in non-ionic surfactant vesicles (niosomes): Self-assembly, fabrication, characterization, drug delivery applications and limitations. *Drug Delivery*, *21*(2), 87–100. https://doi.org/10.3109/10717544.2013.838077

Abdelkader, H., Ismail, S., Kamal, A., & Alany, R. G. (2011). Design and evaluation of controlled-release niosomes and discomes for naltrexone hydrochloride ocular delivery. *Journal of Pharmaceutical Sciences*, *100*(5), 1833–1846. https://doi.org/10.1002/JPS.22422

Ag Seleci, D., Seleci, M., Walter, J. G., Stahl, F., & Scheper, T. (2016). Niosomes as nanoparticular drug carriers: Fundamentals and recent applications. *Journal of Nanomaterials*, *2016*. https://doi.org/10.1155/2016/7372306

Akbari, J., Saeedi, M., Enayatifard, R., Morteza-Semnani, K., Hassan Hashemi, S. M., Babaei, A., Rahimnia, S. M., Rostamkalaei, S. S., & Nokhodchi, A. (2020). Curcumin Niosomes (curcusomes) as an alternative to conventional vehicles: A potential for efficient dermal delivery. *Journal of Drug Delivery Science and Technology*, *60*. https://doi.org/10.1016/J.JDDST.2020.102035

Akula, S., Gurram, A. K., & Devireddy, S. R. (2014). Self-Microemulsifying Drug Delivery Systems: An Attractive Strategy for Enhanced Therapeutic Profile. *International Scholarly Research Notices*, *2014*, 1–11. https://doi.org/10.1155/2014/964051

Al-baker, S., & Dabrowiak, J. C. (1987). Oxidation of a Dinuclear Platinum(II) Complex with Hydrogen Peroxide. *Inorganic Chemistry*, *26*(4), 613–617. https://doi.org/10.1021/ic00251a024

Al-Baker, S., Perez-Soler, R., & Khokhar, A. R. (1992). Synthesis and biological studies of new lipid-soluble cisplatin analogues entrapped in liposomes. *Journal of Inorganic Biochemistry*, *47*(2), 99–108. https://doi.org/10.1016/0162-0134(92)84046-P

Alavizadeh, S. H., Badiee, A., Golmohammadzadeh, S., & Jaafari, M. R. (2014). The influence of phospholipid on the physicochemical properties and anti-tumor efficacy of liposomes encapsulating cisplatin in mice bearing C26 colon carcinoma. *International Journal of Pharmaceutics*, *473*(1–2), 326–333. https://doi.org/10.1016/j.ijpharm.2014.07.020

Alderden, R. A., Hall, M. D., & Hambley, T. W. (2006). The Discovery and Development of Cisplatin. *Journal of Chemical Education*, *83*(5), 728–734. https://doi.org/10.1021/ED083P728

Alemi, A., Zavar Reza, J., Haghiralsadat, F., Zarei Jaliani, H., Haghi Karamallah, M., Hosseini, S. A., & Haghi Karamallah, S. (2018). Paclitaxel and curcumin coadministration in novel cationic PEGylated niosomal formulations exhibit enhanced synergistic antitumor efficacy. *Journal of Nanobiotechnology*, *16*(1). https://doi.org/10.1186/S12951-018-0351-4

Aliabadi, H. M., & Lavasanifar, A. (2006). Polymeric micelles for drug delivery. *Expert Opinion on Drug Delivery*, *3*(1), 139–162. https://doi.org/10.1517/17425247.3.1.139

Allen, T. M., & Cullis, P. R. (2013). Liposomal drug delivery systems: from concept to clinical applications. *Advanced Drug Delivery Reviews*, *65*(1), 36–48. https://doi.org/10.1016/J.ADDR.2012.09.037

Alshammari, B. H., Lashin, M. M. A., Mahmood, M. A., Al-Mubaddel, F. S., Ilyas, N., Rahman, N., Sohail, M., Khan, A., Abdullaev, S. S., & Khan, R. (2023). Organic and inorganic nanomaterials: fabrication, properties and applications. *RSC Advances*, *13*(20), 13735–13785. https://doi.org/10.1039/d3ra01421e

Ang, W. H., Pilet, S., Scopelliti, R., Bussy, F., Juillerat-Jeanneret, L., & Dyson, P. J. (2005). Synthesis and characterization of platinum(IV) anticancer drugs with functionalized aromatic carboxylate ligands: Influence of the ligands on drug efficacies and uptake. *Journal of Medicinal Chemistry*, *48*(25), 8060–8069. https://doi.org/10.1021/jm0506468

Apps, M. G., Choi, E. H. Y., & Wheate, N. J. (2015). The state-of-play and future of platinum drugs. *Endocrine-Related Cancer*, *22*(4), R219–R233. https://doi.org/10.1530/ERC-15-0237

Arduino, I., Depalo, N., Re, F., Dal Magro, R., Panniello, A., Margiotta, N., Fanizza, E., Lopalco, A., Laquintana, V., Cutrignelli, A., Lopedota, A. A., Franco, M., & Denora, N. (2020). PEGylated

solid lipid nanoparticles for brain delivery of lipophilic kiteplatin Pt(IV) prodrugs: An in vitro study. *International Journal of Pharmaceutics*, *583*(January), 119351. https://doi.org/10.1016/j.ijpharm.2020.119351

Attia, M. F., Anton, N., Wallyn, J., Omran, Z., & Vandamme, T. F. (2019). An overview of active and passive targeting strategies to improve the nanocarriers efficiency to tumour sites. *Journal of Pharmacy and Pharmacology*, *71*(8), 1185–1198. https://doi.org/10.1111/JPHP.13098

Bagheri, A., Chu, B. S., & Yaakob, H. (2014). Niosomal drug delivery systems: Formulation, preparation and applications. *World Applied Sciences Journal*, *32*(8), 1671–1685. https://doi.org/10.5829/idosi.wasj.2014.32.08.848

Bahari, L. A. S., & Hamishehkar, H. (2016). The impact of variables on particle size of solid lipid nanoparticles and nanostructured lipid carriers; A comparative literature review. *Advanced Pharmaceutical Bulletin*, *6*(2), 143–151. https://doi.org/10.15171/apb.2016.021

Bahkali, A., Wei, J., & Deng, Y. (2021). *Inorganica Chimica Acta Synthesis and characterization of ethylenediamine platinum (II) complexes containing thiourea derivatives . X-ray crystal structures of [Pt (en) (2-imidazolidinethione) 2](NO 3) 2 and [Pt (en)(1-phenyl-2-thiourea) 2 . 520*(February).

Bas, S., & Soucek, M. D. (2012). Synthesis, characterization and properties of amphiphilic block copolymers of 2-hydroxyethyl methacrylate and polydimethylsiloxane prepared by atom transfer radical polymerization. *Polymer Journal*, *44*(11), 1087–1097. https://doi.org/10.1038/pj.2012.86

Basu, A., & Krishnamurthy, S. (2010). Cellular Responses to Cisplatin-Induced DNA Damage. *Journal of Nucleic Acids*, *2010*, 16. https://doi.org/10.4061/2010/201367

Bayindir, Z. S., & Yuksel, N. (2010). Characterization of niosomes prepared with various nonionic surfactants for paclitaxel oral delivery. *Journal of Pharmaceutical Sciences*, *99*(4), 2049–2060. https://doi.org/10.1002/jps.21944

Belkacemi, L., Atkins, J. L., Yang, L., Gadgil, P., Sater, A. K., Chow, D. S., Bose, R. N., & Zhang, S. X. (2018). Phosphaplatin anti-tumor effect enhanced by liposomes partly via an up-regulation of PEDF in breast cancer. *Anticancer Research*, *38*(2), 623–646. https://doi.org/10.21873/anticanres.12267

Bini, K. B., Akhilesh, D., Prabhakara, P., & Kamath, J. V. (2012). Development and characterization of non-ionic surfactant vesicles (niosomes) for oral delivery of lornoxicam. *International Journal*

of Drug Development and Research, *4*(3), 147–154.

Blint, R. J., Mcmahon, T. B., & Beauchamp, J. L. (1974). Gas-Phase Ion Chemistry of Fluoromethanes by Ion Cyclotron Resonance Spectroscopy. New Techniques for the Determination of Carbonium Ion Stabilities. *Journal of the American Chemical Society*, *96*(5), 1269–1278. https://doi.org/10.1021/JA00812A001/ASSET/JA00812A001.FP.PNG_V03

Boulikas, T. (2007). *Molecular mechanisms of cisplatin and its liposomally encapsulated form , Lipoplatin ™ . Lipoplatin ™ as a chemotherapy and antiangiogenesis drug*. *5*.

Brown, A., Kumar, S., & Tchounwou, P. B. (2019). Cisplatin-Based Chemotherapy of Human Cancers. *Journal of Cancer Science & Therapy*, *11*(4). /pmc/articles/PMC7059781/

Browning, R. J., Reardon, P. J. T., Parhizkar, M., Pedley, R. B., Edirisinghe, M., Knowles, J. C., & Stride, E. (2017). Drug Delivery Strategies for Platinum-Based Chemotherapy. *ACS Nano*, *11*(9), 8560–8578. https://doi.org/10.1021/ACSNANO.7B04092

Carr, J. L., Tingle, M. D., & McKeage, M. J. (2006). Satraplatin activation by haemoglobin, cytochrome C and liver microsomes in vitro. *Cancer Chemotherapy and Pharmacology*, *57*(4), 483–490. https://doi.org/10.1007/s00280-005-0069-5

Chen, J., Wang, X., Yuan, Y., Chen, H., Zhang, L., Xiao, H., Chen, J., Zhao, Y., Chang, J., Guo, W., & Liang, X. J. (2021). Exploiting the acquired vulnerability of cisplatin-resistant tumors with a hypoxia-amplifying DNA repair–inhibiting (HYDRI) nanomedicine. *Science Advances*, *7*(13), 1–13. https://doi.org/10.1126/sciadv.abc5267

Chen, Q., Yang, Y., Lin, X., Ma, W., Chen, G., Li, W., Wang, X., & Yu, Z. (2018). Platinum(iv) prodrugs with long lipid chains for drug delivery and overcoming cisplatin resistance. *Chemical Communications*, *54*(42), 5369–5372. https://doi.org/10.1039/C8CC02791A

Cheng, F., Zhang, R., Sun, C., Ran, Q., Zhang, C., Shen, C., Yao, Z., Wang, M., Song, L., & Peng, C. (2023). Oxaliplatin-induced peripheral neurotoxicity in colorectal cancer patients: mechanisms, pharmacokinetics and strategies. *Frontiers in Pharmacology*, *14*(August), 1–16. https://doi.org/10.3389/fphar.2023.1231401

Chung, T. S., Na, Y. M., Kang, S. W., Jung, O. S., & Lee, Y. A. (2005). Facile generation of platinum(IV) compounds with mixed labile moieties. Hydrogen peroxide oxidation of platinum(II) to platinum(IV) compounds. *Transition Metal Chemistry*, *30*(5), 541–545. https://doi.org/10.1007/s11243-005-2653-2

Cogger, V. C., Roessner, U., Warren, A., Fraser, R., & Le Couteur, D. G. (2013). A sieve-raft hypothesis for the regulation of endothelial fenestrations. *Computational and Structural Biotechnology Journal*, *8*(11), e201308003. https://doi.org/10.5936/csbj.201308003

Cohen, S. M., & Lippard, S. J. (2001). Cisplatin: from DNA damage to cancer chemotherapy. *Prog Nucleic Acid Res Mol Biol*, *67*, 93–130. https://doi.org/10.1016/s0079-6603(01)67026-0

Daley-Yates, P. T., & McBrien, D. C. H. (1985). A study of the protective effect of chloride salts on cisplatin nephrotoxicity. *Biochemical Pharmacology*, *34*(13), 2363–2369. https://doi.org/10.1016/0006-2952(85)90795-6

Dancey, J. E., & Chen, H. X. (2006). Strategies for optimizing combinations of molecularly targeted anticancer agents. *Nature Reviews Drug Discovery 2006 5:8*, *5*(8), 649–659. https://doi.org/10.1038/nrd2089

Date, T., Kuche, K., Ghadi, R., Kumar, P., & Jain, S. (2022). Understanding the Role of Axial Ligands in Modulating the Biopharmaceutical Outcomes of Cisplatin(IV) Derivatives. *Molecular Pharmaceutics*, *19*(5), 1325–1337. https://doi.org/10.1021/acs.molpharmaceut.1c00844

de Brito, R. V., Mancini, M. W., Palumbo, M. D. N., de Moraes, L. H. O., Rodrigues, G. J., Cervantes, O., Sercarz, J. A., & Paiva, M. B. (2022). The Rationale for "Laser-Induced Thermal Therapy (LITT) and Intratumoral Cisplatin" Approach for Cancer Treatment. *International Journal of Molecular Sciences*, *23*(11), 5934. https://doi.org/10.3390/ijms23115934

De Oliveira, M. B., Milled, J., Banks, R. E., Kelland, L. R., McAuliffe, C. A., Mahmood, N., & Rowland, I. J. (1996). New perfluorophtalate complexes of platinum(II) with chemotherapeutic potential. *Metal-Based Drugs*, *3*(3), 117–122. https://doi.org/10.1155/MBD.1996.117

Deo, K. M., Ang, D. L., McGhie, B., Rajamanickam, A., Dhiman, A., Khoury, A., Holland, J., Bjelosevic, A., Pages, B., Gordon, C., & Aldrich-Wright, J. R. (2018). Platinum coordination compounds with potent anticancer activity. *Coordination Chemistry Reviews*, *375*, 148–163. https://doi.org/10.1016/J.CCR.2017.11.014

Deo, K. M., Sakoff, J., Gilbert, J., Zhang, Y., & Aldrich Wright, J. R. (2019). Synthesis, characterisation and influence of lipophilicity on cellular accumulation and cytotoxicity of unconventional platinum(iv) prodrugs as potent anticancer agents. *Dalton Transactions*, *48*(46), 17228–17240. https://doi.org/10.1039/c9dt04049h

Dhar, S., & Lippard, S. J. (2009). Mitaplatin, a potent fusion of cisplatin. *Proceedings of the National*

Academy of Sciences of the United States of America, *106*(52), 22199–22204.

Dhaval, M., Vaghela, P., Patel, K., Sojitra, K., Patel, M., Patel, S., Dudhat, K., Shah, S., Manek, R., & Parmar, R. (2022). Lipid-based emulsion drug delivery systems — a comprehensive review. *Drug Delivery and Translational Research*, *12*(7), 1616–1639. https://doi.org/10.1007/s13346-021-01071-9

Dilruba, S., & Kalayda, G. V. (2016). Platinum-based drugs: past, present and future. *Cancer Chemotherapy and Pharmacology 2016 77:6*, *77*(6), 1103–1124. https://doi.org/10.1007/S00280-016-2976-Z

Doi, T., Hamaguchi, T., Shitara, K., Iwasa, S., Shimada, Y., Harada, M., Naito, K., Hayashi, N., Masada, A., & Ohtsu, A. (2017). NC-6004 phase I study in combination with gemcitabine for advanced solid tumors and population PK/PD analysis. *Cancer Chemotherapy and Pharmacology*, *79*(3), 569–578. https://doi.org/10.1007/s00280-017-3254-4

Dokania, S., & Joshi, A. K. (2015). Self-microemulsifying drug delivery system (SMEDDS)--challenges and road ahead. *Drug Delivery*, *22*(6), 675–690. https://doi.org/10.3109/10717544.2014.896058

Dragovich, T., Mendelson, D., Kurtin, S., Richardson, K., Von Hoff, D., & Hoos, A. (2006). A Phase 2 trial of the liposomal DACH platinum L-NDDP in patients with therapy-refractory advanced colorectal cancer. *Cancer Chemotherapy and Pharmacology*, *58*(6), 759–764. https://doi.org/10.1007/s00280-006-0235-4

Eastman, A. (1987). The formation, isolation and characterization of DNA adducts produced by anticancer platinum complexes. *Pharmacology & Therapeutics*, *34*(2), 155–166. https://doi.org/10.1016/0163-7258(87)90009-X

El-Far, S. W., El-Enin, H. A. A., Abdou, E. M., Nafea, O. E., & Abdelmonem, R. (2022). Targeting Colorectal Cancer Cells with Niosomes Systems Loaded with Two Anticancer Drugs Models; Comparative In Vitro and Anticancer Studies. *Pharmaceuticals*, *15*(7). https://doi.org/10.3390/ph15070816

Faheem, A. M., & Abdelkader, D. H. (2019). Novel drug delivery systems. In *Engineering Drug Delivery Systems*. Elsevier LTD. https://doi.org/10.1016/B978-0-08-102548-2.00001-9

FDA. (2018). Liposome Drug Chemistry, Manufacturing, and Controls; Human Products Pharmacokinetics and Bioavailability; and Labeling Documentation. *Labeling Documentation*

Guidance for Industry, *April*, 15. https://www.fda.gov/regulatory-information/search-fda-guidance-documents/liposome-drug-products-chemistry-manufacturing-and-controls-human-pharmacokinetics-and%0Ahttp://www.fda.gov/Drugs/GuidanceComplianceRegulatoryInformation/Guidances/default.htm

Feng, C. (2019). Approaches to the Search of Platinum Anticancer Agents: Derivatizing Current Drugs and Incorporating HDAC Inhibition. *University of the Pacific Theses and Dissertations*. https://scholarlycommons.pacific.edu/uop_etds/3637

Florea, A. M., & Büsselberg, D. (2011). Cisplatin as an Anti-Tumor Drug: Cellular Mechanisms of Activity, Drug Resistance and Induced Side Effects. *Cancers 2011, Vol. 3, Pages 1351-1371*, *3*(1), 1351–1371. https://doi.org/10.3390/CANCERS3011351

Frezza, M., Hindo, S., Chen, D., Davenport, A., Schmitt, S., Tomco, D., & Ping Dou, Q. (2010). Novel Metals and Metal Complexes as Platforms for Cancer Therapy. *Current Pharmaceutical Design*, *16*(16), 1813–1825. https://doi.org/10.2174/138161210791209009

Gabano, E., Gariboldi, M. B., Marras, E., Barbato, F., & Ravera, M. (2023). Platinum(iv) combo prodrugs containing cyclohexane-1R,2R-diamine, valproic acid, and perillic acid as a multiaction chemotherapeutic platform for colon cancer. *Dalton Transactions*, *52*(32), 11349–11360. https://doi.org/10.1039/d3dt01876h

Gharbavi, M., Amani, J., Kheiri-Manjili, H., Danafar, H., & Sharafi, A. (2018). Niosome: A Promising Nanocarrier for Natural Drug Delivery through Blood-Brain Barrier. *Advances in Pharmacological Sciences*, *2018*. https://doi.org/10.1155/2018/6847971

Ghosh, S. (2019). Cisplatin: The first metal based anticancer drug. *Bioorganic Chemistry*, *88*(March), 102925. https://doi.org/10.1016/j.bioorg.2019.102925

Gindy, M. E., & Prud'homme, R. K. (2009). Multifunctional nanoparticles for imaging, delivery and targeting in cancer therapy. *Http://Dx.Doi.Org/10.1517/17425240902932908*, *6*(8), 865–878. https://doi.org/10.1517/17425240902932908

Giovanni Natile. (2016). Encapsulation of lipophilic kiteplatin Pt(IV) prodrugs in PLGA-PEG micelles. *Journal of the Chemical Society, Dalton Transactions*, *45*(33), 1772. https://doi.org/10.1039/C6DT00763E

Gong, J., Chen, M., Zheng, Y., Wang, S., & Wang, Y. (2012). Polymeric micelles drug delivery

system in oncology. *Journal of Controlled Release*, *159*(3), 312–323. https://doi.org/10.1016/j.jconrel.2011.12.012

Gude, R. P., Jadhav, M. G., Rao, S. G. A., & Jagtap, A. G. (2002). Effects of niosomal cisplatin and combination of the same with theophylline and with activated macrophages in murine B16F10 melanoma model. *Cancer Biotherapy and Radiopharmaceuticals*, *17*(2), 183–192. https://doi.org/10.1089/108497802753773801

Haag, R., & Kratz, F. (2006). Polymer Therapeutics: Concepts and Applications. *Angewandte Chemie International Edition*, *45*(8), 1198–1215. https://doi.org/10.1002/ANIE.200502113

Hall, M. D., & Hambley, T. W. (2002). Platinum(IV) antitumour compounds: Their bioinorganic chemistry. *Coordination Chemistry Reviews*, *232*(1–2), 49–67. https://doi.org/10.1016/S0010-8545(02)00026-7

Hall, M. D., Okabe, M., Shen, D. W., Liang, X. J., & Gottesman, M. M. (2008). The role of cellular accumulation in determining sensitivity to platinum-based chemotherapy. *Annual Review of Pharmacology and Toxicology*, *48*, 495–535. https://doi.org/10.1146/ANNUREV.PHARMTOX.48.080907.180426

Hamaguchi, K., Godwin, A. K., Yakushyi, M., O'Dwyer, P. J., Ozols, R. F., & Hamilton, T. C. (1993). Cross-Resistance to Diverse Drugs Is Associated with Primary Cisplatin Resistance in Ovarian Cancer Cell Lines. *Cancer Research*, *53*(21), 5225–5232.

Hang, Z., Cooper, M. A., & Ziora, Z. M. (2016). Platinum-based anticancer drugs encapsulated liposome and polymeric micelle formulation in clinical trials. *Biochemical Compounds*, *4*(1), 1. https://doi.org/10.7243/2052-9341-4-2

He, R. X., Ye, X., Li, R., Chen, W., Ge, T., Huang, T. Q., Nie, X. J., Chen, H. J. T., Peng, D. Y., & Chen, W. D. (2017). PEGylated niosomes-mediated drug delivery systems for Paeonol: preparation, pharmacokinetics studies and synergistic anti-tumor effects with 5-FU. *Journal of Liposome Research*, *27*(2), 161–170. https://doi.org/10.1080/08982104.2016.1191021

Ho, G. Y., Woodward, N., & Coward, J. I. G. (2016). Cisplatin versus carboplatin: comparative review of therapeutic management in solid malignancies. *Critical Reviews in Oncology/Hematology*, *102*, 37–46. https://doi.org/10.1016/J.CRITREVONC.2016.03.014

Holzer, A. K., Manorek, G. H., & Howell, S. B. (2006). Contribution of the major copper influx transporter CTR1 to the cellular accumulation of cisplatin, carboplatin, and oxaliplatin. *Molecular*

Pharmacology, *70*(4), 1390–1394. https://doi.org/10.1124/MOL.106.022624

Hong, M., Zhu, S., Jiang, Y., Tang, G., & Pei, Y. (2009). Efficient tumor targeting of hydroxycamptothecin loaded PEGylated niosomes modified with transferrin. *Journal of Controlled Release*, *133*(2), 96–102. https://doi.org/10.1016/j.jconrel.2008.09.005

Huang, L., Yang, J., Wang, T., Gao, J., & Xu, D. (2022). Engineering of small-molecule lipidic prodrugs as novel nanomedicines for enhanced drug delivery. *Journal of Nanobiotechnology*, *20*(1), 1–15. https://doi.org/10.1186/s12951-022-01257-4

Iv, D. (1996). *Carboxylation of Dihydroxoplatinum(IV) Complexes via a New Synthetic Pathway*. *Iv*, 1709–1711.

Ivanov, A. I., Christodoulou, J., Parkinson, J. A., Barnham, K. J., Tucker, A., Woodrow, J., & Sadler, P. J. (1998). Cisplatin binding sites on human albumin. *Journal of Biological Chemistry*, *273*(24), 14721–14730. https://doi.org/10.1074/jbc.273.24.14721

Javani, R., Hashemi, F. S., Ghanbarzadeh, B., & Hamishehkar, H. (2021). Quercetin-loaded niosomal nanoparticles prepared by the thin-layer hydration method: Formulation development, colloidal stability, and structural properties. *Lwt*, *141*(November 2020), 110865. https://doi.org/10.1016/j.lwt.2021.110865

Johansson, K., Ito, M., Schophuizen, C. M. S., Mathew Thengumtharayil, S., Heuser, V. D., Zhang, J., Shimoji, M., Vahter, M., Ang, W. H., Dyson, P. J., Shibata, A., Shuto, S., Ito, Y., Abe, H., & Morgenstern, R. (2011). Characterization of new potential anticancer drugs designed to overcome glutathione transferase mediated resistance. *Molecular Pharmaceutics*, *8*(5), 1698–1708. https://doi.org/10.1021/mp2000692

Johnstone, T. C., Alexander, S. M., Wilson, J. J., & Lippard, S. J. (2015). Oxidative halogenation of cisplatin and carboplatin: Synthesis, spectroscopy, and crystal and molecular structures of Pt(iv) prodrugs. *Dalton Transactions*, *44*(1), 119–129. https://doi.org/10.1039/c4dt02627f

Johnstone, T. C., & Lippard, S. J. (2013). The effect of ligand lipophilicity on the nanoparticle encapsulation of Pt(IV) prodrugs. *Inorganic Chemistry*, *52*(17), 9915–9920. https://doi.org/10.1021/ic4010642

Johnstone, T. C., Suntharalingam, K., & Lippard, S. J. (2016). The Next Generation of Platinum Drugs: Targeted Pt(II) Agents, Nanoparticle Delivery, and Pt(IV) Prodrugs. *Chemical Reviews*, *116*(5), 3436–3486. https://doi.org/10.1021/ACS.CHEMREV.5B00597

Johnstone, T. C., Wilson, J. J., & Lippard, S. J. (2013). Monofunctional and higher-valent platinum anticancer agents. *Inorganic Chemistry*, *52*(21), 12234–12249. https://doi.org/10.1021/ic400538c

Joseph, T. M., Kar Mahapatra, D., Esmaeili, A., Piszczyk, Ł., Hasanin, M. S., Kattali, M., Haponiuk, J., & Thomas, S. (2023). Nanoparticles: Taking a Unique Position in Medicine. *Nanomaterials*, *13*(3). https://doi.org/10.3390/nano13030574

Jovanović, S., Petrović, B., Bugarčić, Ž. D., & Van Eldik, R. (2013). Reduction of some Pt(iv) complexes with biologically important sulfur-donor ligands. *Dalton Transactions*, *42*(24), 8890–8896. https://doi.org/10.1039/c3dt50751c

Junyaprasert, V. B., Singhsa, P., & Jintapattanakit, A. (2013). Influence of chemical penetration enhancers on skin permeability of ellagic acid-loaded niosomes. *Asian Journal of Pharmaceutical Sciences*, *8*(2), 110–117. https://doi.org/10.1016/J.AJPS.2013.07.014

Kalinowska-Lis, U., Ochocki, J., & Matlawska-Wasowska, K. (2008). Trans geometry in platinum antitumor complexes. *Coordination Chemistry Reviews*, *252*(12–14), 1328–1345. https://doi.org/10.1016/j.ccr.2007.07.015

Kanaani, L., Javadi, I., Ebrahimifar, M., shahmabadi, H. E., Khiyavi, A. A., & Mehrdiba, T. (2017). Effects of cisplatin-loaded niosomal nanoparticleson BT-20 human breast carcinoma cells. *Asian Pacific Journal of Cancer Prevention*, *18*(2), 365–368. https://doi.org/10.22034/APJCP.2017.18.2.365

Kanaani, L., Mazloumi Tabrizi, M., Akbarzadeh Khiyavi, A., & Javadi, I. (2017). Improving the Efficacy of Cisplatin using Niosome Nanoparticles Against Human Breast Cancer Cell Line BT-20 : An In Vitro Study. *Asian Pacific Journal of Cancer Biology*, *2*(2), 27–29. https://doi.org/10.31557/apjcb.2017.2.2.27-29

Karki, S., Kim, H., Na, S. J., Shin, D., Jo, K., & Lee, J. (2016). Thin films as an emerging platform for drug delivery. *Asian Journal of Pharmaceutical Sciences*, *11*(5), 559–574. https://doi.org/10.1016/j.ajps.2016.05.004

Kartalou, M., & Essigmann, J. M. (2001). Recognition of cisplatin adducts by cellular proteins. *Mutation Research - Fundamental and Molecular Mechanisms of Mutagenesis*, *478*(1–2), 1–21. https://doi.org/10.1016/S0027-5107(01)00142-7

Kasparkova, J., Vojtiskova, M., Natile, G., & Brabec, V. (2008). Unique Properties of DNA Interstrand Cross-Links of Antitumor Oxaliplatin and the Effect of Chirality of the Carrier Ligand. *Chemistry*

– *A European Journal*, *14*(4), 1330–1341. https://doi.org/10.1002/CHEM.200701352

Kauffman, G. B., Pentimalli, R., Doldi, S., & Hall, M. D. (2010). Michele Peyrone (1813-1883), discoverer of Cisplatin. *Platinum Metals Review*, *54*(4), 250–256. https://doi.org/10.1595/147106710X534326

Kaur, D., & Kumar, S. (2018). NIOSOMES: PRESENT SCENARIO AND FUTURE ASPECTS. *Journal of Drug Delivery and Therapeutics*, *8*(5), 35–43. https://doi.org/10.22270/JDDT.V8I5.1886

Kelland, L. R. (1993). New platinum antitumor complexes. *Crit Rev Oncol Hematol*, *15*(3), 191–219. https://doi.org/10.1016/1040-8428(93)90042-3

Kelley, S. L., Basu, A., Teicher, B. A., Hacker, M. P., Hamer, D. H., & Lazo, J. S. (1988). Overexpression of metallothionein confers resistance to anticancer drugs. *Science*, *241*(4874), 1813–1815. https://doi.org/10.1126/science.3175622

Khan, S. R. A., Guzman-Jimenez, I., Whitmire, K. H., & Khokhar, A. R. (2000). Synthesis and characterization of piperidine platinum(II) complexes with dicarboxylates: Crystal and molecular structure of cis-[Pt(piperidine)2Cl2]·H2O. *Polyhedron*, *19*(8), 975–981. https://doi.org/10.1016/S0277-5387(00)00348-X

Kilari, D., Guancial, E., & Kim, E. S. (2016). Role of copper transporters in platinum resistance. *World Journal of Clinical Oncology*, *7*(1), 106. https://doi.org/10.5306/WJCO.V7.I1.106

Klein, A. V, & Hambley, T. W. (2006). *Platinum-Based Anticancer Agents*.

Knox, R. J., Friedlos, F., Lydall, D. A., & Roberts, J. J. (1986). *Mechanism of cytotoxicity of anticancer platinum drugs: Evidence that cis-diamminedichloroplatinum(ii) and cis-diammine-(l,l-cyclobutanedicarboxylato)platinum(ii) differ only in the kinetics of their interaction with dna*. Cancer Research.

Kopermsub, P., Mayen, V., & Warin, C. (2011). Potential use of niosomes for encapsulation of nisin and EDTA and their antibacterial activity enhancement. *Food Research International*, *44*(2), 605–612. https://doi.org/10.1016/J.FOODRES.2010.12.011

Kostrhunova, H., Malina, J., Pickard, A. J., Stepankova, J., Vojtiskova, M., Kasparkova, J., Muchova, T., Rohlfing, M. L., Bierbach, U., & Brabec, V. (2011). Replacement of a thiourea with an amidine group in a monofunctional platinum-acridine antitumor agent. Effect on DNA interactions, DNA adduct recognition and repair. *Molecular Pharmaceutics*, *8*(5), 1941–1954.

https://doi.org/10.1021/MP200309X/SUPPL_FILE/MP200309X_SI_001.PDF

Kumar, G. P., & Rajeshwarrao, P. (2011). Nonionic surfactant vesicular systems for effective drug delivery—an overview. *Acta Pharmaceutica Sinica B*, *1*(4), 208–219. https://doi.org/10.1016/j.apsb.2011.09.002

Kumar, P., Sulakhiya, K., Barua, C. C., & Mundhe, N. (2017). TNF-α, IL-6 and IL-10 expressions, responsible for disparity in action of curcumin against cisplatin-induced nephrotoxicity in rats. *Molecular and Cellular Biochemistry*, *431*(1–2), 113–122. https://doi.org/10.1007/s11010-017-2981-5

Lee, Y. A., Yoo, K. H., & Jung, O. S. (2003). Oxidation of Pt(II) to Pt(IV) complex with hydrogen peroxide in glycols. *Inorganic Chemistry Communications*, *6*(3), 249–251. https://doi.org/10.1016/S1387-7003(02)00752-9

Letchford, K., & Burt, H. (2007). A review of the formation and classification of amphiphilic block copolymer nanoparticulate structures: micelles, nanospheres, nanocapsules and polymersomes. *European Journal of Pharmaceutics and Biopharmaceutics*, *65*(3), 259–269. https://doi.org/10.1016/J.EJPB.2006.11.009

Li, X., Liu, Y., & Tian, H. (2018). Current Developments in Pt(IV) Prodrugs Conjugated with Bioactive Ligands. *Bioinorganic Chemistry and Applications*, *2018*(Ii). https://doi.org/10.1155/2018/8276139

Li, Z., Xu, Q., Lin, X., Yu, K., Lin, L., Liu, Y., Yu, Z., Liu, T., & Luo, D. (2022). Integrating of lipophilic platinum(IV) prodrug into liposomes for cancer therapy on patient-derived xenograft model. *Chinese Chemical Letters*, *33*(4), 1875–1879. https://doi.org/10.1016/J.CCLET.2021.10.077

Lippard, S. J. (2007). Pt-DNA01.pdf. *Chem. Rev.*, *107*(5), 1387.

Liu, D., He, C., Wang, A. Z., & Lin, W. (2013). Application of liposomal technologies for delivery of platinum analogs in oncology. *International Journal of Nanomedicine*, *8*, 3309–3319. https://doi.org/10.2147/IJN.S38354

Liu, P., Chen, G., & Zhang, J. (2022). A Review of Liposomes as a Drug Delivery System : Current. *Molecules*, *27*(4), 1372.

Liu, S., Li, Y., Wang, X., Ma, J., Zhang, L., & Xia, G. (2016). Preparation, Characterization, and Antitumor Activities of Miriplatin-Loaded Liposomes. *Journal of Pharmaceutical Sciences*,

105(1), 78–87. https://doi.org/10.1016/j.xphs.2015.10.026

Loh, S. Y., Mistry, P., Kelland, L. R., Abel, G., & Harrap, K. R. (1992). Reduced drug accumulation as a major mechanism of acquired resistance to cisplatin in a human ovarian carcinoma cell line: Circumvention studies using novel platinum (ii) and (iv) ammine/amine complexes. *British Journal of Cancer*, *66*(6), 1109–1115. https://doi.org/10.1038/bjc.1992.419

Lovejoy, K. S., Todd, R. C., Zhang, S., McCormick, M. S., D'Aquino, J. A., Reardon, J. T., Sancar, A., Giacomini, K. M., & Lippard, S. J. (2008). cis-Diammine(pyridine)chloroplatinum(II), a monofunctional platinum(II) antitumor agent: Uptake, structure, function, and prospects. *Proceedings of the National Academy of Sciences of the United States of America*, *105*(26), 8902–8907. https://doi.org/10.1073/PNAS.0803441105

Lu, O.*Λ*. (2014). Bilgisayar Oyunları ve İnternet Sitelerinde Sanal Şiddet Ögelerinin Değerlendirilmesi. *Cancer Res*, *74*(14), 3913–3922. https://doi.org/10.1158/0008-5472.CAN-14-0247.Say

Madison, B. L., Thyme, S. B., Keene, S., & Williams, B. S. (2007). Mechanistic study of competitive sp3-sp3 and sp 2-sp3 carbon-carbon reductive elimination from a platinum (IV) center and the isolation of a C-C agostic complex. *Journal of the American Chemical Society*, *129*(31), 9538–9539. https://doi.org/10.1021/JA066195D/SUPPL_FILE/JA066195DSI20070622_014101.PDF

Mahale, N. B., Thakkar, P. D., Mali, R. G., Walunj, D. R., & Chaudhari, S. R. (2012). Niosomes: Novel sustained release nonionic stable vesicular systems - An overview. *Advances in Colloid and Interface Science*, *183–184*, 46–54. https://doi.org/10.1016/j.cis.2012.08.002

Malhotra-Kumar, S., Lammens, C., Coenen, S., Van Herck, K., & Goossens, H. (2007). Effect of azithromycin and clarithromycin therapy on pharyngeal carriage of macrolide-resistant streptococci in healthy volunteers: a randomised, double-blind, placebo-controlled study. *The Lancet*, *369*(9560), 482–490. https://doi.org/10.1016/S0140-6736(07)60235-9

Markovic, M., Ben-Shabat, S., Keinan, S., Aponick, A., Zimmermann, E. M., & Dahan, A. (2018). Prospects and Challenges of Phospholipid-Based Prodrugs. *Pharmaceutics*, *10*(4). https://doi.org/10.3390/PHARMACEUTICS10040210

Marzo, T., Pratesi, A., Cirri, D., Pillozzi, S., Petroni, G., Guerri, A., Arcangeli, A., Messori, L., & Gabbiani, C. (2018). Chlorido and bromido oxaliplatin analogues as potential agents for CRC treatment: Solution behavior, protein binding and cytotoxicity evaluation. *Inorganica Chimica Acta*, *470*, 318–324. https://doi.org/10.1016/j.ica.2017.05.067

Matos, M., Pando, D., & Gutiérrez, G. (2019). Nanoencapsulation of food ingredients by niosomes. In *Lipid-Based Nanostructures for Food Encapsulation Purposes: Volume 2 in the Nanoencapsulation in the Food Industry series*. Elsevier Inc. https://doi.org/10.1016/B978-0-12-815673-5.00011-8

Mayer, F., Gillis, A. J. M., Dinjens, W., Oosterhuis, J. W., Bokemeyer, C., & Looijenga, L. H. J. (2002). Microsatellite instability of germ cell tumors is associated with resistance to systemic treatment. *Cancer Research*, *62*(10), 2758–2760.

Meerum Terwogt, J. M., Groenewegen, G., Pluim, D., Maliepaard, M., Tibben, M. M., Huisman, A., Ten Bokkel Huinink, W. W., Schot, M., Welbank, H., Voest, E. E., Beijnen, J. H., & Schellens, J. H. (2002). Phase I and pharmacokinetic study of SPI-77, a liposomal encapsulated dosage form of cisplatin. *Cancer Chemotherapy and Pharmacology*, *49*(3), 201–210. https://doi.org/10.1007/s002800100371

Mishra, V., Nayak, P., Singh, M., Sriram, P., & Suttee, A. (2020). Niosomes: Potential nanocarriers for drug delivery. *International Journal of Pharmaceutical Quality Assurance*, *11*(3), 389–394. https://doi.org/10.25258/ijpqa.11.3.13

Moghassemi, S., & Hadjizadeh, A. (2014). Nano-niosomes as nanoscale drug delivery systems: An illustrated review. *Journal of Controlled Release*, *185*(1), 22–36. https://doi.org/10.1016/j.jconrel.2014.04.015

Moghassemi, S., Hadjizadeh, A., & Omidfar, K. (2017). Formulation and Characterization of Bovine Serum Albumin-Loaded Niosome. *AAPS PharmSciTech*, *18*(1), 27–33. https://doi.org/10.1208/S12249-016-0487-1

Mori, A., Wu, S. P., Han, I., Khokhar, A. R., Perez-Soler, R., & Huang, L. (1996). In vivo antitumor activity of cis-bis-neodecanoato-trans-R,R-1,2-diaminocyclohexane platinum(II) formulated in long-circulating liposomes. *Cancer Chemotherapy and Pharmacology*, *37*(5), 435–444. https://doi.org/10.1007/s002800050409

Mujoriya, R., Bodla, R. B., Dhamande, K., Singh, D., & Patle, L. (2011). Niosomal drug delivery system: The magic bullet. *Journal of Applied Pharmaceutical Science*, *1*(9), 20–23.

Naderinezhad, S., Amoabediny, G., & Haghiralsadat, F. (2017). Co-delivery of hydrophilic and hydrophobic anticancer drugs using biocompatible pH-sensitive lipid-based nano-carriers for multidrug-resistant cancers. *RSC Advances*, *7*(48), 30008–30019. https://doi.org/10.1039/C7RA01736G

Novohradsky, V., Zanellato, I., Marzano, C., Pracharova, J., Kasparkova, J., Gibson, D., Gandin, V., Osella, D., & Brabec, V. (2017). Epigenetic and antitumor effects of platinum(IV)-octanoato conjugates. *Scientific Reports*, *7*(1), 2–5. https://doi.org/10.1038/s41598-017-03864-w

Novohradsky, V., Zerzankova, L., Stepankova, J., Vrana, O., Raveendran, R., Gibson, D., Kasparkova, J., & Brabec, V. (2014). Antitumor platinum(IV) derivatives of oxaliplatin with axial valproato ligands. *Journal of Inorganic Biochemistry*, *140*, 72–79. https://doi.org/10.1016/j.jinorgbio.2014.07.004

Novohradsky, V., Zerzankova, L., Stepankova, J., Vrana, O., Raveendran, R., Gibson, D., Kasparkova, J., & Brabec, V. (2015). New insights into the molecular and epigenetic effects of antitumor Pt(IV)-valproic acid conjugates in human ovarian cancer cells. *Biochemical Pharmacology*, *95*(3), 133–144. https://doi.org/10.1016/J.BCP.2015.04.003

O'Connor, M. J., Boblak, K. N., Topinka, M. J., Kindelin, P. J., Briski, J. M., Zheng, C., & Klumpp, D. A. (2010). Superelectrophiles and the effects of trifluoromethyl substituents. *Journal of the American Chemical Society*, *132*(10), 3266. https://doi.org/10.1021/JA1001482

O'Neill, C. F., Koberle, B., Masters, J. R. W., & Kelland, L. R. (1999). Gene-specific repair of Pt/DNA lesions and induction of apoptosis by the oral platinum drug JM216 in three human ovarian carcinoma cell lines sensitive and resistant to cisplatin. *British Journal of Cancer*, *81*(8), 1294–1303. https://doi.org/10.1038/sj.bjc.6694381

Obeid, M. A., Haifawi, S., & Khadra, I. (2023). The impact of solvent selection on the characteristics of niosome nanoparticles prepared by microfluidic mixing. *International Journal of Pharmaceutics: X*, *5*. https://doi.org/10.1016/J.IJPX.2023.100168

Ogata, Y., Murakami, H., Sasatomi, T., Ishibashi, N., Mori, S., Ushijima, M., Akagi, Y., & Shirouzu, K. (2009). Elevated preoperative serum carcinoembrionic antigen level may be an effective indicator for needing adjuvant chemotherapy after potentially curative resection of stage II colon cancer. *Journal of Surgical Oncology*, *99*(1), 65–70. https://doi.org/10.1002/jso.21161

Oldfield, S. P., Hall, M. D., & Platts, J. A. (2007). Calculation of lipophilicity of a large, diverse dataset of anticancer platinum complexes and the relation to cellular uptake. *Journal of Medicinal Chemistry*, *50*(21), 5227–5237. https://doi.org/10.1021/jm0708275

Olszewski, U., Ulsperger, E., Geissler, K., & Hamilton, G. (2011). Comparison of the effects of the oral anticancer platinum(IV) complexes oxoplatin and metabolite cis-diammine-tetrachlorido-platinum(IV) on global gene expression of NCI-H526 cells. *Journal of Experimental*

Pharmacology, *3*, 43–50. https://doi.org/10.2147/JEP.S13630

Onochie, I. T. O., Nwakile, C. D., Umeyor, C. E., Uronnachi, E. M., Osonwa, U. E., Attama, A. A., & Esimone, C. O. (2013). Formulation and evaluation of niosomes of benzyl penicillin. *Journal of Applied Pharmaceutical Science*, *3*(12), 66–71. https://doi.org/10.7324/JAPS.2013.31212

Osanloo, M., Assadpour, S., Mehravaran, A., Abastabar, M., & Akhtari, J. (2018). Niosome-loaded antifungal drugs as an effective nanocarrier system: A mini review. *Current Medical Mycology*, *4*(4), 31–36. https://doi.org/10.18502/cmm.4.4.384

Ostrowski, A. D., & Ford, P. C. (2009). Metal complexes as photochemical nitric oxide precursors: Potential applications in the treatment of tumors. *Dalton Transactions*, *48*, 10660–10669. https://doi.org/10.1039/b912898k

Pasetto, L. M., D'Andrea, M. R., Rossi, E., & Monfardini, S. (2006). Oxaliplatin-related neurotoxicity: How and why? *Critical Reviews in Oncology/Hematology*, *59*(2), 159–168. https://doi.org/10.1016/j.critrevonc.2006.01.001

Pažout, R., Housková, J., Dušek, M., Maixner, J., & Kačer, P. (2011). Platinum precursor of anticancer drug: A structure fixed by long intermolecular n-h···i and c-h···i hydrogen bonds. *Structural Chemistry*, *22*(6), 1325–1330. https://doi.org/10.1007/s11224-011-9826-8

Perez-Soler, R., Han, I., Al-Baker, S., & Khokhar, A. R. (1994). Lipophilic platinum complexes entrapped in liposomes: improved stability and preserved antitumor activity with complexes containing linear alkyl carboxylato leaving groups. *Cancer Chemotherapy and Pharmacology*, *33*(5), 378–384. https://doi.org/10.1007/BF00686266

Piccart, M. J., Di Leo, A., Beauduin, M., Vindevoghel, A., Michel, J., Focan, C., Tagnon, A., Ries, F., Gobert, P., Finet, C., Closon-Dejardin, M. T., Dufrane, J. P., Kerger, J., Liebens, F., Beauvois, S., Bartholomeus, S., Dolci, S., Lobelle, J. P., Paesmans, M., & Nogaret, J. M. (2001). Phase III trial comparing two dose levels of epirubicin combined with cyclophosphamide with cyclophosphamide, methotrexate, and fluorouracil in node-positive breast cancer. *Journal of Clinical Oncology*, *19*(12), 3103–3110. https://doi.org/10.1200/JCO.2001.19.12.3103

Platts, J. A., Hibbs, D. E., Hambley, T. W., & Hall, M. D. (2001). Calculation of the hydrophobicity of platinum drugs. *Journal of Medicinal Chemistry*, *44*(3), 472–474. https://doi.org/10.1021/jm001080k

Qiu, G. H., Xie, X., Xu, F., Shi, X., Wang, Y., & Deng, L. (2015). Distinctive pharmacological

differences between liver cancer cell lines HepG2 and Hep3B. *Cytotechnology*, *67*(1), 1–12. https://doi.org/10.1007/s10616-014-9761-9

Rajera, R., Nagpal, K., Singh, S. K., & Mishra, D. N. (2011). Niosomes: A controlled and novel drug delivery system. *Biological and Pharmaceutical Bulletin*, *34*(7), 945–953. https://doi.org/10.1248/bpb.34.945

Rathee, S., Nayak, V., Singh, K. R., & Ojha, A. (2022). Nanofortification of vitamin B-complex in food matrix: Need, regulations, and prospects. *Food Chemistry: Molecular Sciences*, *4*(March), 100100. https://doi.org/10.1016/j.fochms.2022.100100

Ratzon, E., Najajreh, Y., Salem, R., Khamaisie, H., Ruthardt, M., & Mahajna, J. (2016). Platinum (IV)-fatty acid conjugates overcome inherently and acquired Cisplatin resistant cancer cell lines: An in-vitro study. *BMC Cancer*, *16*(1), 1–11. https://doi.org/10.1186/S12885-016-2182-8/FIGURES/4

Ravera, M., Gabano, E., McGlinchey, M. J., & Osella, D. (2019). A view on multi-action Pt(IV) antitumor prodrugs. *Inorganica Chimica Acta*, *492*, 32–47. https://doi.org/10.1016/J.ICA.2019.04.025

Ravera, M., Gabano, E., Zanellato, I., Gallina, A., Perin, E., Arrais, A., Cantamessa, S., & Osella, D. (2017). Cisplatin and valproate released from the bifunctional [Pt(IV)Cl2(NH3)2(valproato)2] antitumor prodrug or from liposome formulations: who does what? *Dalton Transactions*, *46*(5), 1559–1566. https://doi.org/10.1039/c6dt03749f

Ravera, M., Zanellato, I., Gabano, E., Perin, E., Rangone, B., Coppola, M., & Osella, D. (2019). Antiproliferative activity of Pt(IV) conjugates containing the non-steroidal anti-inflammatory drugs (NSAIDs) Ketoprofen and Naproxen. *International Journal of Molecular Sciences*, *20*(12), 1–18. https://doi.org/10.3390/ijms20123074

Reithofer, M. R., Bytzek, A. K., Valiahdi, S. M., Kowol, C. R., Groessl, M., Hartinger, C. G., Jakupec, M. A., Galanski, M., & Keppler, B. K. (2011). Tuning of lipophilicity and cytotoxic potency by structural variation of anticancer platinum(IV) complexes. *Journal of Inorganic Biochemistry*, *105*(1), 46–51. https://doi.org/10.1016/j.jinorgbio.2010.09.006

Ringhieri, P., Pannunzio, A., Boccarelli, A., Morelli, G., Coluccia, M., & Tesauro, D. (2016). Effect of cisplatin containing liposomes formulated by unsaturated chain-containing lipids on gynecological tumor cells. *Journal of Liposome Research*, *26*(4), 307–312. https://doi.org/10.3109/08982104.2015.1127257

Rixe, O., Ortuzar, W., Alvarez, M., Parker, R., Reed, E., Paull, K., & Fojo, T. (1996). Oxaliplatin, tetraplatin, cisplatin, and carboplatin: spectrum of activity in drug-resistant cell lines and in the cell lines of the National Cancer Institute's Anticancer Drug Screen panel. *Biochemical Pharmacology*, *52*(12), 1855–1865. https://doi.org/10.1016/S0006-2952(97)81490-6

Rocha, C. R. R., Silva, M. M., Quinet, A., Cabral-Neto, J. B., & Menck, C. F. M. (2018). DNA repair pathways and cisplatin resistance: An intimate relationship. *Clinics*, *73*. https://doi.org/10.6061/CLINICS/2018/E478S

ROGERSON, A., CUMMINGS, J., WILLMOTT, N., & FLORENCE, A. T. (1988). The Distribution of Doxorubicin in Mice Following Administration in Niosomes. *Journal of Pharmacy and Pharmacology*, *40*(5), 337–342. https://doi.org/10.1111/j.2042-7158.1988.tb05263.x

Rosenberg, B., Van Camp, L., & Krigas, T. (1965). Inhibition of Cell Division in Escherichia coli by Electrolysis Products from a Platinum Electrode. *Nature 1965 205:4972*, *205*(4972), 698–699. https://doi.org/10.1038/205698a0

Rottenberg, S., Disler, C., & Perego, P. (2021). The rediscovery of platinum-based cancer therapy. In *Nature Reviews Cancer* (Vol. 21, Issue 1, pp. 37–50). Nature Research. https://doi.org/10.1038/s41568-020-00308-y

Ruckmani, K., & Sankar, V. (2010). Formulation and optimization of zidovudine niosomes. *AAPS PharmSciTech*, *11*(3), 1119–1127. https://doi.org/10.1208/S12249-010-9480-2

Sahin, N. O. (2007). Niosomes as nanocarrier systems. *Nanomaterials and Nanosystems for Biomedical Applications*, 67–81. https://doi.org/10.1007/978-1-4020-6289-6_4

Saimi, N. I. M., Salim, N., Ahmad, N., Abdulmalek, E., & Rahman, M. B. A. (2021). Aerosolized Niosome Formulation Containing Gemcitabine and Cisplatin for Lung Cancer Treatment: Optimization, Characterization and In Vitro Evaluation. *Pharmaceutics*, *13*(1), 1–19. https://doi.org/10.3390/PHARMACEUTICS13010059

Sánchez-Escribano Morcuende, R., Alés-Martínez, J. E., & Aramburo González, P. M. (2007). Low dose Gemcitabine plus cisplatin in a weekly-based regimen as salvage therapy for relapsed breast cancer after taxane-anthracycline-containing regimens. *Clinical and Translational Oncology*, *9*(7), 459–464. https://doi.org/10.1007/s12094-007-0085-5

Sankhala, K. K., Mita, A. C., Adinin, R., Wood, L., Beeram, M., Bullock, S., Yamagata, N., Matsuno, K., Fujisawa, T., & Phan, A. (2009). A phase I pharmacokinetic (PK) study of MBP-426, a novel

liposome encapsulated oxaliplatin. *Journal of Clinical Oncology*, *27*(15_suppl), 2535–2535. https://doi.org/10.1200/jco.2009.27.15_suppl.2535

Sankhyan, A., & Pawar, P. (2012). Recent trends in niosome as vesicular drug delivery system. *Journal of Applied Pharmaceutical Science*, *2*(6), 20–32. https://doi.org/10.7324/JAPS.2012.2625

Sargazi, S., Hosseinikhah, S. M., Zargari, F., Chauhana, N. P. S., Hassanisaadi, M., & Amani, S. (2021). pH-responsive cisplatin-loaded niosomes: synthesis, characterization, cytotoxicity study and interaction analyses by simulation methodology. *Nanofabrication*, *6*(1), 1–15. https://doi.org/10.1515/nanofab-2020-0100

Shahabadi, N., Kashanian, S., Mahdavi, M., & Sourinejad, N. (2011). DNA interaction and DNA cleavage studies of a new platinum(II) complex containing aliphatic and aromatic dinitrogen ligands. *Bioinorganic Chemistry and Applications*, *2011*. https://doi.org/10.1155/2011/525794

Sharma, D., Ali, A. A. E., & Aate, J. R. (2018). Niosomes as Novel Drug Delivery System: Review Article. *Pharmatutor*, *6*(3), 58. https://doi.org/10.29161/PT.V6.I3.2018.58

Shi, M., Fortin, D., Paquette, B., & Sanche, L. (2016). Convection-enhancement delivery of liposomal formulation of oxaliplatin shows less toxicity than oxaliplatin yet maintains a similar median survival time in F98 glioma-bearing rat model. *Investigational New Drugs*, *34*(3), 269. https://doi.org/10.1007/S10637-016-0340-0

Siddik, Z. H. (2003). Cisplatin: Mode of cytotoxic action and molecular basis of resistance. *Oncogene*, *22*(47 REV. ISS. 6), 7265–7279. https://doi.org/10.1038/sj.onc.1206933

Silva, D., & Press, D. (2019). *Characterization , optimization , and in vitro evaluation of Technetium-99m-labeled niosomes*. 1101–1117.

Silverman, A. P., Bu, W., Cohen, S. M., & Lippard, S. J. (2002). 2.4-Å crystal structure of the asymmetric platinum complex {Pt(ammine) (cyclohexylamine)}2+ bound to a dodecamer DNA duplex. *Journal of Biological Chemistry*, *277*(51), 49743–49749. https://doi.org/10.1074/jbc.M206979200

Singh, M. P., Khaket, T. P., Bajpai, V. K., Alfarraj, S., Kim, S. G., Chen, L., Huh, Y. S., Han, Y. K., & Kang, S. C. (2020). Morin Hydrate Sensitizes Hepatoma Cells and Xenograft Tumor towards Cisplatin by Downregulating PARP-1-HMGB1 Mediated Autophagy. *International Journal of Molecular Sciences 2020, Vol. 21, Page 8253*, *21*(21), 8253. https://doi.org/10.3390/IJMS21218253

Sluiter, W. J., Mulder, N. H., Timmer-Bosscha, H., Jan Meersma, G., & de Vries, E. G. E. (1992). Relationship of Cellular Glutathione to the Cytotoxicity and Resistance of Seven Platinum Compounds. *Cancer Research*, *52*(24), 6885–6889.

Spector, D., Erofeev, A., Gorelkin, P., Skvortsov, D., Trigub, A., Markova, A., Nikitina, V., Ul'yanovskiy, N., Shtil', A., Semkina, A., Vlasova, K., Zyk, N., Majouga, A., Beloglazkina, E., & Krasnovskaya, O. (2022). Biotinylated Pt(iv) prodrugs with elevated lipophilicity and cytotoxicity. *Dalton Transactions*, *52*(4), 866–871. https://doi.org/10.1039/d2dt03662b

Stordal, B., & Davey, M. (2007). Understanding cisplatin resistance using cellular models. *IUBMB Life*, *59*(11), 696–699. https://doi.org/10.1080/15216540701636287

Tabbakhian, M., Tavakoli, N., Jaafari, M. R., & Daneshamouz, S. (2006). Enhancement of follicular delivery of finasteride by liposomes and niosomes. 1. In vitro permeation and in vivo deposition studies using hamster flank and ear models. *International Journal of Pharmaceutics*, *323*(1–2), 1–10. https://doi.org/10.1016/j.ijpharm.2006.05.041

Tanaka, K., Kunimatzu, T., Shimakura, J., & Hanada, M. (2011). Development of Miriplatin , a Novel Antitumor Platinum for Hepatocellular Carcinoma. *Sumitomo Kagaku*, 1–12.

Tartaro, G., Mateos, H., Schirone, D., Angelico, R., & Palazzo, G. (2020). *Microemulsion Microstructure (s): A Tutorial Review*. 1–40.

Tavano, L., Aiello, R., Ioele, G., Picci, N., & Muzzalupo, R. (2014). Niosomes from glucuronic acid-based surfactant as new carriers for cancer therapy: Preparation, characterization and biological properties. *Colloids and Surfaces B: Biointerfaces*, *118*, 7–13. https://doi.org/10.1016/j.colsurfb.2014.03.016

Tavano, L., Gentile, L., Oliviero Rossi, C., & Muzzalupo, R. (2013). Novel gel-niosomes formulations as multicomponent systems for transdermal drug delivery. *Colloids and Surfaces B: Biointerfaces*, *110*, 281–288. https://doi.org/10.1016/j.colsurfb.2013.04.017

Thi, T. T. H., Suys, E. J. A., Lee, J. S., Nguyen, D. H., Park, K. D., & Truong, N. P. (2021). Lipid-based nanoparticles in the clinic and clinical trials: From cancer nanomedicine to COVID-19 vaccines. *Vaccines*, *9*(4), 1–29. https://doi.org/10.3390/vaccines9040359

Tsang, R. Y., Al-Fayea, T., & Au, H. J. (2013). Cisplatin Overdose. *Drug Safety 2009 32:12*, *32*(12), 1109–1122. https://doi.org/10.2165/11316640-000000000-00000

Uchino, H., Matsumura, Y., Negishi, T., Koizumi, F., Hayashi, T., Honda, T., Nishiyama, N., Kataoka,

K., Naito, S., & Kakizoe, T. (2005). Cisplatin-incorporating polymeric micelles (NC-6004) can reduce nephrotoxicity and neurotoxicity of cisplatin in rats. *British Journal of Cancer*, *93*(6), 678–687. https://doi.org/10.1038/sj.bjc.6602772

Udofot, O., Affram, K., Smith, T., Tshabe, B., Krishnan, S., Sachdeva, M., & Agyare, E. (2016). Pharmacokinetic, biodistribution and therapeutic efficacy of 5-fluorouracil-loaded pH-sensitive PEGylated liposomal nanoparticles in HCT-116 tumor bearing mouse. *Journal of Nature and Science*, *2*(1), 1–16. http://www.ncbi.nlm.nih.gov/pubmed/27200415%0Ahttp://www.pubmedcentral.nih.gov/articlerender.fcgi?artid=PMC4869888

Ueno, T., Endo, K., Hori, K., Ozaki, N., Tsuji, A., Kondo, S., Wakisaka, N., Murono, S., Kataoka, K., Kato, Y., & Yoshizaki, T. (2014). Assessment of antitumor activity and acute peripheral neuropathy of 1,2-diaminocyclohexane platinum (II)-incorporating micelles (NC-4016). *International Journal of Nanomedicine*, *9*(1), 3005–3012. https://doi.org/10.2147/IJN.S60564

Venkatesh, V., & Sadler, P. J. (2018). Platinum(IV) prodrugs. In *Metallo-Drugs: Development and Action of Anticancer Agents* (Vol. 18, Issue Iv). https://doi.org/10.1515/9783110470734-003

Volovat, S. R., Ciuleanu, T. E., Koralewski, P., Grilley Olson, J. E., Croitoru, A., Koynov, K., Stabile, S., Cerea, G., Osada, A., Bobe, I., & Volovat, C. (2020). A multicenter, single-arm, basket design, phase II study of NC-6004 plus gemcitabine in patients with advanced unresectable lung, biliary tract, or bladder cancer. *Oncotarget*, *11*(33), 3105–3117. https://doi.org/10.18632/oncotarget.27684

Wang, M., Yuan, Y., Gao, Y., Ma, H. M., Xu, H. T., Zhang, X. N., & Pan, W. S. (2012). Preparation and characterization of 5-fluorouracil pH-sensitive niosome and its tumor-targeted evaluation: In vitro and in vivo. *Drug Development and Industrial Pharmacy*, *38*(9), 1134–1141. https://doi.org/10.3109/03639045.2011.641565

Wang, Q., & Pu, S. (2015). *Improved synthesis of miriplatin, an antitumor drug*. *3*(3), 212–215. https://doi.org/10.2991/ic3me-15.2015.41

Wang, Y., Li, H., Rasool, A., Wang, H., Manzoor, R., & Zhang, G. (2024). Polymeric nanoparticles (PNPs) for oral delivery of insulin. *Journal of Nanobiotechnology*, *22*(1), 1–22. https://doi.org/10.1186/s12951-023-02253-y

Wexselblatt, E., & Gibson, D. (2012). What do we know about the reduction of Pt(IV) pro-drugs? *Journal of Inorganic Biochemistry*, *117*, 220–229.

https://doi.org/10.1016/J.JINORGBIO.2012.06.013

Wheate, N. J., Walker, S., Craig, G. E., & Oun, R. (2010). The status of platinum anticancer drugs in the clinic and in clinical trials. *Dalton Transactions*, *39*(35), 8113–8127. https://doi.org/10.1039/C0DT00292E

Wilson, J. J., & Lippard, S. J. (2011). Synthesis, characterization, and cytotoxicity of platinum(IV) carbamate complexes. *Inorganic Chemistry*, *50*(7), 3103–3115. https://doi.org/10.1021/IC2000816/SUPPL_FILE/IC2000816_SI_003.CIF

Wilson, J. J., & Lippard, S. J. (2014a). ChemInform Abstract: Synthetic Methods for the Preparation of Platinum Anticancer Complexes. *ChemInform*, *45*(24), 4470–4495. https://doi.org/10.1002/chin.201424273

Wilson, J. J., & Lippard, S. J. (2014b). Synthetic methods for the preparation of platinum anticancer complexes. *Chemical Reviews*, *114*(8), 4470–4495. https://doi.org/10.1021/CR4004314/ASSET/IMAGES/CR4004314.SOCIAL.JPEG_V03

Witika, B. A., Bassey, K. E., Demana, P. H., Siwe-Noundou, X., & Poka, M. S. (2022). Current Advances in Specialised Niosomal Drug Delivery: Manufacture, Characterization and Drug Delivery Applications. *International Journal of Molecular Sciences*, *23*(17). https://doi.org/10.3390/ijms23179668

Wu, X., Tang, P., Li, S., Wang, S., Liang, Y., Zhong, L., Ren, L., Zhang, T., & Zhang, Y. (2018). A randomized and open-label phase II trial reports the efficacy of neoadjuvant lobaplatin in breast cancer. *Nature Communications*, *9*(1). https://doi.org/10.1038/s41467-018-03210-2

Wu, Y., Xu, X. Y., Yan, F., Sun, W. L., Zhang, Y., Liu, D. L., & Shen, B. (2019). Retrospective study of the efficacy and toxicity of lobaplatin in combined chemotherapy for metastatic breast cancer. *OncoTargets and Therapy*, *12*, 4849–4857. https://doi.org/10.2147/OTT.S192373

Xiaoyong, W., & Zijian, G. (2012). Targeting and delivery of platinum-based anticancer drugs. *Chemical Society Reviews*, *42*(1), 202–224. https://doi.org/10.1039/C2CS35259A

Xu, Z., Wang, Z., Deng, Z., & Zhu, G. (2021). Recent advances in the synthesis, stability, and activation of platinum(IV) anticancer prodrugs. *Coordination Chemistry Reviews*, *442*, 213991. https://doi.org/10.1016/j.ccr.2021.213991

Yang, H., Deng, A., Zhang, J., Wang, J., & Lu, B. (2013). Preparation, characterization and anticancer therapeutic efficacy of cisplatin-loaded niosomes. *Journal of Microencapsulation*, *30*(3), 237–

244. https://doi.org/10.3109/02652048.2012.717116

Yang, X., Tong, J., Guo, L., Qian, Z., Chen, Q., Qi, R., & Qiu, Y. (2017). Bundling potent natural toxin cantharidin within platinum (IV) prodrugs for liposome drug delivery and effective malignant neuroblastoma treatment. *Nanomedicine: Nanotechnology, Biology, and Medicine*, *13*(1), 287–296. https://doi.org/10.1016/j.nano.2016.08.024

Yucel, C., Arslan, F. D., Ekmekci, S., Ulker, V., Kisa, E., Yucel, E. E., Ucar, M., Ilbey, Y. O., Celik, O., Basok, B. I., & Kozacioglu, Z. (2019). Protective Effect of All-Trans Retinoic Acid in Cisplatin-Induced Testicular Damage in Rats. *The World Journal of Men's Health*, *37*(2), 249. https://doi.org/10.5534/WJMH.180105

Zacharie, B., Ezzitouni, A., Duceppe, J. S., & Penney, C. (2009). A simple and efficient large-scale synthesis of metal salts of medium-chain fatty acids. *Organic Process Research and Development*, *13*(3), 581–583. https://doi.org/10.1021/op900038v

Zanellato, I., Bonarrigo, I., Sardi, M., Alessio, M., Gabano, E., Ravera, M., & Osella, D. (2011). Evaluation of Platinum-Ethacrynic Acid Conjugates in the Treatment of Mesothelioma. *ChemMedChem*, *6*(12), 2287–2293. https://doi.org/10.1002/cmdc.201100426

Zaro, J. L. (2015). Lipid-Based Drug Carriers for Prodrugs to Enhance Drug Delivery. *AAPS Journal*, *17*(1), 83–92. https://doi.org/10.1208/s12248-014-9670-z

Zhang, J. Z., Bonnitcha, P., Wexselblatt, E., Klein, A. V., Najajreh, Y., Gibson, D., & Hambley, T. W. (2013). Facile preparation of mono-, Di- and mixed-carboxylato platinum(IV) complexes for versatile anticancer prodrug design. *Chemistry - A European Journal*, *19*(5), 1672–1676. https://doi.org/10.1002/chem.201203159

Zhang, P., & Sadler, P. J. (2017). Redox-Active Metal Complexes for Anticancer Therapy. *European Journal of Inorganic Chemistry*, *2017*(12), 1541–1548. https://doi.org/10.1002/ejic.201600908

Zhang, Q., Kuang, G., Zhang, L., & Zhu, Y. (2023). Nanocarriers for platinum drug delivery. In *Biomedical Technology* (Vol. 2, pp. 77–89). https://doi.org/10.1016/j.bmt.2022.11.011

Zhang, S., Lovejoy, K. S., Shima, J. E., Lagpacan, L. L., Shu, Y., Lapuk, A., Chen, Y., Komori, T., Gray, J. W., Chen, X., Lippard, S. J., & Giacomini, K. M. (2006). Organic cation transporters are determinants of oxaliplatin cytotoxicity. *Cancer Research*, *66*(17), 8847–8857. https://doi.org/10.1158/0008-5472.CAN-06-0769

Zhang, S., Wu, Y., He, B., Luo, K., & Gu, Z. (2014). Biodegradable polymeric nanoparticles based on

amphiphilic principle: construction and application in drug delivery. *Science China Chemistry 2014 57:4*, *57*(4), 461–475. https://doi.org/10.1007/S11426-014-5076-0

Zhao, X., Chen, Q., Liu, W., Li, Y., Tang, H., Liu, X., & Yang, X. (2014). Codelivery of doxorubicin and curcumin with lipid nanoparticles results in improved efficacy of chemotherapy in liver cancer. *International Journal of Nanomedicine*, *10*, 257–270. https://doi.org/10.2147/IJN.S73322

Zhao, Z., Ukidve, A., Kim, J., & Mitragotri, S. (2020). Targeting Strategies for Tissue-Specific Drug Delivery. *Cell*, *181*(1), 151–167. https://doi.org/10.1016/j.cell.2020.02.001

Zheng, X., Xie, J., Zhang, X., Sun, W., Zhao, H., Li, Y., & Wang, C. (2021). An overview of polymeric nanomicelles in clinical trials and on the market. *Chinese Chemical Letters*, *32*(1), 243–257. https://doi.org/10.1016/j.cclet.2020.11.029

Zheng, Y. R., Suntharalingam, K., Johnstone, T. C., Yoo, H., Lin, W., Brooks, J. G., & Lippard, S. J. (2014). Pt(IV) prodrugs designed to bind non-covalently to human serum albumin for drug delivery. *Journal of the American Chemical Society*, *136*(24), 8790–8798. https://doi.org/10.1021/JA5038269

Zhou, N. N., Zhao, Y. Y., Zhai, L. Z., Ruan, C. M., Yang, Y. P., Huang, Y., Hou, X., Chen, L. K., Zhou, T., & Zhang, L. (2018). The efficacy and toxicity of Lobaplatin-contained chemotherapy in extensive-stage small-cell lung cancer. *Journal of Cancer*, *9*(13), 2232–2236. https://doi.org/10.7150/jca.24557

Zhou, Y., Wei, Y., Liu, H., Zhang, G., & Wu, X. (2010). Preparation and in vitro evaluation of ethosomal total alkaloids of Sophora alopecuroides loaded by a transmembrane pH-gradient method. *AAPS PharmSciTech*, *11*(3), 1350–1358. https://doi.org/10.1208/S12249-010-9509-6

Appendix 1 : Each Compounds characterization using Attenuated total reflection (ATR)/Fourier transform infrared spectroscopy (FTIR)

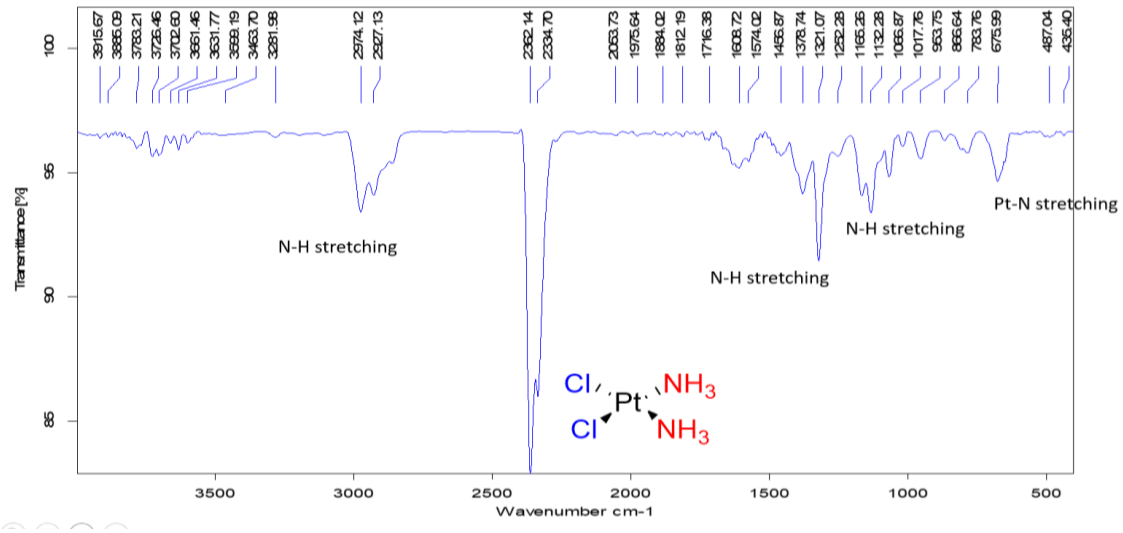

Figure A.1 ATR/FTIR spectra of cisplatin **(10)**

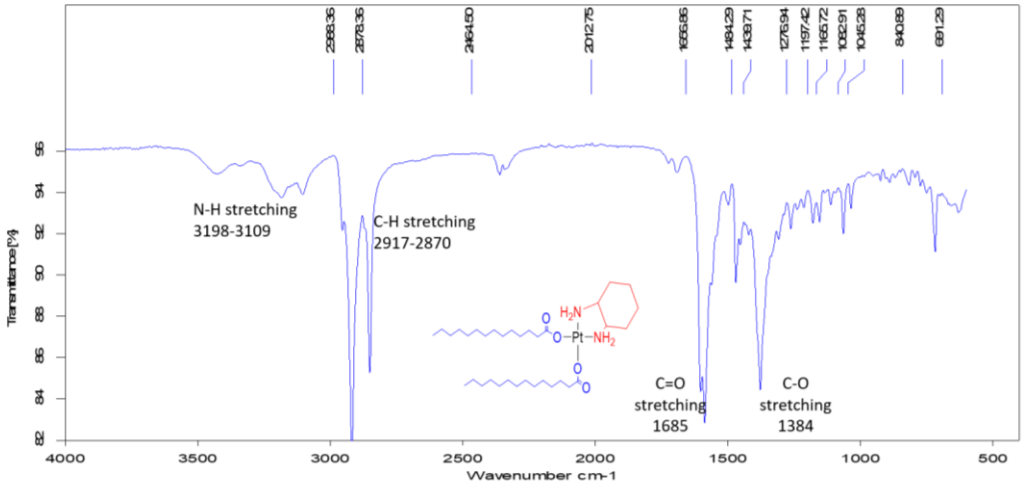

Figure A.2 ATR/FTIR spectra of Miriplatin **(19)**

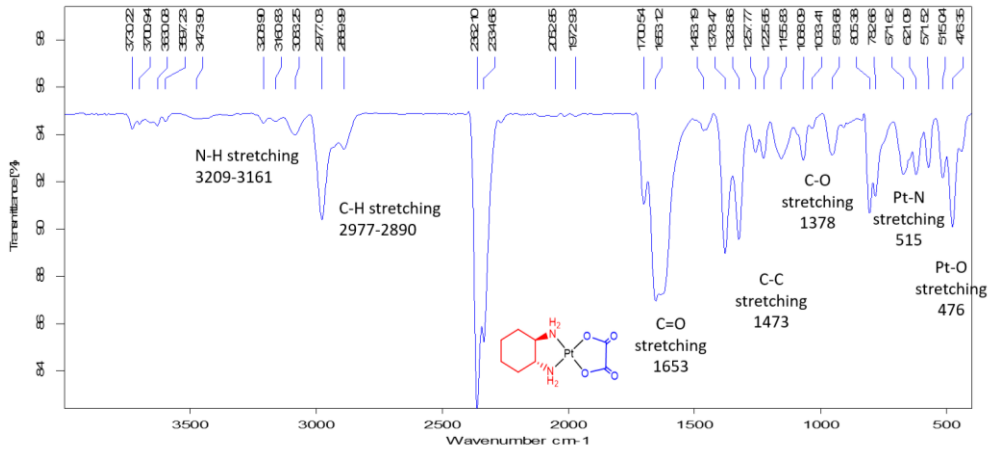

Figure A.3 ATR/FTIR spectra of Oxaliplatin **(23)**

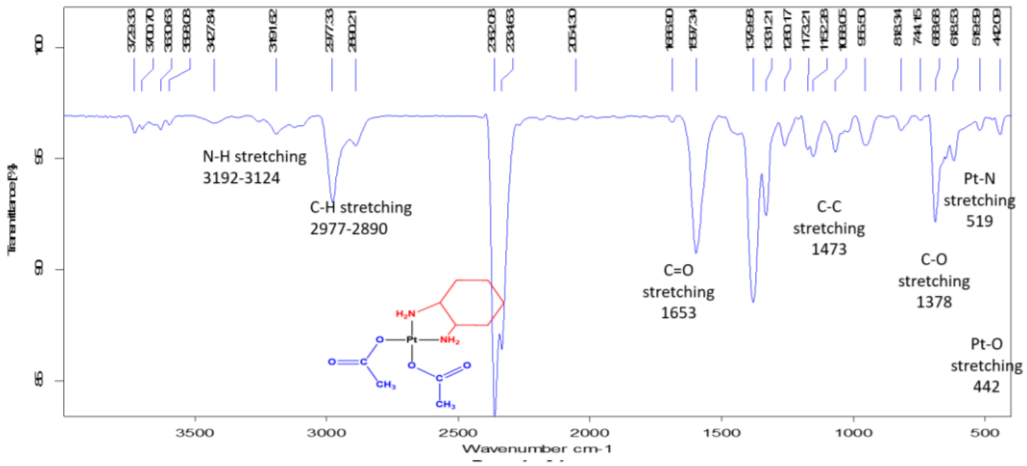

Figure A.4 ATR/FTIR spectra of *Cis*- Pt(DACH)(acetate)$_2$] **(25)**

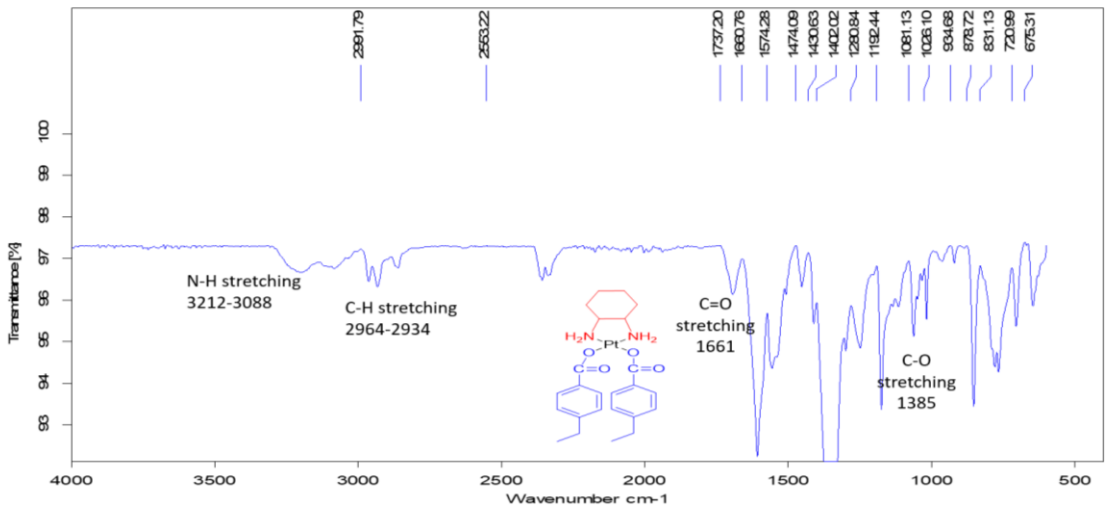

Figure A.5 ATR/FTIR spectra of [*Cis*-Pt(DACH)(EBZ)$_2$] **(26)**

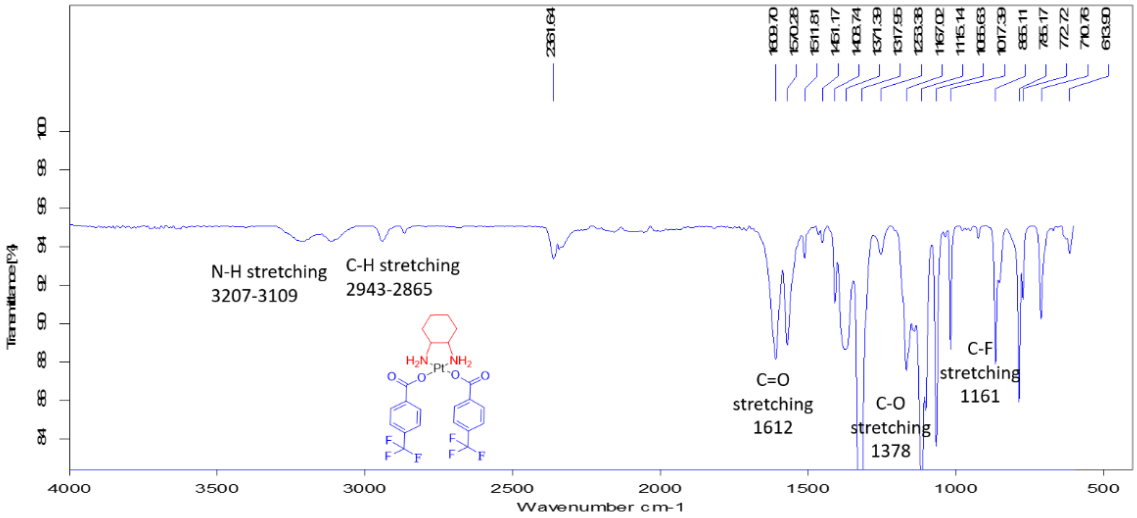

Figure A.6 ATR/FTIR spectra of [*Cis*- Pt(DACH)(TFBA)$_2$] **(27)**

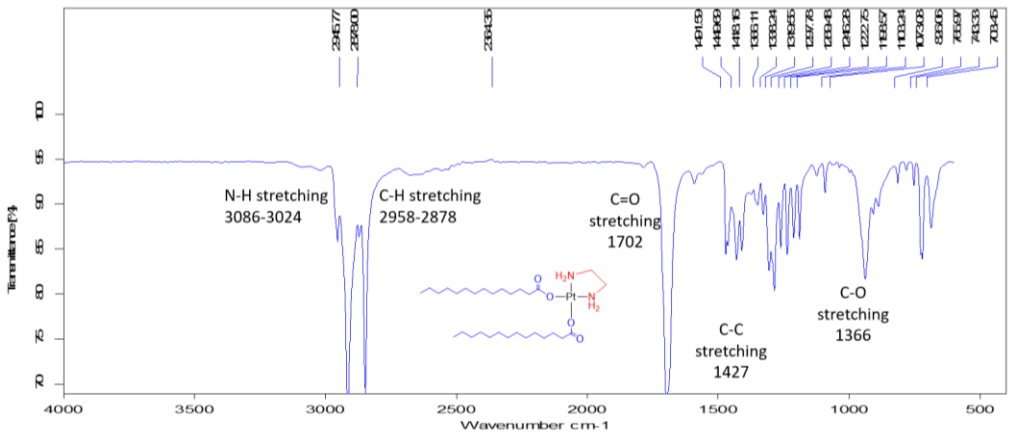

Figure A7 ATR/FTIR spectra of [*Cis*-Pt(EN)(MYR)$_2$] **(30)**

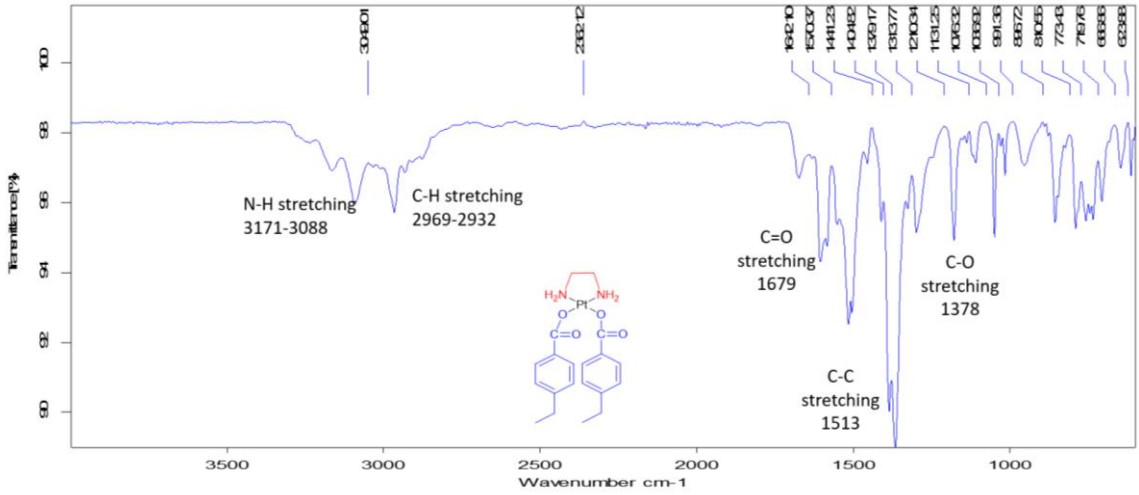

Figure A.8 ATR/FTIR spectra of [*Cis*-Pt(EN)(EZB)$_2$] **(31)**

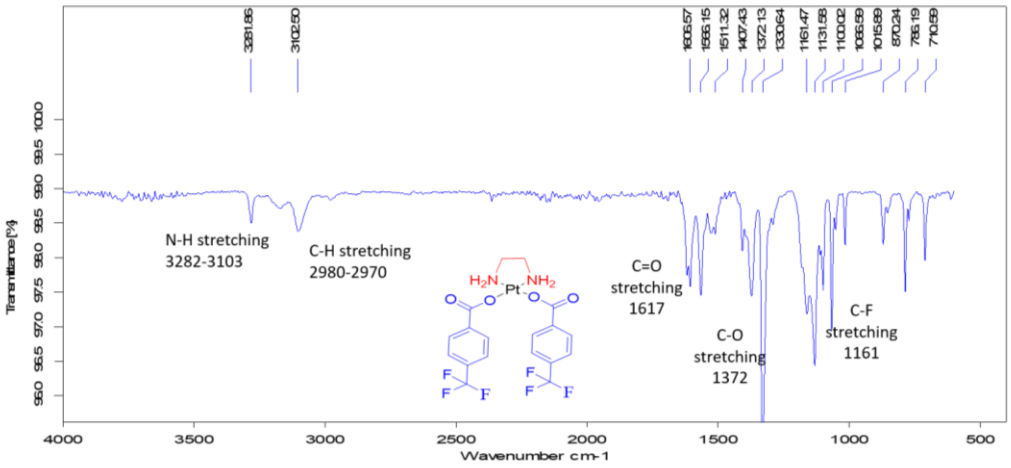

Figure A.9 ATR/FTIR spectra of [*Cis*-Pt(EN)(TFBA)$_2$] **(32)**

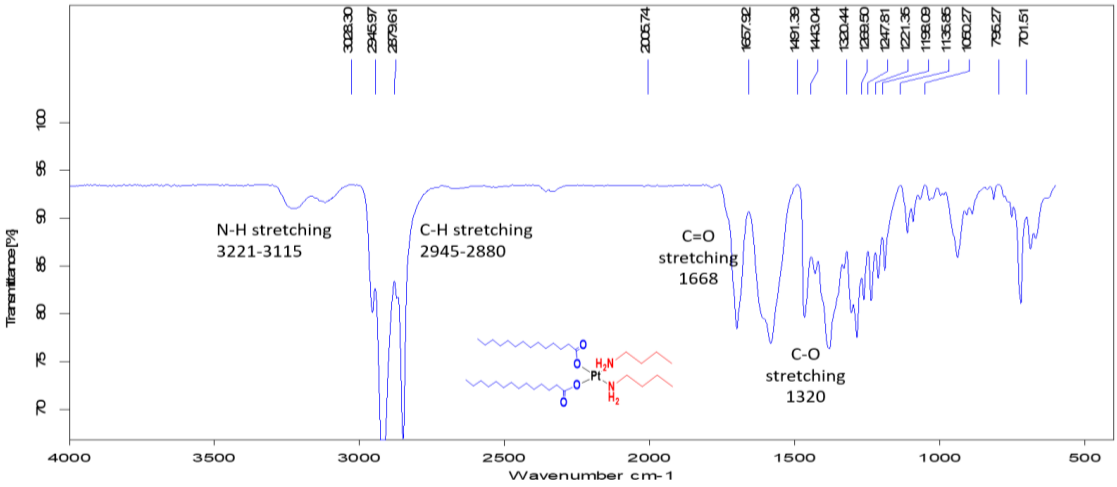

Figure A.10 ATR/FTIR spectra of [*Cis*-Pt(NBA)$_2$(MYR)$_2$] **(35)**

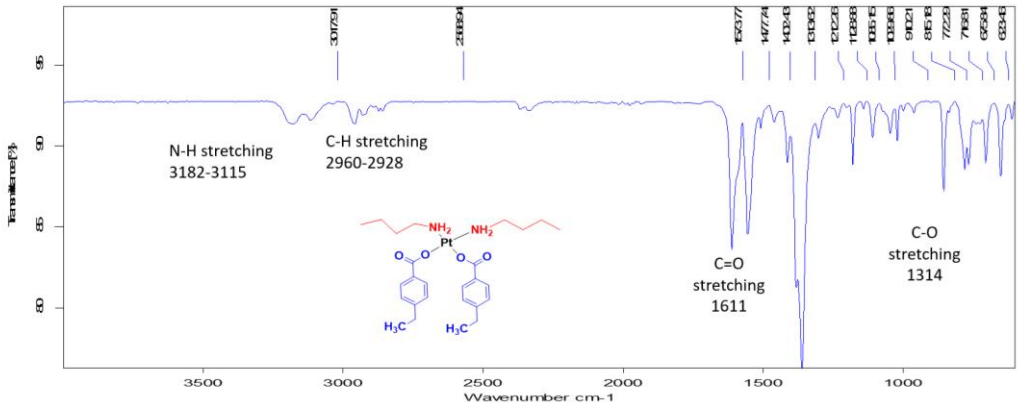

Figure A.11 ATR/FTIR spectra of [*Cis*-Pt(NBA)$_2$(EZB)$_2$] **(36)**

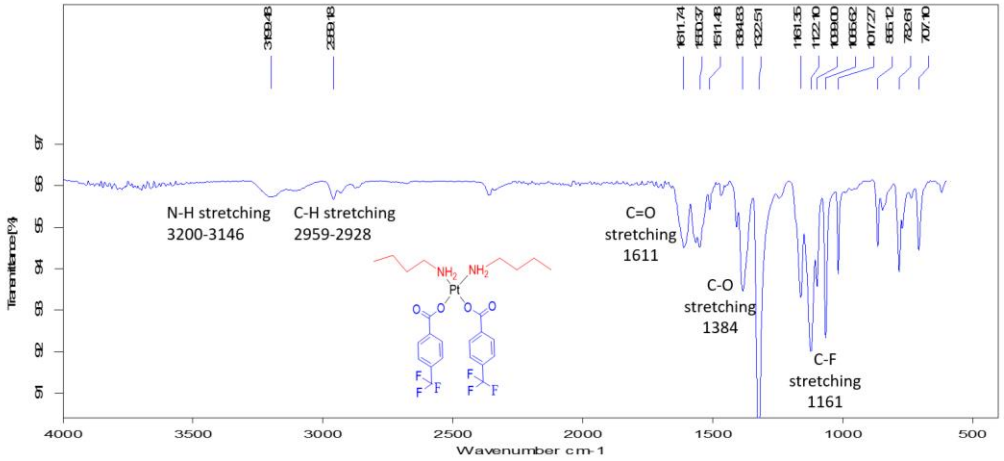

Figure A.12 ATR/FTIR spectra of [*Cis*-Pt(NBA)$_2$(TFBA)$_2$] **(37)**

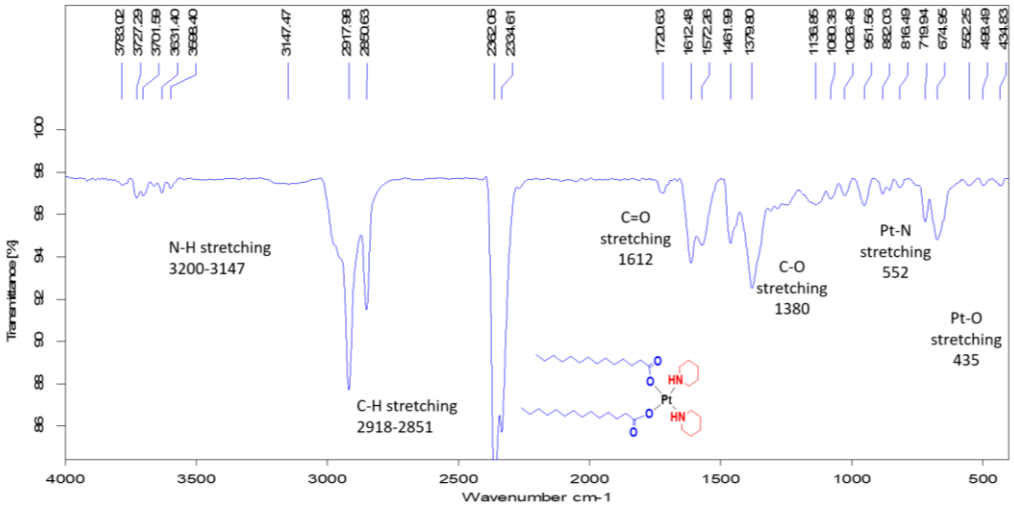

Figure A.13 ATR/FTIR spectra of [*Cis*-Pt(PIP)$_2$(MYR)$_2$] **(40)**

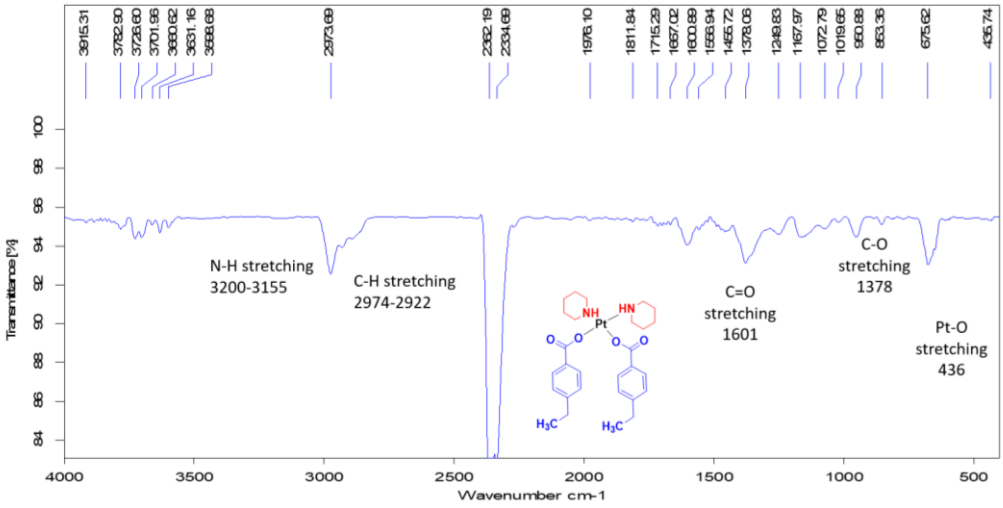

Figure A.14 ATR/FTIR spectra of [*Cis*-Pt(PIP)$_2$(EBZ)$_2$] **(41)**

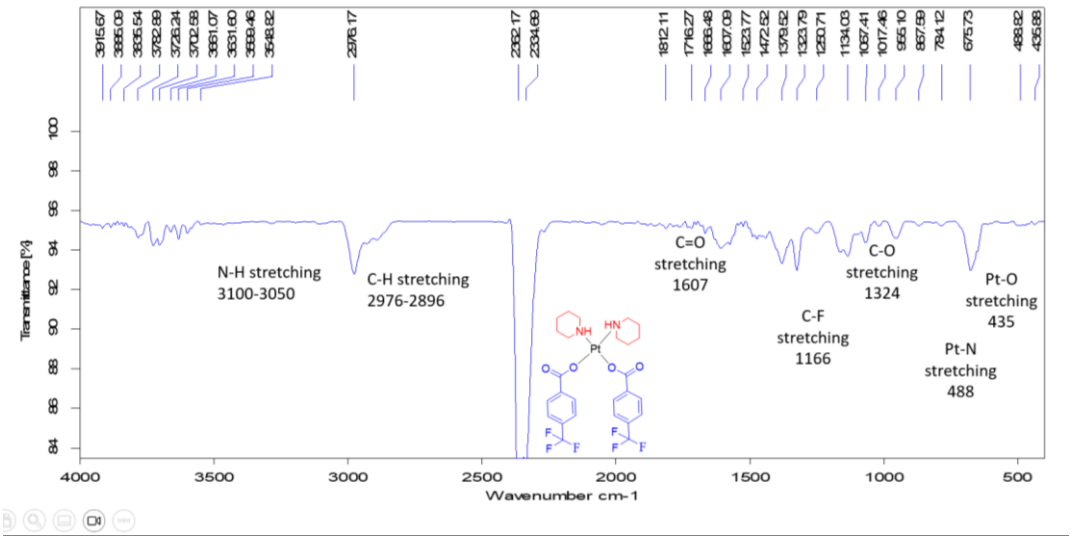

Figure A.15 ATR/FTIR spectra of [*Cis*-Pt(PIP)$_2$(TFBA)$_2$] **(42)**

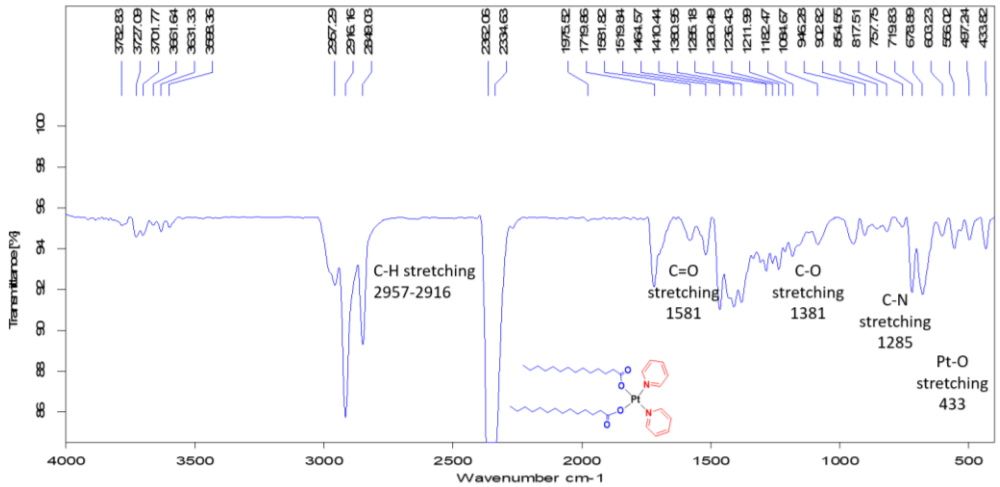

Figure A.16 ATR/FTIR spectra of [*Cis*-Pt(PYR)$_2$(MYR)$_2$] **(47)**

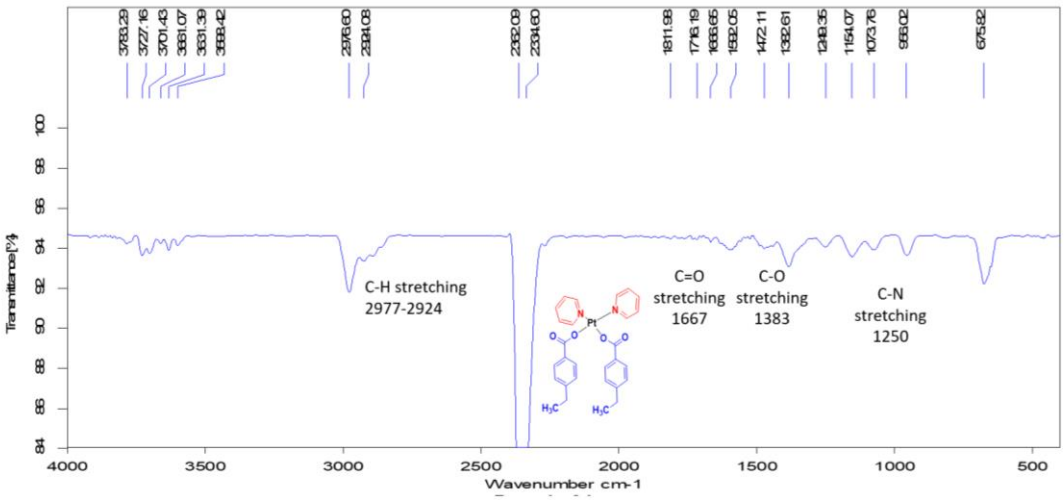

Figure A.17 ATR/FTIR spectra of [*Cis*-Pt(PYR)$_2$(EBZ)$_2$] **(48)**

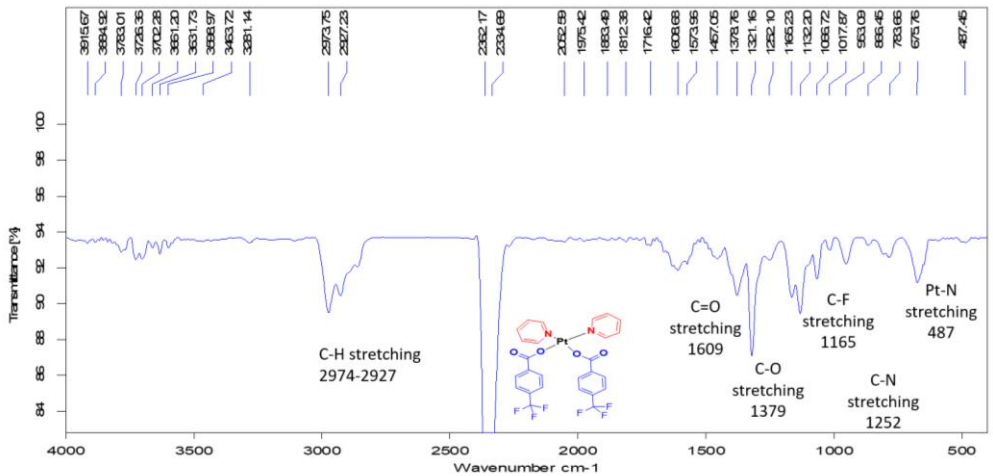

Figure A.18 ATR/FTIR spectra of [*Cis*-Pt(PYR)$_2$(TFBA)$_2$] **(49)**